# Technische Universität München

Lehrstuhl für Bioverfahrenstechnik

# Biphasic whole-cell production of geranyl glucoside by recombinant *Escherichia coli*

## Xenia Laura Priebe

*Wie oft wohl muss einer das, was er weiß, noch einmal lernen, wieder und wieder entdecken, wie viele Verkleidungen abreißen, bis er die Dinge wirklich versteht [...]? Reicht überhaupt eine Lebenszeit dafür aus?*

(Jenny Erpenbeck: Gehen, ging, gegangen)

# Acknowledgments

Manh Dat Hoang and Nicolai Stampfer for their excellent support in the laboratory.

I thank Dr. Carlos Härtel for his supportive mentoring during my master and doctoral studies. Without him, I might not have started working on a doctoral thesis in the first place.

I thank my friends for always having my back and for bringing so much joy and laughter into my life. Hereby, I especially want to thank Lisa, Alex, Nils and Rob for numerous pep talks and constant encouragement.

Last but not least, I thank my entire family for always believing in me, and for supporting my entire course of studies in every respect. Especially my mother and my great-grandmother inspired me with their immense strength and willpower.

# Contents

# 1. Introduction

The chemical industry is an economic sector with an annual turnover of approximately 3.5 trillion € [Verband der chemischen Industrie e.V. 2018] and acts as an important supplier for other commercial sectors such as construction, and automotive and consumer goods industries. To a major extent, the production of basic chemicals, which are starting materials for more advanced fine and specialty chemicals, is still based on petrochemistry [Fischer, L. 2011]. However, due to the finite nature of petroleum and petroleum gas supplies, new raw materials have to be identified. This challenge becomes even more urgent when considering the emission of greenhouse gases related to the use of fossil resources.

Microorganisms can convert renewable resources to valuable products and thus have the potential to take the chemical industry in a new, sustainable direction. In the comparatively new field of industrial biotechnology, microorganisms and their enzymes are used for the production of chemicals [S. Y. Lee et al. 2019; Tang and Zhao 2009]. Matching the diversity of microorganisms, a variety of different, renewable substrates can be converted. Many microorganisms use simple monosaccharides as substrates: for example, the yeast *Saccharomyces cerevisiae* or the bacterium *Escherichia coli* (*E. coli*) can consume glucose. Metabolization of polysaccharides is possible in various bacteria, protozoa and fungi, such as the consumption of pectine by *Aspergillus niger* [Pedrolli et al. 2009]. Different alcohols can serve as substrates, too. For example, *E. coli* and methylotrophic yeasts can use glycerol and methanol, respectively [Murarka et al. 2008; Schmideder et al. 2016a]. Moreover, microalgae and anaerobic acetogenic bacteria can metabolize $CO_2$, CO and $H_2$ [Koller et al. 2017; Mayer and Weuster-Botz 2017].

Besides from the manifold options in natural production strains and raw materials, biotechnology offers the possibility to design microbial "factories" [Almquist et al. 2014] based on process and product requirements. Different metabolic engineering strategies allow for the removal of constraints and bottlenecks in the relevant metabolic pathways and thus for increases in product yields. Such strategies cover the overexpression of target enzymes, the elimination of competing pathways by knocking out the respective enzymes, the insertion of heterologous genetic material, and molecular modifications of the target

enzymes [Kulkarni 2016].

A prominent example for a microorganism frequently used as a cell factory in industrial biotechnology is *E. coli.* This prokaryote is capable of expressing a variety of recombinant enzymes allowing for the production of tailor-made products [Choi et al. 2000; Khalilzadeh et al. 2004; Wong et al. 1998]. Moreover, metabolic engineering is facilitated by different mathematical models describing the cellular metabolic network [Chassagnole et al. 2001; J. W. Schmid et al. 2004] and by extensive databases of the bacterial genome [Keseler et al. 2017].

# 2. Motivation and objectives

The flavor and fragrance (F&F) industry is an important player in the chemical sector, contributing significantly to the appearance and appeal of modern consumer goods such as processed food or cosmetic products. Significant growth is predicted for this industry, especially in the developing markets of Latin America, Africa and Asia [IHS Markit 2018]. In order to guarantee sustained growth, the F&F sector is constantly thriving towards better products and trying to identify and address new customer needs. During the last decade, the demand for natural F&F compounds has increased [Carroll et al. 2016]. According to US and European law, natural F&Fs do not necessarily have to be isolated from a natural source, but can also be produced in "enzymatic or microbiological processes from material of vegetable or animal origin"[1]. This definition, coupled with increasing economic demand, explains why industrial biotechnology has entered the F&F sector and production processes based on the usage of microorganisms or their isolated enzymes have been established [Menzel and Schreier 2007; Schrader 2007].

When it comes to consumer goods containing fragrances, such as body lotions, perfumes and detergents, a second customer need has to be taken into account: The consumer wishes for products whose scents are highly stable and do not disappear during storage or right after application. The volatility of fragrance compounds allows them to enter the human olfactory system and be perceived by the olfactory receptors. Thus, a certain "instability" lies in the nature of fragrances, calling for innovative approaches to stabilize fragrance compounds applied in consumer goods [Schwab et al. 2015a]. The most widely used method for fragrance stabilization is the encapsulation of volatile compounds into polymeric microcapsules. The release of the target compound happens through rupture of the capsule shell, which can be triggered by pressure, increase in temperature, or irradiation [León et al. 2017]. A different approach for fragrance stabilization is based on a mechanism found in nature: In plants, many secondary metabolites such as steroids, flavonoids and terpenoids do not exist in their native form, but are stored as glycoconjugates, i.e. bound to sugars [Bowles et al. 2005]. Such glycosides are less reactive and

---

[1] European law: Council Directive of 22 June 1988, 88/388/EEC, Official Journal of the European Communities, No L 184/61, 1988, Article 1(2)(c)

more hydrophilic than the respective aglycones (aglycone: non-sugar component of a glycoside) [Rivas et al. 2013]. Thus, glycosylation can be a method to create storage-stable fragrance compounds whose scent is set free successively only after hydrolysis of the glycosidic bond [Herrmann 2007]. Hydrolysis can be triggered by light, increase in temperature, pH changes or exposure to hydrolases, which are for example produced by the human skin microbiome [Ikemoto et al. 2002].

In plants, glycosylations are catalyzed by glycosyltranserases (GTs), which transfer sugar moieties from activated donor molecules to acceptor molecules. Most frequently, the donor molecules are nucleotides such as uridine diphosphate (UDP), and hydroxyl groups function as acceptors [Lairson et al. 2008]. A variety of GTs from plants with activities towards industrially relevant fragrance compounds has already been identified and characterized. Huang et al. [2015] isolated GTs from *Catharanthus roseus* with activity towards thymol, menthol and vanillin, whereas Caputi et al. [2008] characterized GTs from *Arabidopsis thaliana* that glycosylate terpenoids such as perillyl alcohol or citronellol. GTs with activity towards linalool, citronellol, nerol and geraniol were isolated from the grapevine species *Vitis vinifera* [Bönisch et al. 2014b].

Geraniol is an acyclic monoterpenoid with a pleasant floral scent present in many plant oils, such as rose oil or palmarosa oil [H. Baydar and N. G. Baydar 2005; Dubey and Luthra 2001]. Due to its wide application in the F&F industry [Rastogi et al. 2001], geraniol is a worthwhile candidate for fragrance stabilization by glycosylation. In *Vitis vinifera*, the glycosyltransferase VvGT14a was shown to have high affinity towards geraniol [Bönisch et al. 2014b]. This enzyme relies on UDP-glucose as a sugar donor and can catalyze the conversion of geraniol to geranyl glucoside. In order to use VvGT14a in industrial biotechnology, the respective gene sequence has to be isolated from *Vitis vinifera* and heterologously expressed in a suitable microbial host. Both *Saccharomyces cerevisiae* and *E. coli* were used as hosts for the recombinant expression of different UDP-glucose dependent GTs in shake flasks [Hirotani et al. 2000; H. I. Lee and Raskin 1999; Moehs et al. 1997; Yamazaki et al. 1999]. However, these studies did not focus on maximizing intracellular GT concentrations, but rather on characterizing GTs regarding their preferred reaction conditions and substrate spectrum. Only two studies emphasize the identification of suitable expression conditions in stirred-tank reactors over subsequent detailed GT characterization: Caputi et al. [2008] successfully produced recombinant GTs from *Arabidopsis thaliana* in *E. coli* in a stirred-tank reactor, however, without quantifying GT concentrations or activities. Schmieder et al. [2016b] used the *E. coli* strain BL21(DE3)pLysS as a host for the recombinant production of VvGT14a during high cell density cultivations in a stirred-tank bioreactor. Hereby, a cell dry weight concentration

of 68 g L$^{-1}$ and a VvGT14a concentration of 2.7 g L$^{-1}$ were obtained within 48 h.

Recombinant protein concentrations in *E. coli* usually range between 1–10 g L$^{-1}$ [Choi et al. 2006]. Thus, the process by Schmieder et al. [2016b] leaves room for further improvements. In the present work, the identical *E. coli* strain is to be used to design a high cell density cultivation process with increased biomass and VvGT14a yields.

After successful production of VvGT14a, the enzyme is to be used for the glucosylation of geraniol to yield geranyl glucoside. As VvGT14a is a UDP-glucose dependent GT, the regeneration of UDP-glucose is crucial for the biotransformation reaction. A very elegant way is the usage of the naturally available UDP-glucose pool in *E. coli* [Arend et al. 2001]. The bacterium uses UDP-glucose as a precursor for different polysaccharides constituting the protective capsule on the cells' surface [Whitfield 2006] and thus constantly synthesizes and regenerates this nucleotide sugar. This makes *E. coli* an attractive whole-cell biocatalyst for the production of geranyl glucoside from geraniol. Thus, in the present study the *E. coli* strain expressing VvGT14a is to be used as a whole-cell biocatalyst.

Geraniol shows cytotoxic activities towards *E. coli* BL21(DE3) and Huang et al. [2016] reported a minimal inhibitory concentration as low as 0.3 g L$^{-1}$. Thus, a biphasic reaction system is beneficial where a second, non-aqueous phase features a significantly higher affinity for geraniol than the aqueous phase does [Déziel et al. 1999]. That way, the non-aqueous phase can function as an *in situ* substrate reservoir in batch processes, preserving the biocatalyst from cytotoxic substrate concentrations. Schmieder et al. [2016b] used the ionic liquid N-hexylpyridinium bis(trifluoromethylsulfonyl)imide as the non-aqueous phase during whole-cell biotransformations of geraniol. However, the commercial unavailability of this ionic liquid impedes a broad application of such a biphasic system. Thus, in the present work a suitable and commercially available sequestering phase for geraniol is to be selected by rational means. Hereby, both adsorbents and liquid and solid absorbents are to be considered. As geranyl glucoside features a minimal inhibitory concentration of 5.5 g L$^{-1}$ [Huang et al. 2016], it can be present in the aqueous phase without harming the biocatalyst. Thus, a non-aqueous phase with high selectivity for geraniol is to be identified, facilitating product isolation from the aqueous phase.

So far, the effect of different process variables on the whole-cell biotransformation of geraniol is unknown. This impedes the design of an efficient biotransformation process. Thus, based on the selection of a suitable sequestering phase, a characterization of the biotransformation reaction system is to be carried out, aiming towards high productivities. In order to conduct these studies efficiently and comparably, they are to be performed in a parallelized reactor system at mL-scale. The reaction engineering studies will cover the identification of an appropriate reaction system composition regarding the components

of the aqueous medium and the fraction of the non-aqueous phase. Moreover, studies on the influence of the biocatalyst concentration, biocatalyst recycling, and pH and temperature changes will be included. Furthermore, potential bottlenecks limiting geranyl glucoside concentrations and yields have to be identified. In this context, an analysis of the UDP-glucose supply during biotransformations is to be carried out in order to determine whether the usage of a strain variant with improved UDP-glucose regeneration is beneficial. Another potential bottleneck that has to be taken into account is the formation of undesired byproducts.

In a last step, the obtained findings are to be combined in order to design a biotransformation process at L-scale. Ideally, higher geranyl glucoside concentrations and yields than described by Caputi et al. [2008] and Schmieder et al. [2016b] can be obtained.

Based on the described objectives, the following approach was defined for the present study:

- Process development for the production of *E. coli* whole-cell biocatalysts expressing the glycosyltransferase VvGT14a in high cell density cultivations at L-scale

- Rational selection of a non-aqueous phase with high affinity and selectivity for geraniol by application of thermodynamic first-principles methods and other rational criteria

- Parallelized reaction engineering studies on the biotransformation system at mL-scale

- Identification and removal of potential bottlenecks constraining the biotransformation of geraniol

- Implementation of the obtained findings in biotransformations at L-scale

# 3. Theoretical background

In the following, the reader will find background knowledge crucial for the evaluation of the results presented in the later course. First, an insight into the biotechnological production of flavors and fragrances will be given. After describing the concept of biphasic reaction systems, the theoretical foundation on the cultivation of microorganisms will be outlined, with a focus on the production of recombinant proteins in *E. coli*. The last chapter deals with fundamentals and applications of whole-cell biocatalysis.

## 3.1. Flavors and fragrances

### 3.1.1. Industrial relevance and manufacturing methods

Flavors and fragrances (F&Fs) fundamentally determine the appearance and appeal of present-day processed food and beverages, as well as household and cosmetic products. Their commercial significance is reflected in the F&F industry's world market value of ~US\$ 40 billion, with rising tendency [IHS Markit 2018]. The characteristics of many consumer goods, e.g. sodas, chewing gum or body lotions, are crucially determined by the addition of F&Fs. Global players like Givaudan, Firmenich and Symrise dominate the F&F industry [Guentert 2007] and use three different main strategies for F&F production: isolation from natural sources, chemical synthesis, and production by biotechnological means. When isolating F&Fs from plant materials, three different techniques can be applied: distillation, extraction and cold pressing. One prominent example for isolation by distillation is *(R)*-(+)-limonene, which can be found in orange peels - an abundant byproduct in orange juice production [Ciriminna et al. 2014].

If the natural source of a F&F molecule is not available in industrially required amounts, or in case the isolation technique is too time-consuming or expensive, synthesis routes become relevant. For example, the global need for vanillin can by far not be met by extracting the component from the seed pods of the vanilla plant *Vanilla planifolia* [Sinha et al. 2008]; thus, chemical synthesis from guaiacol is mostly applied in industry [Fatiadi and Schaffer 1974; Kirk-Othmer 2007]. Chemically synthesized F&F have to be declared

as artificial substances, in spite of being identical (nature-identical) to the molecules occurring in nature [Vandamme and Soetaert 2002]. This is a drawback in the current market situation, where consumers ask for natural products, creating a strong market pull for natural F&Fs [Carroll et al. 2016]. Thus in recent years a successive replacement of chemically produced F&Fs by biotechnologically produced compounds has occurred [D. A. Müller 2007], as these can be labeled *natural* under US and European law as long as precursors isolated from nature are involved[2]. Moreover, the biotechnological production of F&F compounds allows for high chemo-, regio- and stereoselectivity, which is not always the case for chemical reactions. The usage of renewable feedstock instead of petrochemical compounds is an additional benefit of biological processes over chemical synthesis.

Two different approaches exist for the biotechnological production of F&F compounds. On the one hand, biotransformations can be applied. In a biotransformation, a natural precursor of the target compound is transformed in a single-step reaction or a simple reaction cascade. On the other hand, *de novo*, fermentative synthesis from simple molecules such as sugars or amino acids can be used, which exploits the complex metabolic network of a cell [Castiglione and Weuster-Botz 2018; Vandamme and Soetaert 2002]. For both routes either naturally occurring or genetically modified microorganisms can be applied; however, *de novo* routes in the latter might have a more promising future than biotransformations. This is largely due to the fact that no expensive or poorly-available precursors are required, as such routes utilize simple feedstocks such as monosaccharides, amino acids or renewable raw materials. Moreover, continuously improved metabolic engineering strategies for popular microbiological hosts such as *E. coli* and *Saccharomyces cerevisiae* (*S. cerevisiae*) facilitate the design of efficient bioprocesses [Borodina and Nielsen 2014; Carroll et al. 2016]. For example, D. Lee et al. [2016] report the *de novo* production of the aroma compound raspberry ketone in recombinant *S. cerevisiae*, and Rodriguez et al. [2014] describe the production of a variety of fruity ester aromas in recombinant *E. coli*.

### 3.1.2. Classification

The term F&F does not refer to a single chemical class; instead, molecules from a variety of different, structurally non-related chemical classes are used in the F&F industry due

---

[2]  US law: Code of Federal Regulations, Title 21, Food and drugs, part 101, sect 102.22(a)–(i); European law: Council Directive of 22 June 1988, 88/388/EEC, Official Journal of the European Communities, No L 184/61, 1988, Article 1(2)(c)

to their unique aroma or scent. In the following classification, a focus is put on molecules that can be produced biotechnologically.

A differentiation can be made between non-volatile and volatile molecules. As non-volatile compounds are odorless, they only comprise flavor molecules, but no fragrances. Non-volatile flavour compounds induce one of the basic tastes sweet, bitter, salty, sour or umami, and the most prominent substances belong to the class of acids [Schrader 2007]. The industrially most important acid flavour compound is L-glutamic acid which functions as a taste enhancer with an umami taste. Its sodium salt monosodium glutamate can be produced very efficiently by *Corynebacterium glutamicum* at large scales up to several hundred m$^3$ [D. Lee et al. 2016] and is added to many processed food products. Other relevant acids are citric acid with a pleasant acid taste and lactic acid with an enjoyable mild sour taste. Besides glutamic acid, the nucleotides inosine 5'-monophosphate and guanosine 5'-monophosphate are used as taste enhancers, often in conjunction with glutamic acid [Schrader 2007]. Another class of non-volatile flavours are certain polypeptides causing a savoury, umami taste similar to glutamic acid. For example, Y. Wang et al. [2011] report the biotechnological production of the octapeptide "beefy meaty peptide" by recombinant *Pichia pastoris*.

As for volatile compounds, a much higher structural variety can be found, ranging from carboxylic acids, alcohols, aldehydes, ketones and esters to terpenes, lactones, o-heterocycles and S- and N-containing compounds. An overview of the structural classes, based on a classification by Schrader [2007], and of exemplary compounds for each class is given in Table 3.1.

**Terpenes.**   The focus of the present work lies on the monoterpenoid geraniol. Accordingly, special emphasis will be put on the class of terpenes here. The term terpenes refers to an immensely large and diverse group of organic compounds present in plants and some insects. With more than 40,000 molecules, this group is one of the largest among natural products [Rivas et al. 2013]. In spite of the high structural diversity, all terpenes derive from the same precursors, namely isopentenyl diphosphate (IPP) and its isomer dimethylallyl diphosphate (DMAPP), which function as activated isoprene units [Caputi and Aprea 2011]. Two different pathways exist for the synthesis of these building blocks. In the mevalonate pathway, which takes place in the cytosol of eukaryotic cells, acetyl-CoA is used as a carbon source in a reaction cascade to produce IPP and DMAPP [Goldstein and Brown 1990]. In contrast, in the non-mevalonate pathway, also called 2-C-methylerythritol 4-phosphate (MEP) pathway, pyruvate and glyceraldehyde 3-phosphate function as the substrates. This pathway takes place in the plastids of plants

**Table 3.1.:** Overview of the structural classes of volatile flavor and fragrance compounds

| Structural class | Compound | Aliphatic/aromatic | Flavor/scent |
| --- | --- | --- | --- |
| **Carboxylic acids** | Acetic acid | Aliphatic | Sour |
|  | Propanoic acid | Aliphatic | Sour |
| **Alcohols** | Benzyl alcohol | Aromatic | Floral |
|  | 3-Methylbutanol | Aliphatic | Fruity, roasted |
|  | 2-Phenylethanol | Aromatic | Floral |
| **Aldehydes** | Benzaldehyde | Aromatic | Almond |
|  | Isobutyraldehyde | Aliphatic | Malty |
|  | Vanillin | Aromatic | Vanilla |
| **Ketones** | Acetoin | Aliphatic | Creamy, buttery |
|  | 2-Heptanone | Aliphatic | Banana |
|  | Raspberry ketone | Aromatic | Raspberry |
| **Esters** | Butyl butyrate | Aliphatic | Fruity |
|  | Isobutyl acetate | Aliphatic | Fruity |
|  | Geranyl acetate | Aliphatic | Floral |
|  | 2-Phenylethyl acetate | Aromatic | Sweet, honey |
| **Monoterpenes** | *(S)*-Limonene | Aliphatic | Herbal |
| **Monoterpenoids** | Geraniol | Aliphatic | Floral |
|  | Linalool | Aliphatic | Floral |
| **Lactones** | *(R)*-$\gamma$-Decalactone | Aliphatic | Peach |
|  | 6-Pentyl-$\alpha$-pyrone | Aliphatic | Sweet, coconut |
| **O-Heterocycles** | 2,5-Dimethyl-4-hydroxy-2H-furan-3-one | Aliphatic | Pineapple, strawberry |
| **S-containing compounds** | Pineapple mercaptan | Aliphatic | Pineapple |
| **N-containing compounds** | Methylanthranilate | Aromatic | Grape |
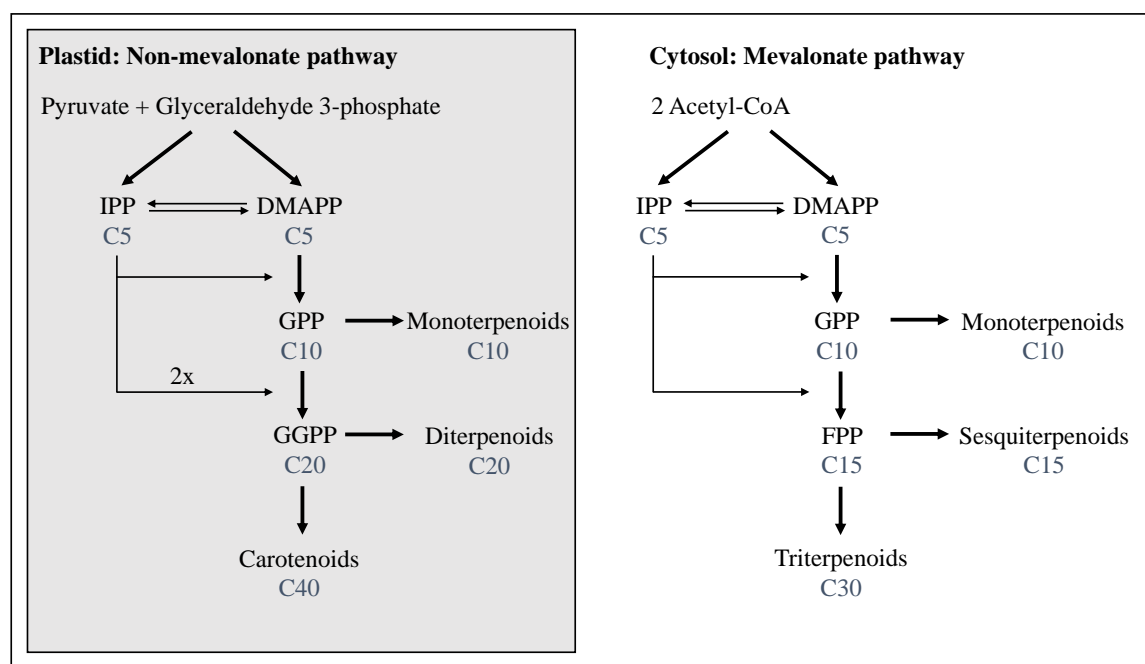
**Figure 3.1.:** Terpene synthesis in plants, adapted from Caputi and Aprea [2011]. Left: Non-mevalonate pathway, taking place in plastids. Right: Mevalonate pathway, taking place in the cytosol. IPP: Isopentenyl diphosphate. DMAPP: Dimethylallyl diphosphate. GPP: Geranyl pyrophosphate. GGPP: Geranylgeranyl pyrophosphate. FPP: Farnesyl pyrophosphate.

[Rohmer 1999]. An overview of the two pathways is given in Figure 3.1. Independently of the prior pathway, IPP and DMAPP are condensed by the action of geranyl pyrophosphate synthase to give geranyl pyrophosphate (GPP) (see Figure 3.2), the precursor for monoterpenes, which have a backbone consisting of 10 carbon atoms. GPP can also be converted to farnesyl pyrophosphate and geranylgeranyl pyrophosphate, which are building blocks for sesquiterpenes (3 isoprene units, thus 15 carbon atoms) and di-/triterpenes (20 and 30 carbon atoms), respectively [Nagegowda 2010]. In general, the biosynthesis of the different terpene classes is catalyzed by terpene synthases. Cyclization reactions at different positions and chemical modifications of the main hydrocarbon backbone provide for the immense chemodiversity of terpenes. Such modifications include hydroxylation, acylation, oxidation and reduction reactions [Caputi and Aprea 2011], yielding modified terpenes called terpenoids. Examples of terpenes and terpenoids are given in Figure 3.3.

In nature, mostly in plants, terpenes perform a variety of different tasks. Most of them are secondary metabolites, and are thus not indispensable to life. However, they confer a competitive edge on their producers: On the one hand, terpenes can function as signaling substances either between individuals of one species, or between different species. As most terpenes are low-weight molecules with high vapor pressures, they can
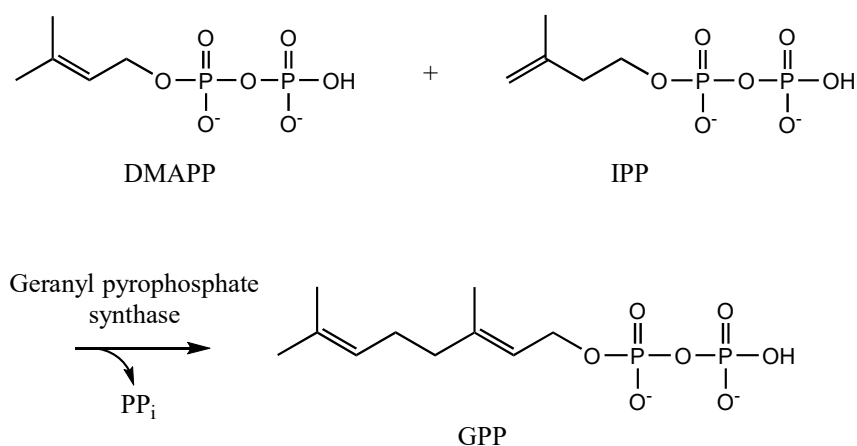
**Figure 3.2.:** Geranyl pyrophosphate (GPP) formation from dimethylallyl diphosphate (DMAPP) and isopentenyl diphosphate (IPP) by the action of geranyl pyrophosphate synthase.
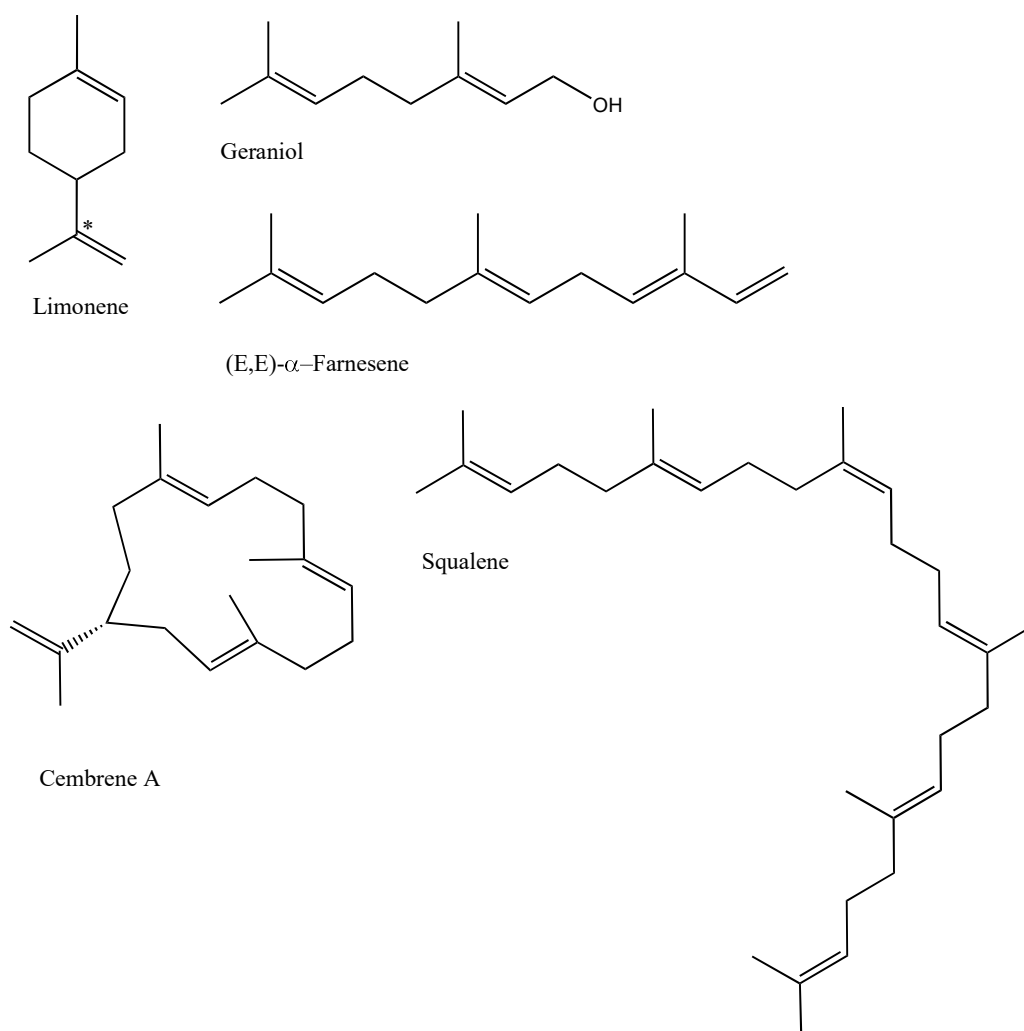


**Figure 3.3.:** Chemical structures of different terpenes and terpenoids. Limonene: Monoterpene. Geraniol: Monoterpenoid. (E,E)-α-Farnesene: Sesquiterpene. Cembrene A: Diterpene. Squalene: Triterpene.

be transported across long distances, and the chemical diversity allows for very specific signals. For example, many terpenes, such as carvone or limonene, attract pollinators with their distinct scent [Gershenzon and Dudareva 2007]. On the other hand, terpenes can protect plants against antagonists, such as predatory herbivores or parasites, by acting as toxins or growth inhibitors [Friedman et al. 2002; S. Lee et al. 2003; Vourc'h et al. 2002]. The precise cellular mechanism of terpene toxicity is not entirely understood, but it is assumed that due to their non-polar, lipophilic character they can interfere with cellular membranes. Their accumulation in membranes can result in increased membrane fluidity and decreased integrity, potentially causing impairment of the electrochemical gradient [Sikkema et al. 1994].

### 3.1.3. Stabilization of alcoholic terpenoids by glycosylation

Terpene toxicity does not only affect the producer's antagonists, but also the producer itself. One way to overcome cytotoxicity is glycosylation: In plants, terpenoids featuring hydroxy groups, such as geraniol, nerol, citronellol or linalool, are not stored in their native form, but mainly as glycoconjugates [Bönisch et al. 2014b; Bowles et al. 2005]. This means that the hydroxy group is bound to a sugar group by a glycosidic bond. Glycoconjugates are less reactive and more hydrophilic and allow for storage in the plant's vacuole [Rivas et al. 2013]. Glycosylation is not only a useful tool for intracellular storage of endogenous plant terpenoids, but also for controlling the compartmentalization and inactivation of xenobiotic terpenoids, which are for example released by insects. Thus, glycosylation is a crucial mechanism for cellular homeostasis in plants [Gachon et al. 2005].

Industrially, the glycosylation of pleasantly scented terpenoids is of strong interest, as the volatility and hydrophobicity of these substances impedes the longevity of the fragrance perception in the products they are used in [Schwab et al. 2015b]. The application of odorless and more hydrophilic glycosides can result in longer shelf life and in the slow release of the fragrance compound once the product is applied, as the sugar moiety can be cleaved successively from the aglycon [Herrmann 2007]. Cleavage of glycosidic bonds can be triggered by variations in temperature, exposure to (day)light, pH changes, or the exposure to hydrolytic enzymes, which are for example produced by the human skin microbiome [Ikemoto et al. 2002] or are present in human saliva.

The industrial synthesis of terpenoid glycosides can be carried out by chemical or enzymatic methods. Chemical synthesis is usually based on the Koenigs-Knorr reaction [Mastelić et al. 2004]. However, this methods suffers from low yields especially when working with badly accessible secondary or tertiary alcohols, from the usage of toxic heavy

metal catalysts and from potential decomposition of the aglycon in the harsh reaction conditions [Kren and Thiem 1997]. Looking at enzymatic means of glycoside production, glycosyltransferases (GTs), glycosidases, transglycosidases and glycoside phosphorylases can be used. The latter two suffer from a small aglycon acceptor spectrum and from low regioselectivity when several hydroxy groups are present in the acceptor molecule [Desmet et al. 2012]. Glycosidases have successfully been used for the production of geranyl, neryl and citronellyl glucoside; however, due to the reaction equilibrium being in favor of hydrolysis and not glycosylation, these processes suffer from low yields [Bachhawat et al. 2004; de Roode et al. 2001; Schwab et al. 2015b]. In contrast to these options, GTs can efficiently glycosylate a variety of acceptor molecules with high regio- and enantioselectivity.

**Glycosyltransferases.** GTs are an ubiquitous family of transferases whose members transfer sugar moieties from activated donor molecules to acceptor molecules such as proteins, lipids, nucleic acids or small molecules, such as alcoholic terpenoids [Schwab et al. 2015a]. Most commonly, the activated donor molecules are nucleotides, for example UDP. Most frequently, the nucleophilic oxygen of a hydroxy group functions as the acceptor, however, nitrogen, sulfur and carbon nucleophiles can be glycosylated as well [Lairson et al. 2008]. More than 2700 GT sequences have been identified so far, and based on sequence similarities they were assigned to 65 different families [Coutinho et al. 2003]. In spite of their immense substrate variety, GTs can be classified into only two structural superfamilies, the GT-A fold and GT-B fold [Hu and Walker 2002]. Both types of enzymes consist of two $\beta/\alpha/\beta$ Rossman-like domains [Rossmann et al. 1974], however less tightly associated for the B fold than for the A fold [Lairson et al. 2008]. Moreover, GTs can be classified according to their reaction mechanism, as the anomeric configuration of the sugar moiety can either be retained or inverted (see Figure 3.4). For inverting GTs, a $S_N2$-like mechanism is assumed, whereas for retaining GTs the mechanism is still not established [Coutinho et al. 2003].

In plants, GTs are located in the cytosol and show activity towards a variety of substrates such as steroids, flavonoids and terpenoids [Bowles et al. 2005]. However, in spite of their extremely broad substrate spectrum, they all belong to the so called plant-specific secondary metabolism glycosyltransferase family and contain a 44-amino acid consensus sequence called plant secondary product glycosyltransferase (PSPG) box [Gachon et al. 2005; J. Hughes and M. A. Hughes 1994]. Within the PSPG box, the highly conserved amino acid motif HCGWNS is suspected to interact with the uracil moiety of sugar donor molecules such as UDP-glucose [Hans et al. 2004]. The characterization of novel GTs and the identification of their natural *in vivo* substrates can be facilitated by generating
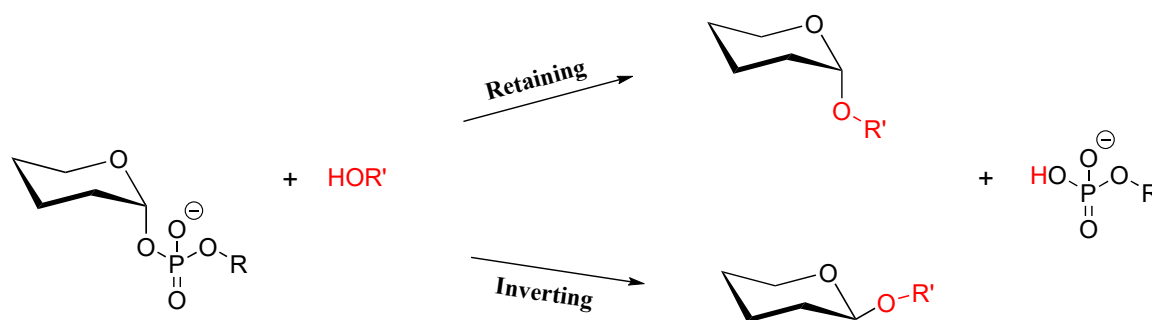
**Figure 3.4.:** Reaction mechanism of glycosyltransferases, adapted from Coutinho et al. [2003]. Typically, the activating group of the sugar donor is a (substituted) phosphate, such as uridine diphosphate. The alcoholic acceptor is depicted as HOR' in red. The anomeric configuration of the donor's sugar moiety can either be retained or inverted.

so called aglycone libraries: In a first step, glycosides are isolated from plant tissue that shows high expression levels of the target GT. Subsequently, the glycosidic extract is subjected to enzymatic hydrolysis and the resulting aglycones are used as substrates for the target GTs in activity assays [Bönisch et al. 2014a].

**Glycosylation of geraniol.**    One example for a monoterpenoid whose industrial application can benefit from enzymatic glycosylation is geraniol. Geraniol is a rose-scented acyclic monoterpenoid (see Figure 3.3), which is present in many essential plant oils, like rose oil [H. Baydar and N. G. Baydar 2005] or palmarosa oil [Dubey and Luthra 2001]. It is an oily liquid with a low water solubility of 0.686 g L$^{-1}$ at 20 °C[3]. In plants, geraniol functions as an insecticide [Barnard and R.-D. Xue 2004], fungicide [Sharma et al. 2016] and shows antimicrobial activities [Friedman et al. 2002]. For example, Huang et al. [2016] report a minimal inhibitory concentration of 0.3 g L$^{-1}$ towards *E. coli* BL21(DE3)pLysS. Moreover, anticancerous properties have been reported, for example by J.-Y. Lee et al. [2016]. Due to its pleasant smell, geraniol has wide applications in the fragrance industry and can be found in a variety of cosmetic and household products [Rastogi et al. 2001]. In these products, the usage of geranyl glycosides instead of the aglycone facilitates a more persistent scent.

By creating aglycone libraries, different GTs from *Vitis vinifera* with activity towards geraniol could be identified. Among these, the inverting VvGT14a has the lowest $K_m$ (9 ± 1.2 µM) and thus highest affinity for the monoterpenoid. This 52.6 kDa enzyme uses UDP-glucose as the sugar donor, yielding geranyl glucoside (see Figure 3.5). It shows the highest activity at pH 8.5 and 30 °C. Other accepted substrates are citronellol,

---
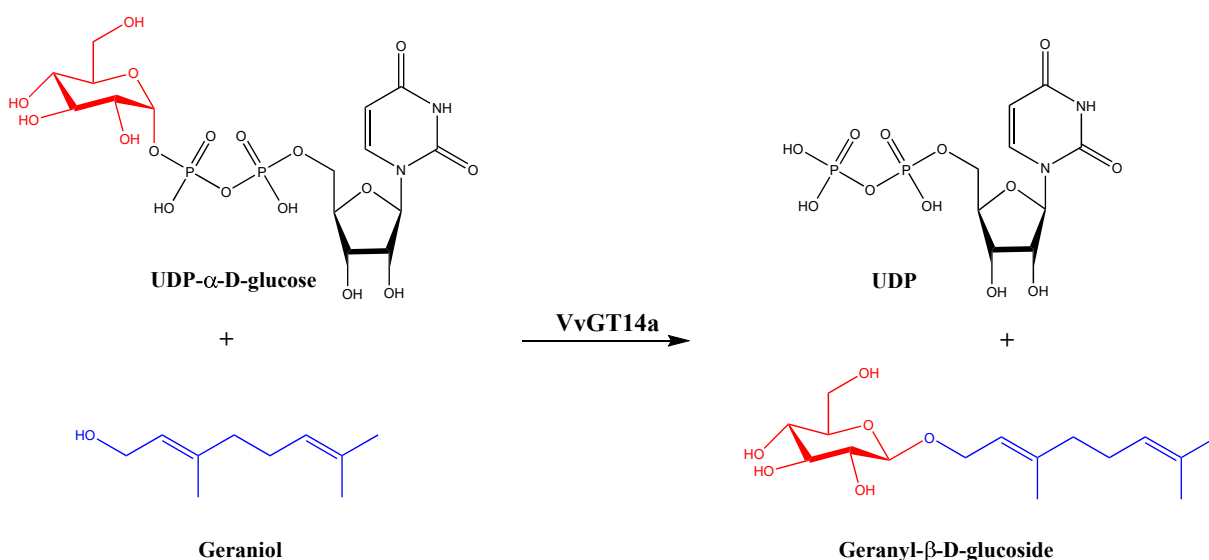
**Figure 3.5.:** UDP-glucose dependent glucosylation of geraniol by glycosyltransferase VvGT14a from *Vitis vinifera*, with the anomeric configuation of glucose being inverted.

nerol, terpineol, linalool and 8-hydroxylinalool, with decreasing affinities [Bönisch et al. 2014a]. Caputi et al. [2008] could identify 15 GTs from *Arabidopsis thaliana* with activity towards geraniol, and Huang et al. [2015] isolated a GT from *Catharanthus roseus* with the capacity to glycosylate the monoterpenoid.

## 3.2. Biphasic reaction systems

The activity of enzymes or microorganisms usually relies on the presence of water. However, certain reactions require the application of biphasic reaction systems, which are characterized by the presence of two different phases. The chemical reaction occurs either in one of the phases or at the phase interface [Déziel et al. 1999]. Both liquid, solid and gaseous phases can be applied, with at least one phase being usually liquid [Castiglione and Weuster-Botz 2018].

### 3.2.1. Biphasic systems for *in situ* substrate supply and product removal

In biotechnology, biphasic reaction systems are used for either *in situ* supply of a substrate, or *in situ* product removal (ISPR). One of the phases has to be aqueous, providing a suitable environment for the applied microorganism or enzyme. In certain cases, minimal amounts of water can be used in a so called micro-aqueous environment [Jakoblinnert and

Rother 2014], however, water fractions are usually higher than the non-aqueous phase fraction.

Substrate supply by a second phase becomes relevant when the substrate is either cyto-toxic at low concentrations or poorly water soluble. Ideally, the second phase absorbs the substrate at much higher levels than the water phase does [Fam and Daugulis 2012]. In certain cases, the second phase does not only act as the sequestering phase, but also as a carbon source for the microorganism, as shown by Braun et al. [2012]: In this work, ethyl oleate serves as a reservoir for the biotransformation substrate progesterone, and as a carbon source for the production host *Yarrowia lipolytica*. Continuous transfer of the target compound from the non-aqueous to the aqueous phase is driven by the ongoing substrate consumption by the microorganism, and by the maintenance of thermodynamic equilibrium between the two phases [Prpich and Daugulis 2004]. Especially in environ-mental biotechnology, where xenobiotics or pollutants are to be degraded microbially, the concept of *in situ* substrate supply is highly relevant [Quijano et al. 2009].

By ISPR, the product(s) of a certain cellular reaction can be removed from the mi-crobial environment directly after formation [Stark and von Stockar 2003]. This method can increase the productivity of biotechnological processes, as cellular inhibition by high product concentrations can be avoided and as product formation can be favored thermo-dynamically. Moreover, undesired product loss by cellular degradation or uncontrolled release (e.g. evaporation) can be circumvented, and the number of downstream steps might be reduced [Freeman et al. 1993]. Besides product extraction by biphasic reaction systems, 4 other main techniques exist for ISPR: Evaporation (e.g. distillation), per-meation (e.g. dialysis), immobilization (e.g. affinity adsorption), and precipitation [Stark and von Stockar 2003].

### 3.2.2. Types of non-aqueous phases

Non-aqueous phases used for *in situ* substrate supply or ISPR can be divided into two main groups - adsorbents and absorbents. Whereas adsorption is a surface-dependent process, absorption is based on the uptake of a target compound by the mass of the absorbent, and not the surface [Mortimer and U. Müller 2007].

**Liquid absorbents.** A variety of different liquid absorbents exists, each with different properties:

- **Water soluble polymers and/or salts:** The usage of water soluble polymers (e.g. polyethylene glycol (PEG)) and/or salts results in the formation of an aqueous

two-phase system (ATPS). Traditionally, such systems are used for the recovery of proteins and antibiotics [Dafoe and Daugulis 2014]. However, they can also be used for the sequestering of small molecules. For example, Rito-Palomares et al. [2001] report the application of an ATPS with PEG 8000 and sodium sulfate for the separation of the lactone 6-pentyl-$\alpha$-pyrone. Nevertheless, ATPSs do not seem to be the ideal choice for the partitioning of small hydrophobic molecules due to low partition coefficients [Dafoe and Daugulis 2014].

- **Organic solvents:** Hydrophobic and potentially cytotoxic compounds can be sequestered by organic solvents - an approach that has been applied extensively in biotechnology since the 1980s [Bang et al. 1983; Braun et al. 2012; Brennan et al. 2012; Hocknull and Lilly 1990]. Water-immiscible solvents cover a broad range of chemical classes like alkanes (e.g. hexadecane), alkenes (e.g. octene), alcohols (e.g. oleyl alcohol), fatty acid esters (e.g. ethyl decanoate) or phthalates (dibutyl phthalate). The organic solvent cannot only serve as the sequestering phase, but can be the reaction's substrate itself [de Smet et al. 1981]. In spite of allowing the extraction of a variety of hydrophobic substances and being an easily available choice, biphasic systems with solvents suffer from explosion hazards, rather high costs and environmental issues related with solvent disposal [Daugulis et al. 2011; Salter and Kelt 1995]. These issues become even more relevant when working at large scales [A. Schmid et al. 1998].

- **Ionic liquids (ILs):** ILs are salts that are liquid below a certain threshold temperature (often 100 °C) and consist of a pair of counter ions [Welton 1999]. By varying the anions and cations, a tremendous variety of compositions and thus characteristics can be obtained, making ILs "designer solvents" [Freemantle 1998]. However, so far no logical correlation between composition and properties (e.g. biocompatibility) could be found, making the rational selection of a suitable ILs for a certain biotechnological application difficult [Roosen et al. 2008]. Nevertheless, ILs have successfully been used in different biphasic biotechnological processes [Bräutigam et al. 2007; Dennewald et al. 2012; Pfründer et al. 2004]. Their nonvolatile and non-flammable nature makes them a promising alternative to organic solvents [Pfründer et al. 2006], with high purchasing prices and the lack of a general waste management concept being relevant challenges though. The recycling of the IL, as described by Dennewald et al. [2011], might be a promising strategy to tackle these problems.

- **Deep eutectic solvents (DES):** DESs consist of halide salts and hydrogen-bond

donors. By mixing these components, their respective crystalline structures are disrupted, resulting in liquids at room temperature. Physicochemically, DESs behave similarly to ILs, but are significantly cheaper and moreover biodegradable [Guajardo et al. 2016]. As for ILs, a structure-function relationship does not exist so far. However, they have already successfully been used in biotechnological processes. For example, whole-cell stereoselective reductions of ketones in a biphasic system containing a choline chloride-glycerol DES were performed by C. R. Müller et al. [2015].

- **Liquid, water-immiscible polymers:** The advantages of liquid polymers over organic solvents are their biocompatibility towards most microorganisms, their inertness towards biodegradation (making them non-bioavailable) and their non-volatility [Dafoe and Daugulis 2014]. A prominent example is silicone oil (polydimethylsiloxane), which has been widely used for the sequestering of hydrophobic target compounds [Morrish and Daugulis 2008; Patel et al. 2017; Zúñiga et al. 2011]. However, certain problems are associated with the application of silicone oil: it features a high viscosity, tends to cause foaming and to adhere to microorganisms, and is expensive in comparison to, for example, organic solvents [Daugulis et al. 2011]. A liquid polymer with potential as a non-aqueous phase in biphasic reaction systems is polytetrahydrofuran, a solid with melting points between 20–30 °C, depending on the polymer length.

**Solid absorbents.**

- **Polymers:** Absorptive polymers, such as Desmopan by Bayer or Hytrel by DuPont, have gained increasing interest as sequestering phases in the last years [Prpich and Daugulis 2004; Rehmann et al. 2007]. As partitioning of target compounds works by the adjustment of thermodynamic equilibrium dependent on the polymers' mass, they can be used as alternatives to organic solvents, however with the advantages of being cheap, easily reusable, non-flammable, non-volatile and biocompatible [Dafoe and Daugulis 2014; Daugulis et al. 2011]. Polymers that have proved to be the most effective ones for sequestering substrates or products of biological reactions are block copolymers, consisting of soft, amorphous segments, and semicrystalline segments. Only soft segments can absorb the target compound, and by increasing the proportion of the soft segments or by engineering the composition of the polymer, solute affinity can be increased [Dafoe et al. 2014].

- **Polyionic liquids:** ILs can be polymerized, yielding solid polyionic liquids that are water-immiscible. Bacon et al. [2017] reports that such polyionic liquids can absorb hydrophilic compounds such as n-butanol efficiently, accompanied with good biocompatibilty, which is in contrast to the IL monomers used for synthesis.

**Adsorbents.** The interaction of a target compound with an adsorbent is based on the adhesion of the molecule to the adsorbent's surface. In order to increase the surface and thus the binding capacity, many commercial adsorbents are highly porous [Dafoe and Daugulis 2014]. These include (XAD) resins, activated charcoal, and zeolites. For each of these compounds, biotechnological applications in biphasic systems are reported [Castiglione et al. 2017; M.-T. Gao et al. 2011; Kühne and Sprecher 1989; Quijano et al. 2009]. Usually, the interactions are of hydrophobic nature, but resins can be functionalized as ion-exchange resins for the partitioning of acids [Y.-P. Xue et al. 2010]. Moreover, besides from inter-molecular interactions, the uptake of target compounds can be based on size exclusion, giving an additional tool for regulating the selectivity. For zeolites, this concept is well described by Ranjan et al. [2009]. The simplicity of implementation has made adsorbents a popular choice for biphasic reaction systems. However, challenges like biofilm formation, poor overall selectivity, and difficult recovery of strongly adsorbed molecules cannot be neglected [Dafoe and Daugulis 2014].

## 3.2.3. Characterization of biphasic systems

In order to gain full understanding of a biphasic system, it has to be characterized regarding the partitioning of the target compound between the two phases. Moreover, the biocompatibility of the non-aqueous phase has to be assessed, and the mass transfer of the target compound between the two phases has to be considered.

**Partitioning of target compounds.** One important criterion for the characterization and assessment of a biphasic system is the partitioning behavior of the target compound. For liquid-liquid systems, partition coefficients (PCs) serve this purpose. When the equilibrium concentration of the target compound in the non-aqueous phase is known, the PC can be calculated directly:

$$PC = \frac{c_S^{org}}{c_S^{aq}} \tag{3.1}$$

$c_S^{org}$    Equilibrium concentration of the target compound (substrate S) in the organic (non-aqueous) phase, g L$^{-1}$

$c_S^{aq}$    Equilibrium concentration of the target compound (substrate S) in the aqueous phase, g L$^{-1}$

When the equilibrium concentration in the non-aqueous phase cannot be measured, following equation can be used:

$$PC = \frac{c_{S,0}^{org} - (\varphi^{-1} - 1) \cdot c_S^{aq}}{c_S^{aq}} \tag{3.2}$$

$c_{S,0}^{org}$    Initial concentration of the target compound (substrate S) in the organic (non-aqueous) phase, g L$^{-1}$

$\varphi$    Fraction of the non-aqueous phase, -

The partitioning of a target compound between an aqueous phase and an absorbing solid polymer can also be characterized by PCs:

$$PC = \frac{\dfrac{m_S^{Pol}}{m_S^{Pol} + m_{Pol,0}^{Pol}}}{\dfrac{m_S^{aq}}{m_S^{aq} + m_{aq,0}^{aq}}} \tag{3.3}$$

$m_S^{Pol}$    Mass of the absorbed target compound, g

$m_{Pol,0}^{Pol}$    Initial mass of the polymer saturated with water, g

$m_S^{aq}$    Mass of the target compound in the aqueous phase after establishment of equilibrium, g

$m_{aq,0}^{aq}$    Mass of the aqueous phase, g

The PC in systems involving absorbing polymers remains constant when changing the polymer mass or the overall target compound concentration [Dafoe and Daugulis 2014]. In contrast, the partitioning behavior of adsorbents has to be described with adsorption isotherms, which can consider the saturation of the adsorbents' surface above a certain target compound concentration. Adsorption isotherms illustrate the mass of the adsorbate (target compound bound to the adsorbent) as a function of the target compound's equilibrium concentration in the liquid phase. Different isotherm models exist, the most commonly used ones being the Henry, Freundlich, Langmuir and BET (Brunauer–Emmett–Teller) isotherms [Bathen and Breitbach 2001]. The isotherms are compared graphically in Figure 3.6.
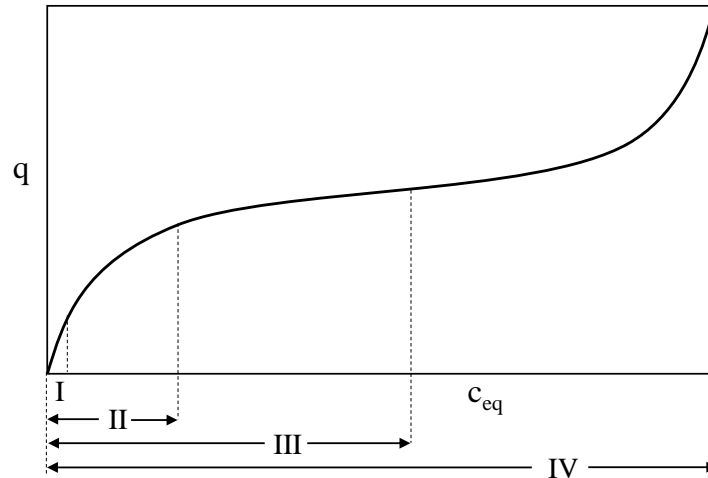
**Figure 3.6.:** Types of adsorption isotherms. I: Henry. II: Freundlich. III: Langmuir. IV: BET. q: Mass of the adsorbate normalized by the mass of the adsorbent. $c_{eq}$: Equilibrium concentration of the target compound in the liquid phase.

At low target compound concentrations, a linear correlation between adsorbate mass and equilibrium concentration in the liquid phase can sometimes still be observed, which can be described with the Henry isotherm (see Equation 3.4, [Henry 1803]). For the Freundlich isotherm (see Equation 3.5), the equation is extended with an empirical exponent, which takes into account the saturation of the adsorbent's surface [Freundlich 1926]. However, as soon as full occupancy of the adsorbent's binding sites is to be described, the Freundlich isotherm does not suffice, and the Langmuir equation (see Equation 3.6) has to be employed [Langmuir 1918]. Whereas the Langmuir isotherm only describes monolayer adsorption, the BET isotherm (see Equation 3.7) considers multilayer adsorption [Bathen and Breitbach 2001].

$$q = K_H \cdot c_{eq} \tag{3.4}$$

$q$      Mass of the adsorbed target compound (adsorbate) normalized by the mass of the adsorbent, g g$^{-1}$

$K_H$    Henry coefficient, L g$^{-1}$

$c_{eq}$    Equilibrium concentration of the target compound in the liquid phase, g L$^{-1}$

$$q = K_F \cdot c_{eq}^{\frac{1}{n}} \tag{3.5}$$

$K_F$    Freundlich coefficient, L g$^{-1}$

$n$      Freundlich exponent

$$q = \frac{c_{eq}}{\frac{1}{K_L} + c_{eq}} \tag{3.6}$$

$K_L$    Langmuir coefficient, L g$^{-1}$

$$q = \frac{K \cdot q_{max} \cdot c_{eq}}{(c_{sat} - c_{eq}) \cdot (1 + \frac{(K-1) \cdot c_{eq}}{c_{sat}})} \tag{3.7}$$

$K$      Sorption coefficient, L g$^{-1}$

$q_{max}$  Maximal mass of the adsorbate in one layer at the adsorbent's surface, normalized by the mass of the adsorbent, g g$^{-1}$

$c_{sat}$  Solubility of the target compound in the liquid phase, g L$^{-1}$

The following paragraphs only refer to systems involving absorbents.

**Biocompatiblity.**  The biocompatibility of liquid absorbents can be assessed by using logP values. The logP is the logarithmic PC of a target compound in a biphasic system consisting of octanol and water and is a measure for the hydrophobicity of a molecule [Laane et al. 1985]. The lower the logP for a molecule, the higher is its hydrophilicity and thus the tendency to accumulate in the aqueous phase, where the biocatalyst is located, and to interfere with the cells' physiological processes [Bruce and Daugulis 1991]. The critical logP, which prevents further metabolic activity, is strongly dependent on the microorganism being used. *E. coli* has a critical logP of approximately 3.4 [Inoue and Horikoshi 1991], whereas *S. cerevisiae* features a critical logP of around 4 [Kollerup and Daugulis 1986]. As an example, Brennan et al. [2012] used a logP larger than 5 as a criterion for a solvent's biocompatibility with *S. cerevisiae* and could thereby successfully pre-select 10 solvents for further studies.

**Mass transfer.**  Efficient mass transfer is crucial for the proper functioning of a biphasic reaction system. Substrates, which are supplied *in situ*, have to be transported across the phase interface from either an organic phase or an absorptive polymer to the cells, and products have to be transferred the other direction. The transfer rate has to keep up with the metabolic activity of the biocatalyst, as otherwise mass transfer limitations or inhibition of the cells occurs. Different studies in stirred bioreactors showed that the mass transfer of apolar substances in liquid-liquid systems is not limiting, even when using viscid silicone oil [Fam and Daugulis 2012; Hernández et al. 2010] or when applying lower power inputs characteristic for industrial-scale reactors [A. Schmid et al. 1998]. In contrast, mass transfer limitations were observed for solid polymers. These can be attributed to a smaller available interface area compared to organic solvents with droplet

sizes in the µm range [Rehmann et al. 2007], and to slow internal diffusion within the polymer [Fam and Daugulis 2012]. These issues can be potentially tackled by smaller polymer beads and polymer material with higher diffusivities [Daugulis et al. 2011].

Interesting findings were made for the oxygen supply in liquid-liquid systems: As organic solvents, mostly hydrocarbons, exhibit 15-20 times higher oxygen solubilities than water, they can significantly increase the oxygen transfer rate from air to the biocatalyst during a bioprocess and are therefore referred to as "oxygen-vectors" [Galaction et al. 2004; Galaction et al. 2005].

### 3.2.4. Rational selection of biphasic systems

When designing a biphasic bioprocess, the selection of the second, non-aqueous phase is a crucial step. In literature, many examples can be found for the usage of a certain phase without providing any rationale [Creuly et al. 1992; Goh et al. 2012; Harrop et al. 1992; Liu et al. 2016], risking the application of a sequestering phase with inadequate characteristics. Another reported approach is based on criteria related to safety, health and environment, with the goal to identify "green" solvents [Prat et al. 2016]. More advanced studies include the assessment of physical parameters like viscosity or water solubility, the determination of PCs and biocompatibility, and the evaluation of potential hurdles in downstream processing [Bräutigam et al. 2007; Brennan et al. 2012]. What all these studies have in common is that they use experimental and/or database results, running the risk of overlooking suitable candidates during the preselection process. A more comprehensive approach consists in the application of thermodynamic first-principles methods that *predict* the affinity between a target compound and a sequestering phase. Not only the affinity can be predicted, but also the biocompatibility by the usage of logP values [Bruce and Daugulis 1991]. A comparison between the predictive and the experimental approach is given in Table 3.2.

**Table 3.2.:** Predictive and experimental approaches for selecting non-aqueous phases. UNIFAC: Universal Quasichemical Functional Group Activity Coefficients. PC: partition coefficient. logP: logarithmic PC in an octanol-water system.

|                  | Predictive                                                        | Experimental |
|------------------|-------------------------------------------------------------------|--------------|
| Affinity         | Thermodynamic first-principles methods (e.g. Hildebrand, Hansen, UNIFAC) | PCs          |
| Biocompatibility | logP                                                              | Assays       |

**Thermodynamic first-principles methods.** High thermodynamic affinity between two compounds implies their miscibility at molecular level. The objective of thermodynamic first-principles methods is to relate the molecular structures of solute and sequestering phase with their affinity to each other [Lei et al. 2008]. Either solubility parameters or activity coefficients can be used for affinity predictions.

In 1962, the *Hildebrand Solubility Parameter* was introduced by Hildebrand and R. L. Scott [1962] with the following equation:

$$\delta = \sqrt{\frac{\Delta H_V}{V}} \tag{3.8}$$

$\delta$      Solubility parameter, MPa$^{0.5}$
$\Delta H_V$   Heat of vaporization, J mol$^{-1}$
$V$      Molar volume of the given molecule, m$^3$ mol$^{-1}$

By describing the cohesive energy density, Hildebrand Solubility Parameters provide a quantitative estimate of the potential interaction between molecules; similar values indicate good miscibility/high affinity. This method is especially suited for apolar molecules, and was for example used by Poleo and Daugulis [2014] for the rational selection of an absorbing polymer for the target compound phenol.

A modification of Hildebrand Solubility Parameters are *Hansen Solubility Parameters* (HSPs), which can be extended to more polar molecules. The underlying equation describes that a liquid's total cohesive energy E, which is identical to the heat of vaporization (see Equation 3.8), is the sum of the dispersion cohesive energy $E_D$, the polar cohesive energy $E_P$, and the hydrogen bonding energy $E_H$:

$$E = E_D + E_P + E_H \tag{3.9}$$

Dividing this by the molar volume gives the square of the overall solubility parameter $\delta$ as the sum of the squares of the D, P, and H components:

$$\delta^2 = \delta_D^2 + \delta_P^2 + \delta_H^2 \tag{3.10}$$

The solubility "distance" $Ra$ between two compounds can be calculated with the equation

$$Ra^2 = 4(\delta_{D2} - \delta_{D1})^2 + (\delta_{P2} - \delta_{P1})^2 + (\delta_{H2} - \delta_{H1})^2 \tag{3.11}$$

The smaller the distance is, the higher is the affinity between two compounds [Hansen 2007]. Jiang et al. [2014] used this method to select a sequestering solvent for dopamine,

and Poleo and Daugulis [2014] could show that predictions based on the Hansen approach match experimental PCs better than Hildebrand predictions.

A different type of thermodynamic methods is based on the prediction of activity coefficients. Activity coefficients account for a mixture's deviation from ideality, and adjust a compound's concentration in a mixture accordingly [Poleo and Daugulis 2014]. Such methods can be divided into two categories: approaches with relations to experimental data, and *ab initio* methods with no relation to experimental data. Group contribution methods, where each compound is broken down into functional groups and the overall activity coefficient is calculated based on existing parameters for the functional groups, belong to the former class [Lei et al. 2008]. Activity coefficients in non-electrolyte mixtures can be determined by the UNIFAC model (Universal Quasichemical Functional Group Activity Coefficients) [Fredenslund et al. 1975]. Based on UNIFAC, Bruce and Daugulis [1991] developed a computer program called ESP (Extractant Screening Program) that can predict PCs for ternary systems, taking into account the effect of the presence of water. This is in contrast to Hildebrand and Hansen parameters, which can only describe binary systems. An example for an *ab inito* approach is COSMO-RS (Conductor like Screening Model for Real Solvents), which is based on unimolecular calculations [Lei et al. 2008]. Janoschek et al. [2018] successfully used this method to predict suitable solvents for the sequestering of the monoterpenes ($S$)-(+)-carvone and terpinen-4-ol. COSMO-RS is a promising tool to rationally select ILs as sequestering phases, whereas methods such as UNIFAC are not very applicable, as only very few experimental data exists [Lei et al. 2008]. COSMO-RS could even be used to identify the most eligible IL structure for a given sequestering task, and hereby do justice to calling ILs "designer solvents" (see Chapter 3.2.2, [Freemantle 1998]).

## 3.3. Microbial cultivation

The biotechnological manufacturing of industrial products is based on the successful cultivation of microorganisms. The term *microorganism* is a combination of the greek terms *mikros*, "small", and *organismós*, "organism", implying the unifying characteristic of small size in the micrometer range. Most of the microorganisms are unicellular, and both prokaroytes and eukaryotes can be found among them. Their vast diversity and species count is underlined by the fact that two of the three domains of life, namely Archaea and Bacteria, are purely made up of microorganisms [Woese and Fox 1977]. Examples for microorganisms are cyanobacteria, microalgae and yeasts.

### 3.3.1. Microbial growth

Microbial growth is defined as an increase in biomass. For unicellular organisms, this usually comes along with an increase in cell number through cell division. Growth can only occur when the cells are located in an environment that provides a suitable temperature, pH, pressure and nutrients [Chmiel et al. 2018].

**Requirements for growth.** The following content is based on information by Chmiel et al. [2018] and Schlegel [1992]. Microorganisms can grow only when all elements involved in the assembly of cell substance are available as metabolizable compounds. The required elements can be divided into macro- and microelements. The macroelements carbon, oxygen, hydrogen, nitrogen, sulfur, phosphorus, potassium, sodium, calcium, magnesium and iron are present at concentrations higher than 50 mg kg$^{-1}$ biomass, whereas the demand for microelements such as zinc, manganese or copper is much lower and varies between different microorganisms. Usually, most of the elements are provided as electrolytes. Moreover, amino acids, purines, pyridines and vitamins are required as growth supplements.

Carbon and energy sources vary between different microorganisms. An overview of the different nutritional groups is given in Table 3.3. Moreover, microorganisms can be classified based on the reducing equivalents they use: organotrophs use organic compounds, whereas lithotrophs use inorganic compounds. It is common practice to refer to the carbon source as the substrate; however, each compound limiting cell growth can be titled a limiting substrate.

**Table 3.3.:** Nutritional groups of microorganisms

| Nutritional group | Source of energy | Source of carbon | Example |
|---|---|---|---|
| **Photoautotroph** | Light | $CO_2$ | Green sulfurbacteria |
| **Chemoautotroph** | Inorganic oxidation | $CO_2$ | Methanogens |
| **Autoheterotroph** | Light | Organic compounds | Heliobacteria |
| **Chemoheterotroph** | Inorganic oxidation | Organic compounds | *Escherichia coli* |

Cultivation media for microorganisms can be divided into two groups. On the one hand, complex media with unknown exact elementary composition can be used, mostly

for demanding microorganisms with unknow nutrient requirements. Such complex media usually consist of extracts from yeast or plant-based/animal sources, and of peptones and glucose. On the other hand, the objective in microbiology is the identification of the minimal nutrient requirements for each organism and the development of a respective minimal/defined cultivation medium [Overmann et al. 2017].

Regarding their relationship to the presence of oxygen, microorganisms can be divided into two groups. Obligate aerobes require the presence of elemental oxygen ($O_2$), whereas anaerobes do not require oxygen for growth. Anaerobes either depend on an oxygen-free environment, as oxygen acts as a cytotoxin on them (obligate anaerobes), or they are facultative anaerobes. Facultative anaerobes can either be aerotolerant, which means that they grow in the presence of oxygen, but not use it. Or they can utilize oxygen, but also have metabolic pathways suitable for anaerobic energy production.

The pH optimum for most microorganisms lies in a neutral range around pH 7. Nevertheless, different examples for divergent optima exist: Alkaliphiles such as certain *Bacillus* species prefer a higher pH, whereas acidophiles such as *Thiobacillus* grow at a pH even smaller than pH 4.

Most of the soil and water bacteria are mesophilic, that is growing optimally at temperatures between 20–42 °C. Organisms with higher temperature tolerance or optima are called thermotolerant and (hyper)thermophilic, respectively. Organisms growing best at temperatures lower than 20 °C are referred to as psychrophilic.

**Characteristic bacterial growth phases.** During batch cultivations, where neither nutrients are added nor metabolites purged during the process, bacteria show a characteristic growth behavior, which can be divided into different phases [Monod 1949] (see Figure 3.7). After inoculation, the cells enter the lag phase with absent cell growth, caused by adaptions to the new environment. As soon as transport systems and enzymes required for the metabolization of the present substrate are available, cell growth accelerates. During the exponential phase, cells grow with the maximal growth rate. From a certain point in time, the high cell density, inhibitory metabolites or limiting substrate concentrations result in the deceleration of growth, followed by the stationary phase, where cell growth is fully compensated with cell death. Subsequently, a death phase can follow, where the death rate is higher than the growth rate.

When cell growth occurs through cell division, the biomass concentration $c_X$ can be calculated from the number of generations n [Chmiel et al. 2018]:

$$c_X = c_{X,0} \cdot 2^n \tag{3.12}$$
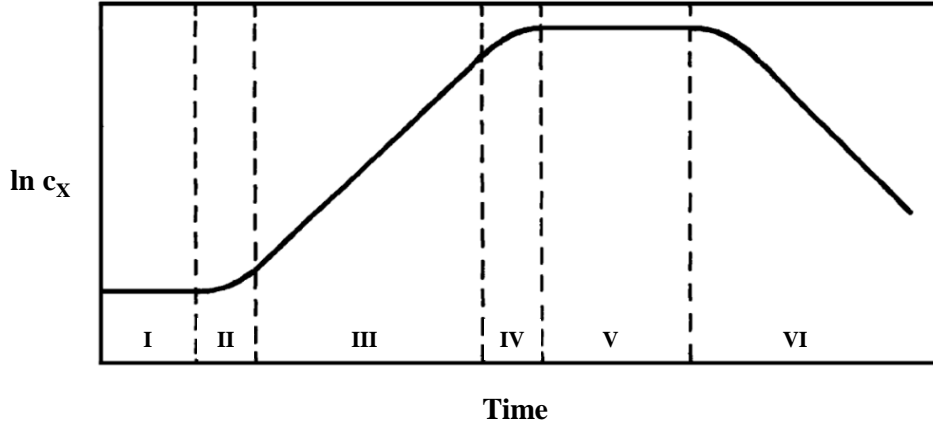
**Figure 3.7.:** Characteristic bacterial growth phases during batch cultivation, adapted from Weber [2010].
The logarithmic biomass concentration is plotted against the process time. I: lag phase, II:
acceleration phase, III: exponential phase, IV: deceleration phase, V: stationary phase, VI:
death phase.

The specific growth rate $\mu$ is defined by

$$\mu \equiv \frac{1}{c_X} \cdot \frac{dc_X}{dt} \tag{3.13}$$

Only during the exponential growth phase cells grow with the maximal growth rate $\mu_{max}$
[Chmiel et al. 2018].

**Growth kinetics.** For the description of growth and of substrate consumption and
product formation rates, non-structured and non-segregated simplifying models can be
used. Such models assume the cells to be uniform units with identical characteristics
suspended in the reaction volume [Chmiel et al. 2018]. By means of the Monod equation
[Monod 1949], the exponential growth phase can be described, as well as the decelera-
tion phase, if it is caused by the depletion of the limiting substrate (substrate limitation
phase). The dependence of the growth rate from the limiting substrate concentration $c_S$
can then be described by the following saturation kinetics:

$$\mu = \mu_{max} \cdot \frac{c_S}{K_S + c_S} \tag{3.14}$$

with $K_S$ being the saturation concentration at which the half-maximal growth rate is
reached.

Prior to cell growth on a certain substrate, the substrate needs to be taken up by the
organism. The specific rate of substrate uptake $q_S$ is defined as

$$q_S = \frac{1}{c_X} \cdot \frac{dc_S}{dt} \tag{3.15}$$

and the specific product formation rate $q_P$ accordingly as

$$q_P = \frac{1}{c_X} \cdot \frac{dc_P}{dt} \tag{3.16}$$

with $c_P$ being the product concentration. The *volumetric* product formation rate $r_P$ is defined as

$$r_P = \frac{dc_P}{dt} = c_X \cdot q_P \tag{3.17}$$

With these rates, yield coefficients for biomass and product formation ($Y_{XS,\mu}$ and $Y_{PS}$) can be defined:

$$Y_{XS} = \frac{\mu}{q_S} = \frac{dc_X}{dc_S} \tag{3.18}$$

$$Y_{PS} = \frac{dc_P}{dc_S} \tag{3.19}$$

With the yield coefficient $Y_{PX}$ (also referred to as specific productivity), product formation can be related to the biomass concentration:

$$Y_{PX} = \frac{dc_P}{dc_X} \tag{3.20}$$

## 3.3.2. Bioreaction engineering

**Bioreactors.** The cultivation of microorganisms can take place in bioreactors which provide a protected environment for their growth. Bioreactors are operated in scales between microfluidic pL [Grünberger et al. 2012] to several 10,000 m$^3$ for biological waste water treatment, and perform five main tasks: They have to homogenize the cultivation broth, and suspend the solid microorganism, sometimes also solid substrates and carrier materials for enzymes, in the broth. Moreover, they disperse gas or non-aqueous phases in the aqueous medium, and guarantee sufficient heat and mass transfer across the reactor boundaries. Last but not least, they function as a sterile barrier [Chmiel et al. 2018].

Based on the method of energy input, different types of bioreactors can be distinguished: Either energy input is achieved by mechanically moving structural elements (stirred-tank reactor), by expansion of a gasphase (bubble column reactor) or by a pump circuit (e.g. packed bed reactor) [Chmiel et al. 2018]. In the biotechnological industry, the stirred-tank

bioreactor is the most important reactor setup [Hortsch and Weuster-Botz 2010]. Parallelized bioprocess development at mL-scale is enabled by the bioREACTOR48 system (2mag AG, Munich), which was originally developed by Puskeiler et al. [2005]. 48 stirred-tank reactors can be operated simultaneously under sterile and controlled conditions and scale-up is enabled by geometrical similarity to L- and $m^3$ stirred-tank reactors and by comparable power inputs and local energy dissipations [Hortsch and Weuster-Botz 2010].

**Generalized mass balance in bioreactors.** In order to describe processes in bioreactors with mathematical models, the reactors are treated as *ideal reactors* whose reaction volume is homogeneously mixed at every point in time. This implies that no spatial gradients in concentrations, temperature, pressure and reaction rates exist [Chmiel et al. 2018]. Every bioprocess taking place in an ideal reactor can be described with a generalized mass balance, irrespective of whether processes are operated in closed systems (batch processes), semi-open systems (fed-batch processes) or open systems (continuous processes):

$$\frac{dm_i}{dt} = \frac{d(c_i \cdot V_R)}{dt} = \underbrace{\dot{V}_{in} \cdot c_{i,in} - \dot{V}_{out} \cdot c_i}_{Convection} + \underbrace{r_i \cdot V_R}_{Reaction} \tag{3.21}$$

| | |
|---|---|
| $m_i$ | Mass of substance i, g |
| $c_i$ | Concentration of substance i, g L$^{-1}$ |
| $V_R$ | Reactor volume, L |
| $\dot{V}_{in}$ | Feed volume flow, L h$^{-1}$ |
| $\dot{V}_{out}$ | Outlet volume flow, L h$^{-1}$ |
| $c_{i,in}$ | Concentration of substance i in the feed solution, g L$^{-1}$ |
| $r_i$ | Volumetric reaction rate of component i, g L$^{-1}$ h$^{-1}$ |

**Batch cultivation.** For batch cultivations, the convection term of the mass balance becomes irrelevant. Moreover, when disregarding slight volume changes due to pH control, addition of antifoam agents and gassing, the reactor volume remains constant, resulting in a simplified mass balance:

$$r_i = \frac{dc_i}{dt} \tag{3.22}$$

As the actual process duration is low compared to reactor downtime for cleaning and sterilization, batch cultivations suffer from a rather low productivity [Srivastava and Gupta 2011]. Increasing the initial substrate concentration in order to improve pro-

ductivity can quickly result in harmful substrate inhibition. For example, *E. coli* is growth-inhibited above following nutrient concentrations: 50 g L$^{-1}$ glucose, 3 g L$^{-1}$ ammonium, 1.15 g L$^{-1}$ iron, 8.7 g L$^{-1}$ magnesium, 10 g L$^{-1}$ phosphorus, and 0.038 g L$^{-1}$ zinc [Riesenberg 1991]. This is why fed-batch cultivations, where substrate concentrations can be kept at low levels by continuous or sequential addition to the initial medium, are often the preferred choice [Salehmin et al. 2013].

**Fed-batch cultivation.** For fed-batch cultivations, the mass balance can be described with

$$\frac{dm_i}{dt} = \frac{d(c_i \cdot V_R)}{dt} = \dot{V}_{in} \cdot c_{i,in} + r_i \cdot V_R \tag{3.23}$$

The substrate S can be balanced by

$$\frac{dc_S}{dt} = \frac{\dot{V}_{in}}{V_R} \cdot (c_{S,in} - c_S) - q_S \cdot c_X \tag{3.24}$$

Here, the convection term takes into account that the substrate concentration in the reactor increases by feeding, but is also diluted by the increase in reactor volume. The feed volume flow can control the specific growth rate, one of the most important process variables of a microbial cultivation [Mears et al. 2017]. Correct adjustment of the feed flow can prevent the production of undesired by-products such as acetate. Formation of this metabolite can happen at high growth rates and/or high glucose uptake rates. It is thought of as a metabolic overflow phenomenon where the acetyl-CoA flux is directed to acetate instead of the overburdened citric acid cycle [Akesson et al. 1999]. For *E. coli*, Aristidou et al. [1994] report acetate concentrations of ~3 g L$^{-1}$ to be growth-inhibiting; whereas concentrations as small as 1 g L$^{-1}$ can already negatively affect gene expression and (recombinant) protein production.

Process intensification of fed-batch cultivations can be achieved by designing a high cell density cultivation (HCDC) process, where final cell densities are maximized by a careful adjustment of the growth rate and feeding profile. For *E. coli*, biomass concentrations of up to 148 g L$^{-1}$ have been reported [Korz et al. 1995]. A common cultivation medium for this microorganism is the "Riesenberg medium" developed by Riesenberg et al. [1991], providing the cells with all essential nutrients. At biomass concentrations above ~50 g L$^{-1}$, exponential growth cannot be maintained and space-time biomass yields decrease [Salehmin et al. 2013]. This is why many HCDC processes are divided into an exponential growth phase (either batch or fed-batch) and a subsequent fed-batch phase with linear growth. The main challenge of HCDC processes is certainly the limited oxy-

gen transfer rate of bioreactors, which can result in anaerobic conditions. In an anaerobic environment, *E. coli* produces different undesired by-products such as acetate, ethanol, lactate and formate by mixed-acid fermentation. Controlling the growth rate $\mu$ and the dissolved oxygen concentration simultaneously by constantly adjusting both the feeding profile and the agitation speed is one strategy to overcome this problem [Riesenberg et al. 1991].

With a defined specific growth rate $\mu_{set}$, the feed volume flow at a certain point in process time can be calculated. By inserting Equation 3.18 in Equation 3.24, one gets

$$\frac{dc_S}{dt} = \frac{\dot{V}_{in}}{V_R} \cdot (c_{S,in} - c_S) - \frac{\mu_{set}}{Y_{XS}} \cdot c_X \tag{3.25}$$

Assuming a constant substrate concentration in the reactor ($\frac{dc_S}{dt} = 0$ due to limiting substrate addition), and the substrate concentration in the reactor being far below the substrate concentration in the feeding solution ($c_{S,in} >> c_S$), following equation results:

$$\dot{V}_{in} = \frac{V_R \cdot \mu_{set} \cdot c_X}{Y_{XS} \cdot c_{S,in}} \tag{3.26}$$

Inserting Equation 3.13 gives

$$\dot{V}_{in} = \frac{V_R \cdot \mu_{set} \cdot c_{X,0}}{Y_{XS} \cdot c_{S,in}} \cdot e^{\mu_{set} \cdot t} \tag{3.27}$$

For *E. coli* growing exponentially on glucose, $Y_{XS}$ amounts to ~0.5  g g$^{-1}$ [Khalilzadeh et al. 2004], and $\mu_{set}$ is usually defined as 0.1–0.3 h$^{-1}$ [S. Y. Lee 1996; Riesenberg et al. 1991].

### 3.3.3. Production of recombinant proteins in *Escherichia coli*

*E. coli*, a resident of the gastrointestinal tract, is a chemoheterotroph (see Table 3.3), facultative anerobic, gram-negative and rod-shaped prokaryote with a length of 2–6 µm. It can either be non-motile or motile with peritrichous flagella, is mesophilic with a temperature optimum of 37 °C and prefers a neutral pH [Croxen et al. 2013; Schlegel 1992]. With its fast growth on inexpensive substrates, short doubling times of 20 min, a deeply investigated genome, a variety of different (engineered) strains and a large number of available genetic vectors and tools, *E. coli* is an organism frequently used for the biotechnological production of recombinant proteins [Baneyx 1999]; for instance human interferon-$\gamma$ [Khalilzadeh et al. 2004], bioadhesive protein from sea mussel [Wong et al. 1998] or alkaline phosphatase from *Bacillus* [Choi et al. 2000]. Nevertheless, certain draw-

backs affecting protein stability and activity can exist when expressing eukaryotic proteins in *E. coli*: The prokayotic host is not capable of conducting post-translational modifications such as glycosylation, acylation, phosphorylation and disulfide-bond formation. Moreover, *E. coli* does not necessarily possess the appropriate chaperons assisting protein folding, and codon usage bias might occur, resulting in insufficient tRNA concentrations [Yesilirmak and Sayers 2009; Yin et al. 2007].

Recombinant gene expression is based on the cloning of heterologous cDNA into plasmids (circular doubled-stranded DNA molecules that replicate independently from chromosomal DNA), which can then be transferred into a bacterial cell by transformation. Cells containing recombinant plasmids can be selected by antibiotic resistance markers located on the plasmids [Baneyx 1999; Schlegel 1992].

The popular T7 expression system (see Figure 3.8) uses the *E. coli* strain BL21(DE3) in combination with a recombinant plasmid (e.g. pET) containing a T7 promoter upstream of the heterologous target gene. The strain BL21(DE3) carries the DNA of the bacteriophage λDE3, which encodes for T7 RNA polymerase (T7RNAP) and for the *lac* repressor, in its genome. Upstream of the T7RNAP gene lie the *lacUV5* promoter and the *lacO* operator; the latter is also part of the operon belonging to the recombinant gene on the expression plasmid. Allolactose or its non-metabolized analogue isopropyl β-D-1-thiogalactopyranoside (IPTG) can be used as inducers for T7RNAP synthesis, as they deactivate the *lac* repressor which is otherwise bound to *lacO*, preventing transcription. T7RNAP can then transcribe the recombinant DNA on the plasmid by binding to the T7 promoter. By integrating an additional plasmid pLysS or pLysE into the cell, a secondary regulation mechanism can avoid basal expression of the target gene: it encodes for the T7 lysozyme, which binds and inactivates basally expressed T7RNAP. Only after induction, T7RNAP concentrations are high enough to outnumber T7 lysozyme.

No positive correlation between IPTG concentration and protein production is reported in literature. On the contrary - IPTG concentrations below 1 mM seem to be advantageous for gene expression, and higher amounts tend to inhibit both cell growth and recombinant protein production [Choi et al. 2006; Faust et al. 2015]. The latter might be explained with overly increased transcription rates, resulting in misfolding of proteins [Donovan et al. 1996]. Not only the IPTG concentration, but also the induction time should be chosen carefully, as induction at low cell densities, as it is for example the case during the early exponential growth phase in a HCDC, can negatively affect recombinant protein concentrations [Choi et al. 2006; Huber et al. 2011]. Instead of one single IPTG pulse, the inducer can also be fed to the reactor, with a feeding rate adapted to biomass growth. This can also reduce the metabolic burden on the cells, and can be used to fine-tune the
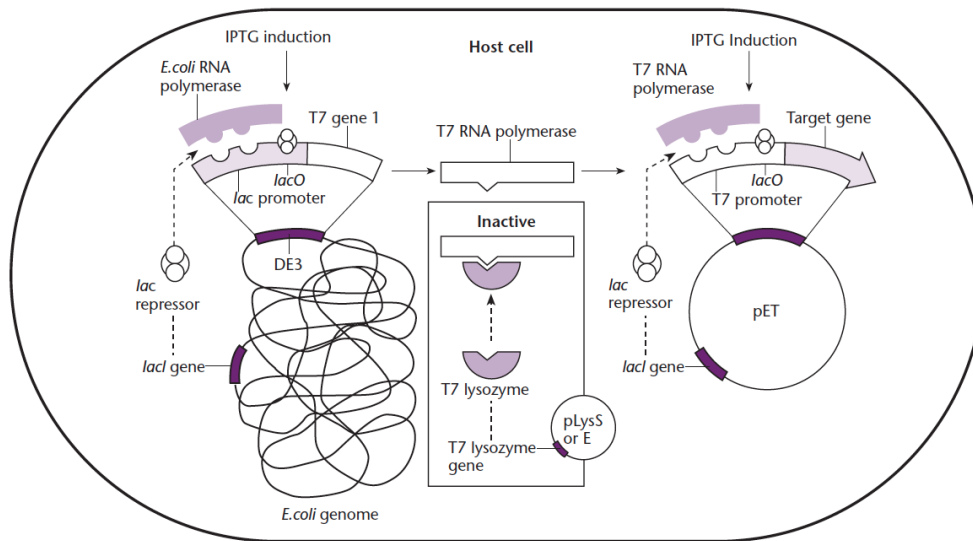
**Figure 3.8.:** T7 expression system in *E. coli* [Primrose and Twyman 2007]. The gene of interest is located on the pET plasmid and is transcribed by the T7 RNA polymerase, which binds to the T7 promotor upstream of the gene of interest. T7 RNA polymerase expression is induced by the addition of IPTG, which deactivates the *lac* repressor. Basal expression of the target gene is prevented by T7 lysozyme, which inactivates basally expressed T7 RNA polymerase.

transcription rate, ideally with positive effects on protein folding [Striedner et al. 2003]. The effect of the post-induction substrate feeding strategy was investigated by Wong et al. [1998] who produced bioadhesive protein in recombinant *E. coli*. By applying a linearly increasing post-induction feeding rate, a 1.7-fold protein concentration could be obtained compared to exponential and constant feeding.

Overexpression of recombinant proteins often comes along with the accumulation of un- or misfolded protein in so called inclusion bodies (IBs). The formation of unfolded proteins or folding intermediates can be caused by excessively high transcription rates, and/or inefficient processing by chaperones. As proteins in IBs are insoluble and inactive, IB formation should be prevented in the first place [Sørensen and Mortensen 2005b]. On the genetic level, low-copy number plasmids can improve soluble protein production. Other approaches include the usage of weaker promoters, the co-expression of specific chaperones, or the linkage of the target protein to solubility tags [Bentley et al. 1990; Sørensen and Mortensen 2005a]. On a process level, a decrease in process temperature is the most powerful tool, as it results in a decrease of transcription rates and diminishes the presence of heat shock proteins. Moreover, lower temperatures result in a reduction of the hydrophobic effect, and thus in a deceleration of protein folding [Schellmann 1997; Sørensen and Mortensen 2005b].

## 3.4. Whole-cell biocatalysis

After the successful production of a recombinant enzyme in a microorganism such as *E. coli*, the enzyme can be used for biotransformations (see Chapter 3.1.1). Biotransformations can either be conducted with purified enzymes (free or immobilized), with crude protein extract, with cellular envelopes containing only the target enzymes [Sührer et al. 2015], or with whole intact cells. The usage of whole-cells as biocatalysts for the synthesis of chemicals is common practice in industry, especially for the production of bulk chemicals like acrylamide, which is produced by *Rhodococcus rhodochrous* at 100,000 ton-scale annually [A. Schmid et al. 2001; Woodley 2006; Yamada and Kobayashi 1996].

When designing a whole-cell biocatalytic process, it is important to differentiate between three different metabolic states of the biocatalyst: truly resting cells, non-growing cells, and growing cells. In truly resting biocatalysts the overall metabolism is shut down and only the target enzymes are active. Such a state can be obtained in a reaction environment consisting only of buffer (e.g. potassium phosphate) and the substrate. It allows for complete temporal and/or spatial separation of biocatalyst production and biotransformation. However, truly resting cells tend to perform poorly, resulting in low product concentrations and/or low biocatalyst stability [Buchhaupt et al. 2012; Castiglione and Weuster-Botz 2018; Willrodt et al. 2016]. The non-growing, metabolically active state can be induced by the depletion of one growth-essential nutrient, such as nitrogen or magnesium. Thereby, competition of the desired biotransformation reaction with the cellular energy and growth metabolism can be avoided. This can allow for increased product concentrations [Julsing et al. 2012; Willrodt et al. 2016]. However, certain biotransformations only work with growing cells that do not face nutrient limitations. One example is the biotransformation of 2,5-dimethylpyrazine (DMP) to 5-methyl-2-pyrazinecarboxylic acid, which is a building block for the synthesis of different pharmaceuticals [Castiglione and Weuster-Botz 2018]. Hereby, the carbon and energy source xylol is required for the induction of enzymes that transform both xylol itself and DMP. Thus, the biotransformation has to be coupled to cell growth.

### 3.4.1. Advantages and challenges

Whole-cell biocatalyis features different advantages over the usage of isolated enzyme, but also has to deal with some challenges. First, biocatalytic transformations using whole-cells allow for less laborious production methods, as process steps like enzyme isolation, purification and immobilization are not necessary. This enables a decrease of process

costs by up to a double-digit factor. Especially for multi-enzyme systems and for larger production scales this can become an important deciding factor [Tufvesson et al. 2011]. Another crucial advantage of whole-cell biocatalysis is that the addition of cofactors becomes obsolete due to intracellular cofactor regeneration. This also allows for additional process cost savings. Particularly reactions involving oxidoreductases, which require the presence of nicotinamide cofactors, are often performed with a whole-cell approach. Another prominent example for whole-cell biotransformations are UDP-glucose-dependent glycosylations (see Chapter 3.1.3). Moreover, whole-cells enable the parallel expression of different enzymes and their subsequent action in a protected environment. This is very advantageous when implementing multi-step enzymatic cascades. If the coexpression of different recombinant enzymes results in an excessively high metabolic burden for the cell though, they can also be produced individually in different strain variants and be combined later within the same reaction medium [Jakoblinnert and Rother 2014].

In many cases, whole cells do not only produce the desired biotransformation product, but also by-products or derived products. Such compounds result from undesired metabolic pathways involving the action of corresponding endogenous enzymes. This problem can be solved by metabolic engineering, e.g. the deletion of respective endogenous enzymes [Castiglione and Weuster-Botz 2018; Liu et al. 2016]. A further challenge in whole-cell biocatalysis is substrate or product inhibition. This problem can, however, be solved by the application of biphasic reaction systems (see Chapter 3.2.1), which specifically are advantageous for poorly water soluble substrates and products. Moreover, thermodynamically unfavorable reactions may be promoted by biphasic reaction systems, as the product can be removed continuously from the cells [Braun et al. 2012; Bräutigam et al. 2007; Castiglione et al. 2017]. However, the application of organic solvents as non-aqueous phase can result in the formation of stable emulsions (interphases), which even persist after attempted phase separation by centrifugation. Brandenbusch et al. [2010] showed that this problem can be tackled by the de-emulsifying action of supercritical carbon dioxide. Another potential bottleneck that has to be considered when working with whole-cell biocatalysts is poor transport of the substrate or product across the cellular membrane [Castiglione and Weuster-Botz 2018]. Insufficient substrate transfer can result in low reaction rates, insufficient product transfer in inhibitory effects and difficulties during downstream processing. Solutions can either be of chemical or physical nature (e.g. solvent treatment, electropermeabilization), or involve molecular engineering. Examples include the display of the respective enzymes on the cellular surface, the co-expression of suitable transport proteins, or an increase in membrane permeability by mutations in membrane proteins or lipoproteins [R. R. Chen 2007; Ni and R. R. Chen 2004].

## 3.4.2. Process characterization

In order to characterize a whole-cell biotransformation process, the conversion of the substrate and the formation of the respective product can be specified mathematically. Moreover, the transport of substrate and product across the cell membrane of the microorganism has to be considered and described. Furthermore, identifying the rate-limiting step during a biotransformation is an important tool for process improvement.

**Process parameters.** For a mathematic description of a biotransformation reaction, different parameters can be used. First, the amount of transformed substrate at a given point in time can be described by the conversion X:

$$X(t) = \frac{n_{S,0} - n_S}{n_{S,0}} \cdot 100 \tag{3.28}$$

$X$     Conversion, %
$n_{S,0}$    Initial substrate amount, mol
$n_S$     Substrate amount at a given point in time t, mol

To describe the amount of formed product at a given point in time, the yield parameter Y can be used:

$$Y(t) = \frac{n_P - n_{P,0}}{n_{S,0}} \cdot \frac{\nu_S}{\nu_P} \cdot 100 \tag{3.29}$$

$Y$     Yield, %
$n_{P,0}$    Initial product amount, mol
$n_P$     Product amount at a given point in time t, mol
$\nu_S$     Stoichiometric coefficient of the substrate, -
$\nu_P$     Stoichiometric coefficient of the product, -

The volumetric productivity of a biotransformation can be described with the space-time yield (STY). It describes the product amount that can be formed in a certain reaction volume within a certain time:

$$STY = \frac{n_P}{t \cdot V_R} \tag{3.30}$$

$STY$    Space-time yield, mol L$^{-1}$ h$^{-1}$
$V_R$     Reaction volume, L

**Membrane transport.** When working with whole cells, the substrate of the biotrans-
formation reaction has to cross the cellular membrane. The membrane of *E. coli*, which is
the whole-cell biocatalyst used in the present work, consists of an inner membrane made
up of a phospholipid bilayer, a peptidoglycan layer stabilizing the periplasm, an outer
membrane with lipopolysaccharides, and a capsule made up of polysaccharides [Whitfield
2006]. It features selective permeability, enabling only the passage of lipophilic, unpolar
and rather small molecules by diffusion, which is driven by concentration gradients. Ions,
hydrophilic and/or larger compounds require the presence of carrier, channel or pump
proteins.

Assuming that the membrane is one homogeneous film, the diffusive transport of small
lipophilic compounds from the extra- to the intracellular space can be described with
Fick's first law:

$$J_S = \frac{\dot{n}_S}{A} = -D_{S,m}\frac{dc_{S,m}}{dx} = -D_{S,m}\frac{c_{S,m}'' - c_{S,m}'}{d_m} \tag{3.31}$$

$J_S$    Diffusion flux of the substrate S, mol cm$^{-2}$ s$^{-1}$

$\dot{n}_S$    Substrate flux, mol s$^{-1}$

$A$    Membrane surface, cm$^2$

$D_{S,m}$    Substrate diffusion coefficient in the membrane, cm$^2$ s$^{-1}$

$c_{S,m}''$    Intracellular equilibrium concentration of the substrate at the membrane,
       mol cm$^{-3}$

$c_{S,m}'$    Extracellular equilibrium concentration of the substrate at the membrane,
       mol cm$^{-3}$

$d_m$    Membrane thickness, cm

When assuming partition equilibrium at the phase boundary of the membrane and the
respective aqueous phase (see Figure 3.9), an equilibrium constant K$_S$ can be defined as
follows:

$$K_S = \frac{c_{S,m}'}{c_{S,w}'} = \frac{c_{S,m}''}{c_{S,w}''} \tag{3.32}$$

$c_{S,w}'$    Substrate concentration in the extracellular space, mol cm$^{-3}$

$c_{S,w}''$    Substrate concentration in the intracellular space, mol cm$^{-3}$

With

$$\Delta c_S = c_{S,w}' - c_{S,w}'' \tag{3.33}$$
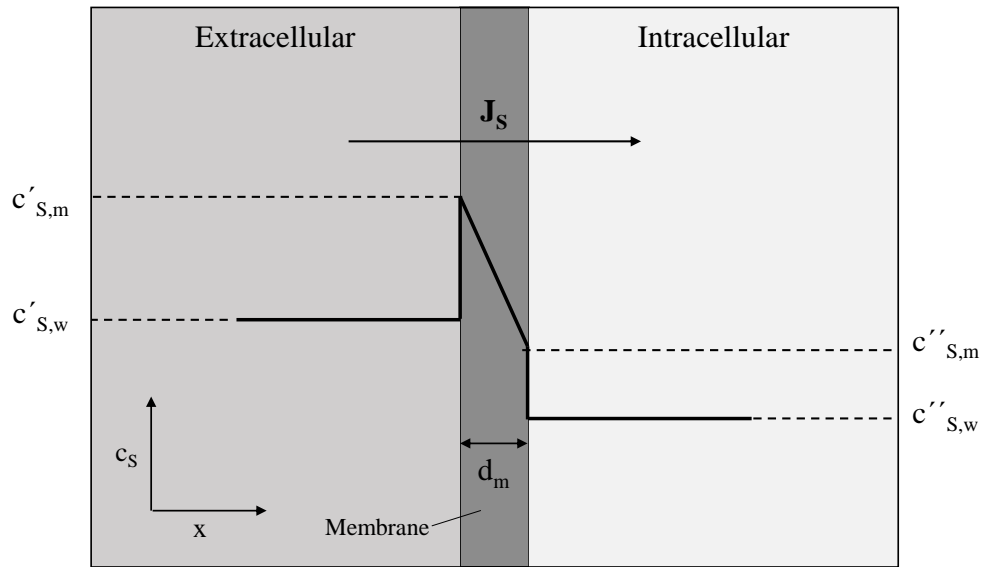
**Figure 3.9.:** Concentration profile for the diffusive transport of a substrate S across a biological membrane, adapted from Bräutigam [2008]. $J_S$: Diffusion flux of the substrate S. $d_m$: Membrane thickness. $c'_{S,m}$: Extracellular equilibrium concentration of the substrate at the membrane. $c''_{S,m}$: Intracellular equilibrium concentration of the substrate at the membrane. $c'_{S,w}$: Substrate concentration in the extracellular space. $c''_{S,m}$: Substrate concentration in the intracellular space.

Equation 3.31 can be written as

$$J_S = \frac{K_S \cdot D_{S,m}}{d_m} \Delta c_S \tag{3.34}$$

with $\frac{K_S \cdot D_{S,m}}{d_m}$ being the permeability coefficient P [Ackermann 1992]. Modified versions of these equations can be used for the calculation of product transfer from the intra- to the extracellular space.

**Rate-limiting steps in biphasic whole-cell biocatalysis.** Three different steps can become rate-limiting during whole-cell biocatalysis in a liquid/liquid biphasic system with *in situ* substrate supply. First, the substrate has to be transported from the non-aqueous phase into the aqueous reaction medium. Different models exist to describe mass transfer across the interphase. The two-film model is based on the assumption that on each side of the interface a boundary layer of the respective phase can be found [Lewis and Whitman 1924]. This concept can be simplified to a one-film model under the assumption that the mass transfer resistance in one of the two boundary layers is negligibly small in comparison to the other. This is usually the case when a substance features a large partition coefficient [Brauer 1978] and can therefore predominantly be found in one of the

two phases (here: organic phase). The one-film model can be illustrated in the same way as the diffusive transport of a substance across a biological membrane (see Figure 3.9) and follows the same equations. Thus, the higher the interfacial area is, the higher is the flux of a substance from one phase into the other (see Equation 3.31). In bioprocess engineering, an increase in the interfacial area can be obtained by decreasing the droplet size of the organic phase, as for example achieved by high stirrer speeds. As described in Chapter 3.2.3, the mass transfer of apolar compounds in liquid-liquid systems in stirred-tank bioreactors is usually not the limiting step during biotransformations, even when working with rather viscous organic phases or when applying comparably low power inputs. However, as soon as very active biocatalysts with high conversion rates are applied, the mass transfer across the interphase might become rate-limiting and thus has to be evaluated thoroughly. The second crucial step, which was described in detail in the preceding paragraph, is the transfer of the substrate from the reaction medium across the cellular membrane into the cell. Low membrane permeabilities can be tackled either by chemical or physical treatment, or by metabolic engineering (see Chapter 3.4.1). When none of the two transfer steps is rate-limiting, the biocatalytic reaction itself or a directly related upstream pathway (e.g. cosubstrate supply) is the bottleneck and metabolic engineering can be used to increase the reaction rate.

### 3.4.3. Whole-cell approach for the glucosylation of geraniol

The glucosylation of geraniol by the glycosyltransferase VvGT14a, described in Chapter 3.1.3 and in Figure 3.5, is a biotransformation predestined for a whole-cell approach: The cosubstrate required for the reaction is UDP-glucose, which has to be provided in stoichiometric amounts. However, its high purchase price of 302.5 € mol$^{-1}$ (Sigma-Aldrich, 28.03.2019) prevents its stoichiometric addition to a glucosylation reaction that is to be somewhat profitable. As they provide for an efficient source of UDP-glucose, *E. coli* cells are convenient whole-cell biocatalysts for the conversion of geraniol by VvGT14a. In *E. coli*, UDP-glucose is a precursor of different polysaccharides constituting the protective capsule on the cells' surface [Whitfield 2006] and thus constantly synthesized and regenerated. The multi-enzyme synthesis pathway of UDP-glucose in *E. coli*, starting from glucose, is depicted in Figure 3.10.

Due to the cytotoxicity of geraniol at concentrations of 0.3 g L$^{-1}$ and higher (see Chapter 3.1.3), its concentrations during whole-cell biotransformations need to be kept strictly below this value. This can either be realized by working with a low overall substrate concentration, by feeding geraniol to the medium with an accurately determined rate,
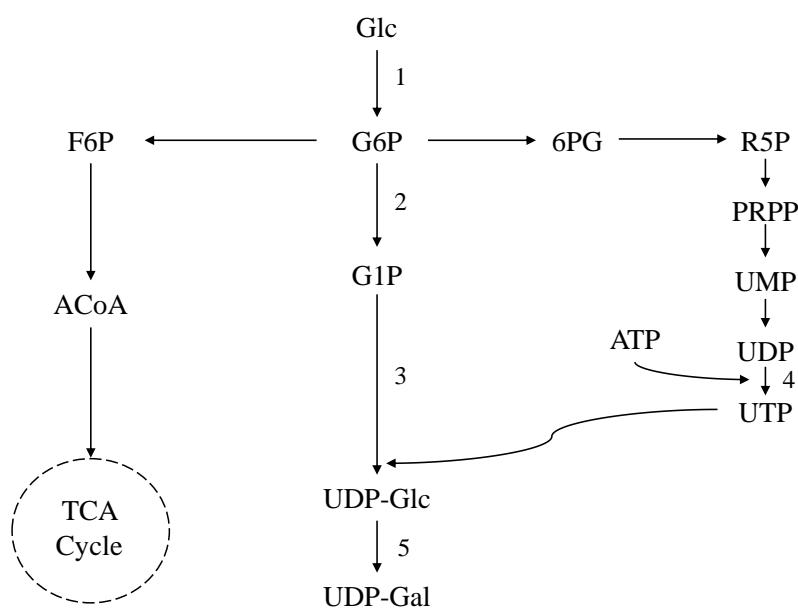
**Figure 3.10.:** UDP-glucose synthesis in *E. coli*, adapted from Mao et al. [2006]. **Metabolites**:
ACoA: acetyl-CoA, ATP: adenosine triphosphate , F6P: fructose-6-phosphate, Glc: gluc-
ose, G1P: glucose-1-phosphate, G6P: glucose-6-phosphate , PRPP: 5-phosphoribosyl-1-
pyrophosphate, 6PG: 6-phosphogluconate, R5P: ribose-5-phosphate, UDP-Gal: UDP-
galactose, UDP-Glc: UDP-glucose, UDP: uridine diphosphate, UMP: uridine monophos-
phate , UTP: uridine triphosphate. TCA cycle: tricarboxylic acid cycle. **Enzymes**: 1:
glucokinase, 2: phosphoglucomutase, 3: UDP-glucose pyrophosphorylase, 4: UDP kinase;,
5: UDP-glucose-4-epimerase.

or by using a biphasic reaction system where a non-aquous phase serves as the *in situ*
substrate reservoir (see Chapter 3.2.1).

Two whole-cell approaches for the glucosylation of geraniol are described in literature:
Caputi et al. [2008] applied a geraniol feed in a biotransformation conducted at L-scale
in a stirred tank reactor, using *E. coli* expressing a glycosyltransferase from *Arabidopsis
thaliana* as a biocatalyst. 0.18 g L$^{-1}$ of geranyl glucoside were obtained, with a space-time
yield of 7.6 mg L$^{-1}$ h$^{-1}$. A biotransformation at mL-scale in stirred tank reactors with a
biphasic system consisting of M9 mineral medium and the water-immiscible ionic liquid
N-hexylpyridinium bis(trifluoromethylsulfonyl)imide was performed by Schmieder et al.
[2016b]. *E. coli* expressing VvGT14a was used as the biocatalyst, yielding 0.29 g L$^{-1}$
geranyl glucoside with a space-time yield of 14.5 mg L$^{-1}$ h$^{-1}$.

# 4. Materials and methods

The following chapter describes the materials and methods used in this work.

## 4.1. Materials

### 4.1.1. Chemicals, consumables and equipment

The used chemicals, consumables and equipment are listed in Tables A.1–A.9.

### 4.1.2. *Escherichia coli* strain variants

The *E. coli* strain BL21(DE3) was used. It has the following genotype:

fhuA2 [lon] ompT gal ($\lambda$ DE3) [dcm] $\Delta$hsdS $\lambda$ DE3 = $\lambda$ sBamHIo

$\Delta$EcoRI-B int::(lacI::PlacUV5::T7 gene1) i21 $\Delta$nin5

The strain contained the expression plasmid pET29a with a kanamycin resistance. The plasmid encodes for the glycosyltransferase VvGT14a from *Vitis vinifera*. Moreover, the strain featured a pLysS plasmid with the genotype [T7p20 ori$_{p15A}$](Cm$^R$). For certain experiments, a strain with a modified pLysS plasmid was used, where the chloramphenicol resistance (Cm$^R$) was replaced by an ampicillin resistance. In the following chapters, the strains will be called BL21(DE3)pLysS pET29a_VvGT14a (abbreviation: pLysS), and BL21(DE3)pLysS**A** pET29a_VvGT14a (abbreviation: pLysSA), respectively. Both strain variants were provided by Prof. Schwab (Associate Professorship of Biotechnology of Natural Products, Technical University of Munich).

Moreover, the two strains *E. coli* BL21(DE3) and *E. coli* BL21(DE3)pLysS were used for certain experiments.

## 4.2. Media and buffers

Media and buffer preparations are described in Tables A.10–A.25. Sterile solutions were first prepared with approximately 90 % of the final volume, and filled up to 100 % with

sterile demineralised water after autoclaving (121 °C, 1 bar excess pressure, 20 min).

## 4.3. Characterization of non-aqueous phases

### 4.3.1. Biocompatibility, biofilm formation and bioavailability

The compatibility of organic solvents with the *E. coli* whole-cell biocatalyst was evaluated by measurement of the optical density and by counting the colonies formed on agar plates after incubation of the whole-cell biocatalysts with the respective solvent. A total reaction volume of 50 mL consisting of 20 % (v/v) of the organic solvent in M9 mineral medium with 5 g L$^{-1}$ glucose was inoculated with the biocatalyst (OD$_{600}$ = 15) in 500 mL shake flasks. After incubation at 30 °C and 200 rpm for 6 h, the optical density of the aqueous phase was measured. Moreover, the aqueous phase was diluted with PBS by 10$^7$, and 100 µL were plated on agar containing 0.1 g L$^{-1}$ kanamycin. After incubation at 37 °C for 24 h, the colonies were counted. Incubation of the biocatalyst in pure M9 mineral medium served as a reference.

Biofilm formation on polymers was evaluated indirectly as described by Morrish and Daugulis [2008]: 300 mg of polymers were added to 10 mL M9 medium containing 20 g L$^{-1}$ glucose and biocatalysts (OD$_{600}$ = 1). Preparations without polymers served as controls. The mixtures were incubated in sealed glass vials, which were agitated at 600 rpm by magnetic stirrers on a multi-stirrer plate at 30 °C. After 24 h, the optical density was measured. A lower optical density in suspensions containing polymers than in the controls was taken as an indicator for adsorption of cells on the polymer surfaces.

The assessment of bioavailability of polymers was performed with the same protocol, however without the addition of glucose. Mixtures without polymers served as controls. If the optical density was higher in suspensions containing polymers, bioavailability of the polymers was assumed.

### 4.3.2. Viscosity

Viscosity measurements of organic solvents were performed with a rotational viscometer (RheolabQC, Anton Paar) at 30 °C with a shear rate range of 100–2000 s$^{-1}$.

### 4.3.3. Partition coefficients and sorption isotherms

**Partition coefficients.** Partition coefficients of geraniol and geranyl glucoside between M9 mineral medium and different organic solvents were determined by adding 10 g L$^{-1}$

geraniol and 2 g L$^{-1}$ geranyl glucoside, respectively, to the sequestering phase, which made up 20 % (v/v) of the total reaction volume of 1 mL. After adding M9 mineral medium, the mixtures were incubated for 1 h at 25 s$^{-1}$ in micro reaction tubes in a mixer mill (MM 200, Retsch Technology). Phases were separated (10 min, 16,249 g, benchtop centrifuge), if necessary diluted, and analyzed by HPLC. Partition coefficients were determined in triplicates.

For F&F compounds that were used as target molecules in the study on a generalized approach for the selection of biphasic systems, a slightly different method was applied. Partition coefficients were determined in triplicate. All preparations were placed in glass scintillation vials with a liquid capacity of 24 mL and foil lined caps. In all cases, the aqueous phase was demineralized water. For liquid-liquid biphasic systems, the target F&F compounds were dissolved in the non-aqueous phases and these mixtures were contacted with water (20 % (v/v) non-aqueous phase mixed with target compound), yielding overall target compound concentrations between 0.4 and 2 g L$^{-1}$. For solid-liquid biphasic systems, the polymers were washed in methanol and subsequently in demineralized water for each 3 h and air-dried overnight before use. The polymers (5 % (w/w)) and demineralized water were placed in scintillation vials, followed by the addition of the target compounds with an aqueous concentration of 2 g L$^{-1}$. All vials were incubated at 30 °C and 180 rpm, either for at least 3 h for liquid-liquid mixtures or for at least 24 h for systems involving polymers. Subsequently, liquid-liquid preparations were centrifuged at 2800 g for 10 min, whereas solid-liquid preparations were processed directly. All aqueous phases were filtered (0.2 µm), if necessary diluted, and aqueous concentrations of the target compounds were quantified either by GC or HPLC. Mass balances were performed to determine the concentrations of the target compounds in the non-aqueous phases and finally partition coefficients were determined by calculating the ratio of the target compound's mass fractions in the non-aqueous and aqueous phase.

**Sorption isotherms.** The sorption of geraniol and geranyl glucoside to different polymers was described by sorption isotherms. For geraniol, different amounts of different polymers (10, 25, 50, 100, 200, 250, 300 mg), which were washed with 2 mL M9 medium beforehand, were mixed with 10 mL of a geraniol solution (0.5 g L$^{-1}$ in M9 medium) and incubated in sealed glass vials, which were agitated at 600 rpm by magnetic stirrers on a multistirrer plate at 30 °C for 8 h. Reactions were performed in triplicates. For geranyl glucoside, different amounts of XAD4 (10, 25, 50, 100, 250 mg) were mixed with 5 mL of a geranyl glucoside solution (0.5 g L$^{-1}$ in M9 medium) and incubated at 30 °C and 600 rpm for 3 h. Reactions were performed in duplicates. The liquid phases were used for subsequent

HPLC analysis.

## 4.3.4. Affinity-based thermodynamic first-principles methods

Hansen Solubility Parameters and associated *Ra* distances were determined with the software HSPiP [Hansen 2016]. The software's "Master Dataset" consisting of 1237 liquid sequestering phases, and a dataset consisting of 530 polymers were used as a starting point for the rational selection of suitable biphasic systems.

As a second thermodynamic method, the Extractant Screening Program introduced by Bruce and Daugulis [1991] was used. ~1500 different solvents were screened in ternary systems consisting of 74 % (w/w) water, 20 % (w/w) solvent and 6 % (w/w) target compound. The systems' temperature was set to 30 °C, as this is a common temperature for bioprocesses.

# 4.4. Production of whole-cell biocatalysts

## 4.4.1. Strain maintenance

The used *E. coli* strain variants were stored as cryo-cultures at -80 °C. To maintain the cell lines, the cultures were grown to a defined optical density, harvested and frozen with a cryoprotective for long-term storage: A test tube was filled with 4.9 mL LB medium, 0.03 g L$^{-1}$ of the respective antibiotics and either 100 µL of the existing cryo-stock or a colony picked from an agar plate, and was incubated at 30 °C and 200 rpm in an incubator shaker. After 16 h, 2.5 mL of this pre-culture, 47.45 mL LB medium and 0.03 g L$^{-1}$ of the respective antibiotics were filled into a 500 mL shake flask and incubated at 37 °C and 250 rpm. As soon as an optical density of 1 was reached, 400 µL-aliquots of the culture were mixed with 800 µL sterile 60 % (v/v) glycerol as a cryoprotective in 1.5 mL micro reaction tubes. The tubes were immediately transferred to -80 °C.

## 4.4.2. High cell density cultivation at L-scale

**Precultures.** 5 test tubes filled with 4.9 mL LB medium, 0.03 g L$^{-1}$ of the respective antibiotics and 100 µL cryostock were prepared under sterile conditions and subsequently incubated over night at 30 °C and 200 rpm on a rotary shaker. After 15 h, 5 unbaffled 500 mL Erlenmeyer flasks were filled with 95 mL sterile RB medium and 5 mL of the overnight-cultures, respectively. The flasks were incubated at 37 °C and 250 rpm until an optical density of 1.5–2 was reached. The inoculum for the main cultivation was

prepared by centrifuging the content of the flasks at 3260 g for 10 minutes, resuspending the cell pellets in fresh RB medium and combining the cell suspensions. The inoculum was transferred to a syringe.

**Main cultivation.**    The main cultivation was performed at L-scale in a jacketed, baffled 7.5 L stirred-tank bioreactor (Labfors 2, INFORS AG) equipped with three Rushton turbines. The reactor cover contained ports for pH and DO (dissolved oxygen) probes, a temperature sensor, and supply air and exhaust gas with gas cooler, as well as ports for sampling and the addition of acid, base, feeding medium and additives such as antifoam agent. The experimental setup is shown in Figure 4.1. Process control and recording was conducted by the software IRIS. The individual components of the system are listed in Table A.4.
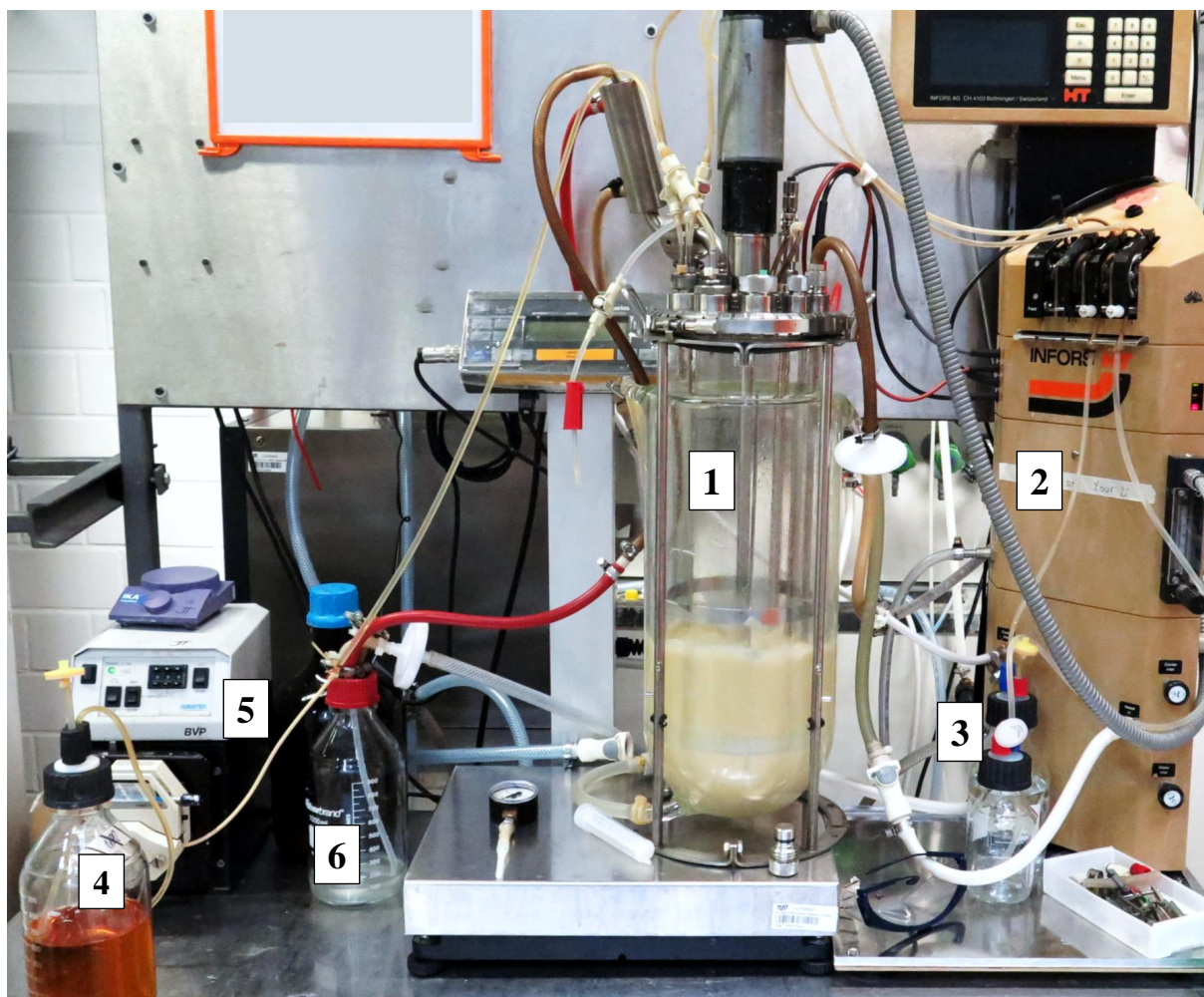


**Figure 4.1.:** Experimental setup for high cell density cultivations at L-scale. (1) 7.5 L stirred-tank reactor, (2) Control unit with pumps for acid and base, (3) Acid and base, (4) Feeding solution, (5) Peristaltic feed pump, (6) Exhaust gas bottle containing antifoam solution.

2 L sterile RB medium, temperated to 37 °C and stirred at 800 rpm, were inoculated to an $OD_{600}$ of 0.5. Immediately after inoculation, exponential feeding with the feeding medium listed in Table A.20 was started, with a set growth rate of 0.18 h$^{-1}$. The feed volume flow was calculated with Equation 3.27. After 18 h, the maximal feeding rate of 8.75 g L$^{-1}$ h$^{-1}$ glucose was reached and kept constant for 3 h. Subsequently, the temperature was lowered to 20 °C and recombinant protein expression was induced with different IPTG concentrations (0.05–1 mM). Different post-induction feeding profiles were applied for the following 27 h. Throughout the entire cultivation, the pH was maintained at pH 6.8 with 28 % (w/v) $H_3PO_4$ and 25 % (v/v) $NH_3$. The DO was maintained above 25 % air saturation by automatic upward regulation of the stirrer speed up to 1200 rpm and of the aeration rate up to 4 vvm. Samples were taken periodically. At the end of the cultivation, the broth was harvested either into 50 mL centrifuge tubes or into 1 L centrifuge beakers.

### 4.4.3. Studies in shake flasks

In order to analyze the effect of different inducer concentrations on VvGT14a expression, protein expression was conducted parallelized in shake flasks. Test tubes filled with 4.9 mL LB medium, 0.03 g L$^{-1}$ of the respective antibiotics and 100 µL cryo-stock of BL21(DE3)pLysS pET29a_VvGT14a were prepared under sterile conditions and subsequently incubated at 37 °C and 250 rpm on a rotary shaker for 6 h. Unbaffled 1000 mL Erlenmeyer flasks were filled with 190.8 mL modified LB medium, 20 g L$^{-1}$ glucose, 0.03 g L$^{-1}$ of the respective antibiotics and the entire content of one test tube, respectively. The flasks were incubated at 37 °C and 250 rpm for 4 h. Subsequently, the flasks were cooled down on ice to 20 °C and different IPTG concentrations (0.1–2.0 mM) were added to induce recombinant protein expression. The production phase lasted 14 h at 250 rpm and 20 °C. Each IPTG concentration was tested in biological duplicates. Samples for protein analytics were taken regularly.

## 4.5. Storage of whole-cell biocatalysts

After harvesting the cells at the end of high cell density cultivations, they were stored in the original RB medium at 4 °C until further use.

For the analysis of different storage conditions, the biocatalysts were stored at 22 °C, 4 °C and -20 °C. Moreover, they were objected to freeze-drying. For this purpose, they were pre-frozen at -80 °C for 2 h, either without cryoprotective, or with 32 % (w/v) sucrose solution as a cryoprotective. Afterwards, the cells were freeze-dried at -50 °C and

0.23 mPa for 4 days and subsequently stored at 4 °C.

# 4.6. Whole-cell biotransformation of geraniol

## 4.6.1. General proceeding

Prior to each biotransformation, the biocatalysts stored at 4 °C were separated from the RB medium by centrifugation (3260 g, 10 min) and resuspended in fresh medium. Usually, this was M9 medium, in certain cases also $KP_i$ buffer or RB/LB/TB medium. Biotransformation systems always contained geraniol as a substrate and glucose as a carbon source. The reactions were either performed as purely aqueous reactions, or in biphasic systems with different non-aqueous phases (liquid or solid).

When using a liquid as a second phase, geraniol was added to this liquid prior to mixing the second phase with the aqueous phase. After the biotransformation, phases were separated by centrifugation at 3260 g.

When working with XAD4 as a solid non-aqueous phase, geraniol was mixed with M9 mineral medium at a maximal concentration of 0.6 g $L^{-1}$ in order to ensure full solubility. The mixture was added to a defined mass of XAD4, which was weighed directly into the reaction vessel and washed twice with M9 mineral medium beforehand. The solid-liquid suspensions were incubated for 3 h at 30 °C at a defined impeller speed to allow adsorption of geraniol to the resin. Subsequently, the biotransformation was started by addition of the whole-cell biocatalyst and glucose. After the biotransformation process, the liquid phase was removed and centrifuged (10 min, 3260 g). The resulting supernatant was used for HPLC analysis. Solutes bound to the adsorbent were eluted with methanol in sealed and stirred glass vials at 20 °C for 2 h. Subsequently, methanol was separated from the solid by centrifugation (10 min, 16,249g, benchtop centrifuge) and the supernatant was used for HPLC analysis.

## 4.6.2. Parallelized biotransformations at mL-scale

Parallelized whole-cell biotransformations of geraniol at mL-scale were performed in a parallel stirred-tank bioreactor system (bioREACTOR, 2mag) equipped with gas-inducing stirrers using sterile single-use unbaffled bioreactors made of polystyrene (2mag, Munich, Germany) with a working volume of 8–15 mL. The reactors had an inner diameter of 20 mm and a height of 86 mm, and were equipped with fluorometric sensors for pH and DO measurements at their bottom. The *on line*, non-invasive measurement of these para-

meters was based on the determination of the fluorescence decay time of fluorescence dyes contained in the sensors. Each sensor contained two different dyes, with one functioning as a reference independent of the actual process parameter and with the other one being sensitive for the actual process value. The reactor supplier provided calibration data for both sensor types, however, calibrations were performed with M9 mineral medium in the present study.

The reaction block (see Figure 4.2) carried 48 reactors, arranged in 6 columns with 8 reactors each. A gas cover on top of the block (see Figure 4.3a) functioned as a sterile barrier and provided the reactors with sterile air: The air was distributed from a central gas inlet across the cover and drawn into the reactors through the hollow axles of the gas-inducing stirrers, which were mounted to the gas cover. Cross holes at the bottom of the stirrers dispersed the air in the reaction medium. In addition to gas supply, the stirrers were responsible for the mixing of the medium, and were powered electromagnetically, with workable stirrer speeds of 500–4000 min$^{-1}$. The headspace of the reaction block was cooled in order to prevent evaporation, whereas the temperature of the reaction space was controlled by an additional heat exchanger. Process temperature, power input and aeration rate could only be defined for the entire reaction block.

The bioreactor system was integrated into an automated liquid handling system (Genesis RSP 150, Tecan) (see Figure 4.3b), which was used for pH control. The pipetting arm with 8 needles (pipetting volume: 0.5–480 µL) could supply 8 reactors of one column in parallel. This allowed for an efficient control of the entire reactor block.

The individual components of the cultivation system are listed in Table A.5.

Process control and recording was carried out by the software Fedbatch-XP. The liquid handler software Gemini was responsible for the execution of the actual pipetting steps.

Whole-cell biotransformations of geraniol at 10 mL-scale were executed at impeller speeds of 2200, 2800 or 4000 rpm, an aeration rate of 0.1 L min$^{-1}$ per reactor, a temperature of 30 or 37 °C, and activated headspace cooling (20 °C) to prevent losses in liquid volume by evaporation. The sterile air was pre-saturated with water at room temperature (23 °C) by applying a gas sparger in a 1 L bottle. In experiments with pH control, 25 % (v/v) NH$_3$ was used to maintain the pH at pH 7. For each data point, biological triplicates, hence 3 reactors, were used. Thereby, the entire content of each reactor was sampled by cannulas while briefly stopping the stirrer.
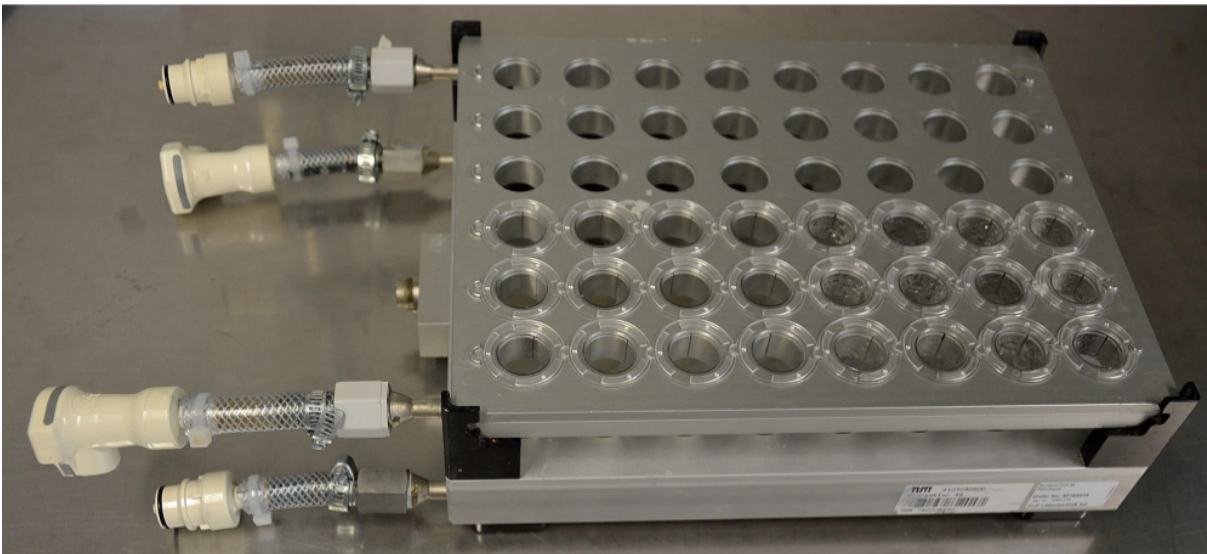
**Figure 4.2.:** Bioreactor block, partly equipped with single-use reactors, for parallelized biotransform-
ations at mL-scale. On the left, the ports for headspace cooling, reaction temperature
control and gas supply are visible.
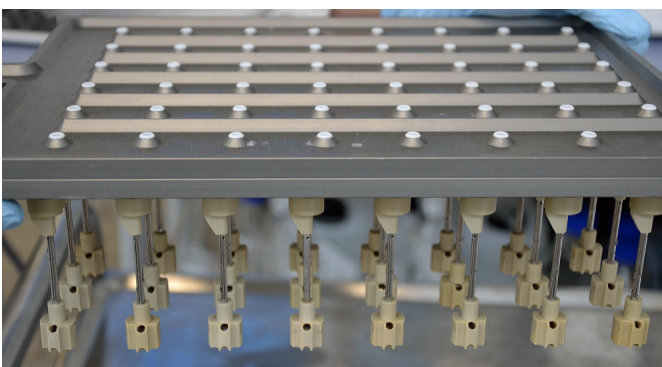


(a) Gas cover of the bioreactor block with mounted gas-
inducing stirrers



(b) Bioreactor block and active pipetting
arm of the liquid handling system (Im-
age copyright: Institute of Biochemical
Engineering, Technical University of Mu-
nich)

**Figure 4.3.:** Bioreactor block system
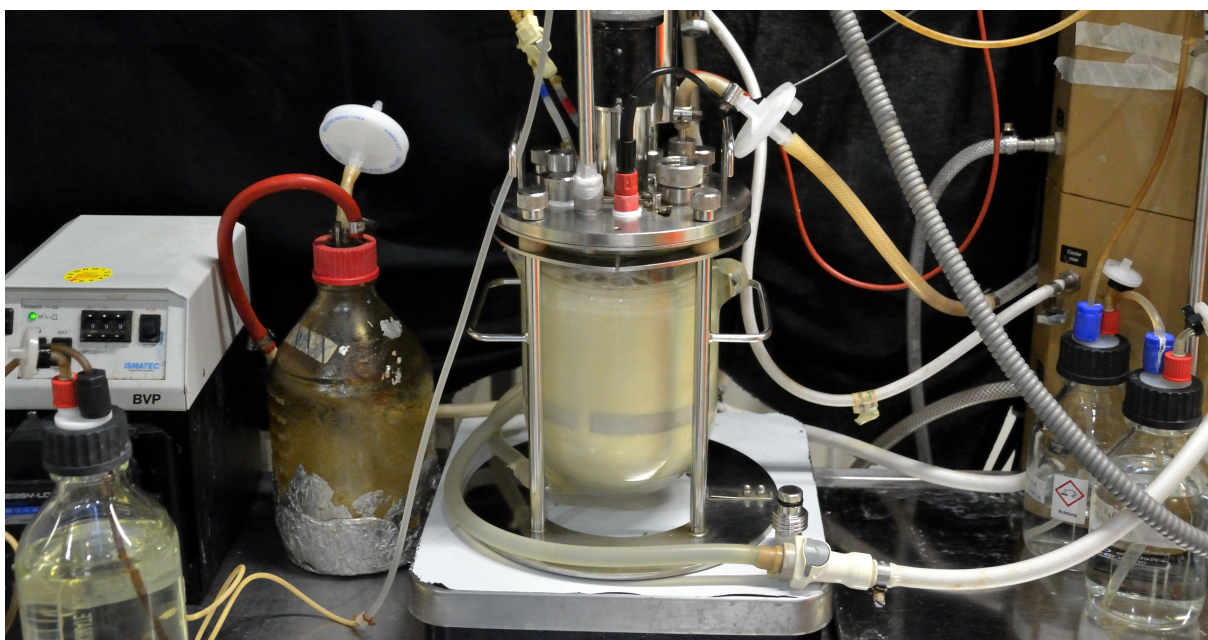
**Figure 4.4.:** Experimental setup for biotransformations at L-scale in a 1.5 L stirred-tank bioreactor

### 4.6.3. Biotransformations at L-scale

Biotransformations at L-scale were either performed in the 7.5 L stirred-tank bioreactor described in Chapter 4.4.2, or in a smaller, 1.5 L stirred-tank bioreactor with identical configuration (see Figure 4.4). The reaction volume amounted to 1 L and the stirrer speed was 1000 rpm. The aeration rate was 2 L min$^{-1}$, the temperature was adjusted to 30 °C or 37 °C, and the pH was controlled to pH 7. 5-mL samples were taken periodically.

### 4.6.4. Parallelized biotransformations at 0.4 L-scale

Parallelized biotransformations at 0.4 L-scale were performed in a parallel reactor system consisting of 4 glass stirred-tank reactors with a maximal working volume of 0.7 L (DASGIP, Eppendorf AG, see Figure 4.5), each equipped with 2 Rushton turbines. Temperature control was realized by a heating/cooling block in which the reactors were put in. Addition of acid (28 % $H_3PO_4$), base (25 % $NH_3$), glucose (500 g L$^{-1}$) and antifoam was realized by 16 individually controllable peristaltic pumps. Measurement of the exhaust gas composition was executed with the device BlueVary (BlueSens). The individual components of the system are listed in Table A.6. Biotransformations were conducted at a temperature of 37 °C, an aeration rate of 2 L min$^{-1}$, a set DO of 30 % regulated by the stirrer speed, and at pH 7. 5-mL samples were taken periodically.
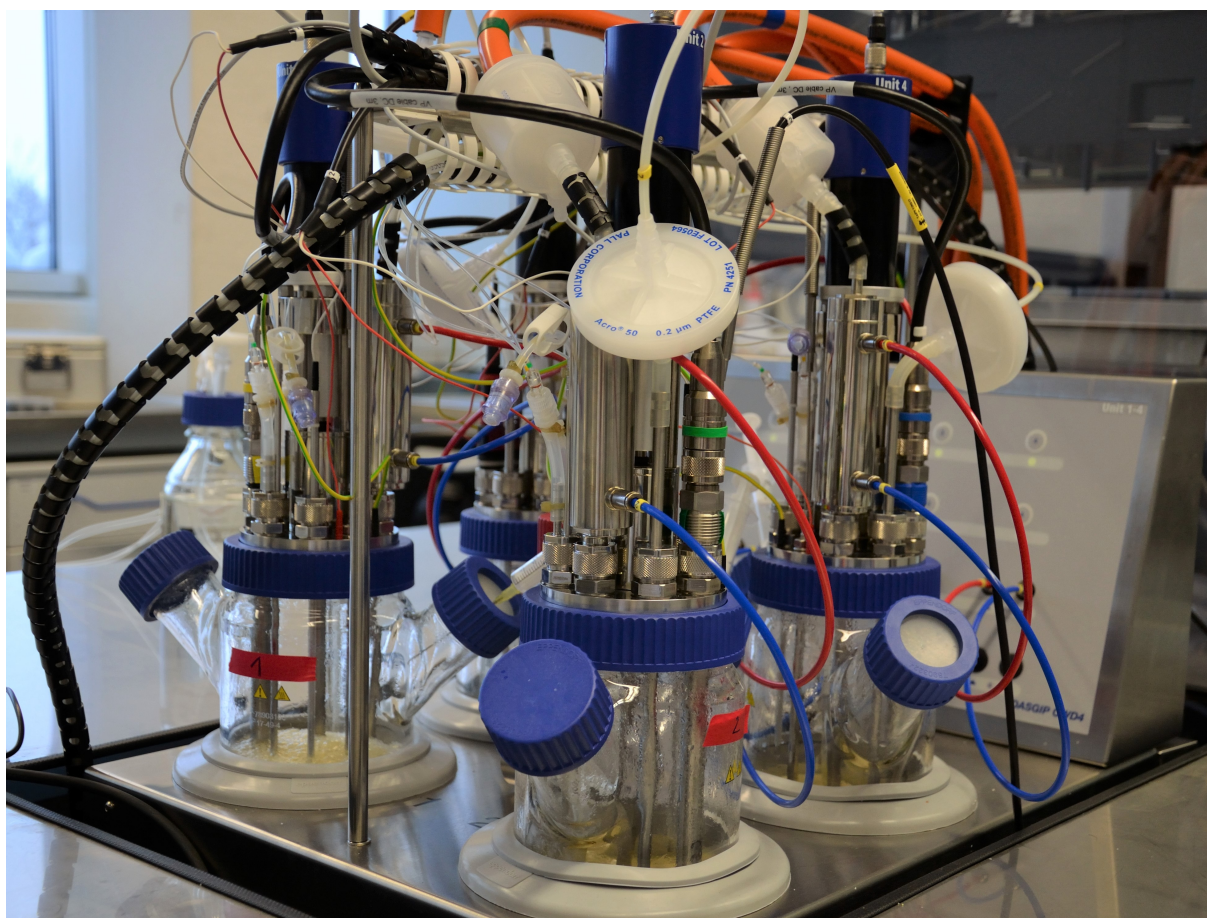
**Figure 4.5.:** Parallel stirred-tank reactor system for biotransformations at 0.4 L-scale

## 4.7. Characterization of whole-cell biocatalysts

### 4.7.1. Effect of freeze-thaw cycles

Investigations on the effect of freeze-thaw cycles on the biocatalytic activity were per-
formed in sealed glass vials with a maximal volume of 10 mL, which were mixed by
magnetic stir bars on a multistirrer plate. As a reference, freshly harvested biocatalysts
were used for the biotransformation; afterwards, one biotransformation was conducted
after each freeze-thaw cycle. First, the total required cell volume was harvested from a
high cell density cultivation process in a 50 mL centrifugation tube. For each freeze-thaw
cycle, the cells were then frozen at -20 °C for 70 min, and thawed for 20 min at room
temperature. The biotransformation systems with a total volume of 5 mL consisted of
20 % (v/v) isopropyl myristate in M9 mineral medium, 1 g L$^{-1}$ geraniol, 10 g L$^{-1}$ glucose
and 4 g L$^{-1}$ *E. coli* BL21(DE3)pLysS pET29a_VvGT14a. The reactions were performed
in triplicates at 30 °C and 500 rpm for 2 h. Afterwards, phases were separated (10 min,

3260 g) and the aqueous phase was used for HPLC analysis.

## 4.7.2. Reusability

Investigations on the reusability of the biocatalyst BL21(DE3)pLysS pET29a_VvGT14a were performed in the bioreactor block (see Chapter 4.2) with a reaction volume of 10 mL. The reaction systems consisted of 30 % (v/v) isopropyl myristate in M9 mineral medium, 0.2 g L$^{-1}$ geraniol, 10 g L$^{-1}$ glucose and 4 g L$^{-1}$ biocatalyst. Reactions were performed in triplicates at 30 °C and 2200 rpm for 18.5 h. After each biotransformation, the cells were separated from the liquid (3260 g, 10 min), resuspended in fresh M9 medium and used for the next biotransformation.

## 4.7.3. Effect of geranyl acetate and UDP on the whole-cell biocatalysts

To assess the effect of different geranyl acetate and UDP concentrations on the biotransformation of geraniol, parallelized biotransformations were conducted in the bioreactor block (see Chapter 4.2) with a reaction volume of 10 mL. The reaction systems consisted of 20 % (v/v) isopropyl myristate in M9 mineral medium, 0.4 g L$^{-1}$ geraniol, 20 g L$^{-1}$ glucose and 6 g L$^{-1}$ *E. coli* BL21(DE3)pLysS pET29a_VvGT14a. Additionally, different amounts of geranyl acetate (0.1/0.2/0.4/0.6/0.8 g L$^{-1}$) and UDP (100/300/600/800/1200 μM) were added. Reactions were performed in triplicates at 30 °C and 2200 rpm for 24 h.
To investigate the effect of geranyl acetate on the viability of the biocatalyst BL21(DE3) pLysS pET29a_VvGT14a, the biocatalyst was incubated with different amounts of geranyl acetate. In 250 mL shake flasks, 0.1–0.8 g L$^{-1}$ geranyl acetate were added to 50 mL LB medium containing 100 μL cryostock and 0.03 g L$^{-1}$ kanamycin. The flasks were incubated at 37 °C and 250 rpm for 7 h and the OD$_{600}$ was measured regularly. A control without geranyl acetate was run in parallel. Reactions were performed in duplicates.

## 4.7.4. Biocatalytic activity of cell lysate

To analyze the activity of cell lysate, 10-mL samples were taken at defined points in time from high cell density cultivations (see Chapter 4.4.2) of the strain BL21(DE3)pLysS pET29a_VvGT14a. The samples were transferred to pre-weighed 15-mL centrifugation tubes and centrifuged at 3260 g and 4 °C for 20 min. Afterwards, the wet weight of the resulting cell pellet was determined and 1 g of the cell pellet was transferred to a 50-mL centrifugation tube. After dissolving the pellet in 5 mL 1 M Tris buffer, 50 μL

phenylmethylsulfonyl fluoride were added to inhibit proteolytic degradation of intracellular proteins. The cells were lysed ultrasonically (5 min, cycles: 5 x 50 %) and centrifuged subsequently (16,249 g, 4 °C, 30 min). The supernatant was then used as the cell lysate in an activity assay. Reactions were performed in triplicate in micro reaction tubes, with the reaction composition shown in Table 4.1.

**Table 4.1.:** Layout of the biocatalytic assay with cell lysate

| Component | Volume, µL |
| --- | --- |
| Cell lysate | 50 |
| 1 M Tris, pH 7.5 | 20 |
| 20 mM UDP-glucose | 5 |
| 60 mM geraniol in DMSO | 2 |
| Demineralized water | 123 |

The tubes were incubated at 500 rpm and 30 °C for 1 h, and subsequently at 75 °C for 15 min. Then, the samples were centrifuged at 16,249 g for 5 min. The supernatant was transferred into a fresh reaction tube and centrifuged again. Afterwards, 100 µl of the fresh supernatant were used for HPLC analysis.

### 4.7.5. Conversion of different alcoholic substrates

The two strains *E. coli* BL21(DE3) and *E. coli* BL21(DE3)pLysS were compared regarding their capacity to esterify different alcoholic substrates. First, the strains were grown overnight at 30 °C and 200 rpm in test tubes containing 4.9 mL modified LB medium, 100 µL cryostock and, for BL21(DE3)pLysS, 0.034 g L$^{-1}$ chloramphenicol. Afterwards, the entire content of the tubes was transferred to 1 L shake flasks containing 242 mL modified LB medium, 6 g L$^{-1}$ glucose, and, for BL21(DE3)pLysS, 0.034 g L$^{-1}$ chloramphenicol. The flaks were incubated for 7 h at 37 °C and 250 rpm. Afterwards, the cells were harvested (3260 g, 10 min) and resuspended in M9 mineral medium.

For each strain, 6 g L$^{-1}$ of cells were used for the inoculation of 10 mL-systems in the bioreactor system (see Chapter 4.2), consisting of 20 % organic phase in M9 mineral medium with 10 g L$^{-1}$ glucose and 1 mM of the substrates chloramphenicol, benzyl alcohol, 2-phenylethanol, vanillin, geraniol and linalool. For the substrates benzyl alcohol, 2-phenylethanol and vanillin, oleyl alcohol was used as the organic phase, whereas isopropyl myristate was used for geraniol and linalool. Chloramphenicol was the only substrate applied in a single-phase aqueous system. Reactions were conducted in triplicate at 30 °C

and 2200 rpm for 15 h. Afterwards, phases were separated by centrifugation (3260 g, 10 min) and analyzed by HPLC.

## 4.8. Analytical methods

### 4.8.1. Determination of optical density and cell dry weight concentration

**Optical density.**   The optical density of cell suspensions was determined photometrically at 600 nm. As the linearity range of the photometer was 0.05–0.3, samples had to be diluted accordingly with PBS. PBS was also used as a blank. Measurements were executed in semi-micro cuvettes.

**Cell dry weight concentration.**   For the determination of the cell dry weight concentration, micro reaction tubes were dried at 80 °C for 24 h and weighed afterwards. The samples were transferred to the tubes and centrifuged at 16,249 g for 10 min. After removal of the supernatants, the pellets were dried at 80 °C for 48 h and subsequently weighed. The cell dry weight concentration was calculated with the following equation:

$$c_X = \frac{m_1 - m_0}{V_{Sample}} \tag{4.1}$$

$c_X$   Cell dry weight concentration, g L$^{-1}$
$m_1$   Mass of the micro reaction tube containing the dried cell pellet, g
$m_0$   Mass of the empty dried micro reaction tube, g

### 4.8.2. pH measurement

The pH of samples was either measured with a regular pH probe (Lab 870, Schott Instruments) or with a micro pH probe for small sample sizes (Lab 850, Schott Instruments). Two-point calibrations were performed prior to probe use.

### 4.8.3. Quantification of extracellular metabolites

**Glucose.**   In order to quantify glucose concentrations in samples, an enzymatic glucose assay was used. The assay kit consisted of Solution 1 (nicotinamide adenine dinucleotide phosphate ($NADP^+$) and adenosine-5'-triphosphate (ATP) in triethanolamine buffer with pH 7.6, and $MgSO_4$), Suspension 2 (320 U hexokinase and 160 U glucose-6-phosphate

dehydrogenase (G6P-DH)) and a glucose assay control solution (0.5 g L$^{-1}$). The control solution was used for the preparation of five standard solutions (0.025, 0.05, 0.1, 0.2 and 0.3 g L$^{-1}$) with demineralised water. Samples were diluted with demineralized water in order to lie in the concentration range of the standard solutions.

Measurements were conducted in microtiter plates according to the assay layout depicted in Table 4.2.

**Table 4.2.:** Layout of the enzymatic glucose assay

| Step | Description | Volume, µL |
|------|-------------|------------|
| 1 | Solution 1 | 50 |
| 2 | Blank/Standard solution/Sample | 20 |
| 3 | Demineralized water | 60 |
| 4 | Mixing, 3 min incubation | |
| 4 | Determination of the extinction $E_1$ at 340 nm | |
| 5 | Suspension 2 | 20 |
| 6 | Mixing, 15 min incubation | |
| 7 | Determination of the extinction $E_2$ at 340 nm | |

Following reactions occur:

$$\text{Glucose} + \text{ATP} \xrightarrow{\text{Hexokinase}} \text{Glucose–6-phosphate} + \text{ADP}$$

$$\text{Glucose–6-phosphate} + \text{NADP}^+ \xrightarrow{\text{G6P-DH}} \text{6-Phosphogluconate} + \text{NADPH}^+$$
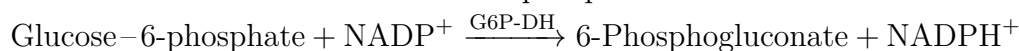
The amount of released NADPH$^+$ is stoichiometrical to the glucose initially present in the system, thus the extinction of NADPH$^+$ at 340 nm can be used as the measurand. With the following equation the extinction difference $\Delta E$ can be calculated:

$$\Delta E = (E_1 - E_2)_{Sample} - (E_1 - E_2)_{Blank} \tag{4.2}$$

By plotting the $\Delta E$ of the standard solutions against their concentrations, a calibration curve was obtained, which allowed the calculation of glucose concentrations in the samples.

For a more rapid determination of the glucose concentration, a glucose measurement device (ACCU-CHEK Comfort, Roche) with the corresponding test strips (GlucoCheck Excellent, aktivmed GmbH) was used. ~1 µL of the sample, if necessary diluted in order to lie in the linearity range of 0.1–6 g L$^{-1}$, was pipetted on the test strip.

**Acetate.** As for glucose, an enzymatic assay kit was used for the quantification of acetate. The assay kit contained Solution 1 (triethanolamine buffer with L-malic acid and

MgCl), Solution 2 (ATP, CoA and NAD$^+$), Solution 3 (1100 U L-malate dehydrogenase (M-DH), 270 U citrate synthase (CS)), Solution 4 (5 U acetyl-CoA synthetase (ACS)) and an acetic acid control solution (0.149 g L$^{-1}$). With the control solution and demineralized water, four additional standard solutions (0.0745, 0.03725, 0.00745, 0.00149 g L$^{-1}$) were prepared. Samples were diluted with demineralized water in order to fall into the concentration range of the calibration curve.

Measurements were conducted in microtiter plates according to the assay layout depicted in Table 4.3.

**Table 4.3.:** Layout of the enzymatic acetate assay

| Step | Description | Volume, µL |
|---|---|---|
| 1 | Solution 1 | 70 |
| 2 | Solution 2 | 12 |
| 3 | Blank/Standard solution/Sample | 20 |
| 4 | Demineralized water | 58 |
| 5 | Mixing, determination of the extinction $E_0$ at 340 nm | |
| 6 | Solution 3 | 20 |
| 7 | Mixing, 3 min incubation | |
| 8 | Determination of the extinction $E_1$ at 340 nm | |
| 9 | Solution 4 | 20 |
| 6 | Mixing, 20 min incubation | |
| 7 | Determination of the extinction $E_2$ at 340 nm | |

Following reactions occur:

$$\text{Acetate} + \text{CoA} + \text{ATP} \xrightarrow{\text{ACS}} \text{Acetyl-CoA} + \text{AMP} + \text{PP}_i$$
$$\text{L-Malate} + \text{NAD}^+ \xrightarrow{\text{M-DH}} \text{Oxaloacetic acid} + \text{NADH}^+$$
$$\text{Acetyl-CoA} + \text{Oxaloacetic acid} + \text{H}_2\text{O} \xrightarrow{\text{CS}} \text{Citrate} + \text{CoA}$$
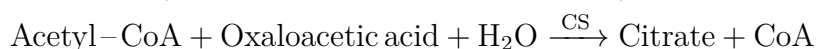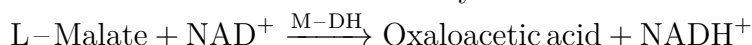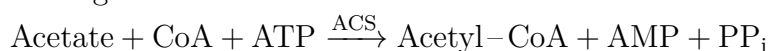
The amount of released NADH$^+$ is stoichiometrical to the acetate initially present in the system, thus the extinction of NADH$^+$ at 340 nm can be used as the measurand. With the following equation the extinction difference $\Delta$E can be calculated, with values indexed with $S$ referring to the sample, and values indexed with $B$ referring to the blank:

$$\Delta E = [(E_1 - E_2)_S - \frac{(E_1 - E_0)_S^2}{(E_2 - E_0)_S}] - [(E_1 - E_2)_B - \frac{(E_1 - E_0)_B^2}{(E_2 - E_0)_B}] \tag{4.3}$$

By plotting the $\Delta$E of the standard solutions against their concentrations, a calibration curve was obtained, which allowed the calculation of the acetate concentrations in the samples.

### 4.8.4. Quantification of intracellular UDP-glucose and UDP

**Sampling.** Both UDP-glucose and its metabolite UDP were quantified intracellulary in order to get a better understanding of the regeneration of UDP-glucose during the biotransformation of geraniol. For this purpose, biotransformations were executed at mL-scale as described in Chapter 4.6. Sampling was conducted by quickly transferring the total content of a reactor to a 50 mL centrifugation tube filled with 20 mL triethanolamine (30 mM, pH 7) temperated to 95 °C. After incubating the sample at 95 °C for precisely 5 min, the tube was centrifuged at 4 °C and 3260 g for 10 min. The resulting aqueous phase was split in six equal parts and the subsamples were mixed with increasing amounts of UDP-glucose and UDP as internal standards, resulting in final known concentrations of 0, 1.25, 5, 25, 35 and 50 µM (see Table 4.4). Subsequently, the mixtures were transferred to LC vials. The internal standard method guarantees that the standard substance is exposed to the same sample matrix as the metabolite that is to be measured in the sample. That way, standard and metabolite experience the same degree of absorptive loss and/or degradation [Bennett et al. 2009; Deutsches Institut für Normung 1998].

**Table 4.4.:** Preparation of internal standards for intracellular UDP-glucose and UDP quantification

|                          | Concentration internal standard, µM | | | | | |
|--------------------------|-------|-------|-----|-----|-----|-----|
|                          | 0     | 1.25  | 5   | 25  | 35  | 50  |
| Sample, µL               | 500   | 500   | 500 | 500 | 500 | 500 |
| $H_2O$, µL               | 500   | 487.5 | 450 | 250 | 150 | 0   |
| 0.2 mM UDP, µL           | 0     | 6.25  | 25  | 125 | 175 | 250 |
| 0.2 mM UDP-glucose, µL   | 0     | 6.25  | 25  | 125 | 175 | 250 |

**LC-MS measurements.** To quantify UDP and UDP-glucose in the prepared samples, an ultrahigh performance liquid chromatography-tandem mass spectrometry (LC-MS) method, as described by Buescher et al. [2010], was applied. First, the compounds were separated with the column Acquity UPLC HSS T3 (Waters Corporation) at 40 °C. A binary gradient was used with Eluent A consisting of 10 mM tributylamine, 15 mM acetic acid and 5 % (v/v) methanol, and Eluent B consisting of 100 % isopropyl (see Table A.7 for the gradient profile). The injection volume amounted to 20 µL.

The ionization of the analytes was achieved by electrospray ionization with nitrogen as sheath gas and argon as auxiliary gas. A triple quadrupole mass spectrometer (TSQ Vantage, Thermo Scientific) was used to detect the negatively charged ions. The software Xcalibur 2.2 (Thermo Fisher Scientific) was used for peak integration and data analysis.

Besides from the prepared samples, 100 µM pulses of UDP and UDP-glucose were injected separately in order to determine their most distinct mass to charge ratios. These were 403 m z$^{-1}$ and 565 m z$^{-1}$, respectively.

The individual components of the LC-MS system are listed in Table A.8.

**Calculation of intracellular concentrations.** The peak areas of one internal standard series (and thus one sample) were plotted against the known UDP or UDP-glucose concentrations. By linear regression calibration curves were created. The analyte's concentration $c_A$ in the sample was calculated from the ratio of the curve's axis intercept and its slope [Deutsches Institut für Normung 1998]. In order to calculate the intracellular concentration, cell dry weights were determined in reactors operated under identical conditions as the sampled reactors. With an intracellular aqueous volume of 1.9 mL g$^{-1}$ for *E. coli* BL21(DE3), as proposed by L. Wang et al. [2013], the total cellular volume $V_X$ in one sample was calculated. By considering the dilution of the aqueous reaction volume by the triethanolamine buffer (20 mL), the intracellular concentration $c_{A,intra}$ was calculated:

$$c_{A,intra} = \frac{c_A}{V_X} \cdot 20 \ mL \tag{4.4}$$

## 4.8.5. Protein detection and quantification

SDS-PAGE (Sodium Dodecyl Sulfate PolyAcrylamide Gel Electrophoresis) was used to detect VvGT14a in cell samples.

For internal comparison of samples on one gel, they were adjusted to an optical density of 2.5 with PBS prior to the electrophoresis. To 100 µL of each sample 20 µL 5x Laemmli buffer were added, and the mixture was incubated at 95 °C for 5 min. The high temperature results in protein denaturation, and 2-Mercaptoethanol, contained in the Laemmli buffer, cleaves disulfid bridges. The negatively charged component sodium dodecyl sulfate contained in the buffer binds to the denatured protein and covers it with a negative charge proportional to the protein's molecular weight. This allows for separation of the proteins based on their molecular mass [Laemmli 1970].

Two different polyacrylamide gel types were used for the electrophoresis: a stacking gel and a separating gel. Both were prepared by polymerization of acrylamide/bis-acrylamide triggered by the addition of ammonium persulfate and tetramethylethylenediamine. The gel compositions are shown in Table 4.5.

4 mL separating gel were pured between two glass plates separated by spacers. After curing, it was covered with 2.5 mL of the stacking gel and a sample comb was inserted

**Table 4.5.:** Composition of stacking and separating gel for SDS-PAGE

| Component | Stacking gel | Separating gel |
|---|---|---|
| Acrylamide/bis-acrylamide 3 % | 5 mL | - |
| Acrylamide/bis-acrylamide 12.5 % | - | 10 mL |
| Ammonium persulfate | 100 µL | 100 µL |
| Tetramethylethylenediamine | 10 µL | 10 µL |

into the gel. After full polymerization and removal of the comb, 5 µL of the samples were loaded into the gel pockets. As a reference, the molecular-weight size marker JustBlue in 10 % TRIS-glycine (Nippon Genetics) was loaded on the gel. After transferring the gel to a gel chamber filled with SDS running buffer, electrophoresis was run at 35 mA and 300 V for 1 h. Due to their negative charge, proteins migrate from the cathode towards the anode, with their migration speed depending on their molecular weight. After the electrophoresis, the gel was stained with heated Fairbanks A and Fairbanks B solution for 5 min, respectively, and destained with 10 % acetic acid for 5 min [Fairbanks et al. 1971]. The concentration of protein bands was determined densitometrically. Hereby, 5 µL of BSA (bovine serum albumin) samples with known concentrations of 0.025, 0.125 and 0.25 g $L^{-1}$ were loaded to the gel and after electrophoresis, the BSA band intensities were determined with the software ImageJ. After creating a calibration curve, the intensities of the target protein bands could be related to their concentration.

### 4.8.6. High-performance liquid chromatography

Geraniol, geranyl acetate and geranyl glucoside were quantified by high-performance liquid chromatography (HPLC). The individual components of the HPLC system are listed in Table A.9. An Accucore C18 column (particle size 2.6 µm; 100 × 4.6 mm; Thermo Fisher Scientific) with a column temperature of 25 °C was used for analyte separation. Detection of the analytes was based on ultraviolet absorbance at 210 nm. The flow rate amounted to 0.8 mL $min^{-1}$, the injection volume was 1 µL. A binary gradient system using water as Eluent A and 100 % acetonitrile as Eluent B was applied. The gradient course was the following: 0–3 min 3-15 % B, 3-5 min 15-50 % B, 5-7 min 50-70 % B, 7-10 min 70-100 % B, 10-11 min 100 % B, 11-12 min 100-3 % B. The column was equilibrated for 2 min prior to each injection. External standards were used for the calculation of geraniol, geranyl acetate and geranyl glucoside concentrations in the samples.

For the quantification of the alcoholic compounds used in Chapter 4.7.5 and their respective esters, the identical measurement method was used, however partly with a UV

wavelength of 280 nm instead of 210 nm. The detection wavelengths and elution times
of all compounds, including geraniol, geranyl acetate and geranyl glucoside, are listed in
Table 4.6.

**Table 4.6.:** HPLC detection wavelengths and elution times of different analytes used in this work

| Analyte | Detection wavelength, nm | Elution time, min |
|---|---|---|
| Geraniol | 210 | 8.6 |
| Geranyl acetate | 210 | 10.5–10.6 |
| Geranyl glucoside | 210 | 6.9–7.0 |
| Chloramphenicol | 280 | 6.8 |
| Chloramphenicol acetate | 280 | 7.5 |
| Benzyl alcohol | 210 | 6.2 |
| Benzyl acetate | 210 | 8.1 |
| 2-Phenylethanol | 210 | 6.8 |
| 2-Phenylethyl acetate | 210 | 8.4 |
| Vanillin | 280 | 6.2 |
| Vanillin acetate | 210 | 7.3 |
| Linalool | 210 | 8.8 |
| Linalyl acetate | 210 | 10.6 |

For F&F compounds involved in the study on a generalized approach for the selection
of biphasic systems, a different HPLC method and device was applied. Benzyl alcohol,
2-phenylethanol, raspberry ketone, vanillin, benzaldehyde, 2-phenylethyl acetate, $(S)$-
limonene, geraniol, linalool and 6-pentyl-$\alpha$-pyrone were quantified with the HPLC device
ProStar (Varian), using a Viva C18 column (particle size 5 µm; 150 x 4.6 mm; Restek)
kept at 60 °C, and UV detection. The flow rate amounted to 1 mL min$^{-1}$, the injection
volume was 10 µL. A binary gradient system consisting of water (solvent A) and 100
% acetonitrile (solvent B) was applied. For benzyl alcohol, 2-phenylethanol, raspberry
ketone and benzaldehyde, the following gradient course was used: 0-1 min 30 % B, 1-3
min 30-100 % B, 3-3.5 min 100 % B, 3.5-4 min 100-30 % B, then 1 min equilibration
time. For vanillin, the following gradient course was used: 0-2.5 min 30 % B, 2.5-3.5 min
30-100 % B, 3.5-4 min 100-30 % B, then 1 min equilibration time. 2-Phenylethyl acetate
was eluted isocratically (50 % acetonitrile) for 6 min, with 1 min equilibration time. For
$(S)$-limonene, geraniol, linalool and 6-pentyl-$\alpha$-pyrone, the following gradient course was

used: 0-1 min 30 % B, 1-3 min 30-100 % B, 3-5 min 100 % B, 5-7 min 100-30 % B, followed by 2 min equilibration time. External standards were used for the calculation of the target compound concentrations in the samples. All wavelengths used for detection and the elution times for the different compounds can be found in Table 4.7.

### 4.8.7. Gas chromatography

Certain F&F compounds involved in the study on a generalized approach for the selection of biphasic systems were quantified by GC (gas chromatography). These were 3-methylbutanol, 2-heptanone, acetoin, isobutyraldehyde, isobutyl acetate, butyl butyrate and $(R)$-$\gamma$-decalactone. The devide 450-GC (Varian) equipped with a Rtx-502.2 column (particle size: 1.4 µm; 30 m x 0.25 mm; Restek) and a flame ionization detector were applied. The carrier gas helium was used at a flowrate of 2.2 mL min$^{-1}$. Nitrogen, hydrogen and air flowrates amounted to 25, 30 and 300 mL min$^{-1}$, respectively. The injection volume amounted to 0.5 µL. Except for the analysis of $(R)$-$\gamma$-decalactone, the injector was kept at 215 °C, the detector at 250 °C and the oven temperature was ramped up from 35 to 215 °C with a rate of 40 °C min$^{-1}$, with an overall run time of 5.5 min and an equilibration time of 2 min. For the quantification of $(R)$-$\gamma$-decalactone, the injector was kept at 250 °C, the detector at 300 °C and the oven temperature was ramped up from 35 to 250 °C with a rate of 40 °C min$^{-1}$, with an overall run time of 6.5 min and an equilibration time of 2 min. External standards were used for the calculation of the target compound concentrations in the samples. The elution times for the different compounds are listed in Table 4.7.

**Table 4.7.:** Quantification of F&F compounds by GC and HPLC: Detection wavelenghts and elution times.

| Compound | Quantified by | Wavelength, nm | Elution time, min |
|---|---|---|---|
| Benzyl alcohol | HPLC | 215 | 2.8 |
| 2-Phenylethanol | HPLC | 215 | 3.2 |
| Raspberry ketone | HPLC | 215 | 3.2 |
| Vanillin | HPLC | 215 | 1.7 |
| Benzaldehyde | HPLC | 215 | 4.3 |
| 2-Phenylethyl acetate | HPLC | 220 | 4.0 |
| $(S)$-Limonene | HPLC | 210 | 7.4 |
| Geraniol | HPLC | 210 | 5.8 |
| Linalool | HPLC | 210 | 5.9 |
| 6-Pentyl-$\alpha$-pyrone | HPLC | 210 | 5.7 |
| 3-Methylbutanol | GC | - | 3.8 |
| 2-Heptanone | GC | - | 4.6 |
| Acetoin | GC | - | 3.8 |
| Isobutyraldehyde | GC | - | 3.0 |
| Isobutyl acetate | GC | - | 4.0 |
| Butyl butyrate | GC | - | 5.0 |
| $(R)$-$\gamma$-decalactone | GC | - | 5.8 |

# 5. Process development for the production of whole-cell biocatalysts

In order to provide active *E. coli* BL21(DE3)pLysS pET29a_VvGT14a whole-cell biocatalysts expressing the glycosyltransferase VvGT14a for subsequent biotransformations of geraniol, a high cell density cultivation process had to be developed. As a starting point, the process described by Schmieder et al. [2016b] was used, where a cell dry weight concentration of $67.6 \pm 1.2$ g L$^{-1}$ and a VvGT14a concentration of $2.7 \pm 0.1$ g L$^{-1}$ was obtained within 48 h. After a 21 hour-long growth phase at 37 °C with the specific growth rate set to 0.20 h$^{-1}$, VvGT14a expression was induced with 0.1 mM IPTG and conducted for 27 hours at 20 °C (see Figure 5.1).

As both the IPTG concentration and the post-induction feeding profile can have major impacts on recombinant protein expression (see Chapter 3.3.3), the effect of both parameters on cell growth and protein production was investigated in the following. The major goal was a further increase in the VvGT14a concentration.
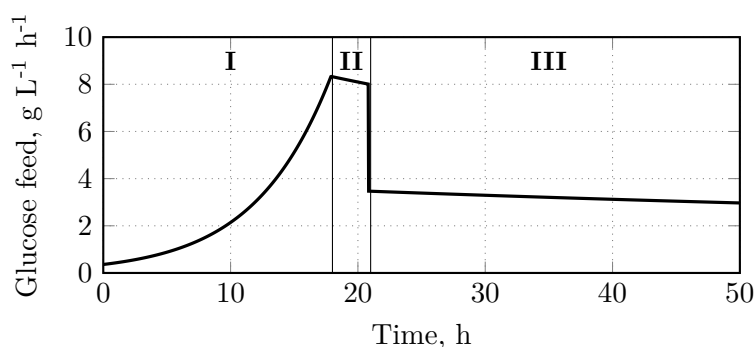


**Figure 5.1.:** Glucose feeding profile for the high cell density cultivation of *E. coli* BL21(DE3)pLysS pET29a_VvGT14a at L-scale in a stirred tank reactor, as described by Schmieder et al. [2016b]. The growth phase is executed at a temperature of 37 °C and is divided into two sections: The 18 hour-long exponential feeding phase (**I**) with $\mu_{set} = 0.20$ h$^{-1}$ is followed by a 3 hour-long constant feeding phase (**II**). At 21 hours, the temperature is lowered to 20 °C and VvGT14a expression is induced by the addition of 0.1 mM IPTG. Protein expression is conducted for 27 hours with glucose being fed to the reactor with a constant rate of 3.9 g L$^{-1}$ h$^{-1}$ (**III**). The effective rate decreases due to a dilution effect caused by an increase in reactor volume.

## 5.1. IPTG concentration

First, the impact of the IPTG concentration on both cell growth and VvGT14a production was investigated. For this purpose, high cell density cultivations were performed at L-scale in a stirred tank bioreactor under the conditions described by Schmieder et al. [2016b]. However, the specific growth rate during the exponential feeding phase was reduced from 0.20 $h^{-1}$ to 0.18 $h^{-1}$, as up to 0.9 g $L^{-1}$ acetate accumulated when applying the higher growth rate (data not shown). Moreover, the process time was increased to 68 hours in order to analyze the effect of a longer protein production phase. Three different IPTG concentrations (0.05, 0.1 and 0.2 mM) were compared. Figure 5.2 shows the courses of the dissolved oxygen (DO), and of the cell dry weight, glucose and acetate concentrations.

Prior to induction, all three process variants show comparable cell growth and thus DO courses. However, after induction, the cultivation with 0.2 mM IPTG deviates from the other two: Whereas the processes using 0.05 and 0.1 mM IPTG result in a final cell dry weight of about 80 g $L^{-1}$, the biomass in the third cultivation reaches a final concentration of 115.6 ± 1.2, coming along with a distinct decrease in oxygen saturation. All three processes run under glucose-limiting conditions after ~5 hours. For the experiments with 0.05 and 0.1 mM IPTG, acetate levels remain below 0.2 g $L^{-1}$, whereas up to 0.6 g $L^{-1}$ acetate are formed with the third process variant.

Table 5.1 summarizes the final cell dry weight concentrations of the three processes. Moreover, it compares the biomass yield coefficients, the densitometrically determined VvGT14a concentrations and the protein yield coefficients at 48 h and 68 h of process time. The cultivations with 0.05 mM and 0.1 mM IPTG result in very similar biomass yield coefficients of 0.45–0.46 g $g^{-1}$, which remain constant between 48 h and 68 h. The biomass yield coefficient in the process using 0.2 mM IPTG is ~11 % higher than in the other two processes, with the value again remaining constant throughout the cultivation. For the experiment with 0.05 mM IPTG, VvGT14a could only be quantified at 48 h of process time resulting in a value of 0.7 ± 0.1 g $L^{-1}$, as afterwards the bands of the target protein were not distinct enough to be analyzed densitometrically (SDS-PAGE gels not shown). The same was true for the process with 0.2 mM IPTG, however, in that case for both 48 h and 68 h of process time. In contrast, VvGT14a could be quantified properly at both points in time for the cultivation with 0.1 mM IPTG, resulting in values of 5.0 ± 0.2 and 5.5 ± 0.5 g $L^{-1}$, respectively.
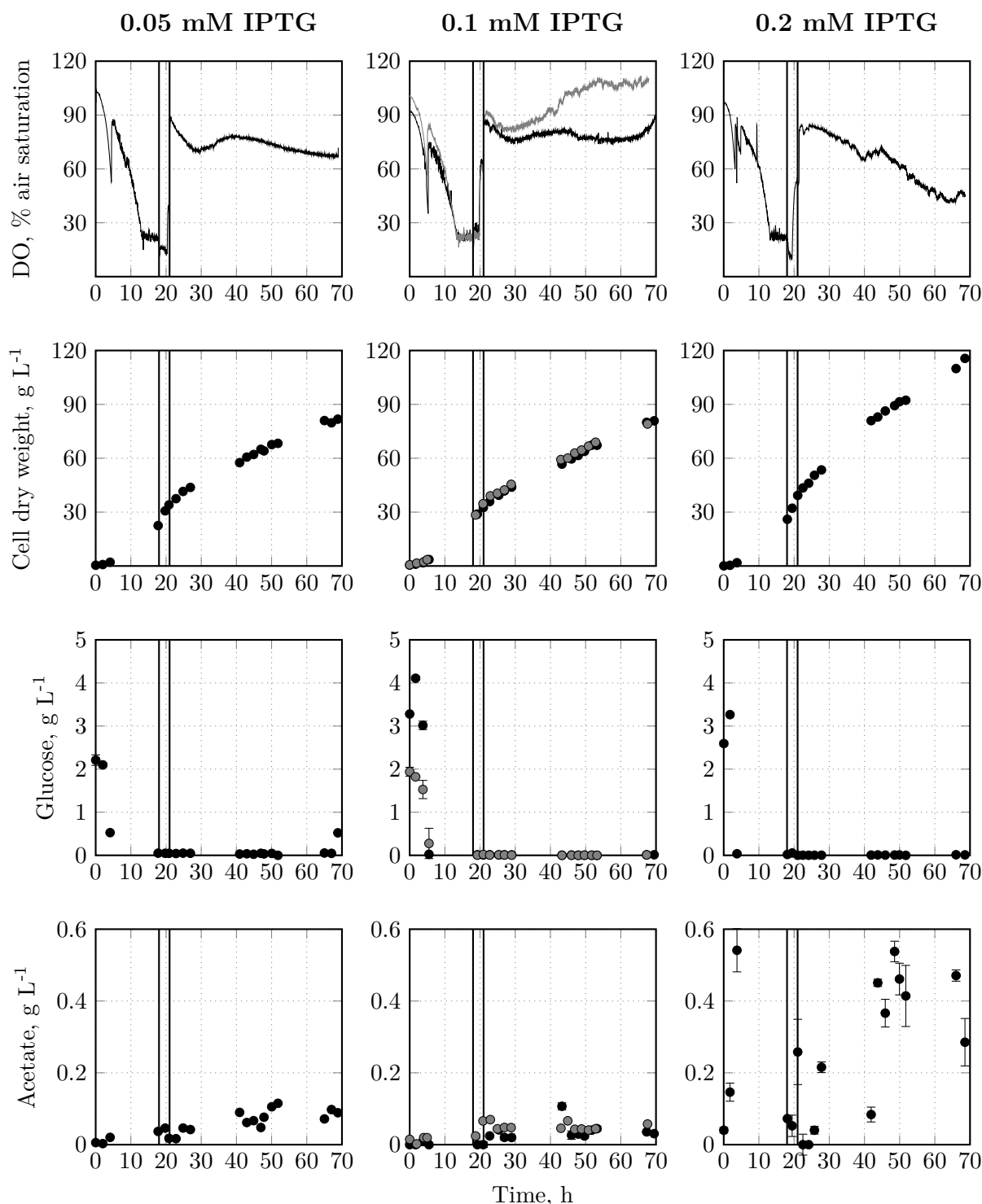
**Figure 5.2.:** Courses of dissolved oxygen (DO), cell dry weight, glucose and acetate concentrations
during high cell density cultivations of *E. coli* BL21(DE3)pLysS pET29a_VvGT14a using
three different IPTG concentrations for induction of VvGT14a production (0.05, 0.1 and
0.2 mM). Duplicated data series are depicted in gray. Fed-batch cultivations were performed
in a stirred tank bioreactor at 2 L-scale. Biomass production phase: 37 °C, exponential
glucose feeding ($\mu_{set} = 0.18$ h$^{-1}$) for 18 hours, followed by constant feeding (8.75 g L$^{-1}$ h$^{-1}$) for
3 hours. Protein production phase: 20 °C, induction with variable IPTG concentrations,
constant post-induction feeding rate of 3.9 g L$^{-1}$ h$^{-1}$. The different process phases are
separated by vertical black lines.

**Table 5.1.:** Final cell dry weight concentrations, biomass yield coefficients ($Y_{XS}$), VvGT14a concentrations and specific productivities ($Y_{PX}$) after high cell density cultivations of *E. coli* with different IPTG concentrations. Cells marked with a dash indicate that the respective values could not be measured/calculated.

| State variable | Process time, h | IPTG, mM | | |
| --- | --- | --- | --- | --- |
| | | 0.05 | 0.1 | 0.2 |
| Cell dry weight, g $L^{-1}$ | 48 | $64.1 \pm 1.3$ | $61.6 \pm 0.1$ | $89.3 \pm 1.6$ |
| | 68 | $81.8 \pm 1.1$ | $80.9 \pm 1.2$ | $115.6 \pm 1.2$ |
| $Y_{XS}$, g $g^{-1}$ | 48 | 0.46 | 0.45 | 0.50 |
| | 68 | 0.45 | 0.45 | 0.50 |
| VvGT14a concentration, g $L^{-1}$ | 48 | $0.7 \pm 0.1$ | $5.0 \pm 0.2$ | - |
| | 68 | - | $5.5 \pm 0.5$ | - |
| $Y_{PX}$, g $g^{-1}$ | 48 | 0.011 | 0.081 | - |
| | 68 | - | 0.068 | - |

## 5.2. Post-induction feeding profile

As a second variable, the post-induction feeding profile was investigated regarding its impact on cell growth and VvGT14a expression. High cell density cultivations were performed as described by Schmieder et al. [2016b], however, a reduced set growth rate of 0.18 h$^{-1}$ during the exponential growth phase was applied again. The processes lasted 68 h and protein expression was induced with 0.1 mM IPTG. In addition to the feeding profile shown earlier in Figure 5.1, where glucose is fed at a constant rate of 3.9 g L$^{-1}$ h$^{-1}$ after induction with IPTG, two linear post-induction feeding profiles were investigated. These profiles also start with a rate of 3.9 g L$^{-1}$ h$^{-1}$, but include a linear gradient of 0.075 g L$^{-1}$ h$^{-2}$ and 0.150 g L$^{-1}$ h$^{-2}$, respectively. The three profiles are shown in Figure 5.3, and will be referred to with Profile 1, 2 and 3 in the following. Figure 5.4 shows the courses of the DO, and of the cell dry weight, glucose and acetate concentrations. The data for Profile 1 is identical with the data for 0.1 mM IPTG shown in Chapter 5.1.

The DO courses prior to induction are very similar for the three processes. After induction, the DO decreases the more, the more glucose is fed to the cultivation medium, reaching values smaller than 25 % with Profile 3. The cells in the experiments with Profile 2 and 3 show identical growth behavior, with the final cell dry weight concentrations
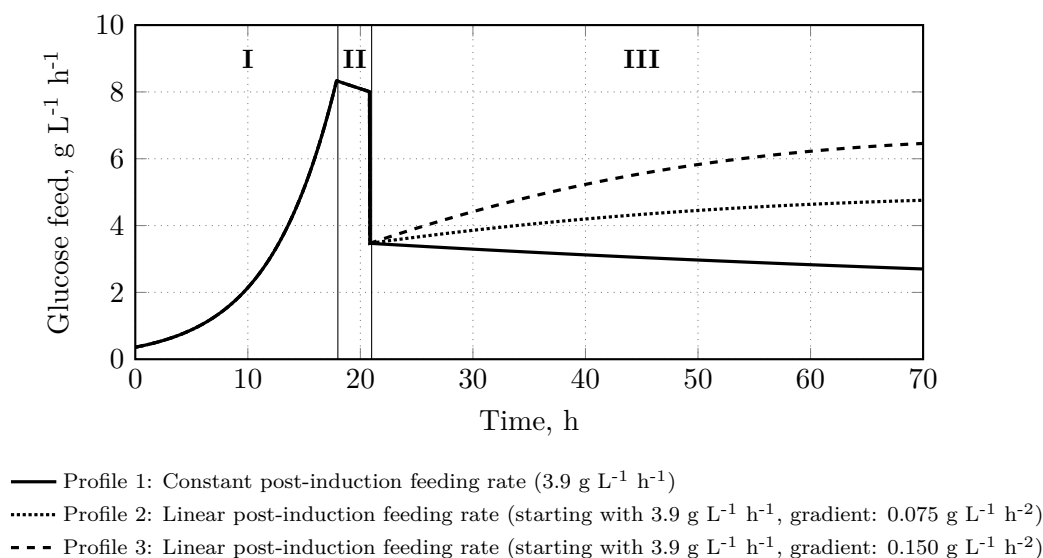
**Figure 5.3.:** Comparison of different post-induction feeding profiles for high cell density cultivations.

being ~16 % higher than with Profile 1. The provided batch glucose is consumed within ~6 hours in all three processes, and the substrate remains constantly limiting afterwards. Whereas the acetate concentration remains notedly below 0.2 g $L^{-1}$ for the cultivation with Profile 1, the metabolite accumulates to up to 0.2 g $L^{-1}$ between 20 h and 24 h during the process with Profile 2, followed by a partial degradation. For the experiment with Profile 3, acetate accumulates rather towards the end of the process, with the concentrations still remaining below 0.2 g $L^{-1}$ though.

Table 5.2 summarizes the final biomass concentrations obtained with the three different processes and shows the biomass yield coefficients and VvGT14a concentrations at 48 h and 68 h of the processes. Additionally, the VvGT14a yield coefficients and the specific VvGT14a activities determined with cell lysate at 48 h and 68 h of process time are depicted.

Whereas the processes with Profile 1 and 2 result in identical biomass yield coefficients, the cultivation with Profile 3 features an 11 % lower coefficient. At 48 h of process time, the VvGT14a concentration determined for the cultivation with Profile 3 is 50 % higher than for the cultivation with Profile 1, and the specific productivity is 40 % higher. This is also reflected in the fact that the specific activities measured with cell lysate from the process with Profile 3 are significantly higher than with Profile 1, with the final value being 61 % higher. While the specific activity decreases between 48 h and 68 h for the cultivation with Profile 1, it significantly increases for the experiment with Profile 3. Looking at the process with Profile 2, one can see that the final specific activity is by 14 % lower than compared to the process with Profile 1.
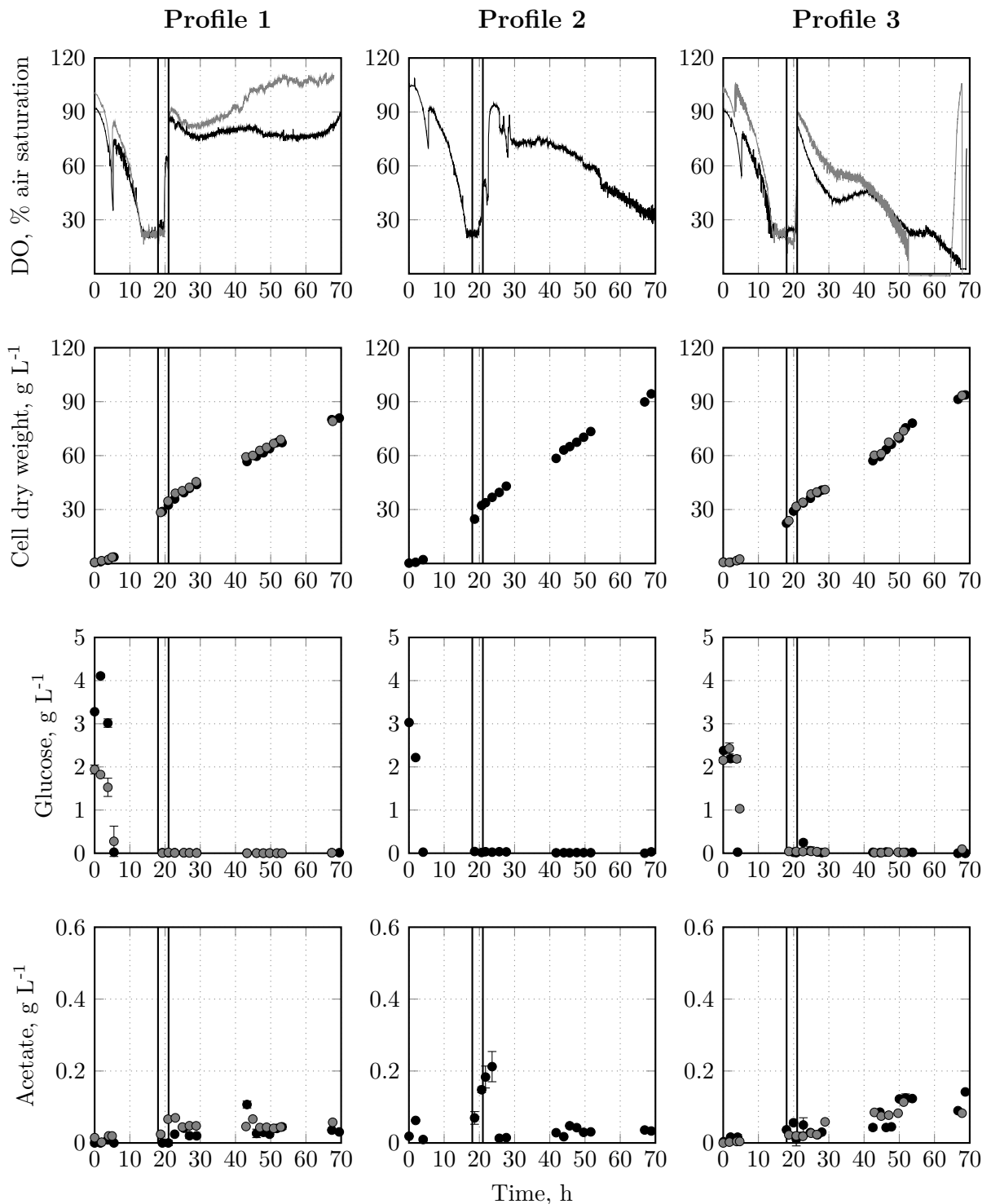
**Figure 5.4.:** Courses of dissolved oxygen (DO), cell dry weight, glucose and acetate concentrations during high cell density cultivations of *E. coli* BL21(DE3)pLysS pET29a_VvGT14a using three different post-induction feeding strategies. Profile 1: constant post-induction feeding rate of 3.9 g L$^{-1}$ h$^{-1}$. Profile 2: linear post-induction feeding rate (starting with 3.9 g L$^{-1}$ h$^{-1}$, gradient: 0.075 g L$^{-1}$ h$^{-2}$). Profile 3: Linear post-induction feeding rate (starting with 3.9 g L$^{-1}$ h$^{-1}$, gradient: 0.150 g L$^{-1}$ h$^{-2}$). Duplicated data series are depicted in gray. Fed-batch cultivations were performed in a stirred tank bioreactor at 2 L-scale. Biomass production phase: 37 °C, exponential glucose feeding ($\mu_{set} = 0.18$ h$^{-1}$) for 18 hours, followed by constant feeding (9.0 g L$^{-1}$ h$^{-1}$) for 3 hours. Protein production phase: 20 °C, induction with 0.1 mM IPTG, different post-induction feeding strategies. The different process phases are separated by vertical black lines.

**Table 5.2.:** Final cell dry weight concentrations, biomass yield coefficients ($Y_{XS}$), VvGT14a concentrations, specific productivities ($Y_{PX}$) and specific VvGT14a activities measured with cell lysate after high cell density cultivations of *E. coli* with different post-induction feeding strategies. Cells marked with a dash indicate that the respective values could not be calculated. Cells marked with *n.a.* refer to values that were not determined.

| State variable | Process time, h | Post-induction feeding profile | | |
| | | 1 | 2 | 3 |
| --- | --- | --- | --- | --- |
| Cell dry weight, g L$^{-1}$ | 48 | 61.6 ± 0.1 | 67.5 ± 0.5 | 66.3 ± 0.2 |
| | 68 | 80.9 ± 1.2 | 94.4 ± 0.8 | 93.8 ± 0.3 |
| $Y_{X/S,\mu}$, g g$^{-1}$ | 48 | 0.45 | 0.44 | 0.40 |
| | 68 | 0.45 | 0.45 | 0.40 |
| VvGT14a concentration, g L$^{-1}$ | 48 | 5.0 ± 0.2 | n.a. | 7.5 ± 0.0 |
| | 68 | 5.5 ± 0.5 | n.a. | n.a. |
| $Y_{PX}$, g g$^{-1}$ | 48 | 0.081 | - | 0.113 |
| | 68 | 0.068 | - | - |
| Specific activity, mU g$_{CDW}$$^{-1}$ | 48 | 174.2 ± 6.6 | n.a. | 220.9 ± 11.4 |
| | 68 | 165.6 ± 0.1 | 143.0 ± 12.1 | 267.1 ± 8.2 |

## 5.3. Discussion

In order to increase the specific productivity for the target protein VvGT14a in comparison to the result by Schmieder et al. [2016b], the effect of the IPTG concentration and the post-induction feeding strategy on cell growth and VvGT14a production during high cell density cultivations was investigated.

Neither decreasing nor increasing the IPTG concentration shows positive effects on VvGT14a production compared to the reference concentration of 0.1 mM. Instead, the enzyme could either not be quantified at all or was produced at a very low concentration. Decreasing the IPTG concentration to 0.05 mM has no effect on cell growth nor on the biomass yield coefficient. However, the IPTG concentration seems to be too low to fully activate VvGT14a production. This result is contrary to observations made by Faust et al. [2015], who showed that IPTG concentrations even lower than 0.05 mM result in full induction of green fluorescent protein synthesis in recombinant *E. coli* harboring a pET28a plasmid. However, there, the strain did not contain a pLysS plasmid, meaning that no

T7 lysozyme was produced (see Chapter 3.3.3). This might explain the need for 0.1 mM IPTG in the present work where the strain does contain the pLysS plasmid: Lower inducer concentrations result in the production of T7 RNA polymerase concentrations possibly not high enough to outnumber the deactivating T7 lysozyme. This hypothesis would have to be verified in follow-up experiments by determining mRNA concentrations of both T7 RNA polymerase and T7 lysozyme by reverse transcription qPCR.

Doubling the IPTG concentration to 0.2 mM results in a significant increase in the final cell dry weight concentration with cell growth being intensified only after induction, however with complete absence of VvGT14a production. The considerably higher biomass yield coefficient compared to the process with 0.1 mM IPTG implies that the glucose fed to the medium is channeled only into cell growth and not at all into VvGT14a production. As described by Choi et al. [2006], high IPTG concentrations can inhibit recombinant protein production (see Chapter 3.3.3), which seems to be the case here. In bacterial cells, a negative correlation between recombinant protein expression and cell growth can exist [M. Scott et al. 2010]. This might be an explanation for the distinct cell growth after induction.

Summarized, high cell density cultivations with the strain *E. coli* BL21(DE3)pLysS pET29a_VvGT14a should be conducted with an IPTG concentration of 0.1 mM. In comparison to the initial reference process described by Schmieder et al. [2016b], the VvGT14a concentration after 48 hours could be increased by 85 %, while the cell dry weight was 8.9 % lower than in the reference process. The significant increase in protein concentration might be explained with the prevention of acetate accumulation by applying a set growth rate of 0.18 h$^{-1}$ instead of 0.20 h$^{-1}$ during the exponential feeding phase. Instead of concentrations up to 0.9 g L$^{-1}$, acetate levels could be kept well below 0.2 g L$^{-1}$. As described by Aristidou et al. [1994], acetate can inhibit recombinant protein production already at levels around 1 g L$^{-1}$, which is consistent with the observations made here. The lower set growth rate can also explain the slightly lower cell dry weight concentration.

Changing the post-induction feeding strategy from a constant to a linearly increasing profile increases cell growth to the same extent for both linear feeding gradients. However, when using the higher gradient, more glucose is channeled into recombinant protein production, recognizable by the decreased biomass yield coefficient. This results in a significantly higher protein concentration and activity compared to the process with the constant feeding profile. The positive effect of a linearly changing post-induction feeding rate on recombinant protein expression was also observed by Wong et al. [1998]. The smaller linear gradient seems to be insufficient to boost protein production. However, it

is unclear why the specific activity of VvGT14a is even lower at process end than with the process applying the constant feeding profile. All in all, 0.1 mM IPTG and a linearly changing post-induction feeding profile with a gradient of 0.150 g L$^{-1}$ h$^{-2}$ were identified as suitable conditions for efficient VvGT14a production during high cell density cultivations of *E. coli* BL21(DE3)pLysS pET29a_VvGT14a.

Moreover, a reduction in process time from 68 h back to 48 h seems reasonable. This is due to the fact that the oxygen saturation in the cultivation broth decreases drastically in the last 20 hours of the process with Profile 3 as the post-induction feeding strategy. In order to avoid exposing the whole-cell biocatalysts to oxygen limiting conditions shortly before cell harvest and storage for successive biotransformations, a reduction in process time is the logical consequence. Moreover, already after 48 h of process time the VvGT14a concentration could be increased by 50 % compared to the process with the constant post-induction feeding profile.

To sum it up, by combining a set growth rate of 0.18 h$^{-1}$ during the exponential growth phase with an IPTG concentration of 0.1 mM and a linear post-induction feeding strategy, the VvGT14a concentration after 48 hours could be increased by 185 % in comparison to the result described by Schmieder et al. [2016b]. Moreover, the specific productivity could be increased by 183 %. Yielding a final VvGT14a concentration of 7.5 g L$^{-1}$, the established process can be classified as a productive process compared to other high cell density cultivations for recombinant protein production, where protein concentrations usually range between 1 and 10 g L$^{-1}$ [Choi et al. 2006]. When assuming that 55 % of the cell dry weight of *E. coli* are made up of proteins [Moran et al. 2010], VvGT14a accounts for 20.5 % of the overall protein amount. This is a value rather in the lower range of specific productivities of 20–50 % for recombinant protein productions reported in literature [Huber et al. 2011; Qing et al. 2004; Riesenberg 1991]. Thus, there is room for further improvement of VvGT14a expression, for example by genetic engineering instead of process engineering. Possible approaches could be the usage of stronger promoters or high copy number plasmids such as the pUC plasmid.

# 6. Rational selection of a biphasic system for the whole-cell glucosylation of geraniol[4]

Due to geraniol´s distinct cytotoxicity towards *E. coli* BL21(DE3)pLysS (minimal inhibitory concentration: 0.3 g L$^{-1}$ [Huang et al. 2016], see Chapter 3.1.3), geraniol concentrations during whole-cell biotransformations need to be kept strictly below this value. As described in Chapter 3.2.1, this can be achieved by using a biphasic reaction system where a non-aquous phase serves as the *in situ* substrate reservoir. The following chapter deals with the rational selection of a non-aqueous phase for *in situ* supply of geraniol.

First, a suitable liquid sequestering phase was to be selected rationally. After selecting a solid sequestering phase as well, the liquid-liquid and solid-liquid systems were to be compared.

## 6.1. Selection of a liquid sequestering phase for geraniol

### 6.1.1. Preselection based on thermodynamic first-principles methods and rational criteria

As a starting point for the rational selection of a liquid sequestering phase for geraniol, the data base by Hansen [2016] comprising 1237 solvents was used. In order to reduce the vast amount of potential liquid sequestering phases, a preselection based on four prefilters was executed.

---

[4] The results of this chapter are published in Priebe et al. (2018): Rational selection of biphasic reaction systems for geranyl glucoside production by *Escherichia coli* whole-cell biocatalysts. *Enzyme Microb Technol*, 112, 79–87; and Priebe et Daugulis (2018): Thermodynamic affinity-based considerations for the rational selection of biphasic systems for microbial flavor and fragrance production. *J Chem Technol Biotechnol*, 93 (3), 656–666.

These were:

- The logP was to be higher than 4 to guarantee biocompatibility with the whole-cell biocatalyst (critical logP for *E. coli*: 3.4 [Inoue and Horikoshi 1991]).

- The solvent´s boiling point was to be at least 120 °C in order to contain safety hazards.

- Neither phthalates nor ionic liquids were to be selected. Phthalates were excluded from the study as their application is associated with severe health concerns, and industry is currently working towards their stepwise replacement [Erickson 2015]. Ionic liquids were excluded due to their high costs and the lack of a general waste management concept, which makes an industrial application questionable.

- The Hansen *Ra* distance between geraniol and the respective solvent was to be at least 4-fold smaller than the *Ra* distance between geraniol and water in order to guarantee an adequate sequestering effect.

The prefilters resulted in the selection of 6 solvents, which are listed in Table 6.1 with their respective chemical category, logP and *Ra* distance to geraniol. For comparative purposes, water is shown in the bottom line. 3 fatty acid esters were preselected, additionally, farnesene belonging to the class of terpenes, and 1-octene and hexadecane, belonging to the class of alkenes and alkanes, respectively. The fatty acid ester ethyl decanoate features the smallest *Ra* distance to geraniol and thus the presumably highest thermodynamic affinity for geraniol, whereas hexadecane shows the highest *Ra* distance.

## 6.1.2. Performance in biotransformations

The 6 preselected solvents were used for parallelized biphasic whole-cell biotransformations of geraniol at mL-scale with an initial overall geraniol concentration of 0.2 g L$^{-1}$. The low substrate concentration guarantees that even in the case of poor geraniol uptake by the applied sequestering phases, the geraniol concentration in the aqueous phases would still be clearly below its minimal inhibitory concentration of 0.3 g L$^{-1}$. A purely aqueous system was used as a reference. The results are shown in Figure 6.1.

Except for the systems with 1-octene and hexadecane as second phases, the biphasic systems result in significantly higher geranyl glucoside concentrations than the purely aqueous system. As the processes with the solvents ethyl oleate and isopropyl myristate feature the highest product concentrations, these systems were characterized further.

**Table 6.1.:** Characteristics of preselected solvents for sequestering of geraniol in a biphasic system, sorted by *Ra* distance. Water is shown as a reference solvent. logP: Logarithmic octanol-water partition coefficient. Values were taken from PubChem (National Center for Biotechnology Information [2019]), where they were calculated with a method described by Cheng et al. [2007]. *Ra* distances were calculated with Hansen Solubility Parameters [Hansen 2016]. The value for water was taken from Hansen [2007].

| Solvent | Chemical category | logP | *Ra* distance to geraniol, mPa$^{0.5}$ | Molar mass, g mol$^{-1}$ |
|---|---|---|---|---|
| Ethyl decanoate | Fatty acid ester | 4.6 | 4.17 | 200.32 |
| Farnesene | Mix of 6 sesquiterpenes | 6.1 | 5.23 | 204.36 |
| Ethyl oleate | Fatty acid ester | 8.0 | 5.32 | 310.52 |
| Isopropyl myristate | Fatty acid ester | 7.2 | 5.61 | 270.46 |
| 1-Octene | Alkene | 4.6 | 6.34 | 112.24 |
| Hexadecane | Alkane | 8.3 | 8.78 | 226.45 |
| Water | - | - | 36.76 | 18.02 |
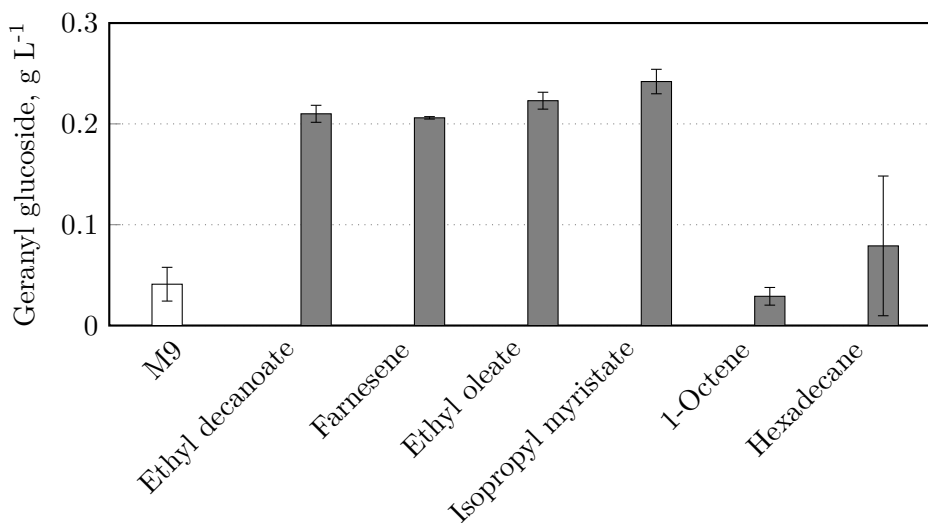


**Figure 6.1.:** Comparison of different biphasic systems with a purely aqueous system (*M9*, white bar) for the whole-cell biotransformation of geraniol at mL-scale. Stirred-tank reactors, V = 10 mL, t = 24 h, T = 30 °C, pH 7, 20 g L$^{-1}$ glucose, 0.2 g L$^{-1}$ geraniol, *E. coli* BL21(DE3)pLysS pET29a_VvGT14a with 4 g L$^{-1}$ dry cell mass in M9 mineral medium or in biphasic systems with different sequestering phases (20 %(v/v)).

**Table 6.2.:** Viscosity, biocompatibility and selectivity of the sequestering phases ethyl oleate and isoproply myristate. The biocompatibility of a sequestering phase was calculated from the ratio of the amount of colony forming units (cfu) after incubation of the biocatalyst in the biphasic (bi) versus the monophasic (mono) system. logPC: Logarithmic partition coefficient for the target compounds geraniol and geranyl glucoside in systems consisting of water and either ethyl oleate or isoproply myristate (20 % (v/v)).

| Solvent | Viscosity, mPa·s | $\frac{cfu_{bi}}{cfu_{mono}}$ | logPC$_{\text{Geraniol}}$, - | logPC$_{\text{Geranyl glucoside}}$, - |
|---|---|---|---|---|
| Ethyl oleate | 5.22 | 1.16 | $2.18 \pm 0.09$ | $-1.57 \pm 0.07$ |
| Isopropyl myristate | 4.28 | 1.00 | $2.42 \pm 0.03$ | $-2.08 \pm 0.05$ |

## 6.1.3. Determination of viscosity, selectivity and biocompatibility

The viscosity, biocompatibility and selectivity for geraniol and geranyl glucoside were determined for ethyl oleate and isoproply myristate and the results are shown in Table 6.2.

Both fatty acid esters feature a viscosity in the same range as grape juice (2–5 mPa·s). Whereas the ratio of colony forming units after incubation of the biocatalyst in the biphasic system versus the monophasic system is larger than 1 for ethyl oleate, the value is exactly 1 for isopropyl myristate. Both solvents feature a high affinity for geraniol, indicated by the respective logP, and show practically no uptake of geranyl glucoside, indicated by the negative logP.

## 6.1.4. Discussion

All in all, the applied theoretical considerations for the selection of suitable liquid sequestering phases show good accordance with the results of biotransformations with the preselected solvents. 4 of the 6 preselected solvents increase product formation when being used as the second phase. However, in spite of complying with the prefilters, 1-octene and hexadecane do not increase geranyl glucoside production in comparison to the aqueous system. The unsuitability of 1-octene might be explained by the solvent´s relatively low molar mass: In contrast to the other solvents, which have molar masses of at least 200 g mol$^{-1}$, 1-octene has a molar mass of only 112.24 g mol$^{-1}$. Brink and Tramper [1985] could show that only solvents having molar masses higher than 200 g mol$^{-1}$ result in activity retention of whole-cell biocatalysts, probably caused by their more distinct (steric) hindrance on their way to or through the cell membrane, leading to a reduced cytotoxicity. These findings match with the results presented here. The unsuitability of

the alkane hexadecane might be explained with the relatively high *Ra* distance to the target compound geraniol, indicating a comparatively low affinity for geraniol. The high *Ra* distance seems to outweigh hexadecane´s high logP value and its rather high molar mass of 226.45 g mol$^{-1}$, underlining the predictive power of Hansen Solubility Parameters, as also described in other publications [Jiang et al. 2014; Poleo and Daugulis 2014; Sicaire et al. 2015].

The biocatalytic productivity of the monophasic system is comparatively low in spite of the initial geraniol concentration being lower than the minimal inhibitory concentration. This might be explained with the fact that despite the concentration being low enough to not kill the cells, geraniol can still interact with the phospholipid bilayer of the cellular membrane, causing harm to the overall viability of the biocatalysts ([J.-C. Chen et al. 2010; Sikkema et al. 1994], see Chapter 3.1.2).

The two solvents ethyl oleate and isoproyl myristate, which result in the highest geranyl glucoside concentration, also prove to be suitable candidates in further characterizations. As both fatty acid esters classify as low-viscosity solvents with their determined viscosities being in the same range as grape juice, they can be easily handled and pipetted in the laboratory. Phase separation after biotransformations is facilitated by the solvents´ insolubility in water (data from suppliers). The biocompatibility of the sequestering phases, which is already indicated by their high logP, guarantees stable biocatalysts throughout the biotransformation process without extensive damage to their cell membrane. However, the ratio of colony forming units of 1.16 for ethyl oleate indicates that this fatty acid ester can be metabolized by the biocatalyst. Comparison of optical densities after incubation of the cells in a purely aqueous system and in the system with ethyl oleate confirms this hypothesis, as the biphasic system results in a 38 % higher optical density (data not shown). The bioavailability of ethyl oleate was shown by Braun et al. [2012] for the yeast *Yarrowia lipolytica*. It might be that the compound can be degraded by the enzymes of the fatty acid synthesis pathway in *E. coli* [Janßen and Steinbüchel 2014], as enzymes can catalyze both directions of a reaction. As the presence of a bioavailable solvent reduces the controllability of a process, ethyl oleate is a less suitable choice than isopropyl myristate. Both sequestering phases exhibit convenient distribution of both substrate and product: whereas geraniol can be mostly found in the organic phase, geranyl glucoside is located entirely in the aqueous phase, facilitating downstream processing steps.

All in all, two suitable liquid sequestering phases could be identified by applying different rational selection criteria and by conducting experimental characterizations, with isopropyl myristate being a better candidate than ethyl oleate.

## 6.2. Selection of a solid sequestering phase for geraniol

### 6.2.1. Preselection based on thermodynamic first-principles methods and rational criteria

In order to broaden the range of studied sequestering phases for geraniol, different solid ab- and adsorbents were investigated in addition to the already described liquid sequestering phases.

For the preselection of different adsorbents, their surface areas were used as the main selection criterion. As non-ionic polymeric resins (XAD) have already successfully been used as adsorbents for the isolation or separation of terpenes or terpenoids in the past [Gunata et al. 1985; Guyot-Declerck et al. 2000; Schievano et al. 2013], different polystyrene and polyacrylic XAD resins covering a broad range of surface areas were preselected. Moreover, the adsorptive resin Sepabeads SP850 was elected in order to increase the covered surface area range upwards. Overall, a range of 300–1000 $m^2$ $g^{-1}$ was covered. As absorptive polymers, the absorbents Desmopan 9370AU and Elvax 40W were preselected due to their commercial availability even in small-scale samples and their low $Ra$ distances to the target solute geraniol. An overview of the preselected solid phases is given in Table 6.3.

**Table 6.3.:** Characteristics of preselected solid phases for sequestering of geraniol in a biphasic system. Surface area data were given by the suppliers. $Ra$ distances were calculated by adding the solubility parameters of the individual components of the polymers, as the exact composition and sequence of the polymers is put under confidentiality by the suppliers. Desmopan 9370AU: 5% butanediol, 20% methyldiisocyanate, 75% tetrahydrofuran. Elvax® 40W: 40% vinyl acetate, 60% ethylene. All indications in (w/w).

| Polymer | Chemical structure | Sorption mechanism | Density, g mL$^{-1}$ | Surface area, m$^2$ g$^{-1}$ | $Ra$ distance to geraniol, mPa$^{0.5}$ |
|---|---|---|---|---|---|
| XAD2 | Polystyrene | Adsorption | 1.02 | 300 | |
| XAD7HP | Polyacrylic | Adsorption | 1.05 | 380 | |
| XAD4 | Polystyrene | Adsorption | 1.02 | 750 | |
| Sepabeads SP850 | Polystyrene | Adsorption | 1.01 | 1000 | |
| Desmopan 9370AU | Thermoplastic polyurethane | Absorption | 1.06 | | 2.14 |
| Elvax 40W | Ethylene vinyl acetate copolymer | Absorption | 0.97 | | 5.25 |

## 6.2.2. Sorption isotherms and adsorption kinetics

In order to characterize the sorption of geraniol to the different polymers, sorption isotherms were established. The data points of adsorbents were fitted with the Freundlich equation, whereas a linear fit was used for the absorbents. The data is shown in Figure 6.2.

Overall, the adsorbents show higher binding capacities for geraniol than the absorbents, with a positive correlation between surface area and binding capacity. The *Ra* distances calculated with the Hansen Solubility Parameters successfully predicted that Desmopan 9370AU exhibits a higher affinity for geraniol than Elvax 40W does, which is reflected in a logarithmic polymer/water partition coefficient of 2.45 for Desmopan 9370AU and of 2.17 for Elvax 40W. All in all, XAD4 and Sepabeads SP850 can adsorb the highest amounts of geraniol, which is why these polymers were subjected to further investigations regarding their biocompatibility. Both resins proved to be fully biocompatible, moreover do not stimulate the formation of biofilms and cannot be degraded by the whole-cell biocatalyst (data not shown). However, Sepabeads SP850 turned out to not be sterilizable through autoclaving, a fact that might hinder a recycling of the material. Thus, this polymer was not further investigated and the focus was laid upon XAD4.

To gain further insight into the adsorption of geraniol to XAD4, the kinetics of the adsorption were examined. The results are depicted in Figure 6.3. The bulk of geraniol is bound to XAD4 within the first 30 min of incubation, independent of the target equilibrium concentration in the liquid phase. A geraniol equilibrium concentration of 0.1 g L$^{-1}$ is reached after 90 min, whereas an equilibrium concentration of 0.01 g L$^{-1}$ is reached after 120 min.

As target molecules interact with adsorbents rather non-specifically, the adsorption of the product geranyl glucoside to XAD4 was analyzed. The results are shown in Figure 6.4. XAD4 has a significantly lower adsorption capacity for geranyl glucoside than for geraniol. However, the fact that geranyl glucoside is both located in the liquid phase and adsorbed to the solid is disadvantageous for downstream processing after biotransformations. Nevertheless, considering the high loading capacity for geraniol, its biocompatibility and thermic stability, XAD4 was selected as the candidate for a direct comparison between liquid-liquid and solid-liquid systems. The two absorbents Desmopan 9370AU and Elvax 40W might in fact be more specific for only the substrate geraniol, yet neither of the two polymers is thermally stable (data not shown) and the partition coefficients are in the same range as those of the previously selected solvents ethyl oleate and isopropyl myristate.
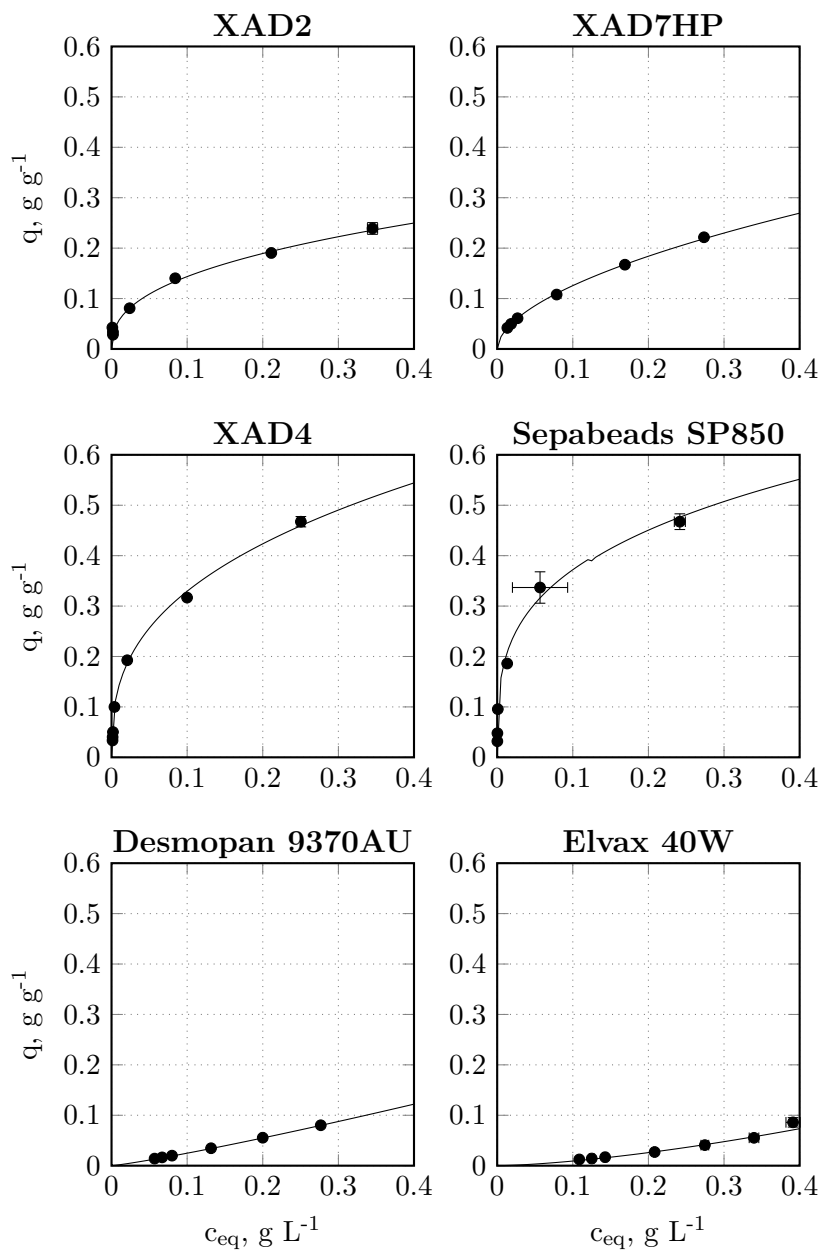
**Figure 6.2.:** Sorption of geraniol to solid sequestering phases with M9 mineral medium as aqueous phase. Standard deviations were calculated from triplicates. q: amount of bound geraniol per gram of solid, $c_{eq}$: geraniol equilibrium concentration in the liquid phase. Isotherms are depicted as continuous lines. Isotherms for adsorbents were calculated with the Freundlich equation, whereas the data points of Desmopan 9370 AU and Elvax 40W were fitted linearly.
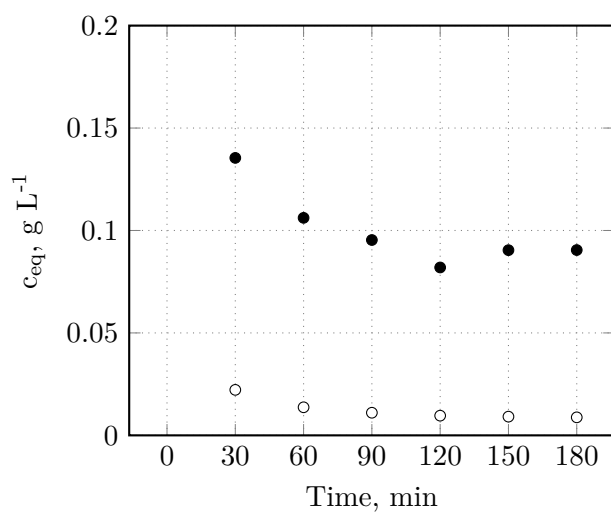
**Figure 6.3.:** Adsorption kinetics of geraniol on XAD4 in a biphasic system with M9 mineral medium as aqueous phase (V = 10 mL, T = 30 °C, n = 600 rpm, 0.49 g $L^{-1}$ initial geraniol). $c_{eq}$: geraniol equilibrium concentration in the liquid phase. Black marks: Kinetics for a target equilibrium concentration of 0.1 g $L^{-1}$. White marks: Kinetics for a target equilibrium concentration of 0.01 g $L^{-1}$. The initial data points of 0.49 g $L^{-1}$ are not depicted.
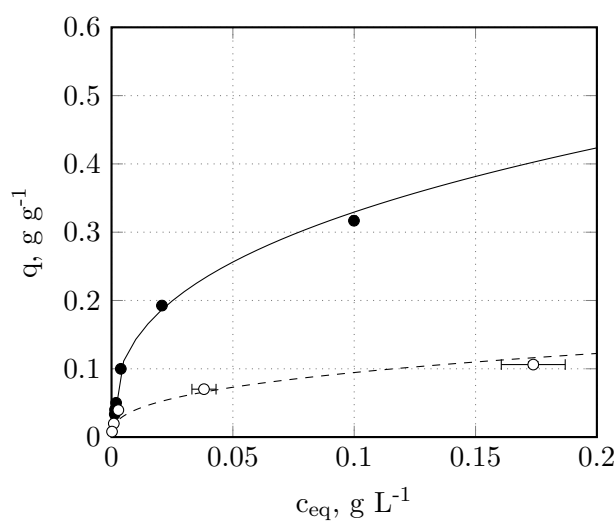


**Figure 6.4.:** Sorption of either geraniol (black circles) or geranyl glucoside (white circles) to XAD4 in a biphasic system with M9 mineral medium as aqueous phase. Standard deviations were calculated from triplicates. q: amount of bound geraniol or geranyl glucoside per gram of solid, $c_{eq}$: geraniol or geranyl glucoside equilibrium concentration in the liquid phase. The isotherms (black: geraniol, dotted: geranyl glucoside) were calculated with the Freundlich equation.

## 6.3.  Direct comparison between liquid-liquid and solid-liquid systems

In order to come to a final decision regarding the most suitable biphasic system for the production of geranyl glucoside by whole-cell biotransformation of geraniol, the three systems with ethyl oleate, isopropyl myristate and XAD4 as sequestering phases were compared in parallel whole-cell biotransformations at mL-scale. The results are depicted in Figure 6.5. It becomes apparent that the biphasic systems are able to at least triple the final geranyl glucoside concentration in comparison to the monophasic system with only M9 mineral medium. The geranyl glucoside concentrations increase in the same order as the binding capacities of the different sequestering phases, which are listed in Table 6.4, together with the prices of the sequestering phases. XAD4 exhibits the highest capacity for the monoterpernoid and is moreover the cheapest choice, followed by isopropyl myristate. Ethyl oleate has the lowest capacity and highest price. However, the prices have less importance when the sequestering phases can be reused.
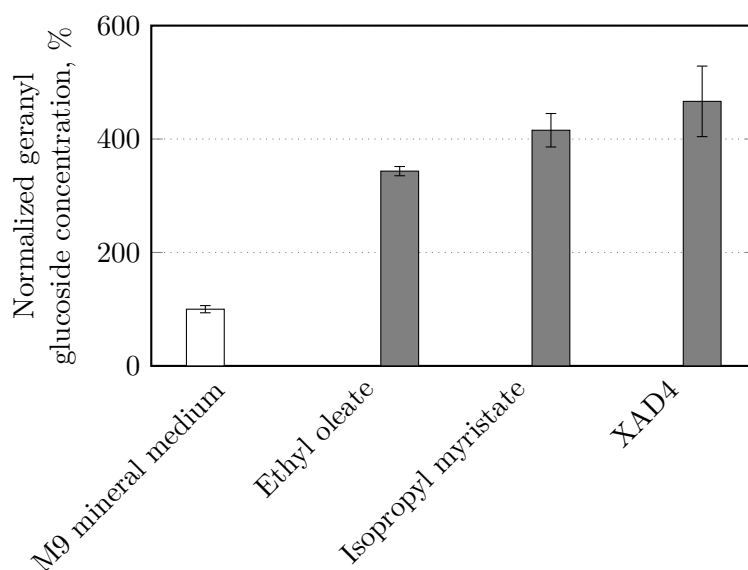


**Figure 6.5.:** Normalized geranyl glucoside concentration with standard deviations (n = 3) after parallel whole-cell biotransformations (stirred-tank reactors, V = 10 mL, t = 24 h, T = 30 °C, pH 7, 20 g L$^{-1}$ glucose, 0.2 g L$^{-1}$ geraniol, 0.01  g L$^{-1}$ geraniol equilibrium concentration, *E. coli* BL21(DE3)pLysS pET29a_VvGT14a with 6 g L$^{-1}$ dry cell mass) in biphasic systems with 20 % (v/v) of either ethyl oleate or isopropyl myristate, or 43.4 mg of XAD4. The geranyl glucoside concentrations were normalized to the concentration measured in a purely aqueous system consisting of M9 mineral medium (white bar).

**Table 6.4.:** Binding capacity (q) of the sequestering phases ethyl oleate, isopropyl myristate and XAD4 for geraniol, and price per gram of bound geraniol. The binding capacity was calculated with a geraniol equilibrium concentration in the aqueous phase (M9 mineral medium) of 0.2 g L$^{-1}$. Prices per gram of bound geraniol are based on purchase prices from the suppliers (Sigma-Aldrich and Carl Roth).

| Sequestering phase | q,  g g$^{-1}$ | Price, € g$_{\text{Geraniol}}^{-1}$ |
|---|---|---|
| Ethyl oleate | 0.036 | 2.42 |
| Isopropyl myristate | 0.063 | 1.12 |
| XAD4 | 0.42 | 0.58 |

**Discussion**

Although the highest product concentration can be reached in the biphasic system with XAD4, this system suffers from two major disadvantages in comparison to the liquid–liquid systems. First, the actual biotransformation needs to be preceded by a time- and labor-intensive adsorption step in order to prevent cytotoxic geraniol concentrations in the aqueous phase. In contrast, geraniol can simply be added to liquid sequestering phases in high concentrations. Second, the product geranyl glucoside is located in both phases at the end of biotransformations in biphasic systems with XAD4, requiring an elution step, e.g. with methanol. On the contrary, the convenient partitioning of geraniol into the organic and of geranyl glucoside into the aqueous phase in biphasic systems with either ethyl oleate or isopropyl myristate facilitates product purification and reduces product loss during downstream processing. Thus, if the slightly lower binding capacity of isopropyl myristate in comparison to XAD4 is no limiting factor, this liquid sequestering phase should be favored for biphasic whole-cell biotransformations of geraniol due to the complete partitioning of the product geranyl glucoside into the aqueous phase and due to a convenient process flow without the necessity for preparatory adsorption or downstream elution steps. Moreover, in contrast to ethyl oleate, isopropyl myristate is not bioavailable.

Isopropyl myristate has already been used as an ISPR phase in a biphasic system for the microbial production of geraniol by Liu et al. [2016], yet without any rationale and preceding rational and systematic screening of different sequestering phases. Moreover, the solvent was suggested as a suitable sequestering phase for the monoterpenes limonene, pinene, terpinene, terpinolene and myrcene by Brennan et al. [2012]. However, no thermodynamic first-principles methods were applied during the selection process, but only logP values, which only makes for a semi-rational approach. Isopropyl myristate represents an

alternative to the ionic liquid N-hexylpyridinium bis(trifluoromethylsulfonyl)imide used by Schmideder et al. [2016b] as sequestering phase for the production of geranyl glucoside from geraniol. As this cost-intensive ionic liquid still lacks a general waste management concept and as pyridine derivatives may accumulate in the aqueous phase during biotransformations, an alternative non-water miscible solvent is beneficial.

All in all, a rational justification for the application of isopropyl myrisate as a sequestering phase for geraniol could be given here.

## 6.4. Generalized approach for the selection of biphasic systems for *de novo* flavor and fragrance synthesis

Many biotechnologically produced F&F compounds exhibit cytotoxicity towards the most common microbiological production hosts *E. coli* and *S. cerevisiae*, making *in situ* product removal (ISPR) strategies using two-phase partitioning bioreactors desirable. Here, the concept used for the rational selection of a sequestering phase for geraniol (see Chapters 6.1-6.3) was extended in a slightly modified way to 17 different F&F compounds, including geraniol. A stronger focus was put on thermodynamic first-principles methods: in addition to Hansen Solubility Parameters (HSP), the Extractant Screening Program (ESP) [Bruce and Daugulis 1991] based on UNIFAC was applied. The objective was to differentiate between sequestering phases with high and low thermodynamic affinity towards the 17 F&F molecules.

### 6.4.1. Selection of representative flavor and fragrance target compounds

In order to create a study as comprehensive as possible, special focus was placed on the selection of target compounds that can adequately represent the vast variety of different classes and structures of F&F molecules by utilizing a range of different selection criteria. First, only compounds with previously-reported *de novo* synthesis routes either in naturally occurring or in genetically modified microorganisms were chosen, reflecting the trend towards the replacement of biotransformations of externally added precursors with more sustainable and economical *de novo* pathways [Carroll et al. 2016]. Second, different structural classes of F&F molecules were selected. As a starting point, the classification of F&Fs by Schrader [2007] was used and six main classes of compounds were selected, namely alcohols, aldehydes, ketones, esters, monoterpenes/-terpenoids and lactones.

Carboxylic acids, such as L-glutamic acid or citric acid, were excluded from the study as their potential dissociation into ions prevents the application of thermodynamic first-principles methods of either Hansen or UNIFAC. Other classes, such as O-heterocycles or compounds containing sulfur and nitrogen, were excluded due to the small number of associated F&F compounds (see also Table 3.1).
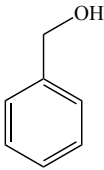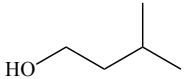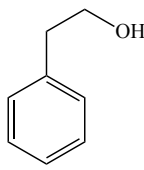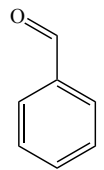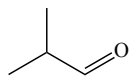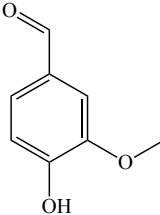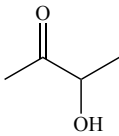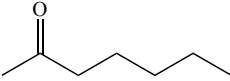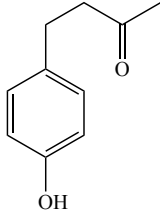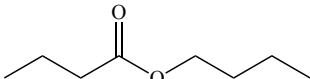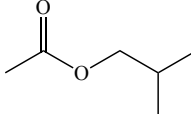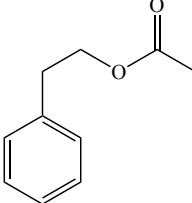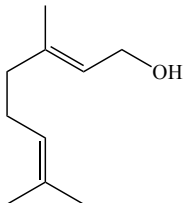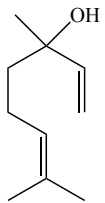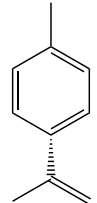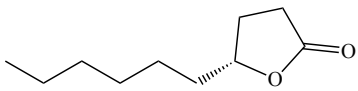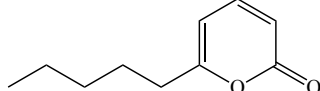
Subsequently, four additional subcriteria were applied to select representative target compounds within each of the six main classes:

- Only molecules with a logP lower than 3.4 were chosen in order to provide a rationale for the use of a biphasic system (critical logP *E. coli*: 3.4 [Inoue and Horikoshi 1991]; critical logP *S. cerevisia*: 4.0 [Kollerup and Daugulis 1986]).

- Compounds with potential industrial relevance, either based on their market volume or on their unique flavor or scent, were picked.

- Within one main class of compounds the structural diversity was to be as high as possible, and thus both aliphatic and aromatic molecules were chosen within a class.

- The selected compounds included ones which have been, and have not yet been, produced using ISPR approaches to allow for a comparison of retrospective and future F&F bioproductions.

All these considerations resulted in the selection of 17 representative F&F target compounds, two within the lactone group and three within all the other main classes, listed in Table 6.5, with chemical structures shown in Figure 6.6. Except for ($S$)-limonene, all compounds meet the criterion of exhibiting a logP lower than 3.4. ($S$)-limonene was included in the selection nonetheless, as on the one hand both enantiomers of this monoterpene (($R$)-enantiomer: orange scent, ($S$)-enantiomer: herbal scent) depict the most commonly used fragrance compounds in household and cosmetic products [Rastogi et al. 2001], and on the other hand this compound, despite its high logP of 4.4 and thus distinctively low water solubility (4.6 mg L$^{-1}$ at 25 °C), exhibits severe toxicity towards *S. cerevisiae* [Brennan et al. 2012].

## 6.4.2. Considered sequestering phases

Only solvents with a logP higher than 4, boiling point higher than 250 °C and melting point lower than 20 °C were considered. The choice of these parameters ensured the solvents' biocompatibility with the production strains *E. coli* and *S. cerevisiae*, reasonably low volatility and hence low associated safety hazards, and liquid state at room

**Figure 6.6.:** Chemical structures and associated classes of selected representative flavors and fragrances.

**Table 6.5.:** Chemical classes, characteristic aromas and scents, and logP of the selected representative flavors and fragrances.

| Compound | Chemical class | Aroma/scent | logP |
|---|---|---|---|
| Benzyl alcohol | Alcohol, aromatic | Floral | 1.1 |
| 3-Methylbutanol | Alcohol, aliphatic | Fruity, roasted | 1.2 |
| 2-Phenylethanol | Alcohol, aromatic | Floral (rose) | 1.4 |
| Benzaldehyd | Aldehyde, aromatic | Almond | 1.5 |
| Isobutyraldehyde | Aldehyde, aliphatic | Malty | 0.7 |
| Vanillin | Aldehyde, aromatic | Vanilla | 1.2 |
| Acetoin | Ketone, aliphatic | Creamy, buttery | -0.4 |
| 2-Heptanone | Ketone, aliphatic | Banana | 2.0 |
| Raspberry ketone | Ketone, aromatic | Raspberry | 1.3 |
| Butyl butyrate | Ester, aliphatic | Fruity | 2.8 |
| Isobutyl acetate | Ester, aliphatic | Fruity | 1.8 |
| 2-Phenylethyl acetate | Ester, aromatic | Honey | 2.3 |
| Geraniol | Monoterpenoid | Floral | 3.2 |
| Linalool | Monoterpenoid | Floral | 3.0 |
| ($S$)-Limonene | Monoterpene | Herbal | 4.4 |
| ($R$)-$\gamma$-Decalactone | Lactone | Peach | 2.7 |
| 6-Pentyl-$\alpha$-pyrone | Lactone | Coconut | 1.8 |

temperature. Phthalates were again excluded from the study due to severe health risks associated with their application. These filters narrowed the database by Hansen [2016] down from 1237 to only 16 solvents (see Table 6.6) and the ESP database was reduced from 1500 to 150 solvents (data not shown).

Solid polymers were screened only with the HSPiP software and not with ESP, as the latter program is not designed to predict partition coefficients for systems involving solids. The HSPiP polymer database consisted of 530 polymers. Only absorbing polymers were considered, as thermodynamic first-principles methods cannot be applied to adsorbents.

## 6.4.3. Application of thermodynamic first-principles methods for affinity predictions

For each target compound, 2–4 sequestering phases with predicted high thermodynamic affinity and 1–2 with predicted low affinity were selected, with 1 of the overall 3–5 sequestering phases being a (solid or liquid) polymer. The terms *high* and *low* were used in a qualitative way, as it is not possible to define one common threshold of *Ra* distances or partition coefficients for all target compounds. The variation in the number of seques-

**Table 6.6.:** Solvent selection from the database by Hansen [2016] after the application of prefilters, sorted by logP.

| Solvent | logP |
|---|---|
| 1-Bromonaphthalene | 4.1 |
| Dibutyl maleate | 4.2 |
| n-Butyl salicylate | 4.6 |
| Trichlorobiphenyl | 5.9 |
| Dibutyl sebacate | 6.3 |
| Acetyltributylcitrate | 6.9 |
| 1-Tetradecene | 7.1 |
| n-Tetradecane | 7.2 |
| Isopropyl myristate | 7.3 |
| Oleyl alcohol | 7.5 |
| Oleic acid | 7.7 |
| Hexadecane | 8.3 |
| Dioctyl adipate | 8.5 |
| Isopropyl palmitate | 8.5 |
| Ethyl oleate | 8.7 |
| Butyl oleate | 9.8 |

tering phases with predicted high thermodynamic affinity preselected for different target compounds can be ascribed to the intention of choosing sequestering phases from a variety of different chemical classes (e.g. alkanes, alkenes, alcohols, esters) represented in the top results of HSPiP and ESP. Owing to different original data sets as well as different algorithms, the HSPiP and ESP ranking results did not generally match up in terms of predicted extractants. Therefore, the top results from each method were picked.

Exemplarily, the HSPiP ranking for the target compound 6-pentyl-$\alpha$-pyrone is shown in Table 6.7, which is based on Table 6.6. Here, the fatty acid ester dibutyl maleate was picked as the solvent with high thermodynamic affinity towards the target compound, and hexadecane as solvent with low affinity.

### 6.4.4. Verification of *in silico* rankings by experimental partition coefficients

In order to verify the *in silico* rankings, partitions coefficients (PCs) were either determined experimentally or - if already reported - taken from literature. In Figures 6.7 and 6.8, PCs for all 17 F&F compounds in the different preselected biphasic systems are presented. Moreover, Table 6.8 lists the target compounds for which PCs were taken from

**Table 6.7.:** Thermodynamic affinities, indicated by *Ra* distance, of prefiltered solvents towards the target compound 6-pentyl-$\alpha$-pyrone. Dibutyl maleate was picked as a solvent with predicted high affinity, hexadecane as a solvent with low affinity.

| Solvent | *Ra* distance to 6-pentyl-$\alpha$-pyrone, mPa$^{0.5}$ |
|---|---|
| **Dibutyl maleate** | **4.6** |
| Dibutyl sebacate | 5.9 |
| Isopropyl palmitate | 6.7 |
| Butyl oleate | 6.8 |
| Trichlorobiphenyl | 7.1 |
| Ethyl oleate | 7.3 |
| Oleic acid | 7.7 |
| Acetyltributylcitrate | 8.1 |
| Oleyl alcohol | 8.1 |
| Dioctyl adipate | 8.3 |
| n-Butyl salicylate | 8.6 |
| Isopropyl myristate | 8.8 |
| 1-Tetradecene | 10.5 |
| 1-Bromonaphthalene | 10.5 |
| **Hexadecane** | **11.7** |
| n-Tetradecane | 11.7 |

literature. In order to make the concept of the graphical representation more accessible, the partitioning of two selected target compounds will be described in more detail in the following.

The partitioning behavior of the compound benzyl alcohol, which is presented in the top left in Figure 6.7, was determined experimentally in four different biphasic systems. Moreover, its uptake by the polymer Hytrel 8171 is already described in literature [Craig and Daugulis 2013] which is why the respective bar on the very right side of the graph is marked with a hash (retrospective) and an asterisk (polymer). Both ESP and HSPiP predicted hexadecane to be a poor extractant for this target compound and the very low experimental PC in the system with this sequestering phase, which is presented on the very left of the graph (dotted bar), confirms these predictions. The systems with the four sequestering phases predicted to be good, 10-undecen-1-ol, dibutyl maleate, oleyl alcohol and Hytrel 8171, exhibit significantly higher PCs.

The second example, the partitioning behavior of the lactone 6-pentyl-$\alpha$-pyrone in five different systems, is depicted in Figure 6.8 at the bottom right. The PCs in the two systems with the sequestering phases predicted to be poor (hexadecane and the
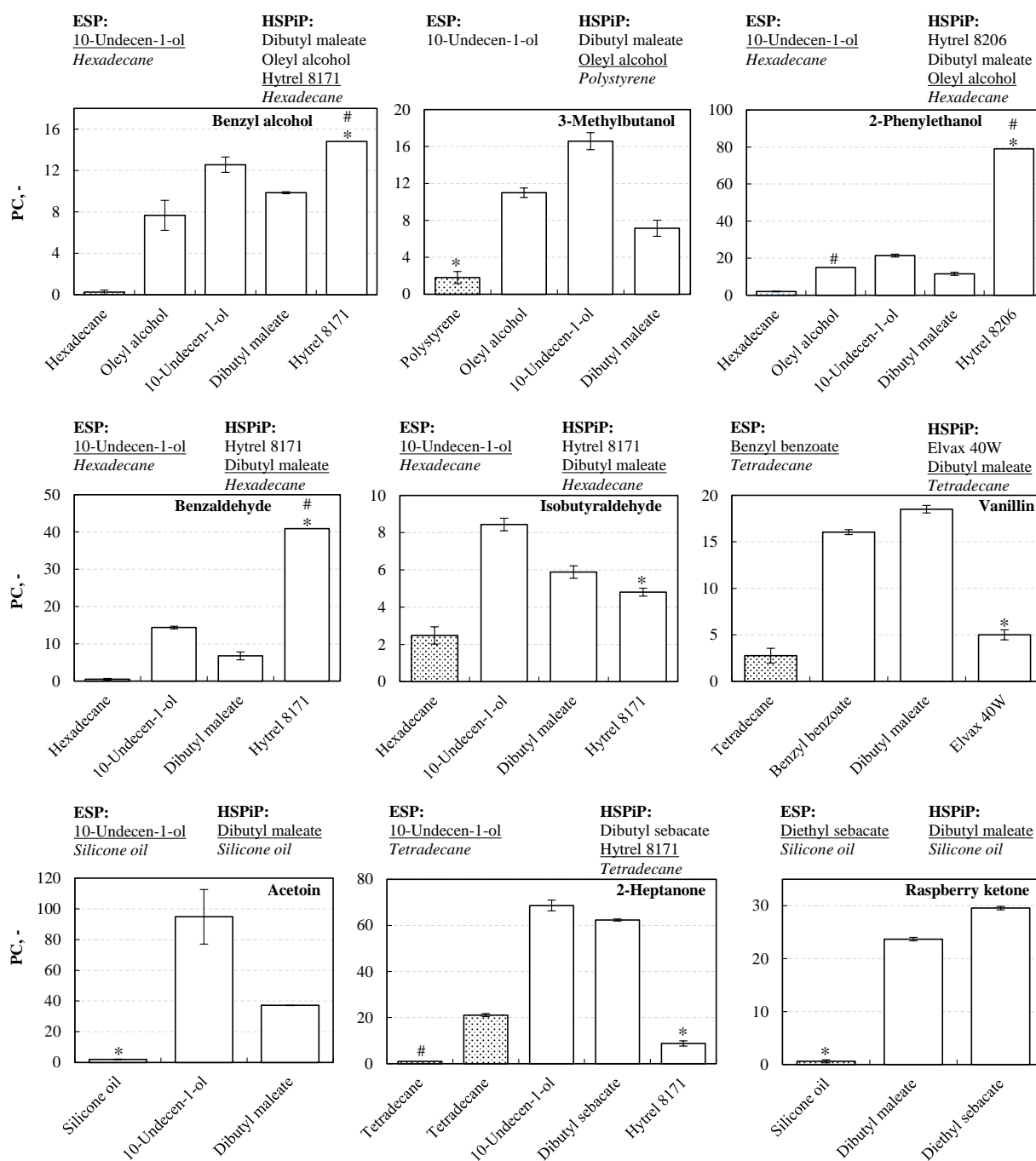
**Figure 6.7.:** Partition coefficients (PCs) with standard deviations (n=3) for flavors and fragrances belonging to the chemical classes of alcohols, aldehydes and ketones in different biphasic systems with water as the aqueous phase. Above each chart, the sequestering phase rankings provided by ESP and HSPiP are listed, with sequestering phases printed in Roman being predicted as effective ones and with sequestering phases printed in *italic* being predicted as poor choices. Effective and unsuitable sequestering phases are separated by a horizontal line. White bars represent PCs in biphasic systems with sequestering phases predicted to be effective, whereas dotted bars are used for systems with sequestering phases predicted to be poor. Asterisks (*) highlight systems which involved a polymer as the sequestering phase, hashes (#) indicate that the respective PCs are reported in literature and were therefore not determined experimentally in this work.

**Table 6.8.:** Target compounds and sequestering phases for which partition coefficients were not determined experimentally, but extracted from literature.

| Target compound | Used sequestering phase | Predicted high (+) or low (-) affinity | Reference |
|---|---|---|---|
| Benzyl alcohol | Hytrel 8171 | + | Craig and Daugulis [2013] |
| 2-Phenylethanol | Hytrel 8206 | + | Etschmann and Schrader [2006] and F. Gao and Daugulis [2009] |
| Benzaldehyde | Hytrel 8171 | + | Craig and Daugulis [2013] and Duff and Murray [1989] |
| 2-Heptanone | Tetradecane | - | Creuly et al. [1992] and Goh et al. [2012] |
| Butyl butyrate | Hexadecane | - | van den Berg et al. [2013] |
| ($S$)-Limonene | Dibutyl phthalate | - | Brennan et al. [2012] and Willrodt et al. [2014] |
| 6-Pentyl-$\alpha$-pyrone | Hexadecane | - | Serrano-Carreón et al. [2002] |
| | PEG 1450 | - | Rito-Palomares et al. [2001] |

polymer PEG 1450) were not determined experimentally in this work, but were taken from literature [Rito-Palomares et al. 2001; Serrano-Carreón et al. 2002]; therefore, the respective dotted bars are again marked with hashes. Again, the sequestering phases predicted to be good, dibutyl maleate, diethyl sebacate and the polymer Hytrel 8171, show significantly higher PCs than the two systems previously described in literature.

When looking at the entirety of the data presented in Figures 6.7 and 6.8, three major trends can be deduced. First, polymers which were predicted by HSPiP to be good sequestering phases, such as DuPont's Hytrels, generally tend to underperform in experimental absorption determinations. In some cases, e.g. Hytrel 8171 for the target compound 2-heptanone, polyethylene for butyl butyrate and polystyrene for 2-phenylethyl acetate, the determined PCs even lie below the PCs of biphasic systems with sequestering phases predicted to be poor.
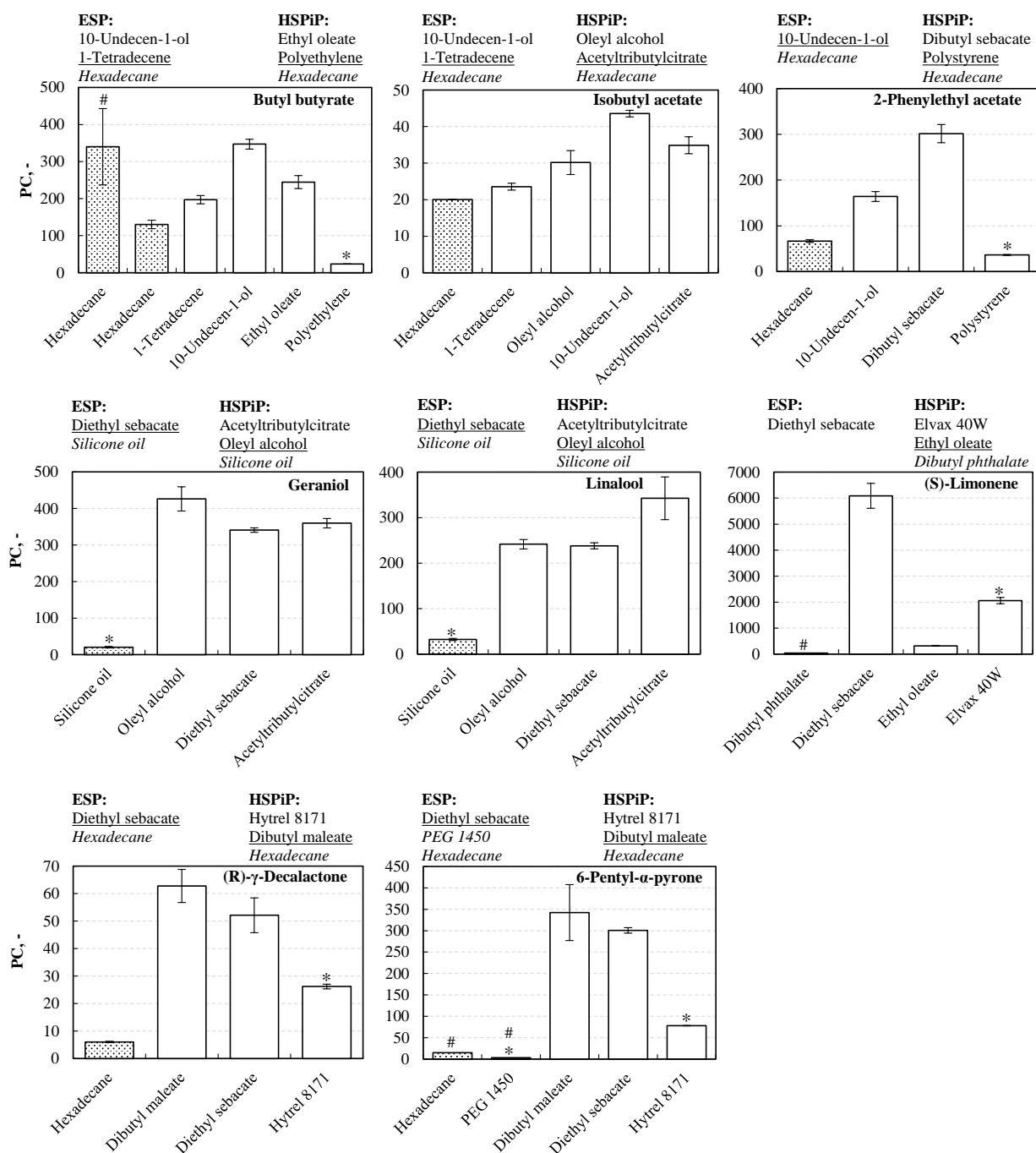
**Figure 6.8.:** Partition coefficients (PCs) with standard deviations (n=3) for flavors and fragrances belonging to the chemical classes of esters, monoterpenes/-terpenoids and lactones in different biphasic systems with water as the aqueous phase. Above each chart, the sequestering phase rankings provided by ESP and HSPiP are listed, with sequestering phases printed in Roman being predicted as effective ones and with sequestering phases printed in *italic* being predicted as poor choices. Effective and unsuitable sequestering phases are separated by a horizontal line. White bars represent PCs in biphasic systems with sequestering phases predicted to be effective, whereas dotted bars are used for systems with sequestering phases predicted to be poor. Asterisks (*) highlight systems which involved a polymer as the sequestering phase, hashes (#) indicate that the respective PCs are reported in literature and were therefore not determined experimentally in this work.

A second trend emerging in the data is the fact that certain chemical classes of liquid extractants were shown to be effective sequestering phases for target compounds across all chemical F&F classes, while liquids from other classes performed very poorly. The two long-chain alcohols oleyl alcohol and 10-undecen-1-ol, and a variety of esters, most frequently dibutyl maleate and diethyl sebacate, were repeatedly top-ranked in ESP and HSPiP across all chemical classes of target compounds, and experimental determination of PCs confirmed their suitability as 'universal' sequestering phases for the absorption of the tested F&F compounds.

The third trend can be best seen in Figure 6.9, where the data from Figures 6.7 and 6.8 is grouped by the chemical classes of the F&F target compounds, and the PCs are normalized to the highest value within the data series of each target compound. Here, it becomes very apparent that the applied approach of preselecting sequestering phases based on thermodynamic affinities predicted by first-principles methods was successful. Sequestering phases which were predicted by ESP and HSPiP to be ineffective for absorbing the target compounds were experimentally proven to indeed be poor, whereas sequestering phases predicted to be effective experimentally resulted in significantly higher PCs than those predicted to be unsuitable. This is true for all target compounds across all chemical classes, except for certain systems where polymers were involved, resulting in unexpectedly low PC values, as described above.

For several of the target compounds, outstanding absorbents resulting in high PCs could be identified, e.g. the ketones acetoin and 2-heptanone partition into 10-undecen-1-ol with experimental PCs of $94.83 \pm 17.75$ and $68.63 \pm 2.31$, respectively, the ester 2-phenylethyl acetate partitions into dibutyl sebacate with a PC of $301.56 \pm 19.97$, and the monoterpene ($S$)-limonene and the lactone 6-pentyl-$\alpha$-pyrone are absorbed by diethyl sebacate with PCs of $6088.41 \pm 478.67$ and $300.67 \pm 6.43$, respectively.

Looking at the target compound geraniol in particular, the two carboxylic acid esters diethyl sebacate and acetyltributylcitrate emerged as the most suitable sequestering phases besides oleyl alcohol. The logarithmic PCs for geraniol (2.53 and 2.56, respectively) lie in the same range as those of systems with the sequestering phases isopropyl myristate and ethyl oleate (2.42 and 2.18, respectively), which were determined to be suitable liquid absorbents for geraniol in Chapter 6.1.

## 6.4.5. Discussion

Overall, the approach to discriminate between good and poor sequestering phases for different F&F compounds by applying thermodynamic first-principles methods emerged

(a) Alcohols/Aldehydes/Ketones

(b) Esters/Monoterpenes,-terpenoids/Lactones
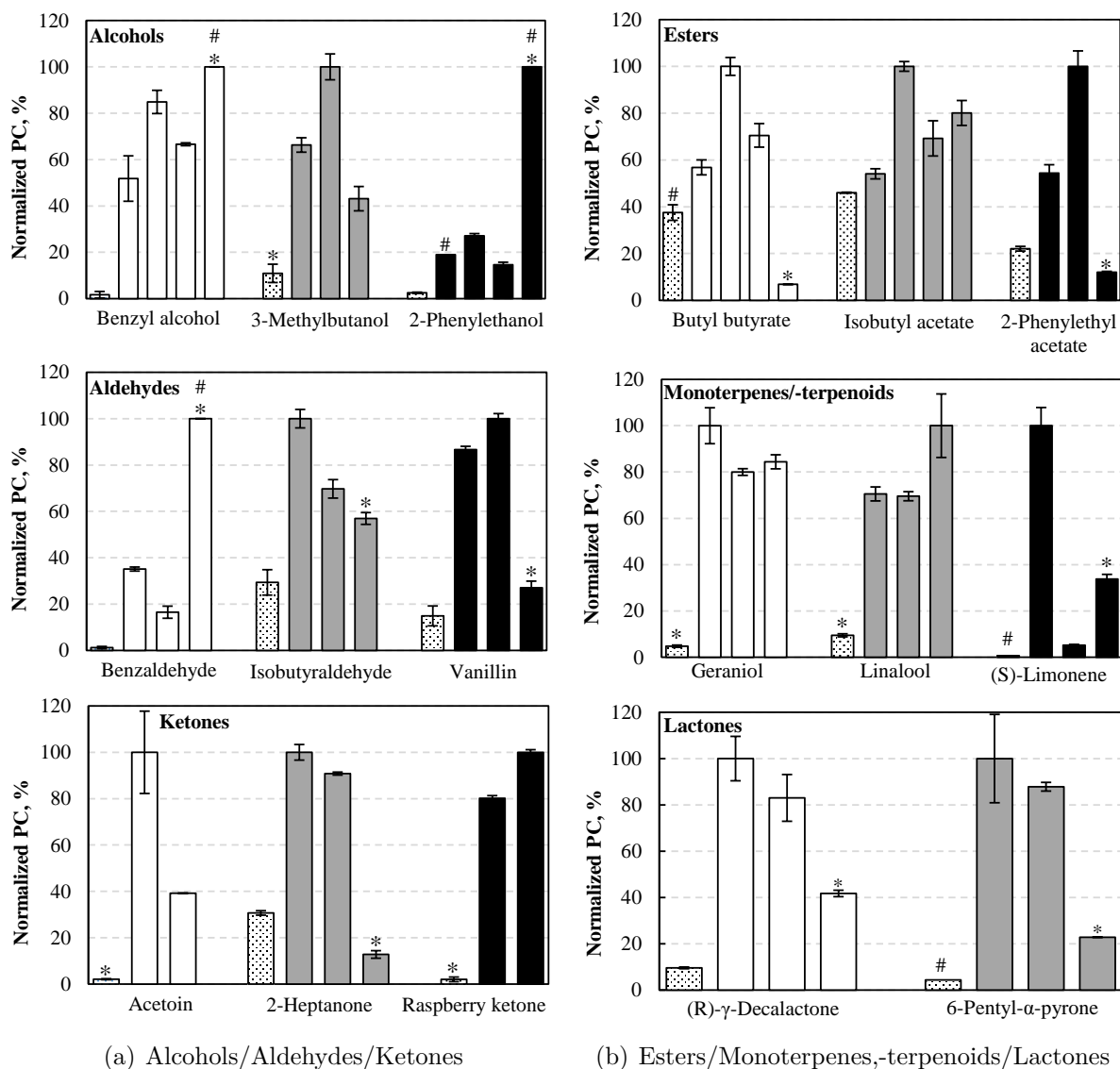
**Figure 6.9.:** Partition coefficients (PCs) with standard deviations (n=3) for flavors and fragrances in different biphasic systems with water as the aqueous phase. Each chart presents data from one chemical class of target compounds, with the target compounds being indicated on the abscissa. Different amounts of shading are used for different target compounds. The PCs were normalized to the highest value for each target compound. Dotted bars, always on the very left side of each data series, are used for systems with sequestering phases predicted to be poor. Asterisks (*) highlight systems that involved a polymer as sequestering phase, hashes (#) indicate that the respective partition coefficient value is reported in literature and was not determined experimentally in this work.

as a successful strategy and outstanding extractants could be identified for several F&F compounds.

The often-low PCs in systems involving polymers can be explained with the fact that by using HSPiP only the predicted thermodynamic affinity between the 'active', absorbing fraction of a polymer and the target compound, and not the polymer as a whole, is considered. Solute uptake is affected by the chain mobility of a polymer and is strongly dependent on the proportion of crystalline/hard segments and amorphous/soft segments: a higher fraction of amorphous/soft segments results in higher overall PCs [Dafoe and Daugulis 2014; Poleo and Daugulis 2014]. As commercially available polymers are often designed to have significant rigidity (e.g. high impact strength) and are not specially designed for ISPR applications (solute absorption), the fraction of the amorphous/soft segments in a polymer, if specified by the manufacturers at all, tends to be rather low. However, this provides significant opportunity for the optimization of biphasic systems involving polymers by selecting specific polymer grades, or designing customized materials with a higher proportion of segments actively participating in the absorption of target compounds. Nevertheless, as shown in Figure 6.7, the three PCs from literature for biphasic systems involving solid polymers (Hytrel 8171 for benzyl alcohol and benzaldehyde, and Hytrel 8206 for 2-phenylethanol, see Table 6.8) are all significantly higher than the other sequestering phases tested for the respective target compounds. This suggests that the amorphous, absorptive components of these polymers are particularly effective at sequestering these particular target molecules.

The thermodynamic affinity between two substances is based on intermolecular interactions [Hansen 2007], and due to their molecular structure (long chains, presence of a double bond in most instances, alcohol and ester functionalities) the effective solvents belonging to the classes of alcohols and esters can interact with the target compounds through nonpolar van der Waals forces, polar dipole–dipole interactions and hydrogen bonding. This also becomes apparent when comparing the HSPs of olelyl alcohol, 10-undecen-1-ol, dibutyl maleate and diethyl sebacate with the HSPs of the alkane hexadecane and the liquid polymer silicone oil (parameters from Hansen [2007], not shown here), which were predicted to be poor sequestering phases for target compounds across all chemical classes. Whereas the suitable extractants exhibit high $\delta_P$ and $\delta_H$ parameters, facilitating strong intermolecular interactions with the target compounds, hexadecane and silicone oil manifest only a modest $\delta_D$ parameter, but very low $\delta_P$ and $\delta_H$ values. Moreover, the $\delta_{tot}$ values of the effective sequestering phases are significantly closer to the $\delta_{tot}$ of the target compounds than those of hexadecane and silicone oil, resulting in smaller $Ra$ distances and thus higher affinities. This is especially true for silicone oil, whose $\delta_{tot}$ of 11.8 is much

smaller than the $\delta_{\text{tot}}$ values of the target molecules. Patel et al. [2017] demonstrated that silicone oil cannot function as an efficient sequestering phase for the absorption of alcohols, ketones or esters – chemical classes which include many F&F compounds – and that only compounds belonging to the classes of alkanes, aromatic hydrocarbons and chlorinated substances partition into silicone oil with high PCs. However, the latter do not constitute F&F compounds and the results shown here confirm that silicone oil is a poor sequestering phase for F&F molecules. In contrast, the use of solvents belonging to the classes of alcohols and esters as sequestering phases for F&F compounds (namely, benzaldehyde, geraniol, limonene and 2-phenylethanol) is already described in literature [Brennan et al. 2012; Duff and Murray 1989; Etschmann and Schrader 2006; Liu et al. 2016], however, with a lack of explanation for the suitability of such solvents based on thermodynamic first-principles methods.

The ESP and HSPiP ranking orders for sequestering phases predicted to be good is not consistently reflected by the order of the experimental PCs, which can be attributed to the fact that preselected sequestering phases often manifest very similar *in silico* PCs (ESP) or Hansen *Ra* distances (HSPiP). Although first-principles methods can never predict the behavior of real systems with full certainty, the main outcome is the fact that the applied approach successfully distinguishes between effective and poor sequestering phases for F&F compounds.

Finally, when looking at the target compound geraniol in particular, it becomes apparent that the two slightly different approaches presented here and in Chapter 6.1 both show that carboxylic acid esters are a suitable choice for the sequestering of geraniol.

# 7. Reaction engineering analysis for geranyl glucoside production with *in situ* geraniol supply

After the selection of isopropyl myristate as a suitable sequestering phase for geraniol, the whole-cell biocatalyst and the biotransformation process were to be characterized.

## 7.1. Investigations on storage conditions for the whole-cell biocatalyst

As the industrial production and actual usage of whole-cell biocatalysts is often conducted by different companies at different locations, the cells preferably exhibit high storage stability. Therefore, the storage stability of *E. coli* BL21(DE3)pLysS pET29a_VvGT14a was investigated. For this purpose, whole-cell biocatalysts were produced by HCDC, stored under different conditions, and afterwards used in parallel biotransformations at mL-scale.

Directly after HCDC, fresh cells were used in a biotransformation to obtain a reference value. The remaining share of the cells was stored at different temperatures and used for biotransformations in certain time intervals (4, 11, 18, 24, 45 and 174 days). The investigated storage temperatures were 22 °C, 4 °C, -20 °C and a temperature change from 4 to -20 °C after 7 days (imitating transportation of the cells at 4 °C and subsequent freezing). Moreover, cells were freeze-dried after pre-freezing them for 2 h at -80 °C. One half of the freeze-dried samples was pretreated with a 32 % (w/v) sucrose solution as a cryoprotective. Figure 7.1 shows the influence of storage duration and storage temperature on the whole-cell biocatalyst activity.

Except for the samples stored at 4 °C, the cells show a decrease in activity after 4 days of storage in comparison to the reference measurement which results in a geranyl glucoside yield of 46.4 %. Cells stored at 4 °C show a similar activity after a storage period of 4 days.
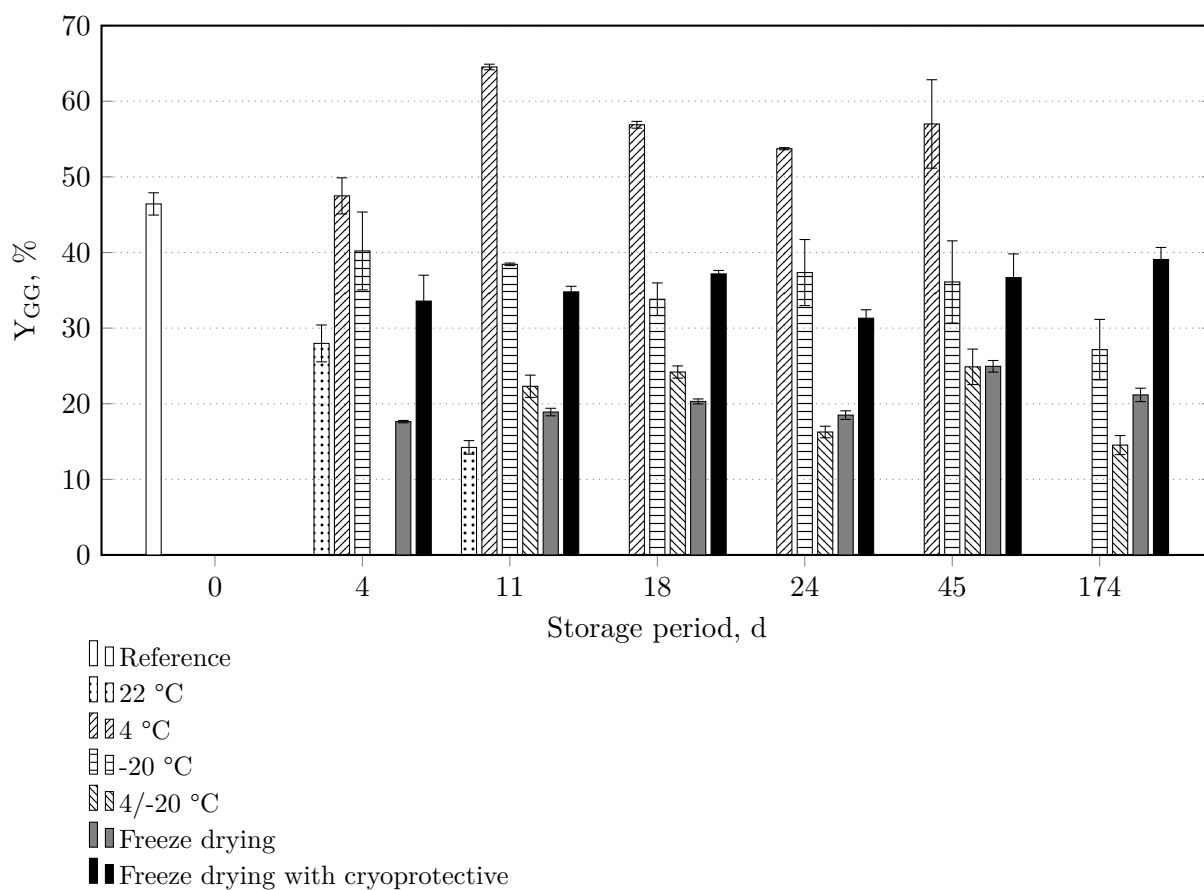
**Figure 7.1.:** Effect of different storage conditions on the activity of the whole-cell biocatalyst *E. coli* BL21(DE3)pLysS pET29a_VvGT14a. $Y_{GG}$: Geranyl glucoside yield. Whole-cell biocatalysts were produced by HCDC. The cells were stored under different conditions in Riesenberg medium and were then used for parallelized biotransformations at mL-scale (Stirred-tank reactors, V = 10 mL, t = 18 h, T = 30 °C, n = 2200 rpm, pH 7, 10 g L$^{-1}$ glucose, 0.2 g L$^{-1}$ geraniol, 4 g L$^{-1}$ dry cell mass in M9 mineral medium with 30 % (v/v) isopropyl myristate). As a reference, cells were used directly after cell harvest. Besides, different storage temperatures and storage periods were tested. Freeze-drying was conducted either without a cryoprotective, or with 32 % (w/v) sucrose solution as a cryoprotective.

After 11 days, a significant increase in activity can be observed, and even afterwards the yields are constantly higher than for the reference. In contrast to this result, cells stored at 22 °C lose their activity completely when stored longer than 11 days. Freeze-dried cells and cells stored at -20 °C or 4/-20 °C show mutually comparable behavior: After a clear decrease in comparison to the reference, their activities stay more or less constant throughout the storage period, although at different levels: Storage at -20 °C and freeze-dried storage with cryoprotective leads to considerably higher yields than storage of freeze-dried cells without cryoprotective, or storage first at 4 °C and then at -20 °C. In order to investigate the long-term storage stability of whole-cell biocatalysts, biotransformations were conducted after 174 days. Then, cells stored at 4 °C show no biocatalytic activity anymore, whereas cells kept at the other storage temperatures still show activity. Thereby, freeze-dried cells mixed with the cryoprotective show no activity loss at all.

When whole-cell biocatalysts are transported or stored in a frozen state, wrong handling can lead to gaps in the cold chain. Therefore, the resistance of cells towards various freeze-thaw cycles was tested. The results are depicted in Figure 7.2, where the geranyl glucoside yield is shown after different counts of freeze-thaw cycles. The yields are normalized to the yield with cells used directly after harvest. The yield increases by more than 10 % after the first freeze-thaw cycle. After the second cycle, the biotransformation yields the same amount of geranyl glucoside as directly after cell harvest. The yield decreases with each following freeze-thaw cycle, with a very distinct decrease after the 4th cycle. After 6 cycles, the normalized yield amounts to 54 %.

After storage at 4°C, when preparing the biocatalysts for the biotransformation, the cells were usually resuspended in the respective medium (e.g. M9 mineral medium) and then stored on ice for ~1 hour until the parallel reactor system was ready for inoculation. Here, it was tested whether an incubation at 30 °C and 800 rpm in an incubator shaker instead of storage on ice is advantageous for the subsequent biotransformation of geraniol. Indeed, a significant increase in geranyl glucoside yield by 41 % was observed (data not shown).

**Discussion.** In spite of the cellular metabolism being decelerated at 4 °C, metabolic processes can still occur up to a certain grade [Batt and Tortorello 2014]. Thus, the increase in biocatalytic activity after storage at 4 °C for 11 days might be explained with enduring protein folding or processing [Gasser et al. 2008], potentially resulting in a higher functional concentration of VvGT14a. The loss in activity after 18 days of storage most likely occurs due to progressing cell aging. In contrast, storage at -20 °C
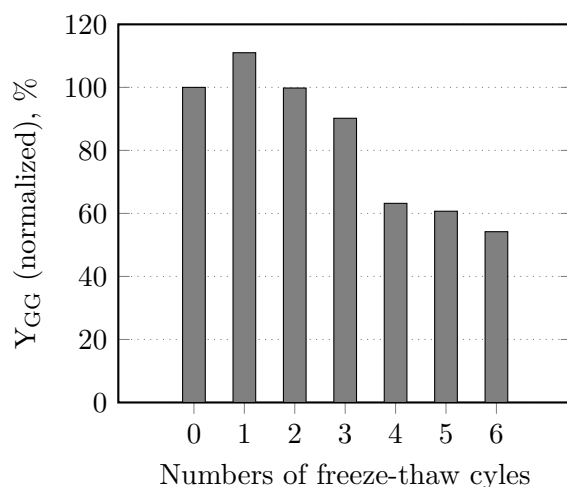
**Figure 7.2.:** Effect of freeze-thaw cycles on the activity of the whole-cell biocatalyst *E. coli*
BL21(DE3)pLysS pET29a_VvGT14a. $Y_{GG}$: Geranyl glucoside yield. Whole-cell biocata-
lysts were produced by HCDC. The cells were subjected to different counts of freeze-thaw
cylces (freezing temperature: -20 °C, freezing time: 60 min) and were then used for par-
allelized biotransformations at mL-scale (glass vials, V = 5 mL, t = 2 h, T = 30 °C,
n = 500 rpm, pH 7, 10 g $L^{-1}$ glucose, 1 g $L^{-1}$ geraniol, 4 g $L^{-1}$ dry cell mass in M9 mineral
medium with 20 % (v/v) isopropyl myristate).

can decelerate aging processes [Gadgil et al. 2005], resulting in more or less constant
biocatalytic activity over 45 days. The initial activity loss in comparison to the reference
with fresh biocatalysts is probably caused by the formation of ice crystals and osmotic
stress induced by freezing. Freeze-drying seems to cause these negative effects to an even
more distinct extent. However, as described by Louis et al. [1994], using the disaccharide
sucrose as a cryoprotective can maintain biocatalytic activity to a higher extent, resulting
in similar yields as cells stored at -20 °C, with the activity even being preserved for half
a year. No other storage condition investigated here allows activity retention for such a
long period.

All in all, whole-cell biocatalysts should be stored differently depending on the reques-
ted storage period: For a storage period of up to 45 days, storage at 4 °C in the HCDC
cultivation broth seems to be the best of the analyzed choices. For longer storage periods,
freeze-drying with the addition of sucrose as a cryoprotective is preferable. For biotrans-
formations described in the following chapters, only cells stored at 4 °C were used. As
data from parallelized experiments at mL-scale was only compared within one experiment,
the cell age can be neglected in these cases. For separate biotransformations at L-scale,

only biocatalysts with similar cell ages were used.

The positive effect of one freeze-thaw cycle on the biocatalytic activity might be explained with a higher membrane permeability caused by extracellular ice crystals which damage the cellular membrane in a non-lethal way [Mazur 1984]. This might result in enhanced trans-membrane transport of geraniol and glucose, boosting the biotransformation. However, the partial damage of the cell membrane seems to become the more harmful the more freeze-thaw cycles have been conducted. All in all, one freeze-thaw cycle prior to the biotransformation could be a promising strategy to increase the yield.

The fact that an incubation of the biocatalysts at 30 °C and 800 rpm for 1 hour prior to the biotransformation is beneficial for geranyl glucoside yields could imply that the incubation results in a shorter adaption phase at the beginning of the biotransformation process, as the cells were already exposed to the actual process temperature and certain shear forces during the prior incubation. This might be of special importance after a longer storage at low temperatures. Moreover, it is possible that the higher temperature of 30 °C allows the cells to activate their metabolism more rapidly, and to potentially degrade cytotoxic compounds such as acetate which might be still present from the HCDC or subsequent, mostly anaerobic, storage. Due to this outcome, biocatalysts were always incubated at 30 °C and 800 rpm for 1 hour prior to biotransformations described in the following chapters.

## 7.2. Recycling of the whole-cell biocatalyst

From an economic point of view, a recycling of the whole-cell biocatalysts is reasonable. This is why a repeated usage of the cells in whole-cell biotransformations of geraniol, each lasting 18.5 h, was tested at mL-scale. Prior to each biotransformation, the cells were separated from the reaction medium and resuspended in fresh M9 mineral medium. The results are depicted in Figure 7.3. Already the first recycling step reduces the activity of the cells by 23 %; after the fourth recycling step, the yield is even 90 % lower than in the process with fresh cells.

**Discussion.** The results imply that the biocatalyst applied in this work is not suited for repeated biotransformations. One recycling step might still be acceptable, depending on yield and concentration requirements, but more recycling steps are not reasonable. Either the biotransformation itself or the subsequent preparation steps for the following
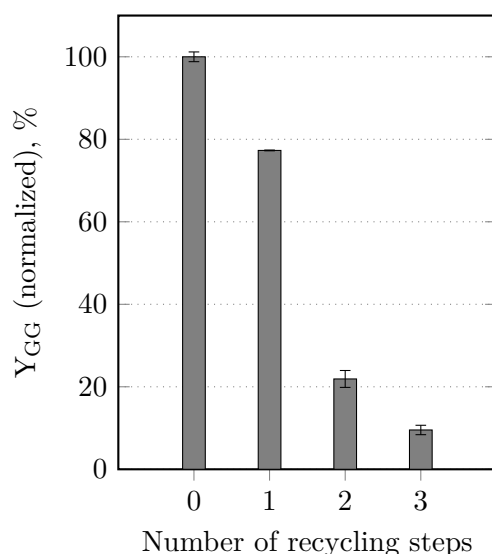
**Figure 7.3.:** Effect of the reuse of whole-cell biocatalysts on the geranyl glucoside yield ($Y_{GG}$) after biotransformations of geraniol at mL-scale (Stirred tank reactors, V = 10 mL, t = 18.5 h, T = 30 °C, n = 2200 rpm, pH 7, 10 g $L^{-1}$ glucose, 0.2 g $L^{-1}$ geraniol, 4 g $L^{-1}$ dry cell mass in M9 mineral medium with 30 % (v/v) isopropyl myristate).

biotransformation (phase separation by centrifugation, resuspension in fresh medium) seem to burden cell vitality to a significant extent. In contrast to this outcome, Richter et al. [2010] reported the reusability of an *E. coli* BL21(DE3) biocatalyst heterologously expressing a glycerol dehydrogenase for 5 biotransformation cycles without any loss in activity. However, the duration of the described biotransformation amounted to only 45 min instead of 18.5 h.

## 7.3. Intracellular UDP-glucose supply during the glucosylation of geraniol

As UDP-glucose is the co-substrate for the glucosylation of geraniol by VvGT14a, the UDP-glucose supply is crucial for the production of geranyl glucoside. To gain a better understanding of the UDP-glucose supply, both UDP-glucose and its metabolite UDP were quantified intracellularly during whole-cell biotransformations at mL-scale. A process without the addition of geraniol served as a reference. The results are depicted in Figure 7.4.

Both the qualitative and quantitative course of UDP-glucose is similar for the biotrans-

formation and the reference process: a linear decrease within the first 10 h of the process is followed by a rather constant course. All measured concentrations lie far above the $K_m$ ($K_m$: substrate concentration at which the reaction rate amounts to half of the maximal rate) of VvGT14a for UDP-glucose as a substrate (16 µM [Bönisch et al. 2014a]). The UDP level increases during the first 10 h of the biotransformation, followed by a decrease. The decrease can also be observed for the reference process, however, the first data point is missing. All measured UDP concentrations lie clearly below the half maximal inhibitory UDP concentration for VvGT14a (600 µM [Huang et al. 2016]). Moreover, it was shown that UDP concentrations up to 1200 µM do not inihibit the whole-cell biotransformation of geraniol (data not shown). Whereas a slight decrease in cell dry weight can be seen for the biotransformation process, the biocatalyst concentration remains rather constant in the reference process, except for an increase between 5 and 10 h of process time. However, the indicated cell dry weight concentrations should not be overrated, as for each data point only one reactor was available. The geranyl glucoside concentration during the biotransformation increases linearly within the first ~12 hours, and remains constant afterwards. The UDP-glucose amount required for the production of the measured geranyl glucoside concentration is ~8.5 times higher than the intracellularly measured decrease in UDP-glucose.

**Discussion.**    The probably most important finding is the fact that not only biocatalysts actively involved in the production of geranyl glucoside consume UDP-glucose, but that the cells of the reference process use the nucleotide sugar to a very similar extent, in spite of not showing much cell growth. This can be attributed to the intracellular usage of UDP-glucose as a precursor and building block for other UDP-sugars and capsular polysaccharides which constitute protective structures on the bacterial surface [Mao et al. 2006; Whitfield 2006]. However, one has to be careful talking about absolute UDP-glucose consumption rates, as each measured value depicts only a snap-shot and not the cells´ capability for UDP-glucose regeneration. Nevertheless, the capability for active UDP-glucose regeneration becomes somewhat apparent when comparing the UDP-glucose amount required for the production of the measured geranyl glucoside concentration to the much lower measured consumption of intracellular UDP-glucose. The decrease in intracellular UDP-glucose during both the biotransformation and the reference process might be primarily explained with full consumption of extracellular glucose within the first 10–15 hours of the processes (data not shown), but another factor might indeed also be an inadequate regeneration rate. UDP-glucose concentrations would have to be measured over longer biotransformation processes in order to assess whether the regeneration rate
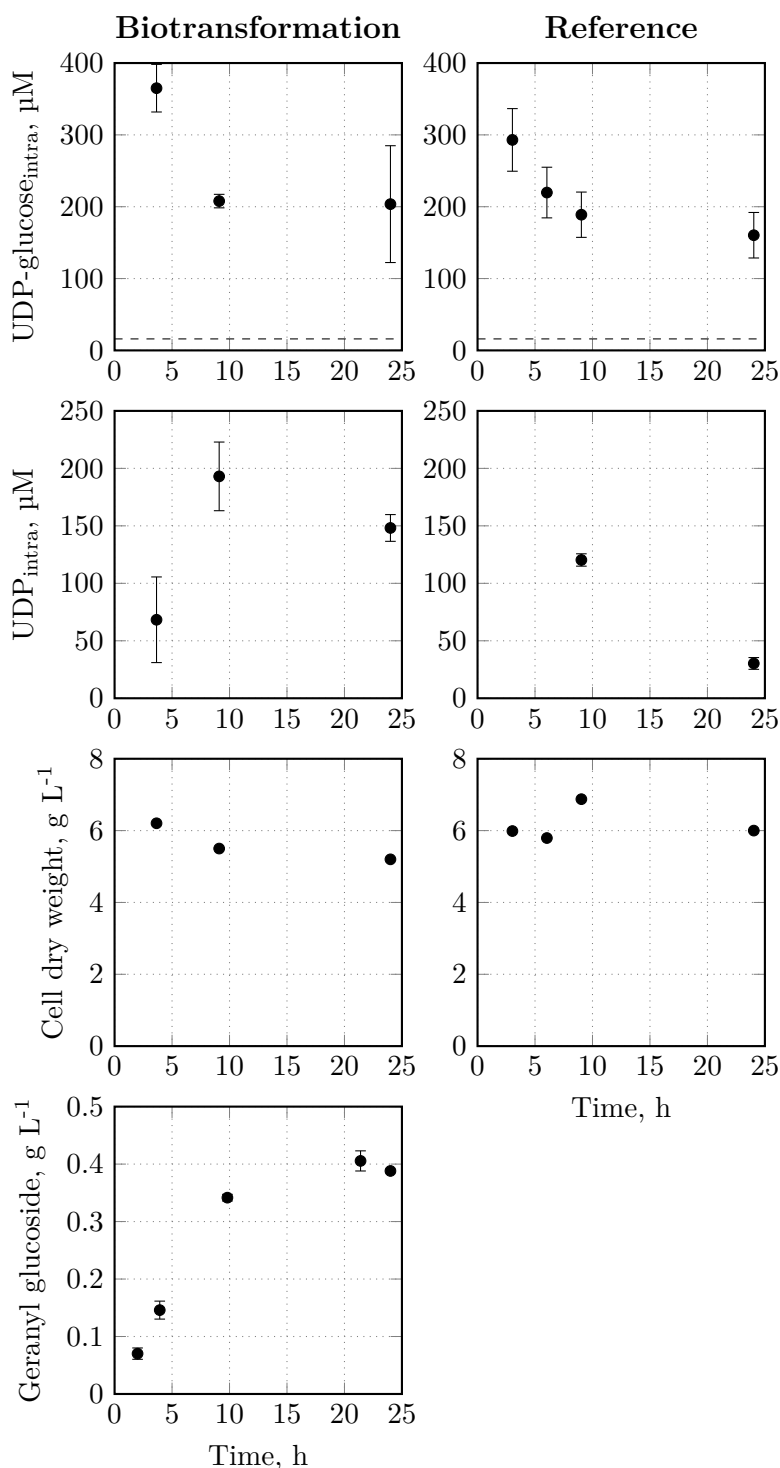
**Figure 7.4.:** Intracellular UDP-glucose and UDP concentrations, as well as cell dry weight and geranyl glucoside concentrations during whole-cell biotransformation of geraniol at mL-scale (stirred-tank reactors, V = 10 mL, t = 24 h, T = 30 °C, n = 2200 rpm, pH 7, 20 g $L^{-1}$ glucose, 0.8 g $L^{-1}$ geraniol, 6 g $L^{-1}$ *E. coli* BL21(DE3)pLysS pET29a_VvGT14a in M9 mineral medium with 40 % (v/v) isopropyl myristate). An identical process, however without the addition of geraniol, was executed for comparative purposes (Reference). The $K_m$ of the glycosyltransferase VvGT14a for UDP-glucose amounts to 16 µM [Bönisch et al. 2014a] and is marked with a dashed line in the upper two graphs. Cell dry weights were determined in separate reactors treated identically to those used for metabolite extraction. Hereby, for each data point 1 reactor was used.

can keep up with the consumption rate. However, with the data presented here, one can rule out that the UDP-glucose concentration is the cause for stagnant geranyl glucoside concentrations after 12 hours. Thus, a different bottleneck seems to exist. However, as soon as the bottleneck can be identified and eliminated, a deeper look would have to be taken into UDP-glucose supply again.

If then, insufficient UDP-glucose supply turns out to be a bottleneck, different strategies exist for improving the regeneration of this co-substrate. Besides deleting *E. coli*-inherent UDP-glucose hydrolases, the overexpression of the key enzymes of the UDP-glucose synthesis pathway, namely phosphoglucomutase and UDP-glucose pyrophosphorylase (see Figure 3.10), are an option [Mao et al. 2006]. Another approach consists in the expression of a sucrose synthase that synthesizes UDP-glucose from sucrose and UDP. This method was already successfully applied *in vitro* for the glycosylation of geraniol by VvGT14a [Huang et al. 2016]. Besides from that, a "split metabolism" could be used, where sucrose and not glucose is used as a carbon source by expressing the sucrose phosphorylase. The resulting fructose is then used for cell growth, whereas the additionally formed glucose-1-phosphate increases UDP-glucose formation [de Bruyn et al. 2015].

Intracellular turnover rates of high-abundance metabolites such as UDP-glucose are assumed to be significantly smaller than those of metabolites of the central metabolism such as the glycolysis: whereas turnover rates as high as $1 \text{ mM s}^{-1}$ are reported for cytosolic glucose, high-abundance compounds are supposed to have turnover rates in the $\text{nM s}^{-1}$ range [de Koning and van Dam 1992; Tweeddale et al. 1998]. As the sampling of each reactor took ~5 s, the turnover of significant UDP-glucose amounts can be ruled out. However, one uncertainty affecting the data has to be considered: For the calculation of intracellular metabolite concentrations the intracellular aqueous volume of an *E. coli* cell is required. Here, a volume of $1.9 \text{ mL g}^{-1}$ determined by L. Wang et al. [2013] for *E. coli* BL21(DE3) was used. Other references, however, describe higher values of $2.15$–$3.2 \text{ mL g}^{-1}$ [Bennett et al. 2008; Park et al. 2011; Volkmer and Heinemann 2011], which would result in lower intracellular metabolite concentrations. As the intracellular volume seems to depend on the overall cell fitness, the carbon source, the growth rate and the type of medium, it is hard to decide which value is the most suitable one for this study. However, the measured UDP-glucose and UDP concentrations seem to lie in a reasonable range when being compared to values measured by Bennett et al. [2009] in exponentially growing cells. The literature values are ~5-fold higher, which seems natural though when comparing exponentially growing cells to rather non-growing biocatalysts.

# 7.4. State variables affecting product concentrations and space-time-yields during biotransformations of geraniol at mL-scale

In the following, different process variables potentially having an impact on product concentrations and space-time-yields during biotransformations of geraniol are investigated at mL-scale.

## 7.4.1. Reaction system composition

The composition of a reaction system can have a significant effect on the reaction's outcome. Therefore, the influence of the aqueous phase composition and of the non-aqueous phase fraction was investigated.

**Aqueous phase**

Different aqueous media were tested in order to identify the best choice for the biotransformation of geraniol. The results are depicted in Figure 7.5. In a single-phase system without a sequestering phase for geraniol, M9 mineral medium shows significantly better results than potassium phosphate buffer. In biphasic systems with isopropyl myristate as the non-aqueous phase, potassium phosphate buffer supplemented with $MgSO_4$ results in significantly lower geranyl glucoside formation as well and, as shown in Figure 7.6, in absent cell growth with a distinct decrease in cell dry weight already within the first hour of the process. The complex medium lysogeny broth results in slightly higher product concentrations, whereas terrific broth does not show differences to M9. Riesenberg medium, which is the medium used for HCDCs for the production of whole-cell biocatalysts, is less suitable than M9.

Moreover, the addition of different components to M9 mineral medium was tested regarding its effect on geranyl glucoside concentrations. The results are shown in Figure 7.7. None of the additives leads to a significant increase in geranyl glucoside concentration, with the addition of $MgSO_4$, $MnCl_2$, $FeSO_4$ and trace solution even resulting in slightly lower product formation. The omission of certain components of M9 (for the M9 composition refer to Table A.21) results in an impairment of the biotransformation. The only M9 variation that leads to identical product concentrations as the regular medium was the one where only $CaCl_2$ and NaCl were left out, with $NH_4Cl$, $Na_2HPO_4$, $KH_2PO_4$ and $MgSO_4$ still being present (data not shown, process duration 2.5 hours).
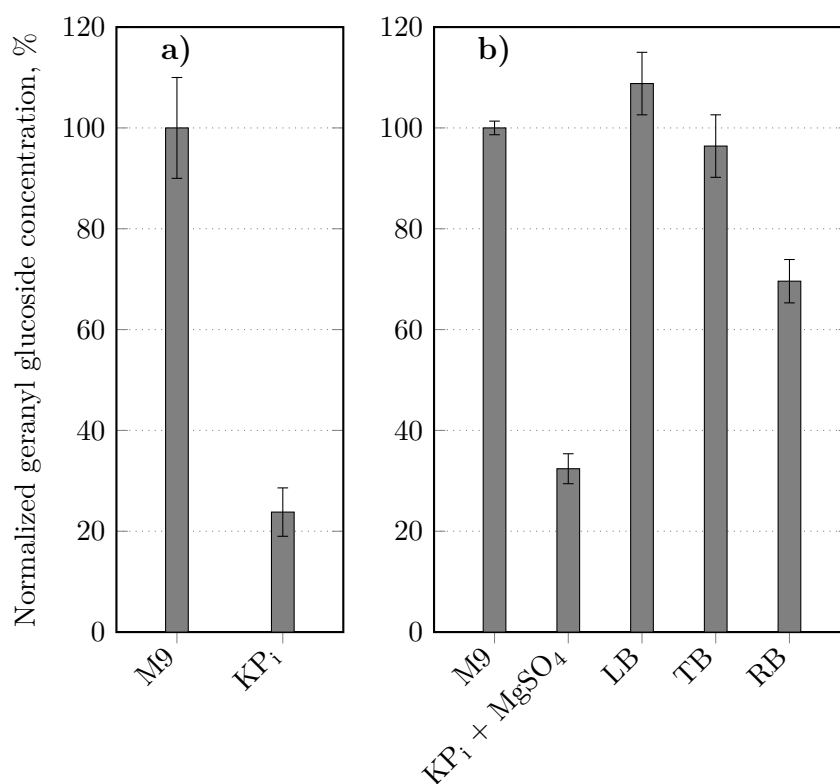
**Figure 7.5.:** Geranyl glucoside formation in parallelized biotransformations with different media at mL-scale. M9 mineral medium served as a reference. All concentrations are normalized to the product concentration formed in systems with M9. $KP_i$: 0.1 M potassium phosphate buffer pH 7. $KP_i$ + $MgSO_4$: 0.1 M potassium phosphate buffer pH 7 supplemented with 0.5 g $L^{-1}$ $MgSO_4$. LB: lysogeny broth. TB: terrific broth. RB: Riesenberg medium. Biotransformation settings: V = 10 mL, T = 30 °C, n = 2200 rpm, pH 7, t = 24 h, 6 g $L^{-1}$ *E. coli* BL21(DE3)pLysS pET29a_VvGT14a, 20 g $L^{-1}$ glucose. **a**: Single-phase system, 0.2 g $L^{-1}$ geraniol. **b**: Biphasic system with 20 % (v/v) isopropyl myristate, 0.8 g $L^{-1}$ geraniol.

**Discussion.**    The fact that whole-cell biotransformations of geraniol performed in potassium phosphate buffer result in significantly lower geranyl glucoside concentrations shows that a decoupling of the cellular metabolism and the biotransformation is not advantageous. Replacing M9 medium with potassium phosphate buffer causes "truly resting cells" [Willrodt et al. 2016], as they face an environment of complete nutrient limitation. This is in contrast to non-growing but metabolically active cells, induced by the omission of only one nutrient essential for growth, like nitrogen or magnesium (see Chapter 3.4). The reason why truly resting cells do not perform well in the biotransformation of geraniol might be attributed to UDP-glucose regeneration that is required for an effective biotransformation of geraniol and that only occurs in metabolically active cells. Buchhaupt et al. [2012] and Julsing et al. [2012] could also show that cofactor-dependent whole-cell bio-
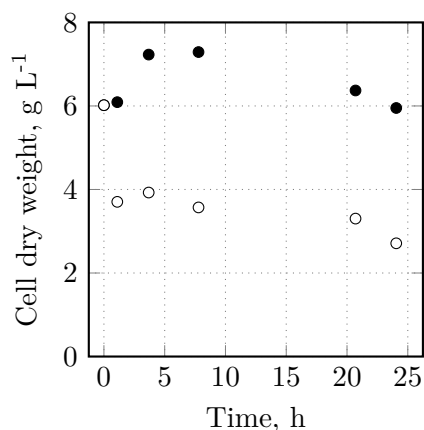
**Figure 7.6.:** Cell growth in potassium phosphate buffer (white circles) compared to M9 mineral medium (black circles) during biotransformations of geraniol at mL-scale. V = 10 mL, T = 30 °C, n = 2200 rpm, pH 7, t = 24 h, 6 g $L^{-1}$ *E. coli* BL21(DE3)pLysS pET29a_VvGT14a, 20 g $L^{-1}$ glucose, 0.8 g $L^{-1}$ geraniol, 20 % (v/v) isopropyl myristate.
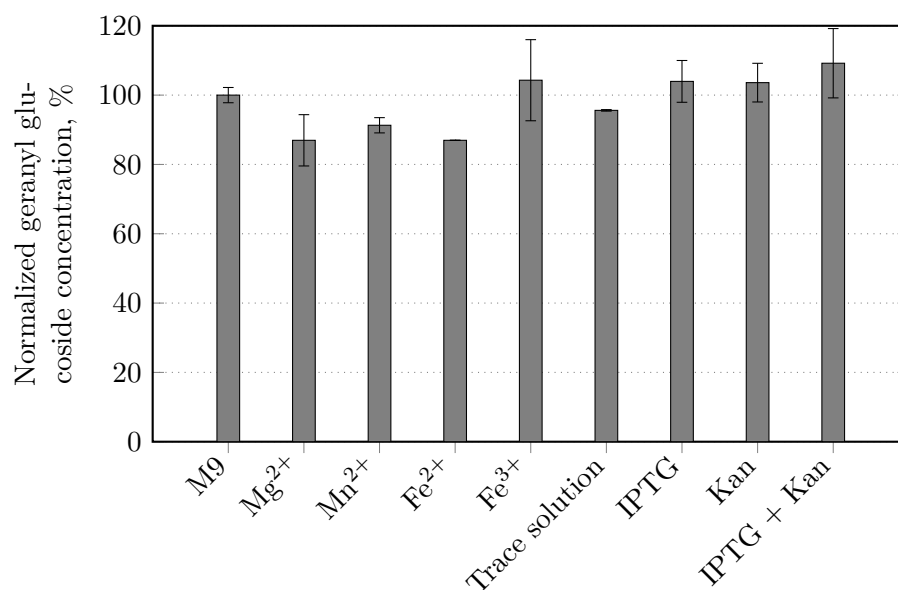


**Figure 7.7.:** Effect of different medium additives on biotransformations at mL-scale. M9 mineral medium served as a reference, and all concentrations are normalized to the product concentration measured in the system with M9. Following components were added to M9 mineral medium: 4 mM $MgSO_4$ ($Mg^{2+}$). 0.08 mM $MnCl_2$ ($Mn^{2+}$). 0.01 mM $FeSO_4$ ($Fe^{2+}$). 0.01 mM ferric citrate ($Fe^{3+}$). 100 µL trace element solution. 1 mM IPTG. 0.03 g $L^{-1}$ kanamycin (Kan). 1 mM IPTG and 0.03 g $L^{-1}$ kanamycin (IPTG + Kan). Biotransformation settings: V = 10 mL, T = 30 °C, n = 2200 rpm, pH 7, t = 24 h, 6 g $L^{-1}$ *E. coli* BL21(DE3)pLysS pET29a_VvGT14a, 20 g $L^{-1}$ glucose, 0.8 g $L^{-1}$ geraniol, 20 % (v/v) isopropyl myristate.

transformations performed in buffer instead of mineral medium result either in lower final product concentrations compared to non-resting cells or in complete activity loss of the biocatalysts within only 1.5 h, in spite of initial production rates being rather high.

Supplementing potassium phosphate buffer with magnesium slightly increases the biotransformation productivity, but still significantly drags behind the system with M9 mineral medium, indicating that other nutrients besides magnesium are required. The fact that biotransformations in M9 show identical results as processes performed in the complex media lysogeny broth and terrific broth shows that the mineral medium does not lack any crucial nutrients. The usage of Riesenberg medium decreases the productivity. Reasons might be the lack of sodium in this medium, or the presence of citric acid or trace solution (for the composition of Riesenberg medium refer to A.19). All in all, as complex media lack consistency in their exact composition and as neither potassium phosphate buffer nor Riesenberg medium show positive effects on the biotransformation of geraniol, M9 mineral medium should be the medium of choice. This medium was also used by Caputi et al. [2008] for the whole-cell glucosylation of different terpenoids, including geraniol.

In spite of Lairson et al. [2008] proposing that $Mg^{2+}$ or $Mn^{2+}$ function as necessary cofactors for certain UDP-dependent glycosyltransferases, an addition of these bivalent cations does not improve the biotransformation of geraniol. Either the magnesium concentration present in the regular M9 composition is sufficiently high, or neither of the cations is a cofactor used by VvGT14a. Paliy and Gunasekera [2007] could show a positive effect of the addition of bivalent iron to M9 medium on the growth of *E. coli* BL21, most likely because the cation is a cofactor for the enzymes of the tricarboxylic acid cycle and the aerobic respiration chain. However, here, no significant positive impact of bivalent iron could be shown, nor of the addition of trivalent iron or trace element solution. The addition of IPTG, kanamycin or a combination of both shows no significant positive effect on the geranyl glucoside concentration either. Antibiotics and inducers can be added to biotransformations to overcome plasmid loss and to potentially effectuate a continued recombinant protein production [Willrodt et al. 2016], in this case of VvGT14a. However, as neither of the components has a positive effect here, it can be assumed that plasmid loss is not a problem and that protein formation either continues anyways or cannot be continued during biotransformations at all. Omitting M9 ingredients decreases final product concentrations. The only M9 variation that leads to similar results as the regular M9 lacks $CaCl_2$ and NaCl - components that are only present in low concentrations of 0.01 and 0.5 g $L^{-1}$, respectively, in regular M9 anyways. Amongst other M9 variants, one tested version was M9 lacking nitrogen in order to channel glucose towards UDP-glucose syn-
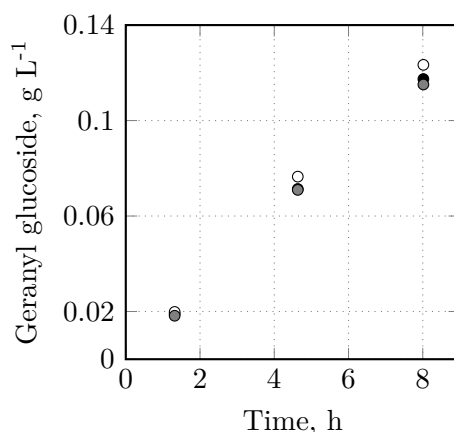
**Figure 7.8.:** Geranyl glucoside formation in systems with different isopropyl myristate fractions of 20 % (black circles), 10 % (white circles) and 5 % (gray circles) during biotransformations of geraniol at mL-scale (V = 10 mL, T = 30 °C, n = 4000 rpm, pH 7, t = 8 h, 6 g L$^{-1}$ *E. coli* BL21(DE3)pLysS pET29a_VvGT14a, 20 g L$^{-1}$ glucose, 0.8 g L$^{-1}$ geraniol).

thesis and not towards cell growth, resulting in non-growing cells. However, the nitrogen limitation does not have a positive effect on the biotransformation here. Willrodt et al. [2016] also concludes that a targeted nitrogen limitation, which impairs the synthesis of nucleic acids and proteins, is not the right strategy for efficient biotransformations.

All in all, the results show that regular M9 mineral medium should be the medium of choice for the whole-cell biotransformation of geraniol presented in this work, and that the whole-cell biocatalysts should not be in a truly resting state.

**Sequestering phase and geraniol**

In a next step, different isopropyl myristate fractions were compared in parallelized bio-transformations at mL-scale. The results are shown in Figure 7.8. It becomes apparent that product formation is identical for the different fractions of 20, 10 and 5 %, with no correlation between geranyl glucoside concentration and isopropyl myristate fraction. One difference became apparent, though: The lower the isopropyl myristate fraction is, the higher is the relative proportion of the interphase after phase separation by centrifugation (data not shown; interphase: stable emulsion of the non-aqueous phase and surface-active components of the aqueous phase [Brandenbusch et al. 2010]).

The amount of geraniol provided in isopropyl myristate for biotransformations has to be adjusted to the minimal inhibitory concentration of 0.3 g L$^{-1}$ in the aqueous phase, using the logarithmic partition coefficient of 2.42 determined in Chapter 6.1. Naturally, the higher the fraction of isopropyl myristate is, the more geraniol can be provided for the biotransformation. However, it was shown that the logarithmic partition coefficient of

geraniol in the actual biotransformation system amounts to only 1.67 (data not shown). A comparison of calculated initial geraniol concentrations in the aqueous phase for the biotransformations described in Figure 7.8 using either a logarithmic partition coefficient of 2.42 or 1.67 is shown in Table 7.1. When using the lower partition coefficient, the overall geraniol concentrations have to be selected more carefully in order to stay below the inhibitory concentration in the aqueous phase.

**Table 7.1.:** Geraniol concentrations in the aqueous phase in systems with different isopropyl myristate fractions (IPM) and an overall geraniol concentration of 0.8 g L$^{-1}$, comparing two different logarithmic partition coefficients (logPC). $c_{aq}$: Geraniol concentration in the aqueous phase.

| | $c_{aq}$ (g L$^{-1}$) in system with | | |
| --- | --- | --- | --- |
| logPC | 20 % IPM | 10 % IPM | 5 % IPM |
| 2.42 | 0.02 | 0.03 | 0.06 |
| 1.67 | 0.08 | 0.14 | 0.24 |

**Discussion.**    The fact that the isopropyl myristate fraction does not affect geranyl glucoside formation underlines the biocompatibility of this non-aqueous phase, as already shown in Chapter 6.1, and shows that even low geraniol concentrations present in the aqueous phase are sufficient for efficient biotransformations. Due to interphase formation, low fractions, especially 5 %, result in a complete "disappearance" of the organic phase after phase separation and therefore make HPLC analysis of the organic phase impossible. Thus, a fraction of 20 % is preferable. Nevertheless, as soon as a process as economically feasible as possible has to be designed, a lower fraction should be taken into consideration. Then, a destabilization of the interphase, e.g. by supercritical carbon dioxide as proposed by Brandenbusch et al. [2010], might be worthwhile.

The fact that the actual partition coefficient in the biotransformation set-up is significantly lower than the one measured in a cell-free M9–isopropyl myristate system might be explained with the interphase formation: As components of the aqueous phase are involved in forming the stable emulsion, the overall volume of the aqueous phase might decrease, resulting in higher aqueous geraniol concentrations. This requires a careful adjustment of the overall provided substrate concentration.

## 7.4.2. Biocatalyst concentration and oxygen availability

In a next step, the impact of the whole-cell biocatalyst concentration on geranyl glucoside formation was investigated in parallelized biotransformations at mL-scale, and the results are shown in Figure 7.9. When increasing the biocatalyst concentration from 4 to 6 g $L^{-1}$, a significant increase in the product concentration can be seen. However, when further increasing the cell concentration, no further increase in geranyl glucoside occurs, but instead even a decrease when using biocatalyst concentrations of 10 and 12 g $L^{-1}$. The reason for this phenomenon can be found in the oxygen supply during biotransformations: Whereas in the system with a biocatalyst concentration of 4 g $L^{-1}$ oxygen is limiting for ~1 hour, the cells in the other systems are exposed to an oxygen limitation for ~2.5–3 h right from the beginning of the process (see Figure 7.10).
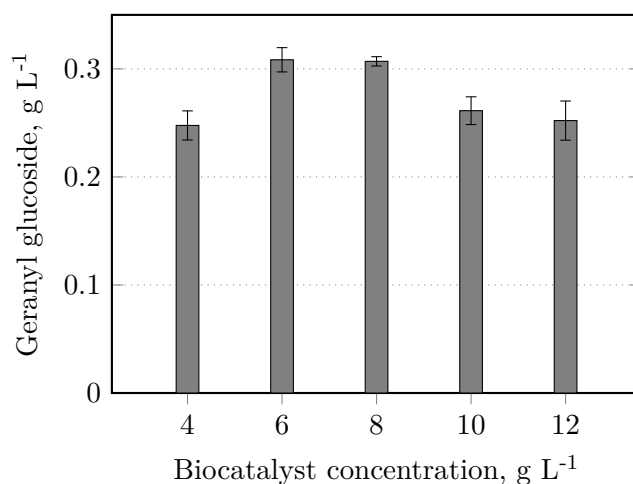


**Figure 7.9.:** Geranyl glucoside formation with different biocatalyst concentrations in biotransformations of geraniol at mL-scale (V = 10 mL, T = 30 °C, n = 2200 rpm, pH 7, t = 24 h, *E. coli* BL21(DE3)pLysS pET29a_VvGT14a whole-cell biocatalyst, 20 g $L^{-1}$ glucose, 0.8 g $L^{-1}$ geraniol, 20 % isopropyl myristate (v/v)).

In order to avoid oxygen limitations during biotransformations, trials with higher stirrer speeds were carried out, all with a biocatalyst concentration of 6 g $L^{-1}$. A stirrer speed of 2800 rpm was investigated (standard speed with baffled reactors [Kusterer 2007]). 4000 rpm was used as the second set point, as this is the highest operable speed at mL-scale. The results are depicted in Figure 7.11. The increase in stirrer speed from 2200 rpm to 2800 rpm does not show a significant effect, however, the increase to 4000 rpm entirely eliminates oxygen limitation. The intermittent drops in dissolved oxygen can be attributed to sampling, where the stirrer had to be stopped briefly in order to sample the entire content of the relevant reactors with cannulas.

A deeper look was taken into a biotransformation at 4000 rpm performed with 6 g $L^{-1}$
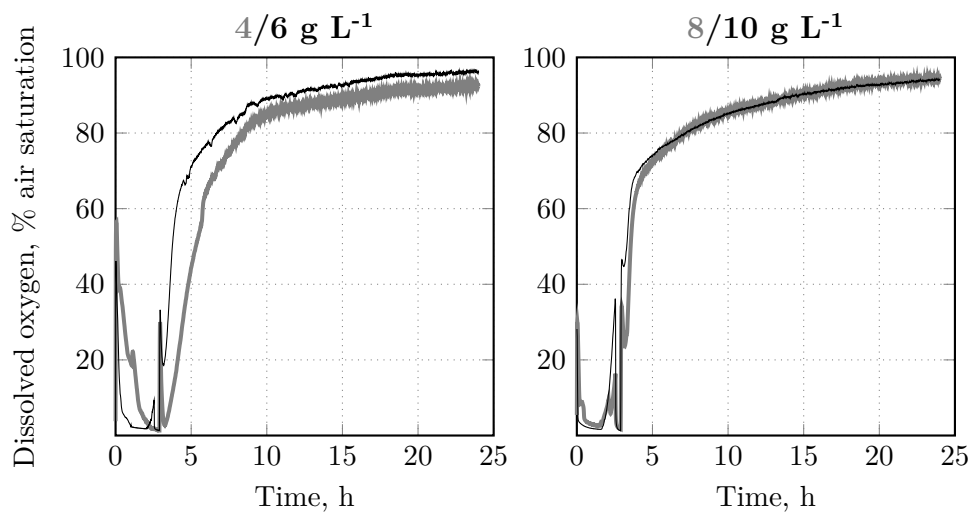
**Figure 7.10.:** Dissolved oxygen concentration during biotransformations with different biocatalyst con-
centrations (V = 10 mL, T = 30 °C, n = 2200 rpm, pH 7, t = 24 h, *E. coli*
BL21(DE3)pLysS pET29a_VvGT14a whole-cell biocatalyst, 20 g L$^{-1}$ glucose, 0.8 g L$^{-1}$
geraniol, 20 % isopropyl myristate (v/v)). Gray lines: 4 and 8 g L$^{-1}$ whole-cell biocatalyst.
Black lines: 6 and 10 g L$^{-1}$.
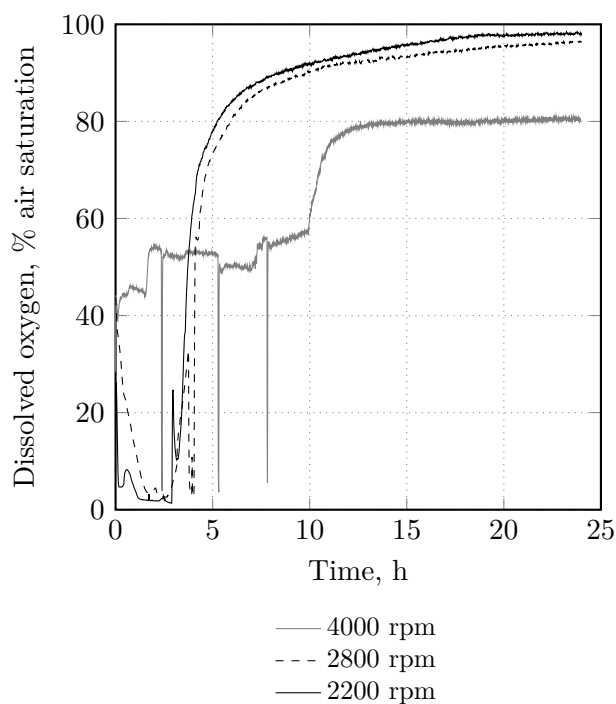


**Figure 7.11.:** Dissolved oxygen courses during biotransformations at different stirrer speeds (V = 10 mL,
T = 30 °C, pH 7, t = 24 h, 6 g L$^{-1}$ *E. coli* BL21(DE3)pLysS pET29a_VvGT14a whole-cell
biocatalyst, 20 g L$^{-1}$ glucose, 0.8 g L$^{-1}$ geraniol, 20 % isopropyl myristate (v/v)).

biocatalysts and was directly compared to the process with 2200 rpm. The respective results are shown in Figure 7.12. It becomes apparent that the oxygen-rich environment created by 4000 rpm results in higher geranyl glucoside concentrations than the process with 2200 rpm, and that full conversion of geraniol can be obtained (however, a lower initial geraniol concentration was used for the experiment at 4000 rpm). Glucose is fully consumed by the cells within ~10 h (no data available for the process with 2200 rpm) and, in contrast to the process performed under oxygen-limiting conditions, no acetate accumulates throughout the process (only endpoint determination for the process with 2200 rpm). The pH courses of the two processes are similar, with the values for 4000 rpm being slightly shifted upwards (both processes were conducted without pH control). In both processes the biocatalyst grows during the first ~10 h. Afterwards, the cells in the process with 4000 rpm are in a stationary phase, whereas the cells in the process with the lower stirrer speed are subjected to cell dying.

With the higher stirrer speed of 4000 rpm, studies on the influence of the biocatalyst concentration on the biotransformation of geraniol were rerun and the resulting geranyl glucoside concentrations are shown in Figure 7.13. In contrast to the results generated at a stirrer speed of 2200 rpm, where an increase of the biocatalyst concentration above 6 g L$^{-1}$ did not result in an increase in product concentrations (see Figure 7.9), here, a significant increase in produced geranyl glucoside can be seen when doubling the cell concentration to 12 g L$^{-1}$. However, the product concentration increases only by 17 %, which is far away from the expected raise by 100 %. No further increase can be seen when increasing the cell concentration to 16 g L$^{-1}$, in spite of still working in an oxygen-abundant environment (data not shown).

One effect that was observed when raising the biocatalyst concentration was an increase in the thickness of the interphase between aqueous and organic phase after phase separation by centrifugation (see also Chapter 7.4.1). Interphase formation and thickness were not affected by different centrifugation temperatures (4/20/30 °C) nor by different sample storage temperatures (4 °C and 20 °C) prior to centrifugation. Increasing the centrifugation speed from 3,260 g to 16,249 g and/or the centrifugation duration from 10 to 20–30 min can result in the re-formation of a small organic phase fraction (10–100 µL), however, these effects were not fully reproducible. The interphase can be separated from the other phases with a spatula (see Figure 7.14), resuspended in methanol and analyzed by HPLC. Thereby, geranyl glucoside could be detected, but only at amounts at most 5 % (w/w) as high as the total produced product (data not shown). However, a carryover of aqueous phase when separating the interphase with a spatula cannot be ruled out.
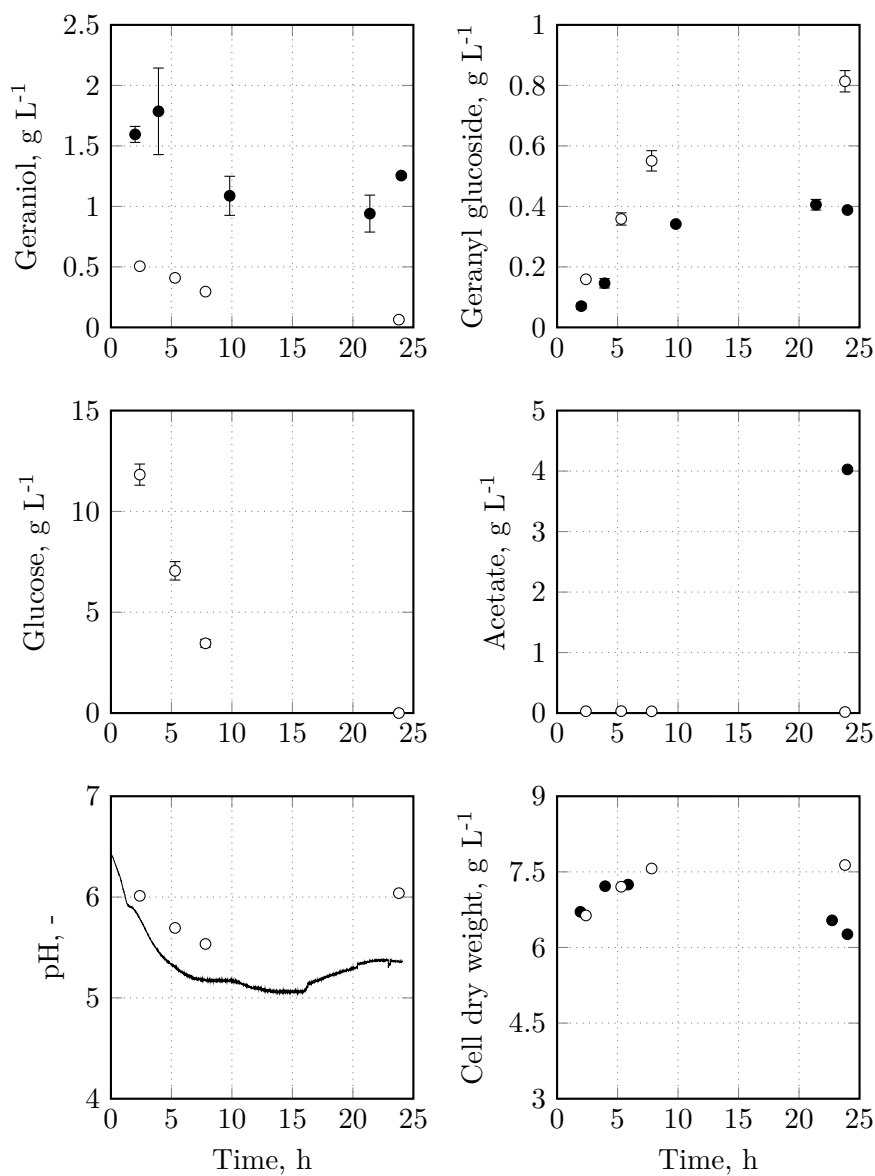
**Figure 7.12.:** Courses of geranyl glucoside, geraniol, glucose, acetate, pH and cell dry weight concentrations during batch biotransformations at mL-scale at either 2200 rpm (black circles/black line) or 4000 rpm (white circles). V = 10 mL, T = 30 °C, 6 g L$^{-1}$ *E. coli* BL21(DE3)pLysS pET29a_VvGT14a whole-cell biocatalyst, 20 g L$^{-1}$ glucose, 0.8 or 1.6 g L$^{-1}$ geraniol, 20 % isopropyl myristate (v/v).
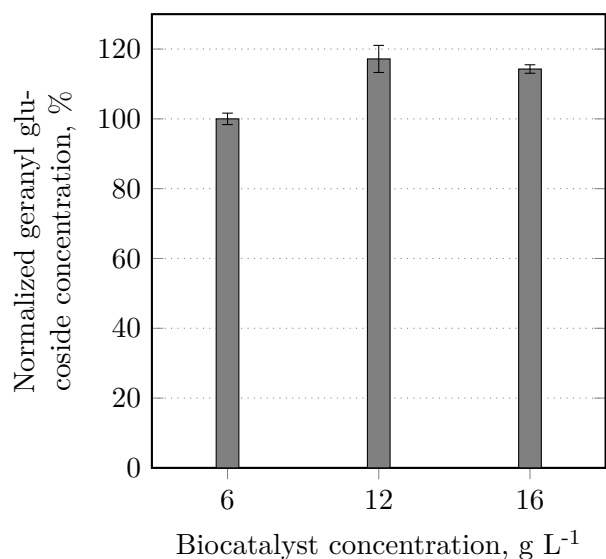
**Figure 7.13.:** Geranyl glucoside formation with different biocatalyst concentrations in biotransformations of geraniol at mL-scale with a stirrer speed of 4000 rpm. Geranyl glucoside concentrations are normalized to the result of the process with a biocatalyst concentration of 6 g $L^{-1}$. V = 10 mL, T = 30 °C, n = 4000 rpm, pH 7, t = 8 h, *E. coli* BL21(DE3)pLysS pET29a_VvGT14a whole-cell biocatalyst, 20 g $L^{-1}$ glucose, 0.8 g $L^{-1}$ geraniol, 20 % isopropyl myristate (v/v).
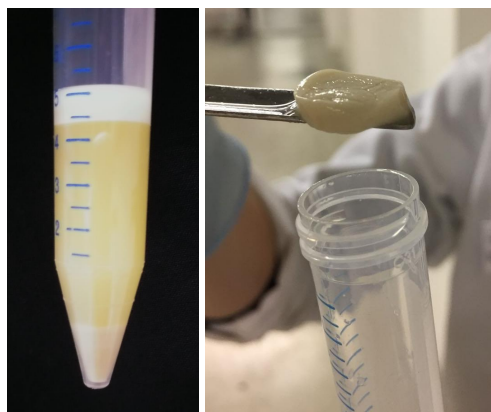


**Figure 7.14.: Left:** Interphase with a volume of ~0.5 mL after phase separation by centrifugation (10 min, 3260 g). The original system contained 5 % (v/v) isopropyl myristate, which "disappears" entirely in the interphase. **Right:** Interphase separated from the medium with a spatula.

**Discussion.**    All in all, the presented results show that an adequate oxygen supply is crucial for the biotransformation of geraniol. Oxygen-limiting conditions result in incomplete conversion of geraniol and strong acetate formation. Acetate is a product of the mixed-acid fermentation, which is induced by anaerobic conditions and/or high glucose concentrations [Schlegel 1992]. The reason for stagnating geranyl glucoside formation might lie in the cytotoxic properties of acetate [de Mey et al. 2007] and a resulting deactivation of the cell metabolism. This finding reinforces the outcome of Chapter 7.4.1, where truly resting cells were found to be unsuitable for the biotransformation of geraniol.

Increasing the stirrer speed from 2200 rpm to 4000 rpm results in improved oxygen supply. However, even under oxygen-rich conditions an increase in biocatalyst concentration does not lead to a proportional increase of the product concentration. This implies that by proper oxygen availability indeed one bottleneck of the biotransformation can be removed, but that a different bottleneck still exists.

Stable emulsions can be formed in biphasic systems consisting of an aqueous phase and a non-miscible organic phase by the interaction of surface-active components, originally located in the water phase, with the organic phase. The formation of such interphases is a well-known problem arising during and after two-liquid-phase biotransformations [van Sonsbeek et al. 1993]. Surface-active substances are amphiphilic molecules, as for example inorganic electrolytes and macromolecules such as proteins or polysaccharides. The compound contributing the most to interphase formation is the microorganism itself though [Brandenbusch et al. 2010], explaining the increase in interphase thickness observed here when raising the biocatalyst concentration. As geranyl glucoside is an amphiphilic molecule, too, its presence in the interphase makes sense. However, the small amounts measured in the interphase here might also originate from the aqueous phase which might have been carried over together with the interphase. All in all, as no way of preventing interphase formation could be identified here, small potential product losses have to be acquiesced.

## 7.4.3. pH and temperature

Schmideder et al. [2016b] could show that the pH optimum for the whole-cell biocatalysis of geraniol with *E. coli* BL21(DE3)pLysS pET29a_VvGT14a in a purely aqueous system consisting of M9 mineral medium lies at pH 7. However, during biotransformations at mL-scale with an initial, uncontrolled pH 7, the value drops to pH 5 (see Figure 7.15 a). Controlling the pH to pH 7 results in a significantly increased geranyl glucoside concentration (see Figure 7.15 b).
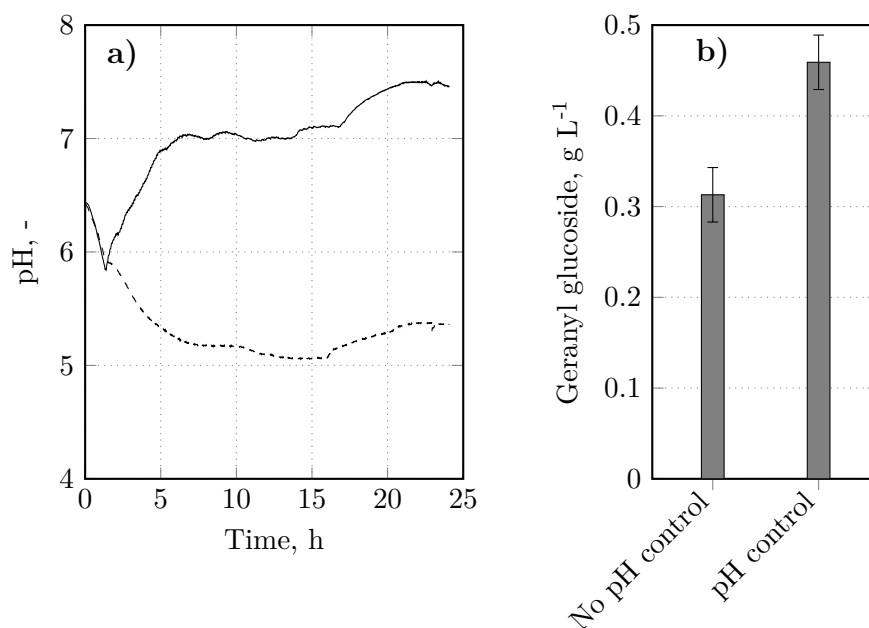
**Figure 7.15.:** Effect of pH control on the pH course (**a**) and the geranyl glucoside formation (**b**) during whole-cell biotransformation of geraniol. Dashed line: no pH control, solid line: pH control (pH 7). V = 10 mL, T = 30 °C, n = 2200 rpm, pH 7, t = 24 h, *E. coli* BL21(DE3)pLysS pET29a_VvGT14a whole-cell biocatalyst, 20 g L$^{-1}$ glucose, 0.8 g L$^{-1}$ geraniol, 20 % isopropyl myristate (v/v).

An increase in the process temperature from 30 °C to 37 °C results in an 1.2-fold increase of the product concentration after 8 h of biotransformation (data not shown).

**Discussion.**    The pH drop in pH-uncontrolled processes can be attributed to the formation of acid metabolic by-products, in this case acetate (the processes described here were still conducted at a stirrer speed of only 2200 rpm). A drop to values around pH 6 is usually not harmful for *E. coli*, as the intracellular pH is regulated independently from the extracellular pH. However, values below pH 6 facilitate the transport of undissociated acids into the cells, resulting in physiological damage [Schlegel 1992]. Thus, pH control during whole-cell biotransformations of geraniol is very reasonable, ideally with higher precision than during the process presented here. The initial pH decrease in the process with pH control can be attributed to the fact that at mL-scale, pH control can only be started 1 h after process start, as the originally dry pH sensors require time to swell in the reaction medium. The pH increase after 15 h of process time can be ascribed to the application of a one-sided pH control, resulting in overtitration once the production of acid metabolites stops.

The positive impact of a temperature increase on product formation can be explained

with the Arrhenius equation, which describes the temperature dependence of reaction rates. The equation states an exponential dependence of the rate constant from temperature [Mortimer and U. Müller 2007]. Here, no exponential dependence of product formation on the reaction temperature can be seen, but only a linear dependence: With an 1.2-fold increase in temperature, a 1.2-fold increase in the geranyl glucoside concentration can be measured. This might be due to other factors affecting the whole-cell biotransformation, e.g. the temperature optimum of purified VvGT14a lying at 30 °C Bönisch et al. [2014a].

## 7.5. By-product formation during whole-cell biotransformations

Even during biotransformations with full conversion of geraniol, the geranyl glucoside yield amounts only to 50-70 %. This is why after biotransformations, the organic phase isopropyl myristate was analyzed by LC-MS, in order to identify potential side products geraniol might be converted to. Such by-products might be nerol, resulting from isomerization of geraniol, or geranial and neral, being formed through dehydrogenization catalyzed by *E. coli* endogenous dehydrogenases [Zhou et al. 2014]. However, none of these molecules were detected, but instead, geranyl acetate was found in notable amounts (data not shown). With this background, geranyl acetate could be quantified by HPLC. A typical course of a biotransformation of geraniol at mL-scale is shown in Figure 7.16. In this case, 12 % geraniol are channeled into geranyl glucoside formation, and 33 % into geranyl acetate production. The incomplete conversion of the substrate can be explained with the oxygen limitation present in this system which was stirred at a speed of only 2200 rpm (see Chapter 7.4.2).

### 7.5.1. Understanding the cause of geranyl acetate formation

In a next step, it was to be clarified why geranyl acetate is formed in such high amounts during the biotransformation of geraniol. In order to investigate whether geranyl acetate is produced in a cell-free system, 2 g L$^{-1}$ acetic acid were incubated with 0.5 g L$^{-1}$ geraniol in M9 medium (pH 7.5) for 24 h. No geranyl acetate could be quantified (data not shown), indicating that the acetylation of geraniol requires the presence of the whole-cell biocatalyst and is therefore an enzymatic process. The acetylation does not only occur in a biphasic system as described earlier, but also during *de novo* synthesis of geraniol in a
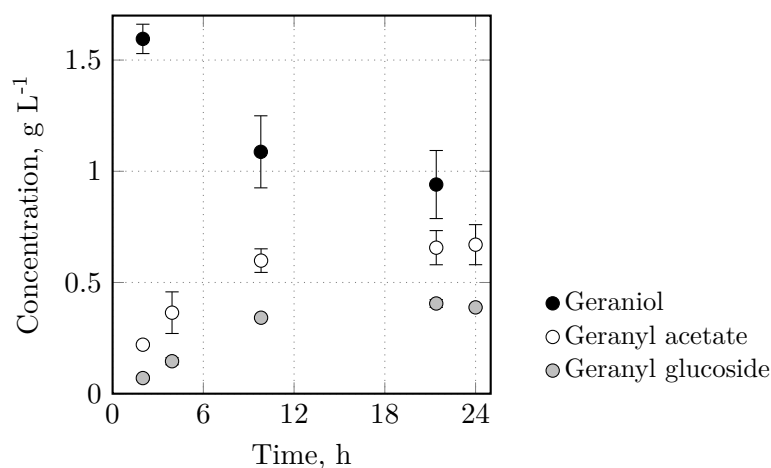
**Figure 7.16.:** Distinct geranyl acetate formation during a biotransformation at mL-scale (V = 10 mL, T = 30 °C, n = 2200 rpm, pH 7, t = 24 h, 6 g L$^{-1}$ *E. coli* BL21(DE3)pLysS pET29a_VvGT14a whole-cell biocatalyst, 20 g L$^{-1}$ glucose, 1.6 g L$^{-1}$ geraniol, 20 % iso-propyl myristate (v/v)).

purely aqueous system [Zhou et al. 2014].

Enzymes that catalyze the acetylation of alcohols are called alcohol O-acetyltransferase. *E. coli* possesses ~10 endogenous O-acetyltransferases [Keseler et al. 2017], thus the identification of the responsible enzyme by knock-out experiments was not possible within the context of this work. Moreover, these enzymes are most likely essential for a functioning metabolism. Zhou et al. [2014] reports that chloramphenicol acetyltransferase (CAT), which is responsible for chloramphenicol resistance, has the capacity to acetylate geraniol. In the biocatalyst *E. coli* BL21(DE3)pLysS pET29a_VvGT14a used in this project, CAT is encoded on the pLysS plasmid and thus might indeed be the reason for geranyl acetate formation.

In order to get a deeper understanding of CAT activity, the capacity for the acetylation of different alcoholic flavor and fragrance substrates was compared for the two *E. coli* strains BL21(DE3) and BL21(DE3)pLysS. Besides chloramphenicol as a reference substrate (see Figure 7.17), benzyl alcohohl, 2-phenylethanol, vanillin, geraniol and linalool were used as substrates (chemical structures are depicted in Figure 6.6). Potential acetylated products were quantified by HPLC and the results are depicted in Figure 7.18.

It becomes apparent that CAT shows the highest activity towards CAM. Besides, the strain BL21(DE3)pLysS containing CAT acetylates all substrates except linalool. Cells of the BL21(DE3) strain show either no activity towards the substrates at all, or a small activity towards benzyl alcohol and geraniol, which is significantly lower than that of the BL21(DE3)pLysS strain.
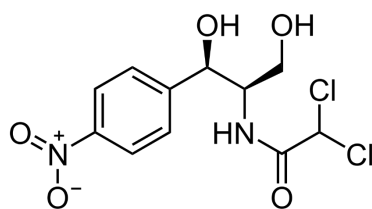
**Figure 7.17.:** Chemical structure of chloramphenicol



BL21(DE3)
BL21(DE3)pLysS
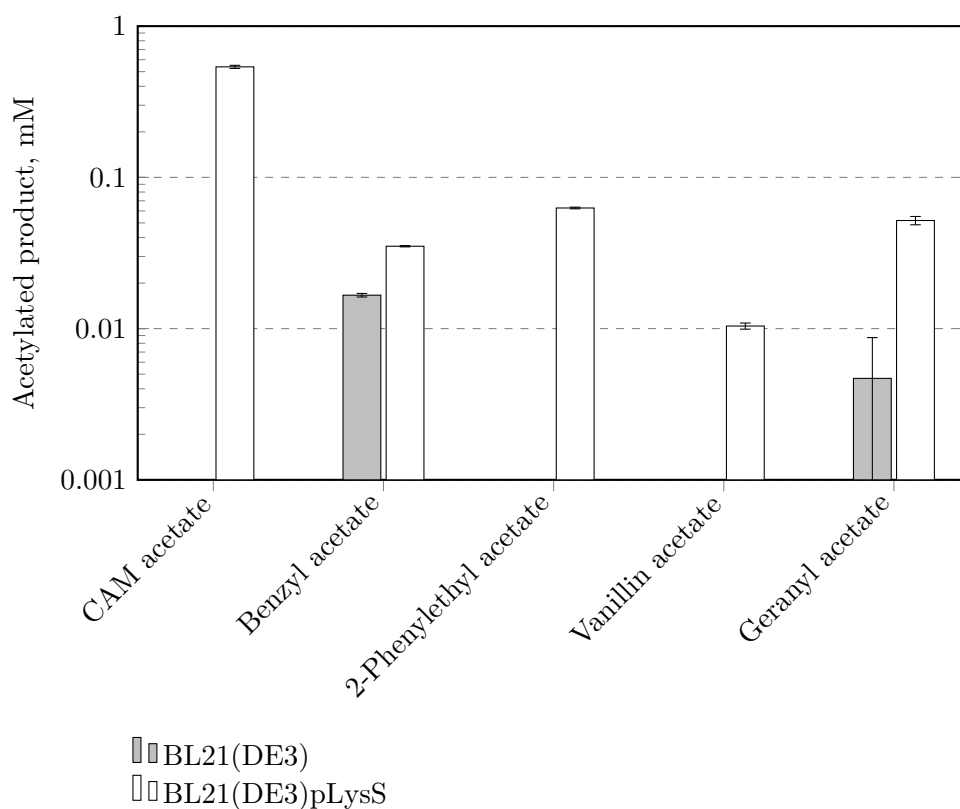
**Figure 7.18.:** Acetylation of different flavors and fragrances by chloramphenicol acetyltransferase (CAT): Comparison of the formation of acetylated substances by *E. coli* BL21(DE3) cells with and without the pLysS plasmid encoding CAT. Cell growth in shake flasks in complex medium, followed by incubation of 6 g $L^{-1}$ cells with 1 mM of either chloramphenicol (CAM), benzyl alcohol, 2-phenylethanol, vanillin, geraniol or linalool in biphasic systems consisting of 20 % (v/v) organic phase in M9 mineral medium at mL-scale for 15 h at 30 °C and 2200 rpm.

**Discussion.**    All in all, a promiscuity of CAT was shown here and it was proven that this o-acetyltransferase is mostly responsible for the formation of geranyl acetate from geraniol. It is not surprising that CAT shows the highest activity towards chloramphenicol among the tested substrates, as promiscuous enzymes exhibit the highest activity towards their native substrate [Khersonsky and Tawfik 2010]. Whereas the acetylation of 2-phenylethanol by CAT is known [Rodriguez et al. 2014], its capacity to acetylate benzyl alcohol and vanillin was shown here for the first time. The fact that benzyl alcohol and geraniol are acetylated even in the absence of CAT implies the presence of inherent *E. coli* enzymes that are capable of acetylating these molecules as well. Moreover, a correlation between the steric accessibility of the alcohol group in a substrate and the extent of its acetylation can be seen: 2-phenylethanol and geraniol possess the easiest accessible alcohol groups and the highest extent of acetylation. Steric hindrance might also explain the entirely absent acetylation of linalool, in spite of this substrate being geraniol's constitutional isomer.

## 7.5.2. Prevention of geranyl acetate formation by strain selection

Geranyl acetate is exclusively located in the organic phase when working with the biphasic biotransformation system consisting of M9 and isopropyl myristate. Thus, no distribution coefficient can be calculated. When being incubated in a purely aqueous system with *E. coli* BL21(DE3)pLysS pET29a_VvGT14a, the substance shows a growth-inhibiting effect at concentrations higher than 0.1 g L$^{-1}$ after 4 h (see Figure 7.19). However, even concentrations as high as 0.8 g L$^{-1}$ do not impair the biotransformation of geraniol in a biphasic system (data not shown), implying a sufficiently fast transport of the cytotoxic substance from the aqueous into the organic phase. Nevertheless, in spite of not affecting the biotransformation itself, a distinct production of geranyl acetate significantly reduces the amount of geraniol available for geranyl glucoside formation. Thus, in order to design an efficient biotransformation process, byproduct formation has to be overcome.

As it was shown that mostly CAT is responsible for geranyl acetate formation in *E. coli* BL21(DE3)pLysS, the project partner (Prof. Schwab, Associate Professorship of Biotechnology of Natural Products, Technical University of Munich) provided a strain carrying a modified pLysS plasmid where the chloramphenicol resistance, thus the CAT gene, is replaced by an ampicillin resistance ($\beta$-lactamase gene). This strain is called *E. coli* BL21(DE3)pLysS**A** pET29a_VvGT14a. The two strains will be abbreviated with pLysS and pLysSA in the following. Just as the reference biocatalyst, the new strain was grown to high cell densities at L-scale. A set growth rate of 0.18 h$^{-1}$ was used during the
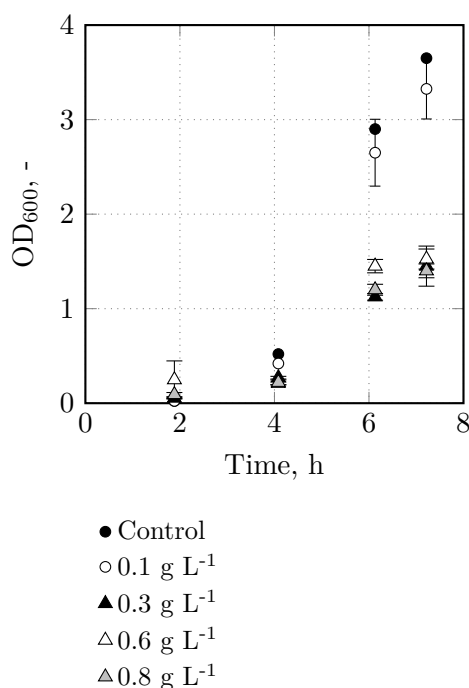
**Figure 7.19.:** Effect of geranyl acetate on the growth of *E. coli* BL21(DE3)pLysS pET29a_VvGT14a. The cells were grown at 37 °C and 250 rpm in shake flasks containing LB medium and different concentrations of geranyl acetate. The control did not contain geranyl acetate. The optical density ($OD_{600}$) was measured regularly.

exponential growth phase, protein expression was induced with 0.1 mM IPTG, a linear post-induction feeding profile with a gradient of 0.150 g $L^{-1}$ $h^{-2}$ was applied, and the process was conducted for 48 h, as these were the conditions defined as the most suitable ones for the reference strain pLysS in Chapter 5.3. Afterwards, a biotransformation was conducted at mL-scale. A comparison between the two strains regarding cell growth during HCDC and product formation during biotransformation is shown in Figures 7.20 and 7.21.

pLysSA shows slightly increased cell growth during the protein expression phase of the HCDC, resulting in a final cell dry weight of 69.9 $\pm$ 0.2 g $L^{-1}$, in comparison to 61.6 $\pm$ 0.1 g $L^{-1}$ for pLysS. The replacement of the antibiotic resistance on the pLysS plasmid fully tackles byproduct formation, as no geranyl acetate is formed during the whole-cell biotransformation of geraniol at all. However, geranyl glucoside formation is drastically affected, too: the obtained final product concentration is 8-times lower than with pLysS. Thus, the expression of VvGT14a during the HCDC of pLysSA was analyzed by SDS-PAGE, and no target protein bands could be seen on the gel (data not shown). In order to potentially increase product formation, the effect of higher IPTG concentrations on geranyl glucoside formation was studied. For this purpose, pLysSA was
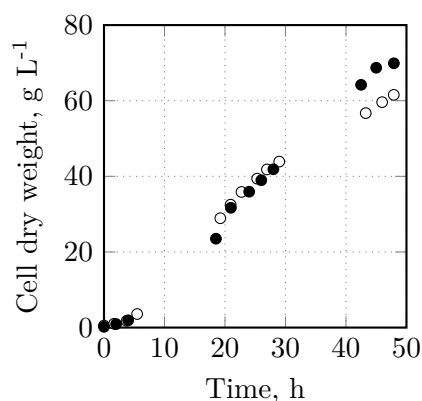
**Figure 7.20.:** Comparison of cell growth during high cell density cultivations of the strains *E. coli* BL21(DE3)pLysS pET29a_VvGT14a (white circles) and *E. coli* BL21(DE3)pLysSA pET29a_VvGT14a (black circles) (V = 2 L, T = 37/20 °C, pH 6.8, DO > 25 %).
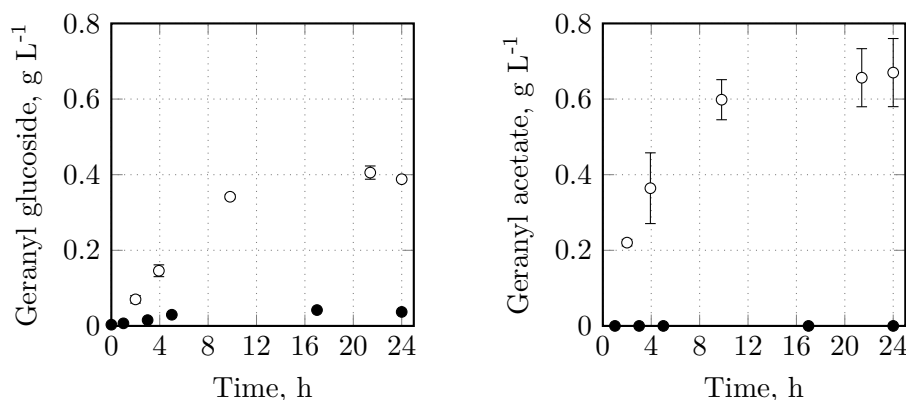


**Figure 7.21.:** Comparison of geranyl glucoside (left graph) and geranyl acetate (right graph) formation for the strains *E. coli* BL21(DE3)pLysS pET29a_VvGT14a (white circles) and *E. coli* BL21(DE3)pLysSA pET29a_VvGT14a (black circles) (Biotransformations: V = 10 mL, T = 30 °C, n = 2200 rpm, pH 7, t = 24 h, 6 g L$^{-1}$ biocatalyst, 20 g L$^{-1}$ glucose, 0.8 g L$^{-1}$ geraniol, 40 % isopropyl myristate (v/v)).

grown in shake flasks and protein production was induced with the IPTG concentrations 0.1, 0.8, 1.0, 1.5 and 2.0 mM. Subsequently, the cells were harvested and used for whole-cell biotransformations at mL-scale. The results are shown in Figure 7.22. It becomes apparent that an increase in IPTG concentration from 0.1 to 0.8 mM has a very distinct positive effect on geranyl glucoside formation, a further increase to 1.0 mM results in a slight further enhancement, afflicted with a rather high standard deviation though. A further raise of IPTG shows no positive effect.

Subsequently, the IPTG concentrations 0.8 and 1.0 mM were tested in HCDCs at L-scale, and again geranyl glucoside formation was measured during successive biotransformations at mL-scale. The courses of the cell dry weight concentrations during HCDCs and
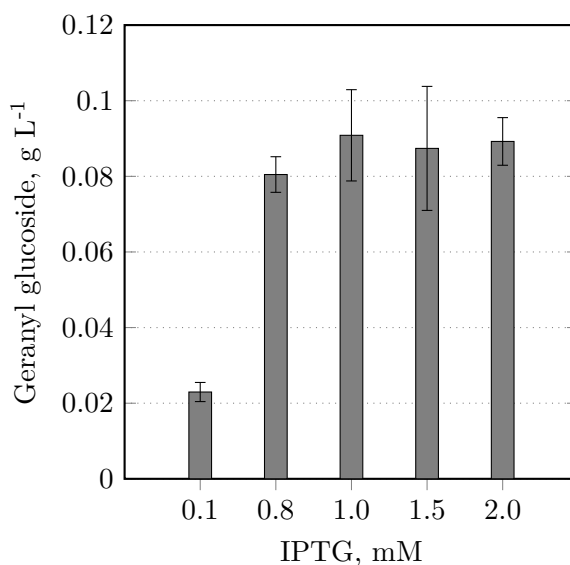
**Figure 7.22.:** Comparison of geranyl glucoside formation by the strain *E. coli* BL21(DE3)pLysSA pET29a_VvGT14a when using different IPTG concentrations for VvGT14a production during preceding biocatalyst expression in shake flasks. Conditions of the biotransformations: V = 10 mL, T = 30 °C, n = 2200 rpm, pH 7, t = 24 h, 6 g $L^{-1}$ biocatalyst, 20 g $L^{-1}$ glucose, 0.8 g $L^{-1}$ geraniol, 40 % isopropyl myristate (v/v).

of geranyl glucoside concentrations during biotransformations are depicted in Figure 7.23. It becomes apparent that no correlation exists between cell growth and applied IPTG concentration for pLysSA, however, a clear interrelation between IPTG concentration and geranyl glucoside formation can be seen: The more IPTG is used for induction of VvGT14a expression, the more geranyl glucoside is formed. Special emphasis should be put on the volumetric product formation rates within the first 5 h of the biotransformations, as the subsequent stagnation of geranyl glucoside formation can be attributed to oxygen-limited conditions (the experiments were conducted at a stirrer speed of only 2200 rpm, resulting in an anaerobic environment and a negative impact on the glucosylation reaction, see Chapter 7.4.2). These rates depict the identical result as the final concentrations: Higher IPTG concentrations lead to higher initial product formation rates. It becomes apparent that with pLysSA induced with 1.0 mM IPTG, the same rate can be reached as with pLysS induced with 0.1 mM IPTG (see Table 7.2). Nevertheless even with 1.0 mM IPTG no target protein bands could be seen on SDS-PAGE gels (data not shown).

In a next step, the temperature during the protein expression phase in the HCDC was increased from 20 to 30 °C, and the influence on cell growth and geranyl glucoside formation was measured, as shown in Figure 7.24. The higher expression temperature results in less distinct cell growth after induction. No impact on geranyl glucoside production can be seen (see Table 7.2), nor could VvGT14a be detected by SDS-PAGE (not shown).
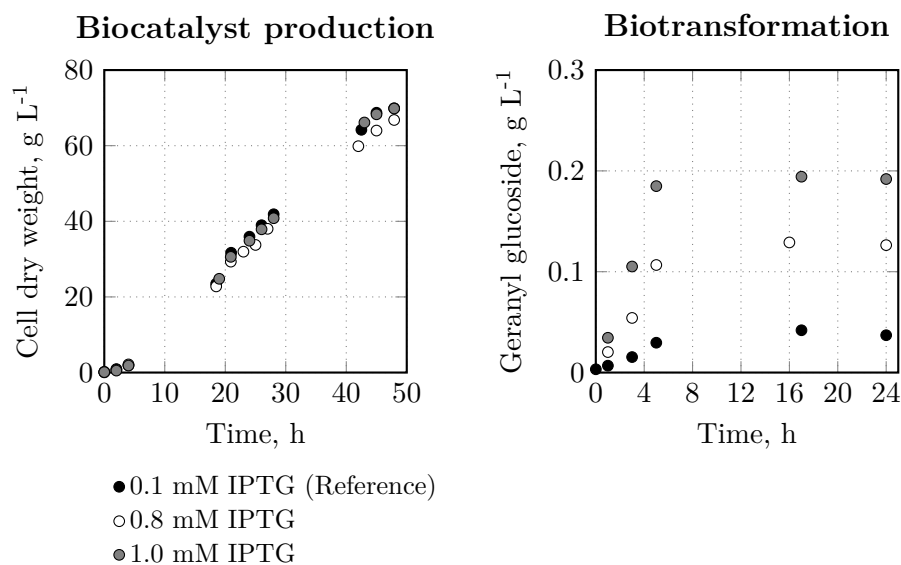
**Figure 7.23.:** Comparison of cell growth during high cell density cultivations (HCDCs) at L-scale and geranyl glucoside formation during biotransformations of geraniol at mL-scale using different IPTG concentrations with the strain BL21(DE3)pLysSA pET29a_VvGT14a (HCDC: V = 2 L, T = 37/20 °C, pH 6.8, DO > 25 %. Biotransformations: V = 10 mL, T = 30 °C, n = 2200 rpm, pH 7, t = 24 h, 6 g L$^{-1}$ biocatalyst, 20 g L$^{-1}$ glucose, 0.8 g L$^{-1}$ geraniol, 40 % isopropyl myristate (v/v)).
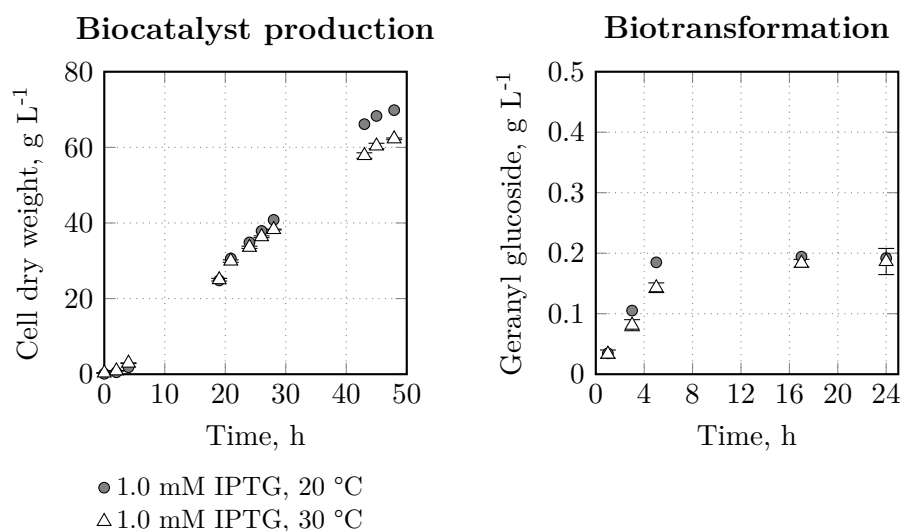


**Figure 7.24.:** Comparison of cell growth during high cell density cultivations (HCDCs) at L-scale and geranyl glucoside formation during biotransformations of geraniol at mL-scale using different IPTG concentrations and expression temperatures with the strain BL21(DE3)pLysSA pET29a_VvGT14a (HCDC: V = 2 L, T = 37/20 or 37/30 °C, pH 6.8, DO > 25 %. Biotransformations: V = 10 mL, T = 30 °C, n = 2200 rpm, pH 7, t = 24 h, 6 g L$^{-1}$ biocatalyst, 20 g L$^{-1}$ glucose, 0.8 g L$^{-1}$ geraniol, 40 % isopropyl myristate (v/v)).

**Table 7.2.:** Comparison of volumetric geranyl glucoside formation rates ($r_{GG}$) for pLysS and pLysSA at mL-scale. The rates were calculated at 5 h of process time.

|  | $r_{GG}$, mg L$^{-1}$ h$^{-1}$ |
| --- | --- |
| **pLysS** | |
| 0.1 mM | 37.1 |
| **pLysSA** | |
| 0.1 mM | 5.9 |
| 0.8 mM | 21.3 |
| 1.0 mM | 37.0 |
| 1.0 mM, 30 °C | 28.6 |

**Discussion.**   All in all, geranyl acetate formation can be prevented by using the pLysSA strain. However, VvGT14a expression seems to be significantly weaker than in pLysS and requires higher IPTG concentrations. The weaker VvGT14a expression seems to have a positive impact on cell growth, as the cell dry weight concentrations during the HCDC expression phase are higher for pLysSA than for pLysS. This negative correlation between VvGT14a expression and cell growth was already observed in Chapter 5.3. The positive correlation between the IPTG concentration and the produced geranyl glucoside amount is contrary to the results described in Chapter 5.3, where even a small increase in IPTG concentration from 0.1 to 0.2 mM resulted in complete suppression of VvGT14a expression in pLysS. It is unclear why the exchange of solely the antibiotic resistance gene on the pLysS plasmid has such a tremendous effect on VvGT14a expression. One explanation might be that CAT acetylates a metabolite or enzyme that is crucially involved in transcription or translation of VvGT14a and that such an acetylation improves the expression significantly. The fact that VvGT14a cannot be detected by SDS-PAGE at all for pLysSA, inspite of the biocatalyst possessing glucosylation activity, might be explained with the low sensitivity of the applied Coomassie Brilliant Blue staining, where the lower detection limit is 50–100 ng [Georgiou et al. 2008]. With the SDS-PAGE method used here (see Chapter 4.8.5), even VvGT14a concentrations of 7.5 g L$^{-1}$, which are commonly produced by pLysS, lie close to the lower limit, making it impossible to detect significantly lower concentrations. An alternative method could be silver staining, featuring a lower detection limit of 0.1–1 ng [Blum et al. 1987].

## 7.6. Process variations at L-scale for increased product concentrations

### 7.6.1. Processes with *E. coli* BL21(DE3)pLysSA pET29a_VvGT14a

After proving that pLysSA is a suitable strain for byproduct-free glucosylation of geraniol and after identifying the IPTG concentration that leads to the maximal observed biocatalytic activity, it was to be investigated whether geranyl glucoside concentrations and yields can be increased further. For this purpose, experiments were conducted in stirred-tank bioreactors at L-scale, as at mL-scale, DO and pH control was technically not feasible at that point in time. The effect of three different variables on geranyl glucoside formation was studied: The glucose supply strategy, the biocatalyst concentration, and the geraniol concentration present in the aqueous phase.

**Glucose supply strategy.**    Preliminary studies at mL-scale, which were conducted over a short process time of 3 h, showed that glucose does not necessarily have to be provided as a batch concentration of 20 g $L^{-1}$. Alternatively, the substrate can be provided as periodic pulses and thereby kept at limiting concentrations without negatively affecting geranyl glucoside production (data not shown). This result was to be reviewed at L-scale over a longer process time of 12 h. Two experiments were conducted: One biotransformation with a batch glucose concentration of 20 g $L^{-1}$ (Experiment A), and one with an initial glucose concentration of 1.5 g $L^{-1}$, followed by a glucose feed (Experiment B). The applied feeding rate of 1.5 g $L^{-1}$ $h^{-1}$ was based on specific glucose consumption rates calculated from earlier experiments (data not shown). The process variables are listed in Table 7.3, where important process results are listed as well. The courses of dissolved oxygen, glucose, acetate, cell dry weight, geranyl glucoside and geraniol concentrations are depicted in Figure 7.25.

The calculated feeding rate in Experiment B results in glucose-limiting conditions throughout the entire process. Thereby, the acetate levels during the first 8 h can be kept lower than for Experiment A. In both processes the cells grow until ~8 h of process time and remain then in a stationary state, potentially caused by acetate accumulation. In spite of the biocatalyst concentrations being very similar and the overall amount of provided glucose being almost identical (A: 20 g $L^{-1}$, B: 19.5 g $L^{-1}$), the biocatalysts in Experiment B consume significantly more oxygen. Limiting glucose concentrations have no negative impact on geranyl glucoside formation, which occurs with a constant production rate throughout the entire Experiment B. This underlines the finding of the pre-study at

**Table 7.3.:** Process variables and results of two biotransformations (A,B) with *E. coli* BL21(DE3)pLysSA pET29a_VvGT14a at L-scale.    GG: Geranyl glucoside.    STY: Space-time yield. Y: Yield.

| Variables and results | A | B |
|---|---|---|
| t, h | 12 | |
| T, °C | 30 | 37 |
| Isopropyl myristate, % (v/v) | 20 | 10 |
| Initial geraniol,  g $L^{-1}$ | 0.8 | 1.6 |
| Initial glucose,  g $L^{-1}$ | 20 | 1.5 |
| Glucose feed, g $L^{-1}$ $h^{-1}$ | - | 1.5 |
| Biocatalyst,  g $L^{-1}$ | 6 | |
| $c_{GG, max}$, g $L^{-1}$ | 0.14 | 0.33 |
| STY, mg $L^{-1}$ $h^{-1}$ | 11.4 | 29.8 |
| $Y_{GG}$, % | 8.3 | 9.9 |

mL-scale. The space-time yield in Experiment B is 2.6-fold higher than in Experiment A. However, the higher yield should not be directly correlated with the glucose-limiting conditions. Most likely, it is a consequence of the higher process temperature of 37 °C, which proved to be advantageous for geranyl glucoside formation in Chapter 7.4.3.

After confirming that a glucose feed is applicable to the biotransformation of geraniol and is moreover advantageous for reducing acetate formation, these findings were to be used for studies on the impact of the biocatalyst concentration and the aqueous geraniol concentration. As these studies were conducted for 48 h and the cells therefore had to be kept vital for this long, low acetate levels were of particular importance.

**Biocatalyst and aqueous geraniol concentration.**    So far, the effect of the biocatalyst concentration on geranyl glucoside formation was only tested for the *E. coli* strain pLysS (see Chapter 7.4.2). Thus, studies with pLysSA were to be conducted here. Moreover, the impact of different aqueous geraniol concentrations on product formation was to be investigated. For pLysS it was shown earlier that the fraction of isopropyl myristate and thus the equilibrium concentration of geraniol in the aqueous phase has no effect (see Chapter 7.4.1). It was to be analyzed whether this result can be confirmed for pLysSA. For this purpose, 4 parallel experiments were performed in stirred-tank reactors (DASGIP system). The process in Reactor 1 (R1) served as a reference. In Reactor 2 (R2), a twofold biocatalyst concentration was used. In Reactor 3 (R3) and 4 (R4), the calculated geraniol concentration in the aqueous phase was increased and decreased, respectively. In all 4

**Figure 7.25.:** Courses of dissolved oxygen (DO), glucose and acetate concentrations, cell dry weight, geranyl glucoside and geraniol concentrations for two biotransformations (A,B) with *E. coli* BL21(DE3)pLysSA pET29a_VvGT14a at L-scale, applying different glucose supply strategies. The process variables are listed in Table 7.3. Universal settings: V = 1 L, n = 1000 rpm, pH 7.

**Table 7.4.:** Process variables and results of parallelized biotransformations in four reactors (R1-R4) with *E. coli* BL21(DE3)pLysSA pET29a_VvGT14a at L-scale. Volumetric product formation rates ($r_{GG}$) were calculated after 3 and 10 h of process time by linear regression, respectively, whereas space-time yields (STY), yields ($Y_{GG}$) and biomass yield coefficients ($Y_{XS,\mu}$) were calculated across the total process time. Biocatalysts were stored for 6 days prior to the biotransformations.

| Variables and results | R1 | R2 | R3 | R4 |
|---|---|---|---|---|
| t, h | | | 48 | |
| T, °C | | | 37 | |
| **Isopropyl myristate, % (v/v)** | 5 | 5 | 5 | 20 |
| **Initial geraniol, g L$^{-1}$** | 0.8 | 0.8 | 1.6 | 1.6 |
| **Initial geraniol concentration aqueous phase, g L$^{-1}$** | 0.06 | 0.06 | 0.11 | 0.03 |
| Initial glucose, g L$^{-1}$ | | | 0.5 | |
| Glucose feed after 4 h, g L$^{-1}$ h$^{-1}$ | | | 2 | |
| **Biocatalyst, g L$^{-1}$** | 16 | 32 | 16 | 16 |
| $c_{GG,max}$, g L$^{-1}$ | 0.49 (10 h) | 0.69 (45 h) | 0.93 (45 h) | 0.54 (45 h) |
| $r_{GG}$ (3 h), mg L$^{-1}$ h$^{-1}$ | 87.0 | 62.6 | 92.3 | 70.3 |
| $r_{GG}$ (10 h), mg L$^{-1}$ h$^{-1}$ | 47.4 | 26.1 | - | 46.6 |
| STY, mg L$^{-1}$ h$^{-1}$ | 10.8 | 15.5 | 20.9 | 12.1 |
| $Y_{GG}$, % | 29.1 | 41.8 | 56.4 | 32.7 |
| $Y_{XS,\mu}$, g g$^{-1}$ | 0.04 | 0.09 | 0.09 | 0.15 |

processes, a glucose feed with a rate of 2 g L$^{-1}$ h$^{-1}$ was started at 4 h of process time.

The process variables are listed in Table 7.4 and the courses of dissolved oxygen, glucose, acetate, cell dry weight, geraniol and geranyl glucoside concentrations are shown in Figures 7.26 and 7.27. Figure A.1 shows the respiratory coefficients (RQ, ratio of carbon dioxide emission rate and oxygen uptake rate) for R1-3, calculated from exhaust gas data.

All processes could be run under glucose-limiting conditions, resulting in low acetate concentrations below 0.5 g L$^{-1}$ throughout the processes. Only during the first few hours higher acetate levels occurred, which were degraded afterwards though. For R2, where the twofold biocatalyst concentration was used, a high acetate concentration of 2.3 g L$^{-1}$ was measured at 3 h of process time, but shortly after, the metabolite was degraded. The cell dry weight concentrations are afflicted with high standard deviations. Nevertheless, certain trends can be seen: In R1, the cells grow up to 25 h and are then subjected to
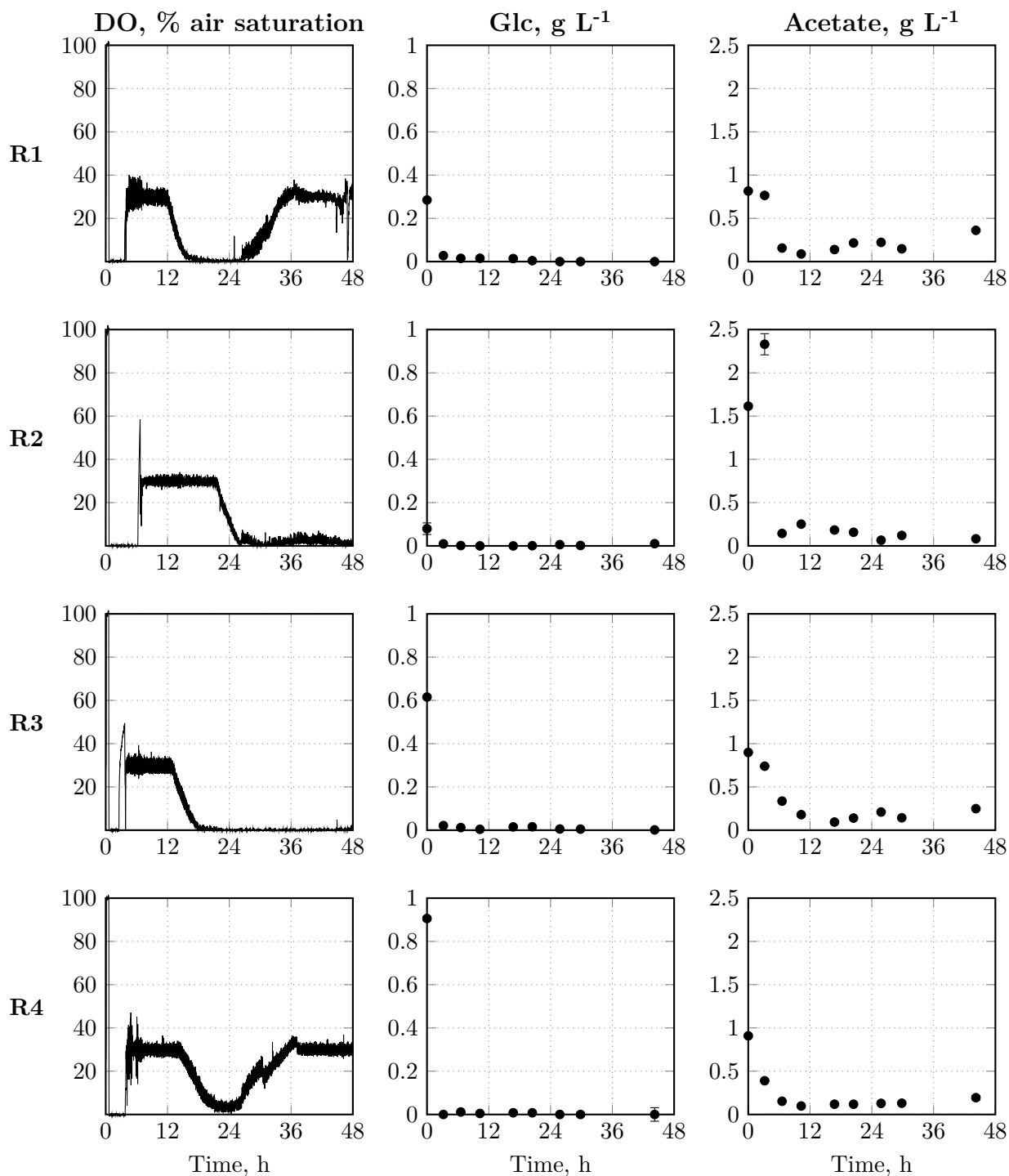
**Figure 7.26.:** Courses of dissolved oxygen (DO), glucose and acetate concentrations for 4 parallelized experimental set-ups (R1-R4) of biotransformations with *E. coli* BL21(DE3)pLysSA pET29a_VvGT14a at L-scale. The different process variables are listed in Table 7.4. Universal settings: V = 0.4 L, $DO_{set}$ = 30 %, pH 7, n = 1400 rpm.
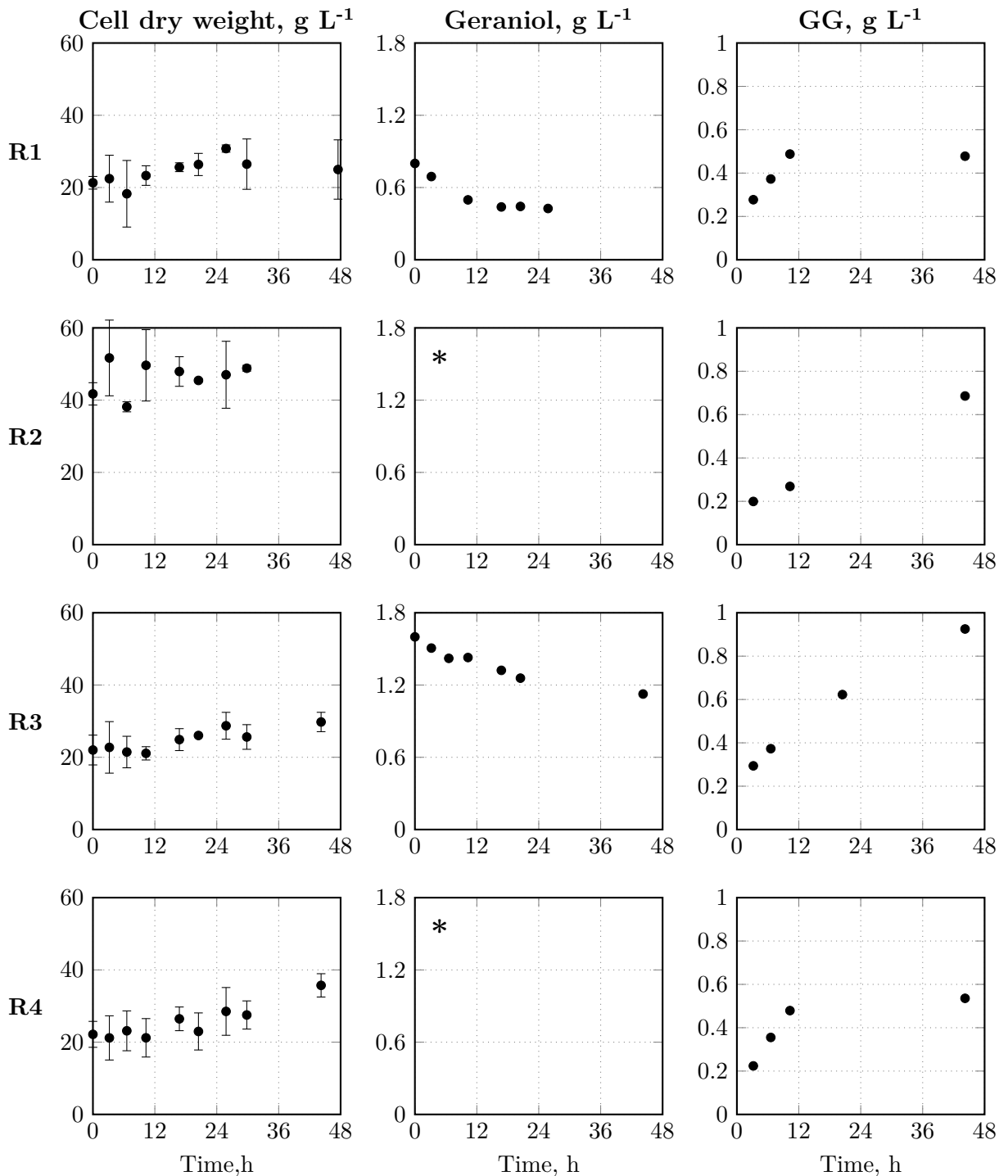
**Figure 7.27.:** Courses of the cell dry weight, geraniol and geranyl glucoside concentrations for 4 parallel-ized experimental set-ups (R1-R4) of biotransformations with *E. coli* BL21(DE3)pLysSA pET29a_VvGT14a at L-scale. The different process variables are listed in Table 7.4. Universal settings: V = 0.4 L, DO$_{set}$ = 30 %, pH 7, n = 1400 rpm. Graphs marked with an asterisk (*) refer to geraniol concentrations that could not be measured due to distinct interphase formation.

slight cell dying. In R2, slight cell growth can be observed until 30 h of process time, afterwards no further data points are available. R3 and R4 show slight cell growth until process end. Volumetric product formation rates are the highest in the first 3 h of all processes and decrease afterwards. The highest maximal geranyl glucoside concentration of 0.93 g L$^{-1}$ was measured in R3, coming along with the highest space-time yield and yield. In R1 and R4, geranyl glucoside formation stagnates after ~15 h, whereas linear formation can be observed for R2 and R3. Oxygen is limiting during the first 5 h for all processes, indicating that the maximal technically feasible oxygen transfer rate was reached. The RQ reaches values higher than 1.0 during this period. Afterwards, the RQ lies in a range between 0.7 and 1.0. All processes enter oxygen-limiting conditions again at 20–25 h of process time. However, whereas R1 and R4 show a distinct increase in dissolved oxygen at ~35 h, R2 and R3 remain oxygen-limited.

**Discussion.**    Doubling the biocatalyst concentration has a negative effect on the product formation rate. This might be due to the distinct acetate formation during the first 3 h of the process. The metabolite can inhibit the cellular metabolism (see Chapter 3.3.2), which might also affect UDP-glucose regeneration. In order to truly investigate the impact of the biocatalyst concentration on geranyl glucoside formation, studies in a reactor setting with higher feasible power input and thus improved oxygen supply would have to be performed. However, it can be expected that no linear correlation between biocatalyst concentration and geranyl glucoside formation exists, as this was already shown for the reference strain pLysS (see Chapter 7.4.2). Nevertheless, increasing the biocatalyst concentration seems to enable continuous geranyl glucoside formation over 45 h; this is in contrast to R1, where already after 15 h no increase in product concentration can be observed. In R2, a higher amount of cells seems to remain alive and is thus capable of carrying on the biotransformation reaction. The similar courses of both dissolved oxygen and geranyl glucoside concentration in R1 and R4 indicate an unknown limitation, which is not present in R2 and R3.

The low biomass yield coefficients for all four experiments underline the absence of strong cell growth. Nevertheless, the measured RQ values show that the cells are highly metabolically active. Thereby, the lowest values were measured for R3, which might correlate with the most distinct product formation [Chmiel et al. 2018]. These results show, especially when looking at the data from R2 and R3, that the biocatalyst does not have to grow during the biotransformation, but has to be in a rather non-growing, but metabolically active state. This confirms the conclusions made in Chapter 7.4.1.

Decreasing the aqueous geraniol concentration (R4) shows no distinct positive effect on

product formation. Apparently, the geraniol amount present in the aqueous phase during the reference process does not negatively affect product formation. Instead, a different limitation seems to exist in both R1 and R4.

However, the process in R3, where the aqueous concentration of geraniol is increased, shows a significantly higher final geranyl glucoside concentration. One assumption could be a mass transfer limitation of geraniol across the cellular membrane: When an increased geraniol concentration is present in the water phase, the concentration gradient across the membrane becomes bigger. As no transporter proteins for geraniol are known in *E. coli*, the trans-membrane transport of geraniol most likely happens by diffusion, whose velocity is driven by the concentration gradient (see Chapter 3.4.2). The fact that one freeze-thaw cycle can improve the glucosylation of geraniol (see Chapter 7.1) can support the hypothesis of a mass transfer limitation. As described by R. R. Chen [2007] and in Chapter 3.4.1, both physical or chemical and molecular engineering approaches exist to tackle mass transfer limitations. Modifying the cellular membrane by genetic engineering seems to be the more elegant and sustainable solution than treatment of the cells with chemicals or exposure to high-voltage pulses for membrane permeabilization. In plants like lavender or *Arabidopsis thaliana*, certain ATP-binding cassette transporter proteins are known to transport monoterpenes like geraniol across the cellular membrane [Demissie et al. 2019]. Heterologoues expression of such transporter in the *E. coli* biocatalyst used here might be a promising strategy to overcome potential membrane transfer limitations. However, all in all, the hypothesis of a mass transfer limitation seems rather unlikely: A doubling of cell concentration, as implemented in R2, results also in a doubling of the available membrane surface, which would then have to lead to an increased trans-membrane geraniol flux and thus an increased product formation rate (see Equation 3.31). However, especially the initial volumetric product formation rates are much higher for R1. Thus, it seems more reasonable to assume a certain constraint occurring in R1 than assuming improved reaction conditions in R3.

Looking at the bigger picture, the low VvGT14a concentration and thus low activity of pLysSA seems to be a rate-limiting factor in the biotransformation of geraniol. Thus, further strain optimization would be necessary, as further adjustments of the expression conditions during HCDCs are not very promising (see Chapter 7.5.2). One idea could be the usage of a different expression plasmid. pET plasmids belong to the group of low copy number plasmids, and using a high copy number plasmid like the pUC plasmid instead might increase the produced VvGT14a concentration. For toxic or unstable proteins low-copy number plasmids are advantageous, however, in contrast, high-copy number plasmids are very beneficial for the overproduction of recombinant proteins [Plotka et al.

**Table 7.5.:** Comparison of the biotransformation in R3 with processes described in literature. **Schmideder et al. [2016b]**: V = 10 mL, T = 20 °C, n = 2200 rpm, pH 7, t = 20 h, 4 g $L^{-1}$ *E. coli* BL21(DE3)pLysS pET29a_VvGT14a, 10 g $L^{-1}$ glucose, 0.2 g $L^{-1}$ geraniol, 5 % (v/v) ionic liquid [HPYR][NTF] in M9 mineral medium. **Caputi et al. [2008]**: V = 1.15 L, T = 25 °C, pH 7.4, t = 22.5 h, ~35 g $L^{-1}$ *E. coli* pGEX-2T_GT73C5 (strain variant unknown), glycerol feed, geraniol feed, M9 mineral medium. GG: Geranyl glucoside. STY: Space-time yield.

| Biotransformation | $c_{GG, max}$, g $L^{-1}$ | STY, mg $L^{-1}$ $h^{-1}$ |
|---|---|---|
| R3, this work | 0.93 | 20.9 |
| Schmideder et al. [2016b] | 0.29 | 14.5 |
| Caputi et al. [2008] | 0.18 | 7.6 |

2017]. A different approach could be the application of a stronger promoter system in the expression plasmid, which features higher affinities for the RNA polymerase and sigma factors. For example, Li et al. [2012] report the usage of promoter clusters consisting of multiple tac-promoters, which can be integrated into the bacterial chromosome and significantly enhance overexpression of recombinant proteins. As described in Chapter 3.3.3, one major drawback of recombinant protein expression in *E. coli* is the cells' inability for post-translational modifications of proteins. It is unknown whether the correct folding and activity of GTs relies to a certain extent on such modifications, like hydroxylation or glycosylation. If so, a different, eukaryotic expression host would be advantageous.

The maximal product formation rates shown in Table 7.4 are all higher than the maximal rates obtained with pLysSA at mL-scale (see Table 7.2). This can be explained with the more controlled reaction environment at L-scale, where pH and DO control was implemented. Moreover, low initial glucose concentrations were applied, a factor that was also shown to be advantageous in the studies on the glucose supply strategy earlier.

The geranyl glucoside concentration obtained with the process in R3 is the highest concentration reported so far (see Table 7.5). Moreover, it is the first process where the formation of geranyl acetate could be deliberately suppressed. Schmideder et al. [2016b] did not explicitly report geranyl acetate formation. However, as the strain pLysS was used, the formation of the byproduct can be expected.

## 7.6.2. Processes with *E. coli* BL21(DE3)pLysS pET29a_VvGT14a

Finally, the "reference" strain pLysS was to be tested again in studies at L-scale in a stirred-tank bioreactor and its performance was compared to pLysSA. As a reference, a process with geraniol and glucose being provided as batch concentrations was run (Expe-

**Table 7.6.:** Process variables and results of different biotransformations (A-C) with *E. coli* BL21(DE3)pLysS pET29a_VvGT14a at L-scale. Maximal volumetric product formation rates ($r_{GG, max}$) were calculated using the first three data points, respectively, whereas space-time yields (STY) and yields ($Y_{GG}$) were calculated across the total process time.

| Variables and results | A | B | C |
|---|---|---|---|
| t, h | 24 | 72 | 28 |
| T, °C | 30 | 30 | 30 |
| Isopropyl myristate, % (v/v) | 20 | 20 | 20 |
| Initial geraniol, g L$^{-1}$ | 0.8 | 0.8 | 3.2 |
| Initial aqueous geraniol concentration, g L$^{-1}$ | 0.01 | 0.01 | 0.06 |
| Geraniol pulses | - | 2x 0.8 g L$^{-1}$ | 1x 3.2 g L$^{-1}$ |
| Initial glucose, g L$^{-1}$ | 20 | 20 | - |
| Glucose pulses | - | 1x 30 g L$^{-1}$, 1x 40 g L$^{-1}$ | - |
| Glucose feed, g L$^{-1}$ h$^{-1}$ | - | - | 1.5 |
| Biocatalyst, g L$^{-1}$ | 6 | 6 | 12 |
| $c_{GG, max}$, g L$^{-1}$ | 1.16 (24 h) | 1.41 (72 h) | 0.82 (28 h) |
| $r_{GG, max}$, mg L$^{-1}$ h$^{-1}$ | 51.1 (3.0 h) | 51.6 (6.0 h) | 33.7 (4.5 h) |
| STY, mg L$^{-1}$ h$^{-1}$ | 48.7 | 19.6 | 28.6 |
| $Y_{GG}$, % | 71.0 | 28.7 | 6.3 |
| $q_{GA, max}$, mg L$^{-1}$ h$^{-1}$ | 46.1 (4.5 h) | 53.3 (6.0 h) | 366.7 (4.5 h) |

riment A). In Experiment B, additional geraniol and glucose pulses were applied, whereby the timing of the geraniol pulses was based on the consumption rate in Experiment A. In Experiment C, a doubled biocatalyst concentration was applied, and geraniol was added both as a batch concentration and by a subsequent puls. No initial glucose was present in the reactor, but the substrate was only provided by a feed beginning only shortly after process start. All experimental conditions and the most important results are listed in Table 7.6. Key questions to be answered were whether the way of providing the cells with glucose plays a role in product formation, whether increasing the biocatalyst concentration can increase geranyl glucoside production, and whether it is possible to reduce or prevent undesired geranyl acetate formation by operating under glucose-limiting conditions from process start.

In Figures 7.28 and 7.29, the courses of dissolved oxygen, glucose and acetate, cell dry weight, geranyl glucoside, geraniol and geranyl acetate concentrations are depicted.
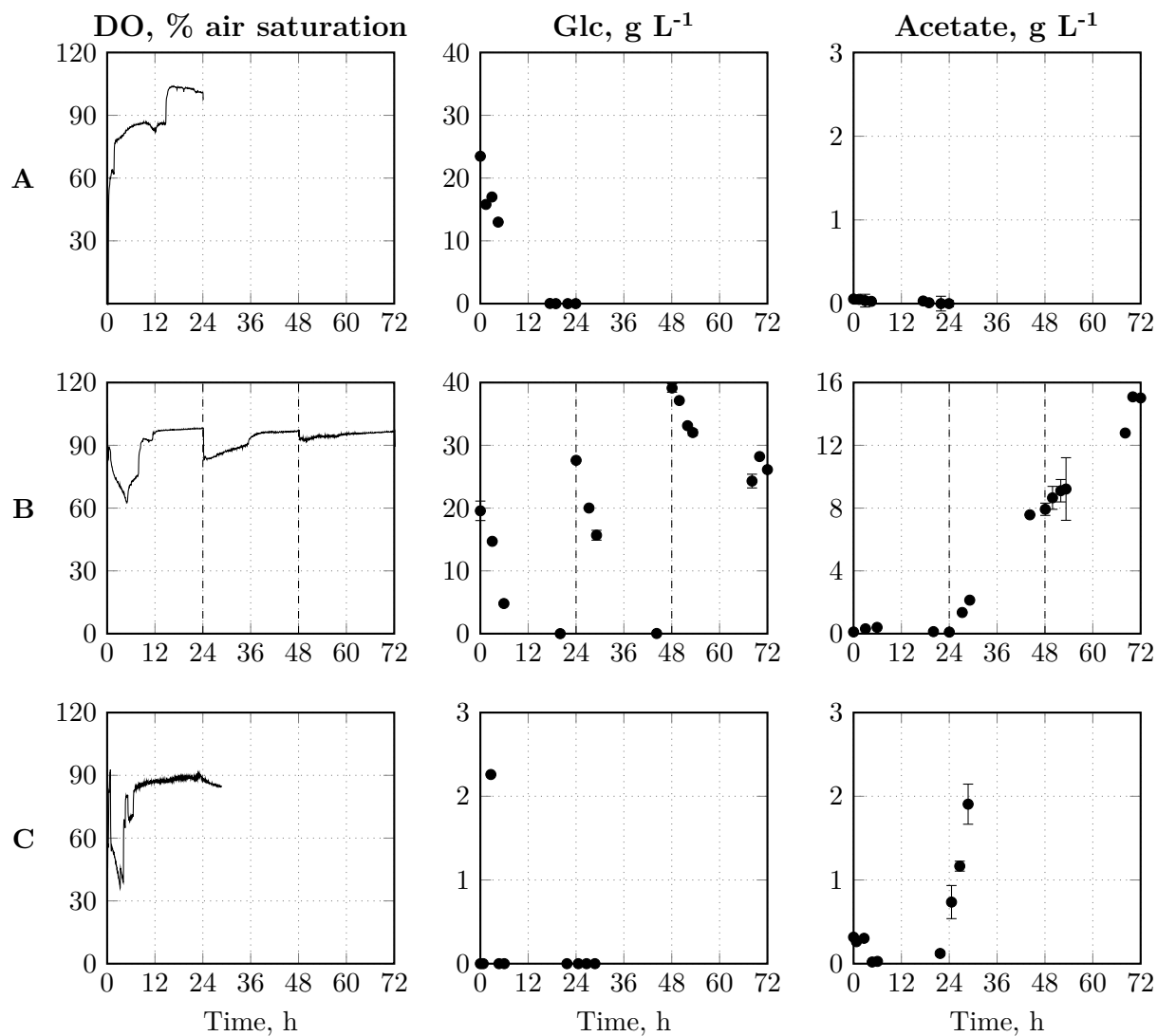
**Figure 7.28.:** Courses of dissolved oxygen (DO), glucose and acetate concentrations for 3 different experimental set-ups (A-C) of biotransformations with *E. coli* BL21(DE3)pLysS pET29a_VvGT14a at L-scale. The process variables are listed in Table 7.6. Universal settings: V = 1 L, n = 1000 rpm, pH 7. Glucose pulses are marked with dashed lines.
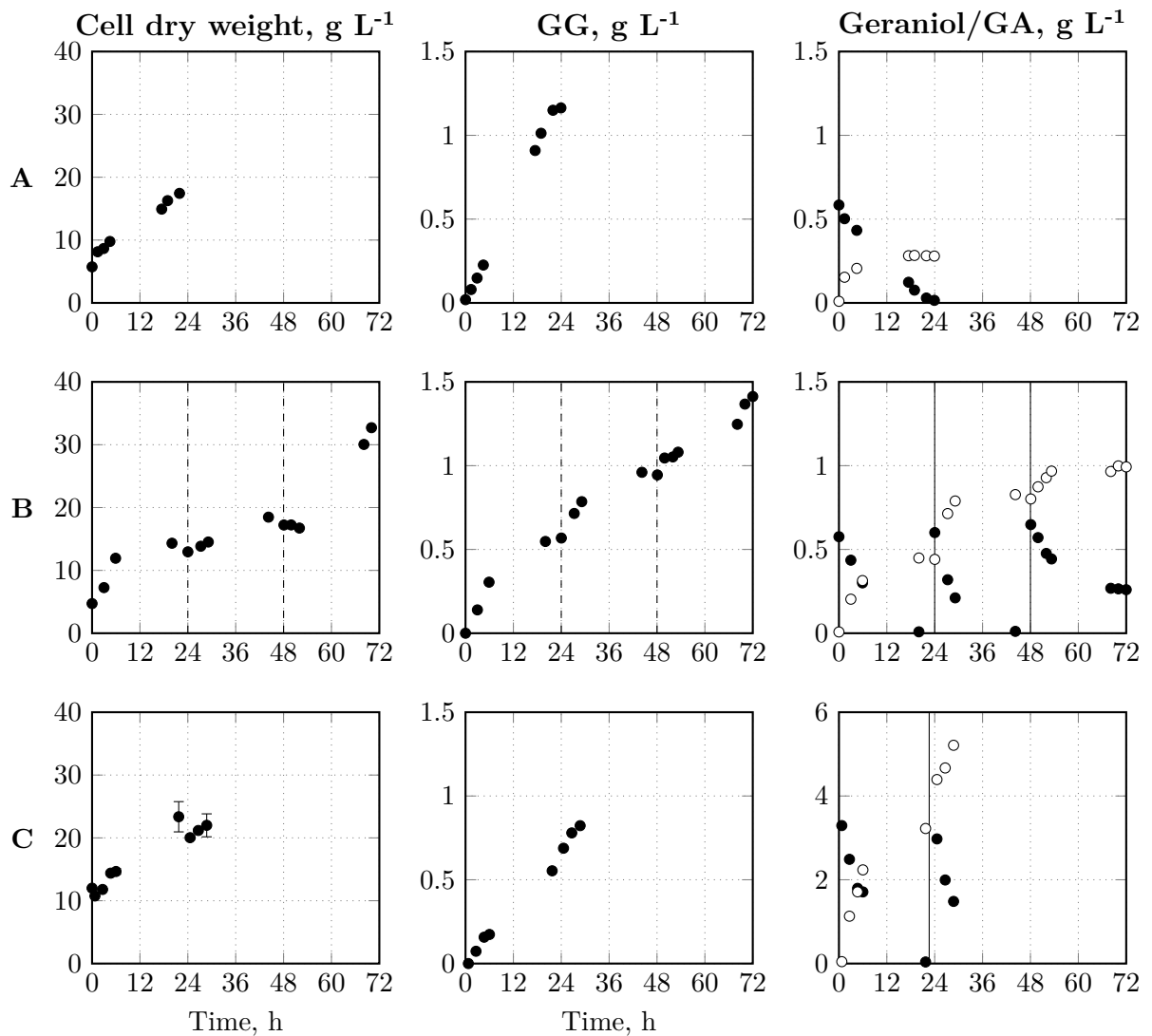
**Figure 7.29.:** Courses of the cell dry weigth, and of geranyl glucoside (GG), geraniol and geranyl acetate (GA) concentrations for 3 different experimental set-ups (A-C) of biotransformations with *E. coli* BL21(DE3)pLysS pET29a_VvGT14a at L-scale. The process variables are listed in Table 7.6. Universal settings: V = 1 L, n = 1000 rpm, pH 7. Glucose pulses are marked with dashed lines, geraniol pulses with solid vertical lines.

The processes were run under oxygen-abundant conditions. Providing the biocatalyst with a batch glucose concentration of 10 or 20 g L$^{-1}$ has a positive impact on the maximal initial product formation rate: Experiment C, where no batch glucose was provided at all, shows a significantly lower initial production rate, in spite of a higher initial biocatalyst concentration. Doubling the biocatalyst concentration shows no positive effect on geranyl glucoside formation here; however, this might be attributed to the glucose limitation at process start of Experiment C. Acetate formation can only be kept low during the first 24 h of the processes; afterwards, the metabolite accumulates in spite of working at fully aerobic conditions. For Experiment B, this can be attributed to the highly concentrated glucose pulses, resulting in an "overflow" of the citric acid cycle (see Chapter 3.3.2). The high acetate levels in Experiment C lack an explanation, as glucose is kept limiting and the reaction environment is fully aerobic. The biocatalysts grow throughout all processes. Geranyl glucoside formation continues throughout the entire process time for all experiments. The doubled biocatalyst concentration combined with the glucose-limiting conditions in Experiment C seems to have a significant effect on the geranyl acetate formation rate which is distinctly the highest among the experiments. A positive correlation between biocatalyst concentration and geranyl acetate formation was also proved in an additional experiment with exactly identical process settings as in Experiment A, but with a doubled cell concentration of 12 g L$^{-1}$ and a shorter process time of 10 h: In contrast to the initial geranyl glucoside formation rate increasing only by 21 %, the geranyl acetate formation rate more than decuples (data not shown).

### 7.6.3.  Discussion

For neither of the two strains used for biotransformations of geraniol, pLysS and pLysSA, a clear proportionality between biocatalyst concentration and geranyl glucoside concentration or production rate could be shown. This outcome underlines the results presented in Chapter 7.4.2, where a doubling of cell concentration did not lead to a doubling of geranyl glucoside concentration, in spite of working under oxygen-abundant conditions. Combining this finding with the fact that the trans-membrane transport of geraniol does not seem to be the rate-limiting step (see Chapter 7.6.1), one can assume a rate-determining parameter within the biocatalyst. A rather weak expression level and/or activity of VvGT14a seems like a plausible hypothesis, especially when assuming that protein expression is not consistent for all cells due to population heterogeneity [Heins and Weuster-Botz 2018]. Further metabolic engineering of the used strains seems like a potential resource: Besides from the usage of a different expression plasmid or promoter system (see Chapter 7.6.1),

the identification of a glycosyltransferase with higher activity towards geraniol might be an option. Such a glycosyltransferase does not necessarily have to derive from *Vitis vinifera* [Bönisch et al. 2014a], but could also have its origin in other plants, such as *Arabidopsis thaliana* [Caputi et al. 2008]. However, not only the glycosylation reaction catalyzed by VvGT14a can be the rate-limiting step, but also the provision with UDP-glucose might be. In Chapter 7.3, UDP-glucose was shown to be sufficiently available, however, the intracellular quantification was executed during an oxygen-limited process. Thus, measurements would have to be repeated for fully aerobic processes.

Initiating the biotransformation process without any provided batch glucose and thereby giving the cells time to metabolize acetate potentially left from HCDC and cell storage cannot prevent geranyl acetate formation. The complete lack of batch glucose even seems to enhance geranyl acetate production and impair geranyl glucoside formation. Thus, a glucose feed should only be applied in combination with batch glucose being provided (as implemented in the parallel experiments shown in Chapter 7.6.1).

The usage of the pLysSA strain can fully prevent byproduct formation. Similar product concentrations and formation rates as with pLysS can be obtained, as shown in Table 7.7 and Figure 7.30. However, this is only feasible when VvGT14a expression is induced with 1.0 mM instead of 0.1 mM IPTG during the HCDC, and when a higher biotransformation temperature and an increased biocatalyst concentration is applied, underlining the already discussed even weaker VvGT14a expression in pLysSA.

For both strains, longer process times may be an option, as product formation proceeds linear courses. However, the process length always has to be evaluated regarding economic viability. Moreover, after a certain point in time, increasing age-caused cell lysis might result in the release of hydrolases that are capable of geranyl glucoside degradation.

The best processes with pLysS and pLysSA presented in this work give significantly better results than the processes described in literature (see Table 7.8), both regarding maximal product concentrations and space-time yields. Especially the comparison with results obtained by Schmideder et al. [2016b] is important, as there, the biocatalyst strain pLysS was used, and as the described process served as a starting point for the work presented here.

**Table 7.7.:** Comparison of the most promising processes at L-scale with *E. coli* BL21(DE3)pLysS pET29a_VvGT14a (pLysS, processes A and B) and BL21(DE3)pLysSA pET29a_VvGT14a (pLysSA, process R3). Process A/B: See Figures 7.28 and 7.29. Process R3: See Figures 7.26 and 7.27. Maximal volumetric product formation rates ($r_{GG, max}$, $r_{GA, max}$; GG: geranyl glucoside, GA: geranyl acetate) were calculated using the first three data points, respectively, whereas space-time yields (STY) and yields ($Y_{GG}$) were calculated across the total process time.

| | pLysS | | pLysSA |
| Variables and results | A | B | R3 |
|---|---|---|---|
| t, h | 24 | 72 | 48 |
| T, °C | 30 | 30 | 37 |
| Isopropyl myristate, % (v/v) | 20 | 20 | 5 |
| Initial geraniol, g $L^{-1}$ | 0.8 | 0.8 | 1.6 |
| Geraniol pulses | - | 2x 0.8 g $L^{-1}$ | - |
| Initial glucose, g $L^{-1}$ | 20 | 20 | 0.5 |
| Glucose pulses | - | 2x 20 g $L^{-1}$ | - |
| Glucose feed | - | - | Yes |
| Biocatalyst, g $L^{-1}$ | 6 | 6 | 16 |
| $c_{GG, max}$, g $L^{-1}$ | 1.16 (24 h) | 1.41 (72 h) | 0.93 (45 h) |
| $r_{GG, max}$, mg $L^{-1}$ $h^{-1}$ | 51.1 (3.0 h) | 51.6 (6.0 h) | 92.3 (3.0 h) |
| STY, mg $L^{-1}$ $h^{-1}$ | 48.7 | 19.6 | 20.9 |
| $Y_{GG}$, % | 71.0 | 28.7 | 56.4 |
| $r_{GA, max}$, mg $L^{-1}$ $h^{-1}$ | 46.1 (4.5 h) | 53.3 (6.0 h) | - |
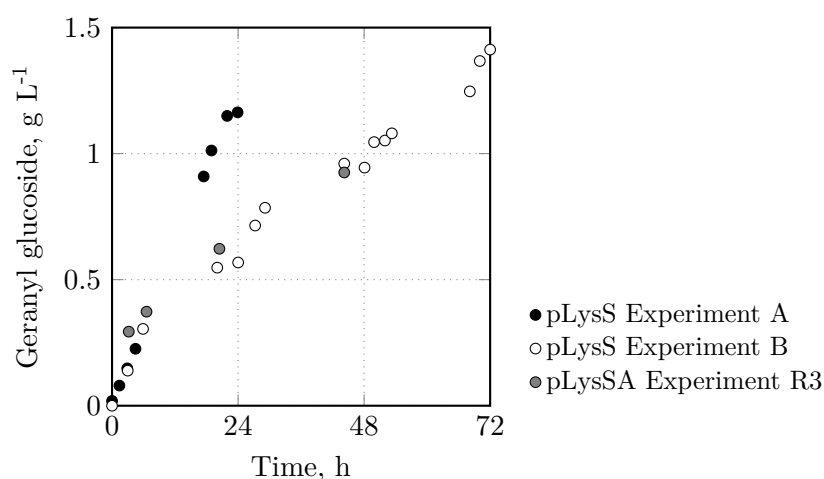


**Figure 7.30.:** Comparison of geranyl glucoside formation by pLysS and pLysSA at L-scale. For pLysS Experiment A and B refer to Figure 7.29, for pLysSA Experiment R3 refer to Figure 7.27.

**Table 7.8.:** Comparison of biotransformations with *E. coli* BL21(DE3)pLysS pET29a_VvGT14a (pLysS) and BL21(DE3)pLysSA pET29a_VvGT14a (pLysSA) with processes described in literature. **pLysS #1**: Process A in Figures 7.28 and 7.29. **pLysS #2**: Process B in Figures 7.28 and 7.29. **pLysSA**: Process R3 in Figures 7.26 and 7.27. **Schmideder et al. [2016b]**: V = 10 mL, T = 20 °C, n = 2200 rpm, pH 7, t = 20 h, 4 g $L^{-1}$ *E. coli* BL21(DE3)pLysS pET29a_VvGT14a, 10 g $L^{-1}$ glucose, 0.2 g $L^{-1}$ geraniol, 5 % (v/v) ionic liquid [HPYR][NTF] in M9 mineral medium. **Caputi et al. [2008]**: V = 1.15 L, T = 25 °C, pH 7.4, t = 22.5 h, ~35 g $L^{-1}$ *E. coli* pGEX-2T_GT73C5 (precise strain unknown), glycerol feed, geraniol feed, M9 mineral medium. GG: Geranyl glucoside. STY: Space-time yield.

| Biotransformation | $c_{GG,\ max}$, g $L^{-1}$ | STY, mg $L^{-1}$ $h^{-1}$ |
|---|---|---|
| pLysS #1, this work | 1.16 (24 h) | 48.7 |
| pLysS #2, this work | 1.41 (72 h) | 19.6 |
| pLysSA, this work | 0.93 (48 h) | 20.9 |
| Schmideder et al. [2016b] | 0.29 (20 h) | 14.5 |
| Caputi et al. [2008] | 0.18 (24 h) | 7.6 |

# 8. Summary

Fragrance compounds are an integral part of many consumer goods such as household and cosmetic products. As customers ask for highly stable scents that do not undergo quick fading, stabilization techniques are required for these volatile molecules. One approach for stabilization is based on a mechanism found in plants: in plant cells, many secondary metabolites such as steroids, flavonoids and terpenoids are stored as glycoconjugates, i.e. bound to a sugar molecule. Such glycosides are more hydrophilic than their respective aglycones, moreover less volatile and thus more stable [Bowles et al. 2005; Schwab et al. 2015a]. Glycosylations can be catalyzed by glycosyltransferases, which transfer a sugar moiety from an activated donor molecule to an acceptor molecule [Gachon et al. 2005].

One acceptor molecule that is of great interest for the consumer goods industry and is used as a fragrance compound in many cosmetic and household products is the monoterpenoid geraniol [Rastogi et al. 2001]. It can be glycosylated at its hydroxy group. The glycosyltransferase VvGT14a from *Vitis vinifera* can transfer glucose from uridine diphosphate glucose (UDP-glucose) to geraniol, giving geranyl glucoside [Bönisch et al. 2014b]. In order to use VvGT14a biotechnologically, the enzyme has to be produced in a recombinant microbial host, e.g. in *E. coli*. As UDP-glucose is an expensive cosubstrate and thus cannot be added in stoichiometric amounts to biotransformation processes, a UDP-glucose regeneration system is required. *E. coli* uses UDP-glucose as a precursor for the synthesis of different polysaccharides shaping the protective capsule on the cells' surface and therefore constantly regenerates this nucleotide sugar [Whitfield 2006]. This makes the whole-cell biotransformation of geraniol in *E. coli* expressing VvGT14a a promising approach for the production of geranyl glucoside.

The recombinant expression of VvGT14a in *E. coli* during high cell density cultivations at L-scale is described by Schmieder et al. [2016b], yielding a cell dry weight concentration of 68 g L$^{-1}$ and a VvGT14a concentration of 2.7 g L$^{-1}$ after 48 h. As recombinant protein concentrations in *E. coli* usually range between 1–10 g L$^{-1}$ [Choi et al. 2006], this process leaves room for further improvements. Thus, the first goal of the present study was the production of whole-cell biocatalysts containing higher concentrations of functional VvGT14a. The obtained biocatalysts were then to be used for the glucosylation

of geraniol to yield geranyl glucoside. As geraniol acts as a cytotoxin for *E. coli* at a concentration as low as 0.3 g $L^{-1}$, a biphasic reaction system is convenient. Thereby, a second, non-aqueous phase serves as an *in situ* geraniol reservoir. For this purpose, a non-aqueous phase with high affinity and selectivity for geraniol had to be selected by thermodynamic first-principles methods and other rational criteria. Up to now, the effect of different process variables on the whole-cell biotransformation of geraniol is unknown, which hampers the design of an efficient biotransformation process. Thus, reaction engineering studies were to be conducted at mL-scale in order to identify a convenient system composition and suitable process variables. Special attention was put on the UDP-glucose supply during the biotransformation, but other potential bottlenecks, such as byproduct formation, were taken into account as well. Last but not least, all obtained findings were to be implemented in controlled biotransformation processes at L-scale in order to produce high concentrations of geranyl glucoside.

The first step in this study consisted in the design of a high cell density cultivation process for the production of active *E. coli* BL21(DE3)pLysS pET29a_VvGT14a whole-cell biocatalysts. Thereby, the earlier mentioned process by Schmieder et al. [2016b] served as a reference process. The effect of a reduced set growth rate during the exponential growth phase, of the IPTG concentration and of the post-induction feeding profile on cell growth and VvGT14a production was investigated. A combination of a set growth rate of 0.18 $h^{-1}$, an IPTG concentration of 0.1 mM and a linear post-induction feeding profile with a gradient of 0.15 g $L^{-1}$ $h^{-2}$ resulted in the highest specific productivity regarding VvGT14a formation: In comparison to the study by Schmieder et al. [2016b], where a growth rate of 0.20 $h^{-1}$ and an IPTG concentration of 0.1 mM were combined with a constant post-induction feeding profile, the productivity could be increased by 183 %, with a final VvGT14a concentration of 7.5 g $L^{-1}$. However, the final cell dry weight concentration could not be increased, most likely as a result of the lower set growth rate during the exponential growth phase. Moreover, the glucose additionally fed to the cultivation medium after induction was channeled into protein formation.

After high cell density cultivations, the whole-cell biocatalysts were not always directly used for biotransformations of geraniol. For a period of up to 45 days, storage at 4 °C in the high cell density cultivation broth consisting of Riesenberg medium turned out to be the best option among different tested storage conditions. Within this period, the cells did not show loss in activity compared to freshly harvested biocatalysts.

In the next step, a non-aqueous phase with high affinity and selectivity for geraniol was selected rationally. Hansen Solubility Parameters (three-dimensional solubility parameters that predict the affinity between two molecules) and octanol/water partition

coefficients were applied in combination with database research to preselect 6 liquid and 6 solid sequestering phases. Subsequently, experimental approaches were used to investigate the suitability of the different sequestering phases. The fatty acid ester isopropyl myristate emerged as the best choice due to its low viscosity, very poor water solubility, low price and compatibility with the whole-cell biocatalyst. A biphasic system containing 20 % (v/v) of this solvent resulted in a 4.2-fold increase in geranyl glucoside concentration compared to a purely aqueous system. Varying the isopropyl myristate fraction between 5–20 % had no effect on the biotransformation reaction, underlining the biocompatiblity of this solvent. Furthermore, isopropyl myristate exhibits advantageous partitioning of geraniol into the organic phase (logarithmic partition coefficient (logPC): 2.42 $\pm$ 0.03) and of geranyl glucoside into the water phase (logPC: -2.08 $\pm$ 0.05). The concept of the rational selection of biphasic reaction systems was afterwards extended to other cytotoxic flavors and fragrances that can be produced microbially. Both Hansen Solubility Parameters and UNIFAC (Universal Functional Group Activity Coefficients) proved as suitable tools to differentiate between sequestering phases with high and poor thermodynamic affinity towards the target compounds.

Subsequently, a deeper look was taken into the biotransformation of geraniol. Product formation stagnated after a certain process time in batch processes, in spite of geraniol still being available. Moreover, an increase in biocatalyst concentration had no clear positive effect on geranyl glucoside production, indicating the presence of a bottleneck. As an increase in biomass concentration comes along with an expansion of the available UDP-glucose pool, an UDP-glucose limitation was rather unlikely. This assumption could be confirmed by measurement of intracellular UDP-glucose concentrations during biotransformations. However, a different bottleneck was identified: The biocatalysts have to be surrounded by an oxygen-abundant medium, as oxygen limitation results in distinct acetate formation and in the transition of the cells into a resting state, which seems to be disadvantageous for the biotransformation of geraniol. This finding could be underlined by the fact that potassium phosphate buffer, which does not provide any essential nutrients, is not a suitable medium for the whole-cell biotransformation of geraniol and results in low geranyl glucoside yields. Instead, M9 mineral medium should be used. A supplementation with electrolytes such as $Mg_2^+$, $Mn_2^+$ or $Fe_3^+$ had no positive effect on product concentrations, neither did the addition of IPTG (isopropyl $\beta$-D-1-thiogalactopyranoside) or kanamycin. Controlling the pH to pH 7 and increasing the temperature from 30 °C to 37 °C can increase geranyl glucoside formation.

Besides the availability of oxygen, the distinct formation of the byproduct geranyl acetate turned out to be a hurdle for productive biotransformations. It was shown that the

acetylation of geraniol is catalyzed by chloramphenicol acetyltransferase, which is encoded on the pLysS plasmid contained in the so far used *E. coli* biocatalyst. By replacing the respective gene on the pLysS plasmid with a $\beta$-lactamase gene (genetic engineering performed by Julian Rüdiger (Associate Professorship of Biotechnology of Natural Products, Technical University of Munich)), byproduct formation could be prevented entirely. However, the modified strain showed very weak VvGT14 expression when being grown in high cell density cultivations with identical conditions as the strain used before, and an 8-times lower geranyl glucoside concentration was measured after biotransformation. This constraint was removed by increasing the IPTG concentration for induction of VvGT14a expression from 0.1 mM to 1.0 mM in the high cell density cultivation process, resulting in identical maximal product formation rates as when utilizing the original strain induced with 0.1 mM IPTG.

Both strains were used for biotransformations in stirred-tank reactors at L-scale. A schematic overview of the reaction system is shown in Figure 8.1. The method of glucose supply (batch, batch with pulses, feed) did not affect geranyl glucoside formation as long as distinct acetate formation could be prevented. Moreover, the geraniol concentration present in the aqueous phase had no effect on product formation in the investigated range of 0.01–0.11 g $L^{-1}$, implying that the trans-membrane transport of geraniol is not the rate-limiting step. Under the assumption that geraniol transfer from the organic into the aqueous phase is not limiting either, a limited biocatalytic activity can be seen as the major bottleneck, especially for the modified strain.

Overall, the highest geranyl glucoside concentration of this study amounted to 1.41 g $L^{-1}$. It was obtained in a process with the original strain BL21(DE3)pLysS pET29a_VvGT14a, which does produce the byproduct geranyl acetate. The process was operated for 72 h at 30 °C with a biocatalyst concentration of 6 g $L^{-1}$, an initial glucose concentration of 20 g $L^{-1}$ and an initial geraniol concentration of 0.8 g $L^{-1}$ in a biphasic system with 20 % (v/v) isopropyl myristate, and included periodic glucose and geraniol pulses. The modified strain with suppressed geranyl acetate formation produced geranyl glucoside at the same rate as the original strain, and a maximal product concentration of 0.93 g $L^{-1}$ was obtained within 48 h (see Figure 8.2). However, this result was only achievable when VvGT14a expression was induced with 1.0 mM instead of 0.1 mM IPTG, and when - compared to the process with the original strain - a higher biotransformation temperature and an increased biocatalyst concentration were applied.
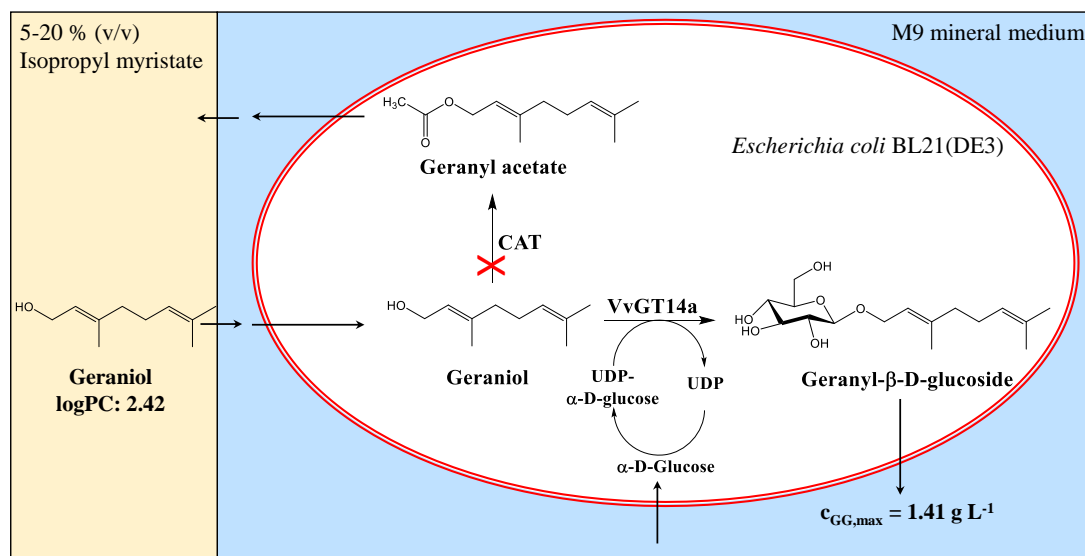
**Figure 8.1.:** Reaction system for the whole-cell biotransformation of geraniol. The conversion of geraniol to geranyl glucoside is catalyzed by the glycosyltransferase VvGT14a, with the respective gene *vvgt14a* being located on the pET29a plasmid of the whole-cell biocatalyst *E. coli* BL21(DE3). The cosubstrate UDP-glucose is regenerated from UDP and glucose by the endogenous *E. coli* metabolism. By the action of chloramphenicol acetyltransferase (CAT), which is encoded on the pLysS plasmid (*camR*), geraniol can be converted to geranyl acetate. *camR* can be replaced by a gene encoding for a $\beta$-lactamase (*ampR*), resulting in the prevention of geranyl acetate formation. The whole-cell biotransformation takes place in the aqueous phase (M9 mineral medium) of a biphasic system. The non-aqueous phase isopropyl myristate acts as an *in situ* substrate reservoir for geraniol and can be applied in phase fractions of 5–20 %. The logarithmic partition coefficient (logPC) of geraniol between isopropyl myristate and M9 is 2.42. Solid arrows indicate mass transfer of involved compounds: Geraniol is pulled from the organic into the aqueous phase, subsequently it diffuses across the cellular membrane. Geranyl glucoside passes the cellular membrane and accumulates in the aqueous phase with a concentration of up to 1.41 g L$^{-1}$ ($c_{GG,max}$). The byproduct geranyl acetate shows even higher affinity for isopropyl myristate than geraniol does and accumulates solely in the organic phase. Glucose is added to the aqueous medium and is transported across the cellular membrane.
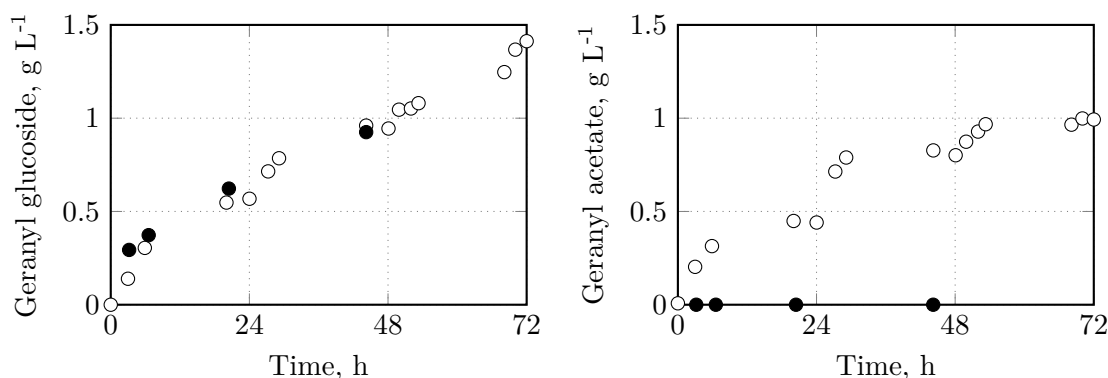


**Figure 8.2.:** Courses of geranyl glucoside (left) and geranyl acetate (right) concentrations during biotransformations of geraniol with *E. coli* BL21(DE3)pLysS pET29a_VvGT14a (white circles) and BL21(DE3)pLysSA pET29a_VvGT14a (black circles) at L-scale.

# 9. Outlook

The present study showed that a major hurdle for higher geranyl glucoside concentrations is the low activity of the whole-cell biocatalyst. Thus, an important objective of future studies should consist in increasing the activity and/or concentration of VvGT14a in whole-cell biocatalysts. One option might be the usage of a BL21(DE3) *E. coli* strain entirely lacking the pLysS plasmid. As in the present work only cells with the regular or modified pLysS plasmid were used, a comparison with cells lacking pLysS would be interesting. The reduced metabolic burden could be advantageous for VvGT14a expression; however, the absence of the T7 lysozyme might cause undesired basal expression of the target protein. Furthermore, the co-expression of a chaperone system promoting protein folding might increase VvGT14a activity. In case these measures are not effective, the usage of high-copy number expression plasmids such as pUC instead of pET plasmids, and the application of stronger promoters as proposed in Chapter 7.6.1 might be an option. Furthermore, the usage of a different glycosyltransferase could be considered. As in *Vitis vinifera* VvGT14a is the glycosyltransferase with the highest known activity towards geraniol [Bönisch et al. 2014a], other plants would have to be taken into account as sources for active glycosyltransferases. An even more fundamental change would consist in the usage of an expression host other than *E. coli*. This prokaryote is not capable of post-translational modifications [Yin et al. 2007], which might be required for full evolvement of glycosyltransferase activity.

In order to design a biotechnological process as sustainable as possible, the substrate both for microbial growth and for the target reaction(s) should originate from a renewable, easily available source. An elegant and sustainable approach is the usage of sugar monomers originating from residual biomass of the agriculture and forestry industry [Robak and Balcerek 2018]. These sugars can be used for the *de novo* synthesis of desired compounds in genetically engineered microbial "factories" [Almquist et al. 2014]. In the context of the present work, a *de novo* synthesis of geranyl glucoside might be an interesting approach. Instead of using geraniol as the direct precursor of geranyl glucoside, glucose is used as the substrate for both cell growth and geranyl glucoside production. Liu et al. [2016] proposes

the recombinant expression of the mevalonate pathway (see Chapter 3.1.2) and of geranyl diphosphate synthase and geraniol synthase in recombinant *E. coli*; that way, 2 g L$^{-1}$ geraniol were synthesized from glucose. When combining this system with the recombinant expression of VvGT14a, a biphasic reaction system might not even be necessary, as geraniol is directly converted to geranyl glucoside within the cells. In case the different recombinant enzymes cause an excessively high metabolic burden, two different *E. coli* biocatalysts could be combined in the same reaction medium [Jakoblinnert and Rother 2014] - one strain for the production of geraniol, the other for the biotransformation of geraniol. In such a system, a non-aqueous phase might be necessary, depending on geraniol synthesis rates and geraniol conversion rates.

# Bibliography

Ackermann, T. (1992). *Physikalische Biochemie: Grundlagen der physikalisch-chemischen Analyse biologischer Prozesse* (1st ed.). Berlin: Springer-Verlag.

Akesson, M., Nordberg Karlsson, E., Hagander, P., Axelsson, J. P. & Tocaj, A. (1999). On-line detection of acetate formation in *Escherichia coli* cultures using dissolved oxygen responses to feed transients. *Biotechnol Bioeng, 64*, 590–598.

Almquist, J., Cvijovic, M., Hatzimanikatis, V., Nielsen, J. & Jirstrand, M. (2014). Kinetic models in industrial biotechnology - improving cell factory performance. *Metab Eng, 24*, 38–60.

Arend, J., Warzecha, H., Hefner, T. & Stöckigt, J. (2001). Utilizing genetically engineered bacteria to produce plant-specific glucosides. *Biotechnol Bioeng, 76*, 126–131.

Aristidou, A., San, K. & Bennett, G. (1994). Modification of central metabolic pathway in *Escherichia coli* to reduce acetate accumulation by heterologous expression of the *Bacillus subtilis* acetolactate synthase gene. *Biotechnol Bioeng, 44*, 944–951.

Bachhawat, P., Mishra, S., Bhatia, Y. & Bisaria, V. S. (2004). Enzymatic synthesis of oligosaccharides, alkyl and terpenyl glucosides, by recombinant *Escherichia coli*-expressed *Pichia etchellsii* $\beta$-glucosidase II. *Appl Biochem Biotechnol, 118*(1-3), 269–282.

Bacon, S. L., Ross, R. J., Daugulis, A. J. & Parent, J. S. (2017). Imidazolium-based polyionic liquid absorbents for bioproduct recovery. *Green Chem, 19*(21), 5203–5213.

Baneyx, F. (1999). Recombinant protein expression in *Escherichia coli*: Review. *Curr Opin Biotechnol, 10*, 411–421.

Bang, W.-G., Lang, S., Sahm, H. & Wagner, F. (1983). Production of L-tryptophan by *Escherichia coli* cells. *Biotechnol Bioeng, 25*, 999–1011.

Barnard, D. R. & Xue, R.-D. (2004). Laboratory evaluation of mosquito repellents against *Aedes albopictus*, *Culex nigripalpus*,and *Ochlerotatus triseriatus* (Diptera: Culicidae). *J Med Entomol, 41*(4), 726–730.

Bathen, D. & Breitbach, M. (2001). *Adsorptionstechnik*. VDI-Buch.

Batt, C. A. & Tortorello, M.-L. (Eds.). (2014). *Encyclopedia of Food Microbiology* (2nd ed.). London: Elsevier.

Baydar, H. & Baydar, N. G. (2005). The effects of harvest date, fermentation duration and Tween 20 treatment on essential oil content and composition of industrial oil rose (*Rosa damascena* Mill). *Ind Crops Prod*, *21*(2), 251–255.

Bennett, B. D., Kimball, E. H., Gao, M., Osterhout, R., van Dien, S. J. & Rabinowitz, J. D. (2009). Absolute metabolite concentrations and implied enyzme active site occupancy in *Escherichia coli*. *Nat Chem Biol*, *5*, 593–599.

Bennett, B. D., Yuan, J., Kimball, E. H. & Rabinowitz, J. D. (2008). Absolute quantitation of intracellular metabolite concentrations by an isotope ratio-based approach. *Nat Protoc*, *3*, 1299–1311.

Bentley, W. E., Mirjalili, N., Andersen, D. C., Davis, R. H. & Kompala, D. S. (1990). Plasmid-encoded protein: The prinicipal factor in the metabolic burden associated with recombinant bacteria. *Biotechnol Bioeng*, *35*, 668–681.

Blum, H., Beier, H. & Gross, H. J. (1987). Improved silver staining of plant proteins, RNA and DNA in polyacrylamide gels. *Electrophoresis*, *8*(2), 93–99.

Bönisch, F., Frotscher, J., Stanitzek, S., Rühl, E., Wüst, M., Bitz, O. & Schwab, W. (2014a). A UDP-glucose:monoterpenol glucosyltransferase adds to the chemical diversity of the grapevine metabolome. *Plant Physiol*, *165*, 561–581.

Bönisch, F., Frotscher, J., Stanitzek, S., Rühl, E., Wüst, M., Bitz, O. & Schwab, W. (2014b). Activity-based profiling of a physiologic aglycone library reveals sugar acceptor promiscuity of Family 1 UDP-glucosyltransferases from grape. *Plant Physiol*, *166*, 23–39.

Borodina, I. & Nielsen, J. (2014). Advances in metabolic engineering of yeast *Saccharomyces cerevisiae* for production of chemicals. *Biotechnol J*, *9*(5), 609–620.

Bowles, D., Isayenkova, J., Lim, E.-K. & Poppenberger, B. (2005). Glycosyltransferases: Managers of small molecules: Review. *Curr Opin Plant Biol*, *8*, 254–263.

Brandenbusch, C., Bühler, B., Hoffmann, P., Sadowski, G. & Schmid, A. (2010). Efficient phase separation and product recovery in organic-aqueous bioprocessing using supercritical carbon dioxide. *Biotechnol Bioeng*, *107*(4), 642–651.

Brauer, H. (1978). Unsteady state mass transfer through the interface of spherical particles. I Physical and mathematical description of the mass-transfer problem. II - Discussion of results obtained by theoretical methods. *Int J Heat Mass Transfer*, *21*, 445–453.

Braun, A., Geier, M., Bühler, B., Schmid, A., Mauersberger, S. & Glieder, A. (2012). Steroid biotransformations in biphasic systems with *Yarrowia lipolytica* expressing human liver cytochrome P450 genes. *Microb Cell Fact*, *11*.

Bräutigam, S. (2008). *Ganzzell-Biokatalyse in Gegenwart ionischer Flüssigkeiten mit rekombinanten escherichia coli* (Dissertation, TU München).

Bräutigam, S., Bringer-Meyer, S. & Weuster-Botz, D. (2007). Asymmetric whole cell biotransformations in biphasic ionic liquid/water-systems by use of recombinant *Escherichia coli* with intracellular cofactor regeneration. *Tetrahedron: Asymmetry*, *18*, 1883–1887.

Brennan, T. C. R., Turner, C. D., Krömer, J. O. & Nielsen, L. K. (2012). Alleviating monoterpene toxicity using a two-phase extractive fermentation for the bioproduction of jet fuel mixtures in *Saccharomyces cerevisiae*. *Biotechnol Bioeng*, *109*, 2513–2522.

Brink, L. E. & Tramper, J. (1985). Optimization of organic solvent in multiphase biocatalysis. *Biotechnol Bioeng*, *27*(8), 1258–1269.

Bruce, L. J. & Daugulis, A. J. (1991). Solvent selection strategies for extractive biocatalysis. *Biotechnol Prog*, *7*, 116–124.

Buchhaupt, M., Guder, J. C., Etschmann, M. M. W. & Schrader, J. (2012). Synthesis of green note aroma compounds by biotransformation of fatty acids using yeast cells coexpressing lipoxygenase and hydroperoxide lyase. *Appl Microbiol Biotechnol*, *93*(1), 159–168.

Buescher, J. M., Moco, S., Sauer, U. & Zamboni, N. (2010). Ultrahigh performance liquid chromatography-tandem mass spectrometry method for fast and robust quantification of anionic and aromatic metabolites. *Anal Chem*, *82*, 4403–4412.

Caputi, L. & Aprea, E. (2011). Use of terpenoids as natural flavouring compounds in food industry: Review. *Recent Pat Food, Nutr Agric*, *3*, 9–16.

Caputi, L., Lim, E.-K. & Bowles, D. (2008). Discovery of new biocatalysts for the glycosylation of terpenoid scaffolds. *Chem - Eur J*, *14*, 6656–6662.

Carroll, A. L., Desai, S. H. & Atsumi, S. (2016). Microbial production of scent and flavor compounds. *Curr Opin Biotechnol*, *37*, 8–15.

Castiglione, K., Fu, Y., Polte, I., Leupold, S., Meo, A. & Weuster-Botz, D. (2017). Asymmetric whole-cell bioreduction of (*R*)-carvone by recombinant *Escherichia coli* with in situ substrate supply and product removal. *Biochem Eng J*, *117*, 102–111.

Castiglione, K. & Weuster-Botz, D. (2018). Enzymatische Prozesse. In *Bioprozesstechnik* (pp. 403–447). Berlin.

Chassagnole, C., Fell, D. A., Raïs, B., Kudla, B. & Mazat, J.-P. (2001). Control of the threonine-synthesis pathway in *Escherichia coli*: A theoretical and experimental approach. *Biochem J*, *356*(2), 433–444.

Chen, J.-C., Chen, Q.-H., Guo, Q., Ruan, S., Ruan, H., He, G.-Q. & Gu, Q. (2010). Simultaneous determination of acetoin and tetramethylpyrazine in traditional vinegars by HPLC method. *Food Chem*, *122*(4), 1247–1252.

Chen, R. R. (2007). Permeability issues in whole-cell bioprocesses and cellular membrane engineering. *Appl Microbiol Biotechnol*, *74*, 730–738.

Cheng, T., Zhao, Li, X., Lin, F., Xu, Y., Zhang, X., . . . Lai, L. (2007). Computation of octanol-water partition coefficients by guiding an additive model with knowledge. *J Chem Inf Model*, *47*(6), 2140–2148.

Chmiel, H., Takors, R. & Weuster-Botz, D. (Eds.). (2018). *Bioprozesstechnik* (4th ed.). Berlin: Springer Spektrum.

Choi, J. H., Jeong, K. J., Kim, S. C. & Lee, S. Y. (2000). Efficient secretory production of alkaline phosphatase by high cell density culture of recombinant *Escherichia coli* using the *Bacillus* sp. endoxylanase signal sequence. *Appl Microbiol Biotechnol*, *53*(6), 640–645.

Choi, J. H., Keum, K. C. & Lee, S. Y. (2006). Production of recombinant proteins by high cell density culture of *Escherichia coli*: Review. *Chem Eng Sci*, *61*, 876–885.

Ciriminna, R., Lomeli-Rodriguez, M., Demma Carà, P., Lopez-Sanchez, J. A. & Pagliaro, M. (2014). Limonene: A versatile chemical of the bioeconomy. *Chem Comm*, *50*(97), 15288–15296.

Coutinho, P. M., Deleury, E., Davies, G. J. & Henrissat, B. (2003). An evolving hierarchical family classification for glycosyltransferases. *J Mol Biol*, *328*(2), 307–317.

Craig, T. & Daugulis, A. J. (2013). Polymer characterization and optimization of conditions for the enhanced bioproduction of benzaldehyde by *Pichia pastoris* in a two-phase partitioning bioreactor. *Biotechnol Bioeng*, *110*(4), 1098–1105.

Creuly, C., Larroche, C. & Gros, J.-B. (1992). Bioconversion of fatty acids into methyl ketones by spores of *Penicillium roquefortii* in a water-organic solvent, two-phase system. *Enzyme Microb Technol*, *14*(8), 669–678.

Croxen, M. A., Law, R. J., Scholz, R., Keeney, K. M., Wlodarska, M. & Finlay, B. B. (2013). Recent advances in understanding enteric pathogenic *Escherichia coli*. *Clin Microbiol Rev*, *26*(4), 822–880.

Dafoe, J. T. & Daugulis, A. J. (2014). In situ product removal in fermentation systems: Improved process performance and rational extractant selection. *Biotechnol Lett*, *36*(3), 443–460.

Dafoe, J. T., Parent, J. S. & Daugulis, A. J. (2014). Block copolymers as sequestering phases in two-phase biotransformations: Effect of constituent homopolymer properties on solute affinity. *J Chem Technol Biotechnol*, *89*(9), 1304–1310.

Daugulis, A. J., Tomei, M. C. & Guieysse, B. (2011). Overcoming substrate inhibition during biological treatment of monoaromatic compounds: Recent advances in bioprocess design. *Appl Microbiol Biotechnol*, *90*, 1589–1608.

de Koning, W. & van Dam, K. (1992). A method for the determination of changes of glycolytic metabolites in yeast on a subsecond time scale using extraction at neutral ph. *Anal Biochem*, *204*(1), 118–123.

de Bruyn, F., de Paepe, B., Maertens, J., Beuaprez, J., de Cocker, P., Mincke, S., ... de Mey, M. (2015). Development of an in vivo glucosylation platform by coupling production to growth: Production of phenolic glucosides by a glycosyltransferase of *Vitis Vinifera*. *Biotechnol Bioeng*, *112*, 1594–1603.

de Mey, M., de Maeseneire, S., Soetaert, W. & Vandamme, E. (2007). Minimizing acetate formation in *E. coli* fermentations: Review. *J Ind Microbiol Biotechnol*, *34*, 689–700.

de Roode, B. M., Oliehoek, L., van der Padt, A., Franssen, M. C. R. & Boom, R. M. (2001). Downstream processing of enzymatically produced geranyl glucoside. *Biotechnol Prog*, *17*, 881–886.

de Smet, M.-J., Wynberg, H. & Witholt, B. (1981). Synthesis of 1,2-epoxyoctane by *Pseudomonas oleovorans* during growth in a two-phase system containing high concentrations of 1-octene. *Appl Environ Microbiol*, *42*, 811–816.

Demissie, Z. A., Tarnowycz, M., Adal, A. M., Sarker, L. S. & Mahmoud, S. S. (2019). A lavender ABC transporter confers resistance to monoterpene toxicity in yeast. *Planta*, *249*(1), 139–144.

Dennewald, D., Hortsch, R. & Weuster-Botz, D. (2012). Evaluation of parallel milliliter-scale stirred-tank bioreactors for the study of biphasic whole-cell biocatalysis with ionic liquids. *J Biotechnol*, *157*, 253–257.

Dennewald, D., Pitner, W.-R. & Weuster-Botz, D. (2011). Recycling of the ionic liquid phase in process integrated biphasic whole-cell biocatalysis. *Process Biochem*, *46*, 1132–1137.

Desmet, T., Soetaert, W., Bojarová, P., Křen, V., Dijkhuizen, L., Eastwick-Field, V. & Schiller, A. (2012). Enzymatic glycosylation of small molecules: Challenging substrates require tailored catalysts. *Chem Eur J*, *18*(35), 10786–10801.

Deutsches Institut für Normung. (1998). Verfahren der Standardaddition: Verfahren, Auswertung.

Déziel, E., Comeau, Y. & Villemur, R. (1999). Two-liquid-phase bioreactors for enhanced degradation of hydrophobic/toxic compounds. *Biodegradation*, *10*(3), 219–233.

Donovan, R. S., Robinson, C. W. & Glick, B. R. (1996). Review: Optimizing inducer and culture conditions for expression of foreign proteins under the control of the lac promoter. *J Ind Microbiol*, *16*, 145–154.

Dubey, V. S. & Luthra, R. (2001). Biotransformation of geranyl acetate to geraniol during palmarosa (*Cymbopogon martinii*, Roxb. wats. var. motia) inflorescence development. *Phytochemistry*, *57*(5), 675–680.

Duff, S. J. B. & Murray, W. D. (1989). Oxidation of benzyl alcohol by whole cells of *Pichia pastoris* and by alcohol oxidase in aqueous and nonaqueous reaction media. *Biotechnol Bioeng*, *34*, 153–159.

Erickson, B. E. (2015). Pressure on plasticizers - Toxicity concerns prompt retailers, regulators to phase out widely used phthalates. *Chem Eng News*, *93*, 11–15.

Etschmann, M. & Schrader, J. (2006). An aqueous–organic two-phase bioprocess for efficient production of the natural aroma chemicals 2-phenylethanol and 2-phenylethyl acetate with yeast. *Appl Microbiol Biotechnol*, *71*(4), 440–443.

Fairbanks, G., Steck, T. L. & Wallachl, D. F. H. (1971). Electrophoretic analysis of the major polypeptides of the human erythrocyte membrane. *Biochemistry*, *10*, 2606–2617.

Fam, H. & Daugulis, A. J. (2012). Substrate mass transport in two-phase partitioning bioreactors employing liquid and solid non-aqueous phases. *Bioprocess Biosyst Eng*, *35*, 1367–1374.

Fatiadi, A. J. & Schaffer, R. (1974). An improved procedure for synthesis of DL-4-hydroxy-3-methoxymandelic acid. *J Res Natl Bur Stan Sect A*, *78A*(3), 411.

Faust, G., Stand, A. & Weuster-Botz, D. (2015). IPTG can replace lactose in auto-induction media to inhance protein expression in batch-cultured *Escherichia coli*. *Eng Life Sci*, *15*(8), 824–829.

Fischer, L. (2011). Was kommt nach der Petrochemie?

Fredenslund, A., Jones, R. L. & Prausnitz, J. M. (1975). Group-contribution estimation of activity coefficients in nonideal liquid mixtures. *AIChE Journal*, *21*(6), 1086–1099.

Freeman, A., Woodley, J. M. & Lilly, M. D. (1993). In situ product removal as a tool for bioprocessing. *Nat Biotechnol*, *11*(9), 1007–1012.

Freemantle, M. (1998). Designer solvents - Ionic liquids may boost clean technology development. *Chem Eng News*, *76*, 32–37.

Freundlich, H. (1926). *Colloid and Capillary Chemistry*. London: Methuen & Co.

Friedman, M., Henika, P. R. & Mandrell, R. E. (2002). Bactericidal activities of plant essential oils and some of their isolated constituents against *Campylobacter jejuni*, *Escherichia coli*, *Listeria monocytogenes*, and *Salmonella enterica*. *J Food Prot*, *65*(10), 1545–1560.

Gachon, C. M. M., Langlois-Meurinne, M. & Saindrenan, P. (2005). Plant secondary metabolism glycosyltransferases: The emerging functional analysis: Review. *Trends Plant Sci*, *10*, 542–549.

Gadgil, M., Kapur, V. & Hu, W.-S. (2005). Transcriptional response of *Escherichia coli* to temperature shift. *Biotechnol Prog*, *21*(3), 689–699.

Galaction, A.-I., Cascaval, D., Onicscu, C. & Turnea, M. (2004). Enhancement of oxygen mass transfer in stirred bioreactors using oxygen-vectors. 1. Simulated fermentation broths. *Bioprocess Biosyst Eng*, *26*, 231–238.

Galaction, A.-I., Cascaval, D., Turnea, M. & Folescu, E. (2005). Enhancement of oxygen mass transfer in stirred bioreactors using oxygen-vectors. 2. *Propionibacterium shermanii* broths. *Bioprocess Biosyst Eng*, *27*, 263–271.

Gao, F. & Daugulis, A. J. (2009). Bioproduction of the aroma compound 2-phenylethanol in a solid-liquid two-phase partitioning bioreactor system by *Kluyveromyces marxianus*. *Biotechnol Bioeng*, *104*(2), 332–339.

Gao, M.-T., Shimamura, T., Ishida, N. & Takahashi, H. (2011). pH-uncontrolled lactic acid fermentation with activated carbon as an adsorbent. *Enzyme Microb Technol*, *48*(6-7), 526–530.

Gasser, B., Saloheimo, M., Rinas, U., Dragosits, M., Rodríguez-Carmona, E., Baumann, K., . . . Villaverde, A. (2008). Protein folding and conformational stress in microbial cells producing recombinant proteins: A host comparative overview. *Microb Cell Fact*, *7*, 11.

Georgiou, C. D., Grintzalis, K., Zervoudakis, G. & Papapostolou, I. (2008). Mechanism of Coomassie brilliant blue G-250 binding to proteins: A hydrophobic assay for nanogram quantities of proteins. *Anal Bioanal Chem*, *391*(1), 391–403.

Gershenzon, J. & Dudareva, N. (2007). The function of terpene natural products in the natural world. *Nat Chem Biol*, *3*, 408–414.

Goh, E.-B., Baidoo, E. E. K., Keasling, J. D. & Beller, H. R. (2012). Engineering of bacterial methyl ketone synthesis for biofuels. *Appl Environ Microbiol*, *78*(1), 70–80.

Goldstein, J. L. & Brown, M. S. (1990). Regulation of the mevalonate pathway. *Nature*, *343*(6257), 425–430.

Grünberger, A., Paczia, N., Probst, C., Schendzielorz, G., Eggeling, L., Noack, S., . . . Kohlheyer, D. (2012). A disposable picolitre bioreactor for cultivation and investigation of industrially relevant bacteria on the single cell level. *Lab Chip*, *12*(11), 2060–2068.

Guajardo, N., Müller, C. R., Schrebler, R., Carlesi, C. & Domínguez de María, P. (2016). Deep eutectic solvents for organocatalysis, biotransformations, and multistep organocatalyst/enzyme combinations. *ChemCatChem*, *8*, 1020–1027.

Guentert, M. (2007). The flavour and fragrance industry - Past, present, and future. In *Flavours and Fragrances* (pp. 1–14). Berlin.

Gunata, Y. Z., Bayonove, C. L., Baumes, R. L. & Cordonnier, R. E. (1985). The aroma of grapes. Extraction and determination of free and glykosidically bound fractions of some grape aroma components. *J Chromatogr*, *331*, 83–90.

Guyot-Declerck, C., Chevance, F., Lermusieau, G. & Collin, S. (2000). Optimized extraction procedure for quantifying norisoprenoids in honey and honey food products. *J Agric Food Chem*, *48*(12), 5850–5855.

Hans, J., Brandt, W. & Vogt, T. (2004). Site-directed mutagenesis and protein 3D-homology modelling suggest a catalytic mechanism for UDP-glucose-dependent betanidin 5-O-glucosyltransferase from *Dorotheanthus bellidiformis. Plant J*, *39*, 319–333.

Hansen, C. M. (2007). *Hansen Solubility Parameters: A User´s Handbook* (2nd ed.). Florida: CRC Press.

Hansen, C. M. (2016). HSPiP Software.

Harrop, A. J., Woodley, J. M. & Lilly, M. D. (1992). Production of naphtalene-cis-glycol by *Pseudomonas putida* in the presence of organic solvents. *Enzyme Microb Technol*, *14*, 725–730.

Heins, A.-L. & Weuster-Botz, D. (2018). Population heterogeneity in microbial bioprocesses: Origin, analysis, mechanisms, and future perspectives. *Bioprocess Biosyst Eng*, *41*(7), 889–916.

Henry, W. (1803). Experiments on the quantity of gases absorbed by water, at different temperatures, and under different pressures. *Phil Trans R Soc Lon*, *93*, 29–274.

Hernández, M., Quijano, G., Thalasso, F., Daugulis, A. J., Villaverde, S. & Muñoz, R. (2010). A comparative study of solid and liquid non-aqueous phases for the biodegradation of hexane in two-phase partitioning bioreactors. *Biotechnol Bioeng*, *106*(5), 731–740.

Herrmann, A. (2007). Controlled release of volatiles under mild reaction conditions: From nature to everyday products. *Angew Chem, Int Ed*, *46*, 5836–5863.

Hildebrand, J. H. & Scott, R. L. (1962). *Regular Solutions.* Englewood Cliffs: Prentice-Hall Inc.

Hirotani, M., Kuroda, R., Suzuki, H. & Yoshikawa, T. (2000). Cloning and expression of UDP-glucose: Flavonoid 7-O-glucosyltransferase from hairy root cultures of *Scutellaria baicalensis. Planta, 210*(6), 1006–1013.

Hocknull, M. D. & Lilly, M. D. (1990). The use of free and immobilised *Arthrobacter simplex* in organic solvent/aqueous two-liquid-phase reactors. *Appl Microbiol Biotechnol, 33,* 148–153.

Hortsch, R. & Weuster-Botz, D. (2010). Power consumption and maximum energy dissipation in a milliliter-scale bioreactor. *Biotechnol Progr, 26,* 595–599.

Hu, Y. & Walker, S. (2002). Remarkable structural similarities between diverse glycosyltransferases. *Chem Biol, 9*(12), 1287–1296.

Huang, F.-C., Hinkelmann, J., Hermenau, A. & Schwab, W. (2016). Enhanced production of $\beta$-glucosides by *in-situ* UDP-glucose regeneration. *J Biotechnol, 69,* 5238–5242.

Huang, F.-C., Hinkelmann, J. & Schwab, W. (2015). Glucosylation of aroma chemicals and hydroxy fatty acids. *J Biotechnol, 216,* 100–109.

Huber, R., Roth, S., Rahmen, N. & Büchs, J. (2011). Utilizing high-throughput experimentation to enhance specific productivity of an *E. coli* T7 expression system by phosphate limitation. *BMC Biotechnol, 11.*

Hughes, J. & Hughes, M. A. (1994). Multiple secondary plant product UDP-glucose glucosyltransferase genes expressed in cassava (*Manihot esculenta* crantz) cotyledons. *DNA Sequence, 5*(1), 41–49.

IHS Markit. (2018). Flavors and Fragrances: Specialty Chemicals Update Program.

Ikemoto, T., Okabe, B.-I., Mimura, K. & Kitahara, T. (2002). Formation of fragrance materials from odourless glycosidically-bound volatiles by skin microflora (Part 1). *Flavour Fragrance J, 17,* 452–455.

Inoue, A. & Horikoshi, K. (1991). Estimation of solvent-tolerance of bacteria by the solvent parameter logP. *J Ferment Bioeng, 71*(3), 194–196.

Jakoblinnert, A. & Rother, D. (2014). A two-step biocatalytic cascade in micro-aqueous medium: Using whole-cells to obtain high concentrations of a vicinal diol. *Green Chem, 16,* 3472–3482.

Janoschek, L., Grozdev, L. & Berensmeier, S. (2018). Membrane-assisted extraction of monoterpenes: From in silico solvent screening towards biotechnological process application. *R Soc Open Sci, 5*(4).

Janßen, H. J. & Steinbüchel, A. (2014). Fatty acid synthesis in *Escherichia coli* and its applications towards the production of fatty acid based biofuels. *Biotechnol Biofuels*, *7*(1), 7.

Jiang, X., Wang, Y. & Li, M. (2014). Selecting water-alcohol mixed solvent for synthesis of polydopamine nano-spheres using solubility parameter. *Sci Rep*, *4*, 6070.

Julsing, M. K., Kuhn, D., Schmid, A. & Bühler, B. (2012). Resting cells of recombinant *E. coli* show high epoxidation yields on energy source and high sensitivity to product inhibition. *Biotechnol Bioeng*, *109*(5), 1109–1119.

Keseler, I. M., Mackie, A., Santos-Zavaleta, A., Billington, R., Bonavides-Martínez, C., Caspi, R., . . . Karp, P. D. (2017). The EcoCyc database: Reflecting new knowledge about *Escherichia coli* K-12. *Nucleic Acids Res*, *45*, 543–550.

Khalilzadeh, R., Shojaosadati, S. A., Bahrami, A. & Maghsoudi, N. (2004). Fed-batch cultivation of recombinant *Escherichia coli* producing human interferon-$\gamma$ under controlled specific growth rate. *Iran J Biotechnol*, *2*, 113–122.

Khersonsky, O. & Tawfik, D. S. (2010). Enzyme promiscuity: A mechanistic and evolutionary perspective. *Annu Rev Biochem*, *79*(1), 471–505.

Kirk-Othmer. (2007). *Food and Feed Technology* (1st ed.). Wiley.

Koller, A. P., Wolf, L. & Weuster-Botz, D. (2017). Reaction engineering analysis of *Scenedesmus ovalternus* in a flat-plate gas-lift photobioreactor. *Bioresour Technol*, *225*, 165–174.

Kollerup, F. & Daugulis, A. J. (1986). Ethanol production by extractive fermentation - solvent identification and prototype development. *Can J Chem Eng*, *64*(4), 598–606.

Korz, D. J., Rinas, U., Hellmuth, K., Sanders, E. A. & Deckwer, W.-D. (1995). Simple fed-batch technique for high cell density cultivation of *Escherichia coli*. *J Biotechnol*, *39*, 59–65.

Kren, V. & Thiem, J. (1997). Glycosylation employing bio-systems: From enzymes to whole cells. *Chem Soc Rev*, *26*, 463–473.

Kühne, B. & Sprecher, E. (1989). Enhancement of the production of fungal volatiles employing different adsorbents. *Flavour Fragrance J*, *4*, 77–79.

Kulkarni, R. (2016). Metabolic engineering: Biological art of producing useful chemicals. *Resonance*, *21*(3), 233–237.

Kusterer, A. (2007). *Reaktionstechnische Optimierung von Parallelreaktoren für kontrollierte Bioprozesse* (Dissertation, TU München).

Laane, C., Boeren, S. & Vos, K. (1985). On optimizing organic solvents in multi-liquid-phase biocatalysis. *Trends Biotechnol*, *3*(10), 251–252.

Laemmli, U. K. (1970). Cleavage of structural proteins during the assembly of the head of bacteriophage T4. *Nature*, *227*(5259), 680–685.

Lairson, L. L., Henrissat, B., Davies, G. J. & Withers, S. G. (2008). Glycosyltransferases: Structures, functions, and mechanisms: Review. *Annu Rev Biochem*, *77*, 521–555.

Langmuir, I. (1918). The adsorption of gases on plane surfaces of glass, mica and platinum. *J Am Chem Soc*, *40*(9), 1361–1403.

Lee, D., Lloyd, N. D. R., Pretorius, I. S. & Borneman, A. R. (2016). Heterologous production of raspberry ketone in the wine yeast *Saccharomyces cerevisiae* via pathway engineering and synthetic enzyme fusion. *Microb Cell Fact*, *15*, 49.

Lee, H. I. & Raskin, I. (1999). Purification, cloning, and expression of a pathogen inducible UDP-glucose:salicylic acid glucosyltransferase from tobacco. *J Biol Chem*, *274*(51), 36637–36642.

Lee, J.-Y., Na, Y.-A., Kim, E., Lee, H.-S. & Kim, P. (2016). The actinobacterium *Corynebacterium glutamicum*, an industrial workhorse. *J Microbiol Biotechnol*, *26*(5), 807–822.

Lee, S. Y. (1996). High cell-density culture of *Escherichia coli*: Review. *Trends Biotechnol*, *14*, 98–105.

Lee, S. Y., Kim, H. U., Chae, T. U., Cho, J. S., Kim, J. W., Shin, J. H., . . . Jang, Y.-S. (2019). A comprehensive metabolic map for production of bio-based chemicals. *Nat Catal*, *2*(1), 18–33.

Lee, S., Peterson, C. J. & Coats, J. R. (2003). Fumigation toxicity of monoterpenoids to several stored product insects. *J Stored Prod Res*, *39*(1), 77–85.

Lei, Z., Chen, B., Li, C. & Liu, H. (2008). Predictive molecular thermodynamic models for liquid solvents, solid salts, polymers, and ionic liquids. *Chem Rev*, *108*(4), 1419–1455.

León, G., Paret, N., Fankhauser, P., Grenno, Erni, P., Ouali, L. & Berthier, D. L. (2017). Formaldehyde-free melamine microcapsules as core/shell delivery systems for encapsulation of volatile active ingredients. *RSC Adv*, *7*(31), 18962–18975.

Lewis, W. K. & Whitman, W. G. (1924). Principles of gas absorption. *Ind Eng Chem*, *16*(12), 1215–1220.

Li, M., Wang, J., Geng, Y., Li, Y., Wang, Q., Liang, Q. & Qi, Q. (2012). A strategy of gene overexpression based on tandem repetitive promoters in *Escherichia coli*. *Microb Cell Fact*, *11*, 19.

Liu, W., Xu, X., Zhang, R., Cheng, T., Cao, Y., Li, X., . . . Xian, M. (2016). Engineering *Escherichia coli* for high-yield geraniol production with biotransformation of geranyl acetate to geraniol under fed-batch culture. *Biotechnol Biofuels*.

Louis, P., Trüper, G. H. & Galinski, E. A. (1994). Survival of *Escherichia coli* during drying and storage in the presence of compatible solutes. *Appl Microbiol Biotechnol*, *41*, 684–688.

Mao, Z., Shin, H.-D. & Chen, R. R. (2006). Engineering the *E. coli* UDP-glucose synthesis pathway for oligosaccharide synthesis. *Biotechnol Prog*, *22*, 369–374.

Mastelić, J., Jerkovic, I., Vinković, M. & Džolić, Z. (2004). Synthesis of selected naturally occurring glucosides of volatile compounds. Their chromatographic and spectroscopic properties. *Croat Chem Acta*, *77*, 491–500.

Mayer, A. & Weuster-Botz, D. (2017). Reaction engineering analysis of the autotrophic energy metabolism of *Clostridium aceticum*. *FEMS Microbiol Lett*, *364*(22).

Mazur, P. (1984). Freezing of living cells: mechanisms and implications. *Am J Physiol*, *247*, 125–142.

Mears, L., Stocks, S. M., Sin, G. & Gernaey, K. V. (2017). A review of control strategies for manipulating the feed rate in fed-batch fermentation processes. *J Biotechnol*, *245*, 34–46.

Menzel, M. & Schreier, P. (2007). Enzymes and Flavour Biotechnology. In *Flavours and Fragrances: Chemistry, Bioprocessing and Sustainability*. Berlin.

Moehs, C. P., Allen, P. V., Friedman, M. & Belknap, W. R. (1997). Cloning and expression of solanidine UDP-glucose glucosyltransferase from potato. *Plant J*, *11*(2), 227–236.

Monod, J. (1949). The growth of bacterial cultures. *Annu Rev Microbiol*, *3*(1), 371–394.

Moran, U., Phillips, R. & Milo, R. (2010). Snapshot: Key numbers in biology. *Cell*, *141*(7), 1262–1262.e1.

Morrish, J. L. E. & Daugulis, A. J. (2008). Improved reactor performance and operability in the biotransformation of carveol to carvone using a solid-liquid two-phase partitioning bioreactor. *Biotechnol Bioeng*, *101*, 946–956.

Mortimer, E. M. & Müller, U. (2007). *Chemie: Das Basiswissen der Chemie* (9th ed.). Stuttgart: Georg Thieme Verlag.

Müller, C. R., Lavandera, I., Gotor-Fernández, V. & Domínguez de María, P. (2015). Performance of recombinant-whole-cell-catalyzed reductions in deep-eutectic-solvent-aqueous-media mixtures. *ChemCatChem*, *7*, 2654–2659.

Müller, D. A. (2007). Flavours: The Legal Framework. In *Flavours and Fragrances: Chemistry, Bioprocessing and Sustainability* (pp. 15–24). Berlin.

Murarka, A., Dharmadi, Y., Yazdani, S. S. & Gonzalez, R. (2008). Fermentative utilization of glycerol by *Escherichia coli* and its implications for the production of fuels and chemicals. *Appl Environ Microbiol*, *74*(4), 1124–1135.

Nagegowda, D. A. (2010). Plant volatile terpenoid metabolism: Biosynthetic genes, transcriptional regulation and subcellular compartmentation. *FEBS Lett*, *584* (14), 2965–2973.

National Center for Biotechnology Information. (2019). PubChem.

Ni, Y. & Chen, R. R. (2004). Accelerating whole-cell biocatalysis by reducing outer membrane permeability barrier. *Biotechnol Bioeng*, *87*, 804–811.

Overmann, J., Abt, B. & Sikorski, J. (2017). Present and future of culturing bacteria. *Annu Rev Microbiol*, *71*, 711–730.

Paliy, O. & Gunasekera, T. S. (2007). Growth of *E. coli* BL21 in minimal media with different gluconeogenic carbon sources and salt contents. *Appl Microbiol Biotechnol*, *73* (5), 1169–1172.

Park, C., Lee, Y., Lee, S. Y., Oh, H. B. & Lee., J. (2011). Determination of the intracellular concentrations of metabolites in *Escherichia coli* collected during the exponential and stationary growth phases using liquid chromatography-mass spectrometry. *Bull Korean Chem Soc*, *32*, 524–530.

Patel, M. J., Popat, S. C. & Deshusses, M. A. (2017). Determination and correlation of the partition coefficients of 48 volatile organic and environmentally relevant compounds between air and silicone oil. *Chem Eng J*, *310, Part 1*, 72–78.

Pedrolli, D. B., Monteiro, A. C., Gomes, E. & Carmona, E. C. (2009). Pectin and pectinases: Production, characterization and industrial application of microbial pectinolytic enzymes. *Open Biotechnol J*, *3* (1), 9–18.

Pfründer, H., Amidjojo, M., Kragl, U. & Weuster-Botz, D. (2004). Efficient whole-cell biotransformation in a biphasic ionic liquid/water system. *Angew Chem, Int Ed*, *43*, 4529–4531.

Pfründer, H., Jones, R. & Weuster-Botz, D. (2006). Water immiscible ionic liquids as solvents for whole cell biocatalysis. *J Biotechnol*, *124*, 182–190.

Plotka, M., Wozniak, M. & Kaczorowski, T. (2017). Quantification of plasmid copy number with single colour droplet digital PCR. *PLoS One*, *12* (1).

Poleo, E. E. & Daugulis, A. J. (2014). A comparison of three first principles methods for predicting solute–polymer affinity, and the simultaneous biodegradation of phenol and butyl acetate in a two-phase partitioning bioreactor. *J Chem Techol Biotechnol*, *89* (1), 88–96.

Prat, D., Wells, A., Hayler, J., Sneddon, H., McElroy, C. R., Abou-Shehada, S. & Dunn, P. J. (2016). CHEM21 selection guide of classical and less classical solvents. *Green Chem*, *18* (1), 288–296.

Primrose, S. B. & Twyman, R. M. (2007). *Principles of Gene Manipulation and Genomics* (7. ed., 4. print). Malden, MA: Blackwell.

Prpich, G. P. & Daugulis, A. J. (2004). Polymer development for enhanced delivery of phenol in a solid-liquid two-phase partitioning bioreactor. *Biotechnol Prog, 20*(6), 1725–1732.

Puskeiler, R., Kaufmann, K. & Weuster-Botz, D. (2005). Development, parallelization, and automation of a gas-inducing milliliter-scale bioreactor for high-throughput bioprocess design (HTBD). *Biotechnol Bioeng, 89*, 512–523.

Qing, G., Ma, L.-C., Khorchid, A., Swapna, G. V. T., Mal, T. K., Takayama, M. M., . . . Inouye, M. (2004). Cold-shock induced high-yield protein production in *Escherichia coli. Nat Biotechnol, 22*(7), 877–882.

Quijano, G., Hernandez, M., Thalasso, F., Munoz, R. & Villaverde, S. (2009). Two-phase partitioning bioreactors in environmental biotechnology. *Eur J Appl Microbiol Biotechnol, 84*(5), 829–846.

Ranjan, R., Thust, S., Gounaris, C. E., Woo, M., Floudas, C. A., Keitz, M. v., . . . Tsapatsis, M. (2009). Adsorption of fermentation inhibitors from lignocellulosic biomass hydrolyzates for improved ethanol yield and value-added product recovery. *Microporous Mesoporous Mater, 122*(1), 143–148.

Rastogi, S. C., Heydorn, S., Johansen, J. D. & Basketter, D. A. (2001). Fragrance chemicals in domestic and occupational products. *Contact Dermatitis, 45*, 221–225.

Rehmann, L., Sun, B. & Daugulis, A. J. (2007). Polymer selection for biphenyl degradation in a solid-liquid two-phase partitioning reactor. *Biotechnol Prog, 23*, 814–819.

Richter, N., Neumann, M., Liese, A., Wohlgemuth, R., Weckbecker, A., Eggert, T. & Hummel, W. (2010). Characterization of a whole-cell catalyst co-expressing glycerol dehydrogenase and glucose dehydrogenase and its application in the synthesis of L-glyceraldehyde. *Biotechnol Bioeng, 106*, 541–552.

Riesenberg, D. (1991). High-cell-density cultivation of *Escherichia coli. Curr Opin Biotechnol, 2*, 380–384.

Riesenberg, D., Schulz, V., Knorre, W. A., Pohl, H.-D., Korz, D., Sanders, E. A., . . . Deckwer, W.-D. (1991). High cell density cultivation of *Escherichia coli* at controlled specific growth rate. *J Biotechnol, 20*, 17–28.

Rito-Palomares, M., Negrete, A., Miranda, L., Flores, C., Galindo, E. & Serrano-Carreón, L. (2001). The potential application of aqueous two-phase systems for in situ recovery of 6-pentyl-$\alpha$-pyrone produced by *Trichoderma harzianum. Enzyme Microb Technol, 28*(7–8), 625–631.

Rivas, F., Parra, A., Martinez, A. & Garcia-Granados, A. (2013). Enzymatic glycosylation of terpenoids: Review. *Phytochem Rev, 12*, 327–339.

Robak, K. & Balcerek, M. (2018). Review of second generation bioethanol production from residual biomass. *Food Technol Biotechnol, 56*(2), 174–187.

Rodriguez, G. M., Tashiro, Y. & Atsumi, S. (2014). Expanding ester biosynthesis in *Escherichia coli. Nat Chem Biol, 10*(4), 259–265.

Rohmer, M. (1999). The discovery of a mevalonate-independent pathway for isoprenoid biosynthesis in bacteria, algae and higher plants. *Nat Prod Rep, 16*(5), 565–574.

Roosen, C., Müller, P. & Greiner, L. (2008). Ionic liquids in biotechnology: Applications and perspectives for biotransformations: Review. *Appl Microbiol Biotechnol, 81*, 607–614.

Rossmann, M. G., Moras, D. & Olsen, K. W. (1974). Chemical and biological evolution of a nucleotide-binding protein. *Nature, 250*(5463), 194–199.

Salehmin, M. N., Annuar, M. S. M. & Chisti, Y. (2013). High cell density fed-batch fermentations for lipase production: Feeding strategies and oxygen transfer: Review. *Bioprocess Biosyst Eng, 36*, 1527–1543.

Salter, G. J. & Kelt, D. B. (1995). Solvent selection for whole cell biotransformations in organic media. *Crit Rev Biotechnol, 15*, 139–177.

Schellmann, J. A. (1997). Temperature, stability, and the hydrophobic interaction. *Biophys J, 73*, 2960–2964.

Schievano, E., D'Ambrosio, M., Mazzaretto, I., Ferrarini, R., Magno, F., Mammi, S. & Favaro, G. (2013). Identification of wine aroma precursors in Moscato Giallo grape juice: A nuclear magnetic resonance and liquid chromatography-mass spectrometry tandem study. *Talanta, 116*, 841–851.

Schlegel, H. G. (1992). *Allgemeine Mikrobiologie* (7th ed.). Stuttgart: Thieme.

Schmid, A., Dordick, J. S., Hauer, B., Kiener, A., Wubbolts, M. & Witholt, B. (2001). Industrial biocatalysis today and tomorrow. *Nature, 409*, 258–268.

Schmid, A., Kollmer, A., Mathys, R. G. & Witholt, B. (1998). Developments toward large-scale bacterial bioprocesses in the presence of bulk amounts of organic solvents. *Extremophiles, 2*, 249–256.

Schmid, J. W., Mauch, K., Reuss, M., Gilles, E. D. & Kremling, A. (2004). Metabolic design based on a coupled gene expression-metabolic network model of tryptophan production in *Escherichia coli. Metab Eng, 6*(4), 364–377.

Schmieder, A., Hensler, S., Lang, M., Stratmann, A., Giesecke, U. & Weuster-Botz, D. (2016a). High-cell-density cultivation and recombinant protein production with

*Komagataella pastoris* in stirred-tank bioreactors from milliliter to cubic meter scale. *Proc Biochem, 51*(2), 177–184.

Schmieder, A., Priebe, X., Rubenbauer, M., Hoffmann, T., Huang, F.-C., Schwab, W. & Weuster-Botz, D. (2016b). Non-water miscible ionic liquid improves biocatalytic production of geranyl glucoside with *Escherichia coli* overexpressing a glucosyltransferase. *Bioprocess Biosyst Eng, 39*, 1409–1414.

Schrader, J. (2007). Microbial Flavour Production. In *Flavours and Fragrances: Chemistry, Bioprocessing and Sustainability* (pp. 507–574). Berlin.

Schwab, W., Fischer, T. C., Giri, A. & Wüst, M. (2015a). Potential applications of glucosyltransferases in terpene glucoside production: Impacts on the use of aroma and fragrance: Review. *Appl Microbiol Biotechnol, 99*, 165–174.

Schwab, W., Fischer, T. C. & Wüst, M. (2015b). Terpene glucoside production: Improved biocatalytic processes using glycosyltransferases: Review. *Eng Life Sci, 15*, 376–386.

Scott, M., Gunderson, C. W., Mateescu, E. M., Zhang, Z. & Hwa, T. (2010). Interdependence of cell growth and gene expression: Origins and consequences. *Science, 330*(6007), 1099–1102.

Serrano-Carreón, L., Balderas-Ruíz, K., Galindo, E. & Rito-Palomares, M. (2002). Production and biotransformation of 6-pentyl-$\alpha$-pyrone by *Trichoderma harzianum* in two-phase culture systems. *Eur J Appl Microbiol Biotechnol, 58*(2), 170–174.

Sharma, Y., Khan, L. A. & Manzoor, N. (2016). Anti-*Candida* activity of geraniol involves disruption of cell membrane integrity and function. *J Mycol Med, 26*, 244–254.

Sicaire, A. G., Vian, M., Fine, F., Joffre, F., Carré, P., Tostain, S. & Chemat, F. (2015). Alternative bio-based solvents for extraction of fat and oils: Solubility prediction, global yield, extraction kinetics, chemical composition and cost of manufacturing. *Int J Mol Sci, 16*(4), 8430–8453.

Sikkema, J., de Bont, J. A. & Poolman, B. (1994). Interactions of cyclic hydrocarbons with biological membranes. *J Biol Chem, 269*(11), 8022–8028.

Sinha, A. K., Sharma, U. K. & Sharma, N. (2008). A comprehensive review on vanilla flavor: Extraction, isolation and quantification of vanillin and others constituents. *Int J Food Sci Nutr, 59*(4), 299–326.

Sørensen, H. P. & Mortensen, K. K. (2005a). Advanced genetic strategies for recombinant protein expression in *Escherichia coli*: Review. *J Biotechnol, 115*, 113–128.

Sørensen, H. P. & Mortensen, K. K. (2005b). Soluble expression of recombinant proteins in the cytoplasm of *Escherichia coli. Microb Cell Fact, 4*.

Srivastava, A. K. & Gupta, S. (2011). Fed-Batch Fermentation - Design Strategies. In *Comprehensive Biotechnology* (pp. 515–526).

Stark, D. & von Stockar, U. (2003). In situ product removal (ISPR) in whole cell biotechnology during the last twenty years. *Adv Biochem Eng/Biotechnol*, *80*, 149–175.

Striedner, G., Cserjan-Puschmann, M., Pötschacher, F. & Bayer, K. (2003). Tuning the transcription rate of recombinant protein in strong *Escherichia coli* expression systems through repressor titration. *Biotechnol Prog*, *19*, 1427–1432.

Sührer, I., Langemann, T., Lubitz, W., Weuster-Botz, D. & Castiglione, K. (2015). A novel one-step expression and immobilization method for the production of biocatalytic preparations. *Microb Cell Fact*, *14*, 180.

Tang, W. L. & Zhao, H. (2009). Industrial biotechnology: Tools and applications. *Biotechnol J*, *4*(12), 1725–1739.

Tufvesson, P., Lima-Ramos, J., Nordblad, M. & Woodley, J. M. (2011). Guidelines and cost analysis for catalyst production in biocatalytic processes. *Org Process Res Dev*, *15*(1), 266–274.

Tweeddale, H., Notley-McRobb, L. & Ferenci, T. (1998). Effect of slow growth on metabolism of *Escherichia coli*, as revealed by global metabolite pool ("metabolome") analysis. *J Bacteriol*, *180*(19), 5109–5116.

van den Berg, C., Heeres, A. S., van der Wielen, L. A. M. & Straathof, A. J. J. (2013). Simultaneous clostridial fermentation, lipase-catalyzed esterification, and ester extraction to enrich diesel with butyl butyrate. *Biotechnol Bioeng*, *110*(1), 137–142.

van Sonsbeek, H. M., Beeftink, H. H. & Tramper, J. (1993). Two-liquid-phase bioreactors. *Enzyme Microb Technol*, *15*(9), 722–729.

Vandamme, E. J. & Soetaert, W. (2002). Bioflavours and fragrances via fermentation and biocatalysis. *J Chem Technol Biotechnol*, *77*(12), 1323–1332.

Verband der chemischen Industrie e.V. (2018). Chemiemärkte weltweit (Teil 1): Umsatz, Handel, Verbrauch von Chemikalien und Investitionen in der Chemie.

Volkmer, B. & Heinemann, M. (2011). Condition-dependent cell volume and concentration of *Escherichia coli* to facilitate data conversion for systems biology modeling. *PLoS One*, *6*.

Vourc'h, G., Garine-Wichatitsky, M., Labbé, A., Rosolowski, D., Martin, J.-L. & Fritz, H. (2002). Monoterpene effect on feeding choice by deer. *J Chem Ecol*, *28*(12), 2411–2427.

Wang, L., Zhou, Y. J., Ji, D. & Zhao, Z. K. (2013). An accurate method for estimation of the intracellular aqueous volume of *Escherichia coli* cells. *J Microbiol Methods*, *93*, 73–76.

Wang, Y., Meng, Q., Gao, W., Hou, J. & Ahmed, Z. (2011). Expression and purification of beefy meaty peptide in *Pichia pastoris. Korean J Chem Eng, 28*(3), 848–852.

Weber, H. (2010). *Mikrobiologie der Lebensmittel: Band 1: Grundlagen.* Behr's Verlag.

Welton, T. (1999). Room-temperature ionic liquids. Solvents for synthesis and catalysis. *Chem Rev, 99*(8), 2071–2084.

Whitfield, C. (2006). Biosynthesis and assembly of capsular polysaccharides in *Escherichia coli. Annu Rev Biochem, 75*, 39–68.

Willrodt, C., David, C., Cornelissen, S., Bühler, B., Julsing, M. K. & Schmid, A. (2014). Engineering the productivity of recombinant *Escherichia coli* for limonene formation from glycerol in minimal media. *Biotechnol J, 9*(8), 1000–1012.

Willrodt, C., Hoschek, A., Bühler, B., Schmid, A. & Julsing, M. K. (2016). Decoupling production from growth by magnesium sulfate limitation boosts de novo limonene production. *Biotechnol Bioeng, 113*(6), 1305–1314.

Woese, C. R. & Fox, G. E. (1977). Phylogenetic structure of the prokaryotic domain: The primary kingdoms. *Proc Natl Acad Sci USA, 74*(11), 5088–5090.

Wong, H. H., Kim, Y. C., Lee, S. Y. & Chang, H. N. (1998). Effect of post-induction nutrient feeding strategies on the production of bioadhesive protein in *Escherichia coli. Biotechnol Bioeng, 60*, 271–276.

Woodley, J. M. (2006). Choice of biocatalyst form for scalable processes. *Biochem Soc Trans, 34*, 301–303.

Xue, Y.-P., Liu, Z.-Q., Xu, M., Wang, Y.-Y., Zheng, Y.-G. & Shen, Y.-C. (2010). Enhanced biotransformation of (*R,S*)-mandelonitrile to (*R*)-(−)-mandelic acid with in situ production removal by addition of resin. *Biochem Eng J, 53*(1), 143–149.

Yamada, H. & Kobayashi, M. (1996). Nitrile hydratase and its application to industrial production of acrylamide. *Biosci, Biotechnol, Biochem, 60*(9), 1391–1400.

Yamazaki, M., Gong, Z., Fukuchi-Mizutani, M., Fukui, Y., Tanaka, Y., Kusumi, T. & Saito, K. (1999). Molecular cloning and biochemical characterization of a novel anthocyanin 5-O-glucosyltransferase by mRNA differential display for plant forms regarding anthocyanin. *J Biol Chem, 274*(11), 7405–7411.

Yesilirmak, F. & Sayers, Z. (2009). Heterelogous expression of plant genes. *Int J Plant Genomics, 2009*, 296482.

Yin, J., Li, G., Ren, X. & Herrler, G. (2007). Select what you need: A comparative evaluation of the advantages and limitations of frequently used expression systems for foreign genes: Review. *J Biotechnol, 127*, 335–347.

Zhou, J., Wang, C., Yoon, S.-H., Jang, H.-J., Choi, E.-S. & Kim, S.-W. (2014). Enginee-
   ring *Escherichia coli* for selective geraniol production with minimized endogenous
   dehydrogenation. *J Biotechnol, 169*, 42–50.

Zúñiga, C., Morales, M., Le Borgne, S. & Revah, S. (2011). Production of poly-$\beta$-hydroxy-
   butyrate (PHB) by *Methylobacterium organophilum* isolated from a methanotrophic
   consortium in a two-phase partition bioreactor. *J Hazard Mater, 190*(1-3), 876–882.

# List of abbreviations

| Abbreviation | Definition |
| --- | --- |
| Acetyl-CoA | Acetyl coenzyme A |
| BSA | Bovine serum albumin |
| cDNA | Complementary deoxyribonucleic acid |
| CDW | Cell dry weight concentration |
| DMAPP | Dimethylallyl diphosphate |
| DMP | 2,5-Dimethylpyrazine |
| DMSO | Dimethyl sulfoxide |
| DNA | Deoxyribonucleic acid |
| DO | Dissolved oxygen |
| *E. coli* | *Escherichia coli* |
| F&F | Flavor and fragrance |
| GA | Geranyl acetate |
| GG | Geranyl glucoside |
| Glc | Glucose |
| GPP | Geranyl pyrophosphate |
| GT | Glycosyltransferase |
| h | Hour |
| $H_2O$ | Water |
| HCDC | High cell density cultivation |
| HPLC | High performance liquid chromatography |
| [HPYR] [NTF] | Hexylpyridinium bis(trifluoromethylsulfonyl)imide |
| HSP | Hansen Solubility Parameter |
| IB | Inclusion body |
| IL | Ionic liquid |
| IPP | Isopentenyl diphosphate |
| IPTG | Isopropyl $\beta$-D-1-thiogalactopyranoside |
| ISPR | *in situ* product removal |

| Abbreviation | Definition |
| --- | --- |
| KP$_i$ | Potassium phosphate buffer |
| L | Liter |
| LB | Lysogeny broth |
| LC-MS | Liquid chromatography–mass spectrometry |
| logP | Logarithmic octanol/water partition coefficient |
| M | Molar |
| M9 | M9 mineral medium |
| MEP | 2-C-methylerythritol 4-phosphate |
| min | Minute |
| mL | Milliliter |
| mm | Millimeter |
| mM | Millimolar |
| mRNA | Messenger ribonucleic acid |
| MW | Molar mass, g mol$^{-1}$ |
| µL | Microliter |
| OD | Optical density |
| OD$_{600}$ | Optical density at 600 nm |
| PBS | Phosphate-buffered saline |
| PC | Partition coefficient |
| pLysS | *E. coli* BL21(DE3)pLysS pET29a_VvGT14a |
| pLysSA | *E. coli* BL21(DE3)pLysSA pET29a_VvGT14a |
| PP$_i$ | Inorganic pyrophosphate |
| PSPG | Plant secondary product glycosyltransferase |
| qPCR | Quantitative polymerase chain reaction |
| RB | Riesenberg medium |
| RNA | Ribonucleic acid |
| RP | Reversed-phase |
| rpm | revolutions per minute |
| RQ | Respiration coefficient |
| s | Second |
| *S. cerevisiae* | *Saccharomyces cerevisiae* |
| SDS | Sodium dodecyl sulfate |
| SDS-PAGE | Sodium dodecyl sulfate polyacrylamide gel electrophoresis |
| T7RNAP | T7 RNA polymerase |

| Abbreviation | Definition |
|---|---|
| TB | Terrific broth |
| Tris | Tris(hydroxymethyl)aminomethane |
| tRNA | Transfer ribonucleic acid |
| U | *Unit* (enzyme activity, µmol min$^{-1}$) |
| UDP | uridine diphosphate |
| UDP-glucose | Uridine diphosphate glucose |
| VvGT14a | A glycosyltransferase from *Vitis vinifera* |
| vvm | Volume of air per volume of reaction medium per minute |

# List of symbols

| Symbol | Definition |
|---|---|
| $A$ | Membrane surface, cm$^2$ |
| $c_A$ | Concentration of an analyte A, g L$^{-1}$ |
| $c_{A,intra}$ | Intracellular concentration of an analyte A, g L$^{-1}$ |
| $c_{eq}$ | Equilibrium concentration, g L$^{-1}$ |
| $c_{i,in}$ | Concentration of substance i in a feed solution, g L$^{-1}$ |
| $c_P$ | Product concentration, g L$^{-1}$ |
| $c_S$ | Substrate concentration, g L$^{-1}$ |
| $c'_{S,m}$ | Extracellular equilibrium concentration of the substrate S at the membrane, mol cm$^{-3}$ |
| $c''_{S,m}$ | Intracellular equilibrium concentration of the substrate S at the membrane, mol cm$^{-3}$ |
| $c'_{S,w}$ | Substrate concentration in the extracellular space, mol cm$^{-3}$ |
| $c''_{S,w}$ | Substrate concentration in the intracellular space, mol cm$^{-3}$ |
| $c_X$ | Cell dry weight concentration, g L$^{-1}$ |
| cSt | Centistoke as the unit of kinematic viscosity, 1 cSt = 10$^{-6}$ m$^2$ s$^{-1}$ |
| $d_m$ | Membrane thickness, cm |
| $D_{S,m}$ | Substrate diffusion coefficient in the membrane, cm$^2$ s$^{-1}$ |
| $\delta$ | Overall solubility parameter, MPa$^{0.5}$ |
| $\delta_D$ | Dispersion part of the solubility parameter, MPa$^{0.5}$ |
| $\delta_H$ | Hydrogen bonding part of the solubility parameter, MPa$^{0.5}$ |
| $\delta_P$ | Polar bonding part of the solubility parameter, MPa$^{0.5}$ |
| $E$ | Extinction, - |
| $E$ | Total cohesive energy or energy of vaporization, J mol$^{-1}$ |
| $E_D$ | Dispersion cohesive energy, J mol$^{-1}$ |
| $E_H$ | Hydrogen bonding energy, J mol$^{-1}$ |

*Continued on the next page*

| Symbol | Definition |
| --- | --- |
| $E_P$ | Polar cohesive energy, J mol$^{-1}$ |
| $\Delta H_V$ | Heat of vaporization, J mol$^{-1}$ |
| $J$ | Diffusion flux, mol cm$^{-2}$ s$^{-1}$ |
| $K_F$ | Freundlich coefficient, L g$^{-1}$ |
| $K_H$ | Henry coefficient, L g$^{-1}$ |
| $K_L$ | Langmuir coefficient, L g$^{-1}$ |
| $K_m$ | Michaelis constant, g L$^{-1}$ |
| $K_S$ | Equilibrium constant, - |
| $K_S$ | Half-saturation constant, g L$^{-1}$ |
| $\mu$ | Specific growth rate, h$^{-1}$ |
| $\mu_{max}$ | Maximal specific growth rate, h$^{-1}$ |
| $\mu_{set}$ | Set point for the specific growth rate, h$^{-1}$ |
| $m_i$ | Mass of a substance i |
| $n$ | Number of generations |
| $n$ | Stirrer speed, rpm |
| $\dot{n}$ | Substrate flux, mol s$^{-1}$ |
| $n_P$ | Product amount, mol |
| $n_S$ | Substrate amount, mol |
| $\nu_P$ | Stoichiometric coefficient of the product, - |
| $\nu_S$ | Stoichiometric coefficient of the substrate, - |
| $q$ | Mass of the adsorbate normalized by the mass of the adsorbent, g g$^{-1}$ |
| $q_P$ | Specific product formation rate,  g L$^{-1}$ h$^{-1}$ |
| $q_S$ | Specific substrate uptake rate,  g L$^{-1}$ h $^{-1}$ |
| $Ra$ | $Ra$ distance as the measure of thermodynamic affinity between two substances according to their Hansen Solubility Parameters, mPa$^{0.5}$ |
| $r_i$ | Volumetric reaction rate of component i, g L$^{-1}$ h $^{-1}$ |
| $t$ | Time, h |
| $STY$ | Space-time yield, mol L$^{-1}$ h$^{-1}$ |
| T | Temperature, °C |
| $V$ | Molar volume, m$^3$ mol$^{-1}$ |
| $V$ | Volume, L |
| $\dot{V}_{in}$ | Feed volume flow, L h$^{-1}$ |

| Symbol | Definition |
|--------|-----------|
| $\dot{V}_{out}$ | Outlet volume flow, L h$^{-1}$ |
| $V_R$ | Reactor volume, L |
| $\varphi$ | Phase fraction of a non-aqueous phase, - |
| $X$ | Conversion, % |
| $Y$ | Yield, % |
| $Y_{PS}$ | Specific product yield coefficient, g g$^{-1}$ |
| $Y_{PX}$ | Specific product yield related to biomass formation (or: specific productivity), g g$^{-1}$ |
| $Y_{XS,\mu}$ | Specific biomass yield coefficient, g g$^{-1}$ |

# A. Appendix

# A.1. Chemicals, consumables and equipment

## A.1.1. Chemicals

**Table A.1.:** Chemicals used in this work

| Chemical | Supplier | Article number |
|---|---|---|
| Acetic acid | Carl Roth | 4483.1 |
| Acetoin | Sigma-Aldrich | W200832 |
| Acetone | Carl Roth | T906.1 |
| Acetonitrile | J.T.Baker | JB9017.2500 |
| Acetyltributyl citrate | Sigma-Aldrich | 1009901 |
| Acrylamide/Bisacrylamide | Carl Roth | T802.1 |
| Agar | Carl Roth | 6494.3 |
| Albumin | Carl Roth | Q0163.2 |
| Ammonia 25 % (v/v) | Carl Roth | 6774.2 |
| Ammonium chloride, $NH_4Cl$ | Carl Roth | 5470.2 |
| Antifoam 204 | Sigma-Aldrich | A6426 |
| Assay kit acetic acid | R-Biopharm | 10148261035 |
| Asssay kit glucose | R-Biopharm | 10716251035 |
| Benzaldehyde | Sigma-Aldrich | B1334 |
| Benzyl alcohol | Sigma-Aldrich | 305197 |
| Benzyl acetate | Sigma-Aldrich | 50475 |
| Benzyl benzoate | Sigma-Aldrich | B6630 |
| Boric acid, $BH_3O_3$ | Sigma-Aldrich | B6768 |
| Bromphenol blue | Carl Roth | A512.1 |
| Butyl butyrate | Sigma-Aldrich | 281964 |
| Calcium chloride, $CaCl_2$ | Carl Roth | A119.1 |
| Chloramphenicol | Carl Roth | 3886.2 |
| Chloramphenicol acetate | Santa Cruz Biotechnology | sc-391764 |
| Citric acid monohydrate | Carl Roth | 6490.1 |
| Cobalt chloride hexahydrate, $CoCl_2 \cdot 6\,H_2O$ | Carl Roth | 7095.1 |

*Continued on the next page*

**Table A.1.:** Chemicals used in this work: continued

| Chemical | Supplier | Article number |
|---|---|---|
| Cooling liquid | Conzelmann Schweißgesellschaft | HKF 15.1 MW65 |
| Coomassie Brilliant Blue | Sigma-Aldrich | 1.15444 |
| Copper chloride dihydrate, $CuCl_2 \cdot 2\,H_2O$ | Merck | 1.02733.0250 |
| $\gamma$-Decalactone | Sigma-Aldrich | W236012 |
| Desmopan 9370AU | Covestro | |
| Diammonium hydrogen phosphate, $(NH_4)_2HPO_4$ | Carl Roth | 0268.3 |
| Dibutyl maleate | Sigma-Aldrich | D47102 |
| Dibutyl phthalate | Sigma-Aldrich | 524980 |
| Dibutyl sebacate | Sigma-Aldrich | 84840 |
| Diethyl sebacate | Sigma-Aldrich | 246077 |
| Dipotassium hydrogen phosphate, $K_2HPO_4$ | Carl Roth | P749.3 |
| Disodium phosphate, $Na_2HPO_4$ | Merck | F1021786125 |
| EDTA | AppliChem | 141026.1211 |
| Elvax 40W | DuPont | D12950143 |
| Ethanol 99 % (v/v) | CLN | 1004/25/21001 |
| Ethyl decanoate | Sigma-Aldrich | W243205 |
| Ethyl oleate | Sigma-Aldrich | 75100-1L |
| Farnesene | Sigma-Aldrich | W383902 |
| Geraniol | Carl Roth | 4988.2 |
| Geranyl acetate | Sigma-Aldrich | 173495 |
| D-Glucose monohydrate | Carl Roth | 6887.5 |
| Glyerol (87 %) | Merck | 1.04091 |
| Glyerol (99 %) | Carl Roth | 3783.3 |
| 2-Heptanone | | 537683 |
| Hexadecane | Sigma-Aldrich | H6703 |
| Hydrogen chloride, HCl | Honeywell | 10314253 |
| Hyrtel 8171 | DuPont | |

**Table A.1.:** Chemicals used in this work: continued

| Chemical | Supplier | Article number |
|---|---|---|
| Hytrel 8206 | DuPont | |
| IPTG | Carl Roth | CN08.4 |
| Iron(III) citrate, $C_6H_5FeO_7$ | Sigma-Aldrich | F6129 |
| Isobutyl acetate | Sigma-Aldrich | W217506 |
| Isobutyraldehyde | Sigma-Aldrich | 320358 |
| Isopropyl myristate | Carl Roth | 5527.1 |
| JustBlue Marker | Nippon Genetics | MWP05 |
| Kanamycin sulfate | Roth | T832.3 |
| Linalool | Sigma-Aldrich | L2602 |
| Linalyl acetate | Sigma-Aldrich | W263605 |
| Magnesiumsulfate heptahydrate, $MgSO_4 \cdot 7\,H_2O$ | Carl Roth | T888.2 |
| Manganese(II) chloride tetrahydrate, $MnCl_2 \cdot 4\,H_2O$ | VWR | 25222.233 |
| Methanol | X948.1 | Carl Roth |
| 3-Methylbutanol | Sigma-Aldrich | 59090 |
| Monopotassium phosphate, $KH_2PO_4$ | Merck | P018.1 |
| Nitrogen | Air Liquide | |
| 1-Octene | Sigma-Aldrich | O4806 |
| Oleyl alcohol | Sigma-Aldrich | 369314 |
| 6-Pentyl-$\alpha$-pyrone | Sigma-Aldrich | W369608 |
| Peptone from casein | Biofoxx | 1298KG2P5 |
| 2-Phenylethanol | Sigma-Aldrich | 77861 |
| 2-Phenylethyl acetate | Sigma-Aldrich | W285706 |
| Phosphoric acid | Honeywell | 10314209 |
| Polyethylene, medium density | Sigma-Aldrich | 332119 |
| Polystyrene | Sigma-Aldrich | 81401 |
| Potassium chloride, KCl | Carl Roth | 6781.1 |
| Potassium hydroxide, KOH | Carl Roth | 6751.1 |

**Table A.1.:** Chemicals used in this work: continued

| Chemical | Supplier | Article number |
|---|---|---|
| Raspberry ketone | Sigma-Aldrich | W258814 |
| ($S$)-Limonene | Sigma-Aldrich | 218367 |
| SDS | Carl Roth | 2326.1 |
| Sepabeads SP850 | Sigma-Aldrich | 13597-U |
| Silicone oil (viscosity: 10 cSt, MW: 700 g mol$^{-1}$) | Scientific Polymer Products | |
| Sodium chloride, NaCl | Sigma-Aldrich | SZBD1000V |
| Sodium hydroxide, NaOH | Carl Roth | 6771.2 |
| Sodium molybdate dihydrate, $Na_2MoO_4 \cdot 2\,H_2O$ | Carl Roth | 0274.2 |
| D(+)-Sucrose | Carl Roth | 4621.2 |
| TEMED | Carl Roth | 2367.3 |
| Tetradecane | Sigma-Aldrich | 172456 |
| 1-Tetradecene | Sigma-Aldrich | T9805 |
| TRIS | Carl Roth | 4855.2 |
| Toluol | Carl Roth | 7346.2 |
| Tris-Glycin 10 % | Carl Roth | 3060.2 |
| 10-Undecen-1-ol | Sigma-Aldrich | U2008 |
| Vanillin | Sigma-Aldrich | 94752 |
| Vanillin acetate | Sigma-Aldrich | W310808 |
| XAD-2 | Sigma-Aldrich | 9003-70-7 |
| XAD-4 | Sigma-Aldrich | 6444 |
| XAD-7HP | Sigma-Aldrich | BCBR6699V |
| Yeast extract | Deutsche Hefewerke | 253-3 |
| Zinc acetate dihydrate, $Zn(CH_3CO_2)_2 \cdot 2\,H_2O$ | Merck | 1.08802.0250 |

## A.1.2. Consumables

**Table A.2.:** Consumables used in this work

| Article | Model/Size | Supplier |
|---|---|---|
| Cannulas | 0.6 x 30 mm | Becton Dickinson |
| Cannulas | 0.8 x 120 mm | B. Braun Melsungen |
| Centrifuge tubes | 15/50 mL | Greiner Bio-One |
| Cuvettes, semi-micro | 1.6 mL, thickness 10 mm | Ratiolab |
| Disposable gloves | S | Meditrade |
| Disposable petri dishes | 90 mm | Greiner Bio-One |
| Disposable pipette tips | 200/1000 µL | B. Braun Melsungen |
| Exhaust air filter | 0.2 µm | Pall Corporation |
| Glas vials | 15 mL | Thermo Fisher |
| Glucose test strips | GlucoCheck Excellent | aktivmed GmbH |
| HPLC vials | 1.5 mL | neoLab |
| HPLC vial inserts | 15 mm | Macherey-Nagel |
| Micro reaction tubes | 1.5/2 mL | Greiner Bio-One |
| Microwell plates | 96 wells | Greiner Bio-One |
| Pipette tips | 5/10 mL | Gilson |
| Safe-lock micro reaction tubes | 1.5 and 2 mL | Eppendorf |
| Silicone septum | 19 mm | Infors |
| Sterile filter | 0.2 µm | Macherey-Nagel |
| Sterile filter | 0.22 µm | Millipore |
| Supply air filter | 0.2 µm | Pall Corporation |
| Syringes | 1/5/10/20 mL | B. Braun Melsungen |
| Vial crimp caps | 11 mm | Thermo Fisher |

## A.1.3. Equipment

**Table A.3.:** Universal equipment used in this work

| Component | Model | Manufacturer |
| --- | --- | --- |
| Autoclave | VX-150 | Systec |
| Centrifuge | MIKRO 20 | Hettich |
| Centrifuge | ROTIXA 50 RS | Hettich |
| Electrophoresis power source | Power Source 300 V | VWR |
| Electrophoresis system | CVS10TETRAD0.75 | Cleaver Scientific |
| Freeze dryer | Alpha 1–2 LD | Christ |
| Glucose measurement device | ACCU-CHEK Comfort | Roche |
| Heatblock | Standard Heatblock | VWR |
| Incubator | | Binder |
| Incubator shaker | Multitron | Infors |
| Incubator shaker | WiseCube | Wisd Laboratory Instruments |
| Microtiter plate photometer | MULTISCAN FC | Thermo Scientific |
| Mixer mill | MM 200 | Retsch Technology |
| pH probe | Lab 870 | Schott Instruments |
| pH probe | Lab 850 | Schott Instruments |
| Photometer | GENESYS 10uv | Thermo Scientific |
| Ultrasonic homogenizer | Sonopuls | Bandelin |
| Viscosimeter | RheolabQC | Anton Paar |

**Table A.4.:** Components of the high cell density cultivation system

| Component | Model | Manufacturer |
| --- | --- | --- |
| Reaction vessel 7.5 L | Labfors | Infors |
| Vessel equipment | Labfors | Infors |
| Control unit | Labors | Infors |
| Peristaltic feed pump | BVP | ISMATEC |
| Recirculating chiller | minichiller 600 | Huber Kältetechnik |
| pH probe | 405-DPAS-SC-K8S/425 | Mettler-Toledo |
| Dissolved oxygen probe | InPro6820/12/420 | Mettler-Toledo |
| Software | Iris V5 | Infors |

**Table A.5.:** Components of the mL-scale parallel bioreactor system

| Component | Model | Manufacturer |
| --- | --- | --- |
| Reactor block | bioREACTOR 48 | 2mag |
| Single-use bioreactors | Unbaffled | 2mag |
| Stirrer control | | 2mag |
| Optical sensor scanner bars | MCR 8pH-8oxygen | PreSens |
| Heater | W15 | Haake |
| Recirculating chiller | | FRYKA Kältetechnik |
| Gas mixer | 0254 | Brooks Instrument |
| Liquid handling system | Genesis RSP150 | Tecan |
| Software liquid handling system | Gemini V4.2.17.304 | Tecan |
| Software process control | Fedbatch-XP 1.0.248 | DASGIP |

**Table A.6.:** Components of the 0.4 L-scale parallel bioreactor system

| Component | Model | Manufacturer |
| --- | --- | --- |
| Reaction vessel | DASGIP DS0700ODSS 250 mL–700 mL | Eppendorf |
| Vessel equipment | DASGIP | Eppendorf |
| Stirrer motor | DASGIP RE40, 100–1.600 rpm | Eppendorf |
| Heating and cooling block | DASGIP Bioblock | Eppendorf |
| Gas mixer | DASGIP MX4/4 | Eppendorf |
| Temperature and stirrer control | DASGIP TC4SC4 | Eppendorf |
| pH and dissolved oxygen read-out device | DASGIP PH4PO4L | Eppendorf |
| Peristaltic pumps | DASGIP MP8 | Eppendorf |
| Exhaust gas analytics | BlueVary | BlueSens |
| pH probe | EasyFerm Plus PHI K8 225 | Hamilton |
| Dissolved oxygen probe | VisiFerm DO ECS 225HO | Hamilton |
| Software | DASware® control | Eppendorf |

**Table A.7.:** Elution gradient for LC-MS measurements

| Time, min | Flow, mL min⁻¹ | Eluent B, % |
|---|---|---|
| 0 | 0.40 | 0 |
| 5 | 0.4 | 0 |
| 10 | 0.4 | 2 |
| 11 | 0.35 | 9 |
| 16 | 0.25 | 9 |
| 18 | 0.25 | 9 |
| 19 | 0.15 | 50 |
| 25 | 0.15 | 50 |
| 26 | 0.15 | 0 |
| 32 | 0.4 | 0 |
| 36 | 0.4 | 0 |

**Table A.8.:** Components for LC-MS measurements

| Component | Model | Manufacturer |
|---|---|---|
| Pump/pump degasser | Acella | Thermo Scientific |
| Sampler | PAL CTC | CTC Analytics |
| Column oven | MistraSwitch | Mayland |
| Column | Acquity HSS T3 150 mm x 2.1 mm × 1,8 µm, 100 Å | Waters Corporation |
| Guard column | VanGuard 2,1 mm x 5,0 mm | Waters |
| Mass spectrometer | TSQ Vantage | Thermo Scientic |
| Software | Xcalibur 2.2 | Thermo Fisher Scientific |

**Table A.9.:** Components for HPLC measurements

| Component | Model | Manufacturer |
|---|---|---|
| Pump | UltiMate LPG-3400SD | Thermo Scientific |
| Sampler | UltiMate WPS-3000 SplitLoop | Thermo Scientific |
| Detector | UltiMate DAD-3000 | Thermo Scientific |
| Software | Chromeloen 7 | Thermo Scientific |
| Column oven | Mistral | Spark Holland |
| Column | Accucore C18 (particle size 2.6 µm; dimensions: 100 × 4.6 mm) | Thermo Scientific |
| Guard column | SecurityGuard KJ0-4282 | Phenomenex |

## A.2. Media and buffer compositions

**Table A.10.:** Composition of phosphate-buffered saline (PBS). The pH was adjusted to pH 7.4.

| Component | Concentration, g L$^{-1}$ |
|---|---|
| NaCl | 8.0 |
| KCl | 0.2 |
| Na$_2$HPO$_4$ | 1.44 |
| KH$_2$PO$_4$ | 0.24 |

**Table A.11.:** Composition of 0.1 M potassium phosphate buffer pH 7 (KP$_i$)

| Component | Concentration, g L$^{-1}$ |
|---|---|
| K$_2$HPO$_4$ | 9.344 |
| KH$_2$PO$_4$ | 6.309 |

**Table A.12.:** Composition of lysogeny broth (LB). The pH was adjusted to pH 7.

| Component | Concentration, g L$^{-1}$ |
|---|---|
| Peptone from casein | 10 |
| Yeast extract | 5 |
| NaCl | 10 |

**Table A.13.:** Composition of modified lysogeny broth (LB$_{mod}$). The pH was adjusted to pH 7.

| Component | Concentration, g L$^{-1}$ |
| --- | --- |
| Peptone from casein | 20 |
| Yeast extract | 10 |
| NaCl | 5 |
| K$_2$HPO$_4$ | 2.5 |
| MgSO$_4$ · 7 H$_2$O | 1 |

**Table A.14.:** Composition of lysogeny broth for agar plates. The pH was adjusted to pH 7.

| Component | Concentration, g L$^{-1}$ |
| --- | --- |
| Peptone from casein | 10 |
| Yeast extract | 5 |
| NaCl | 5 |
| Agar | 12 |
| Addition of sterile antibiotics after autoclaving and cooling to 60 °C. Pouring in petri dishes and airtight storage at 4 °C. | |

**Table A.15.:** Composition of terrific broth (TB)

| Component | Amount |
| --- | --- |
| Tryptone from casein | 12 g L$^{-1}$ |
| Yeast extract | 24 g L$^{-1}$ |
| Glycerol | 4 mL |
| KP$_i$ buffer (0.17 M KH$_2$PO$_4$, 0.72 M K$_2$HPO$_4$) | 100 mL |

**Table A.16.:** 250 g L$^{-1}$ magnesium sulfate heptahydrate stock solution

| Component | Concentration, g L$^{-1}$ |
| --- | --- |
| MgSO$_4$ · 7 H$_2$O | 250 |

**Table A.17.:** 500 g L$^{-1}$ glucose stock solution

| Component | Concentration, g L$^{-1}$ |
| --- | --- |
| D(+)-glucose monohydrate | 550 |

**Table A.18.:** Composition of the trace element stock solution

| Component | Concentration, g L$^{-1}$ |
|---|---|
| $BH_3O_3$ | 0.3 |
| $CoCl_2 \cdot 6\,H_2O$ | 0.25 |
| $C_{10}H_{16}N_2O_8$ (EDTA) | 0.84 |
| $C_6H_5FeO_7$ | 6 |
| $CuCl_2 \cdot 2\,H_2O$ | 0.18 |
| $MnCl_2 \cdot 4\,H_2O$ | 1.95 |
| $Na_2MoO_4 \cdot 2\,H_2O$ | 0.3 |
| $Zn(CH_3CO_2)_2 \cdot 2\,H_2O$ | 0.96 |

**Table A.19.:** Riesenberg medium for high cell density cultivations. Composition according to Riesenberg et al. [1991], however without the addition of thiamine.

| Component | Concentration, g L$^{-1}$ |
|---|---|
| $KH_2PO_4$ | 13.3 |
| $(NH_4)_2HPO_4$ | 4 |
| $C_6H_8O_7 \cdot H_2O$ (Citric acid monohydrate) | 1.87 |
| pH 6.8 with 10 M KOH | |
| Addition of following components after autoclaving | Amount |
| $MgSO_4 \cdot 7\,H_2O$ (from stock) | 1.2 g L$^{-1}$ |
| Glucose (from stock) | 2 g L$^{-1}$ |
| Trace element solution (from stock) | 10 mL |
| Antifoam | 1 mL |
| Kanamycin | 1 mL |

**Table A.20.:** Composition of the feeding medium for high cell density cultivations

| Component | Concentration, g L$^{-1}$ |
|---|---|
| D(+)-glucose monohydrate | 660 |
| $MgSO_4 \cdot 7\,H_2O$ | 15 |

**Table A.21.:** Composition of M9 mineral medium for whole-cell biotransformations of geraniol. Adjustment of pH 7 with KOH or $H_3PO_4$.

| Component | Concentration, g L$^{-1}$ |
|---|---|
| $NH_4Cl$ | 1 |
| $CaCl_2$ | 0.0111 |
| $Na_2HPO_4$ | 6 |
| $KH_2PO_4$ | 3 |
| $MgSO_4 \cdot 7\,H_2O$ | 0.246 |
| $NaCl$ | 0.5 |

**Table A.22.:** Composition of 5x Laemmli buffer [Laemmli 1970]

| Component | Concentration |
| --- | --- |
| Tris/HCl pH 6.8 | 300 mM |
| Glycerol | 50 % (w/v) |
| 2-Mercaptoethanol | 5 % (w/v) |
| Bromphenol blue | 0.05 % (v/v) |
| Sodium dodecyl sulfate | 10 % (w/v) |

**Table A.23.:** Composition of SDS running buffer

| Component | Concentration |
| --- | --- |
| Tris/HCl pH 6.8 | 300 mM |
| Glycerol | 50 % (w/v) |
| Sodium dodecyl sulfate | 10 % (w/v) |

**Table A.24.:** Composition of Fairbanks A solution [Fairbanks et al. 1971]

| Component | Concentration |
| --- | --- |
| Isopropanol | 25 % (v/v) |
| Acetic acid | 10 % (v/v) |
| Coomassie Brilliant Blue | 0.05 % (w/v) |

**Table A.25.:** Composition of Fairbanks B solution [Fairbanks et al. 1971]

| Component | Concentration |
| --- | --- |
| Isopropanol | 10 % (v/v) |
| Acetic acid | 10 % (v/v) |
| Coomassie Brilliant Blue | 0.005 % (w/v) |

## A.3. Supplementary figures
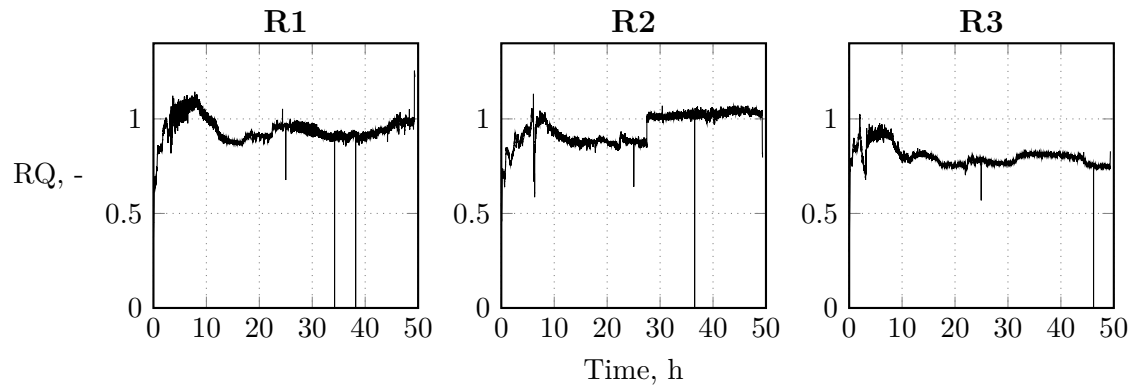


**Figure A.1.:** Respiration coefficients (RQ) for 3 parallelized experimental set-ups (R1-R3) of biotransformations with *E. coli* BL21(DE3)pLysSA pET29a_VvGT14a at L-scale. The process variables are listed in Table 7.4. Universal settings: V = 0.4 L, $DO_{set}$ = 30 %, pH 7.